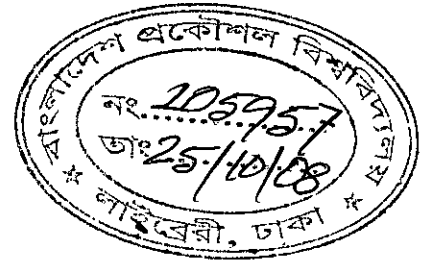
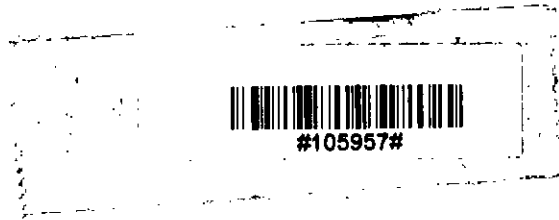


**AN EXPERIMENTAL STUDY OF HEAT TRANSFER IN TURBULENT  
FLOW THROUGH A TUBE WITH PERFORATED RECTANGULAR STRIP  
INSERT**



By

**Muhammad Mostafa Kamal Bhuiya**



In partial fulfillment of the requirements for the degree of  
**MASTER OF SCIENCE IN MECHANICAL ENGINEERING**

**Department of Mechanical Engineering  
BANGLADESH UNIVERSITY OF ENGINEERING AND TECHNOLOGY,  
BUET**

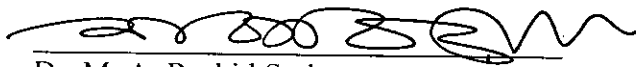
**Dhaka, Bangladesh**

**June 2008**

## CERTIFICATION OF RESEARCH

The thesis entitled " An Experimental Study of Heat Transfer in Turbulent Flow Through a Tube with Perforated Rectangular Strip Insert," submitted by Muhammad Mostafa Kamal Bhuiya, Roll no.: 040410090F, Session: April, 2004 has been accepted as satisfactory in partial fulfillment of the requirement for the degree of MASTER OF SCIENCE IN MECHANICAL ENGINEERING on 21 June, 2008.

### BOARD OF EXAMINERS

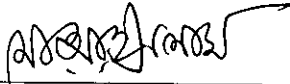


Dr. M. A. Rashid Sarkar  
Professor

Department of Mechanical Engineering, BUET,  
Dhaka, Bangladesh.

(Supervisor)

Chairman



Dr. Md. Ashraful Islam  
Professor

Department of Mechanical Engineering, BUET,  
Dhaka, Bangladesh

Member

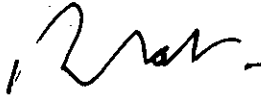


Dr. Abu Rayhan Md. Ali  
Professor & Head

Department of Mechanical Engineering, BUET,  
Dhaka, Bangladesh

(Ex-officio)

Member



Dr. Bodius Salam  
Associate Professor & Head

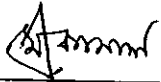
Department of Mechanical Engineering, CUET,  
Chittagong, Bangladesh

(External)

Member

## DECLARATION

It is hereby declared that this thesis or any part of it has not been submitted elsewhere for the award of any degree.



---

Muhammad Mostafa Kamal Bhuiya  
Author

*Dedicated*  
*To*  
*My Younger Brother*  
*Late Altaf Hossain*

## TABLE OF CONTENTS

<b>TITLE</b> -----	Page i
<b>THESIS APPROVAL</b> -----	ii
<b>DECLARATION</b> -----	iii
<b>DEDICATION</b> -----	iv
<b>TABLE OF CONTENTS</b> -----	v-vii
<b>LIST OF FIGURES AND TABLES</b> -----	viii-xvi
<b>NOMENCLATURE</b> -----	xvii-xviii
<b>ACKNOWLEDGEMENT</b> -----	xix
<b>ABSTRACT</b> -----	xx
<b>CHAPTER-1</b>	
<b>INTRODUCTION</b> -----	1-3
<b>1.1 General</b> -----	1
<b>1.2 The Enhancement Techniques</b> -----	1
<b>1.3 Objectives</b> -----	3
<b>CHAPTER-2</b>	
<b>LITERATURE SURVEY</b> -----	4-14
<b>CHAPTER-3</b>	
<b>THEORY</b> -----	15-22
<b>3.1 General</b> -----	15
<b>3.2 Hydraulic Diameter</b> -----	15
<b>3.3 Reynolds Number</b> -----	16
<b>3.4 Pressure Drop and Fanning Friction Factor</b> -----	16
<b>3.5 Porosity</b> -----	17
<b>3.6 Heat Transfer Rate</b> -----	17
<b>3.7 Bulk Fluid Temperature</b> -----	18
<b>3.8 Heat Transfer Coefficient</b> -----	19
<b>3.9 Nusselt Number</b> -----	19
<b>3.10 Blower Power</b> -----	20
<b>3.11 Effectiveness</b> -----	20

3.12 Performance Parameter -----	21
<b>CHAPTER – 4</b>	
<b>EXPERIMENTAL FACILITY AND PROCEDURE -----</b>	<b>23-29</b>
4.1 General -----	23
4.2 Experimental Facility -----	23
4.2.1 Test Section -----	23
4.2.2 Inlet Section -----	24
4.2.3 Air Supply System -----	24
4.2.4 Heating Arrangemnts -----	25
4.3 Measurement Systems -----	25
4.3.1 Flow Measuring System -----	25
4.3.2 Pressure Measuring System -----	26
4.3.3 Temperature Measuring System -----	26
4.4 Experimental Procedures -----	27
4.5 Uncertainty Analysis -----	28
<b>CHAPTER-5</b>	
<b>RESULTS AND DISCUSSIONS -----</b>	<b>38-53</b>
5.1 General -----	38
5.2 Temperature Distribution -----	39
5.2.1 Effect of Reynolds Numbers and Porosity of the Rectangular Strip on Local and Average Tube Wall and Fluid Bulk Temperatures -----	39
5.2.2 Effect of Reynolds Numbers and Porosity of the Rectangular Strip on Dimensionless Temperature Differences -----	41
5.3 Heat Transfer Characteristics -----	42
5.3.1 Effect of Reynolds Numbers and Porosity of the Rectangular Strip on Heat Transfer Coefficient ---	43
5.3.2 Effect of Reynolds Numbers and Porosity of the Rectangular Strip on Nusselt Number -----	44
5.3.3 Effect of Reynolds Numbers and Porosity of the Rectangular Strip on Heat Transfer Rate -----	46

<b>5.4 Fluid Flow Characteristics -----</b>	<b>46</b>
<b>5.4.1 Effect of Reynolds Numbers and Porosity of the           Rectangular Strip on Pressure Drop-----</b>	<b>47</b>
<b>5.4.2 Effect of Reynolds Numbers and Porosity of the           Rectangular Strip on Friction Factor -----</b>	<b>48</b>
<b>5.5 Blower Power -----</b>	<b>49</b>
<b>5.6 Effectiveness -----</b>	<b>49</b>
<b>5.7 Performance Parameter -----</b>	<b>50</b>
<b>5.8 Comparison of the Results with the Previous Results ----</b>	<b>50</b>
<b>5.9 Data Reduction -----</b>	<b>52</b>
<b>CHAPTER-6</b>	
<b>CONCLUSSION AND RECOMMENDATION -----</b>	<b>102-104</b>
<b>REFERENCES -----</b>	<b>105-108</b>
<b>APPENDICES</b>	
<b>APPENDIX-A SPECIFICATION OF THE EQUIPMENTS ----</b>	<b>A-1</b>
<b>APPENDIX-B SAMPLE CALCULATION -----</b>	<b>B.1-B.11</b>
<b>APPENDIX-C DETERMINATION OF LOCATION OF           MEASURING INSTRUEMENTS -----</b>	<b>C.1-C.3</b>
<b>APPENDIX-D UNCERTAINTY ANALYSIS -----</b>	<b>D.1-D.6</b>
<b>APPENDIX-E DATA TABLES-----</b>	<b>E.1-E.27</b>
<b>APPENDIX-F PHOTOGRAPHS -----</b>	<b>F.1-F.10</b>

## LIST OF FIGURES AND TABLES

---

	Page
Fig. 4.1 : Schematic diagram of the experimental facility.	30
Fig.4.2a : Schematic diagram of the experimental facility with dimensions	31
Fig.4.2b : Cross- section of the test section with insulations.	31
Fig.4.3a : Cross- section of the test section with perforated rectangular strip insert.	32
Fig.4.3b : Isometric view of the perforated rectangular strip insert with dimensions.	32
Fig.4.3c : Schematic diagram of the hole position in the strip with dimensions.	32
Fig. 4.4 : Shaped inlet section	33
Fig. 4.5 : Electrical circuit diagram for the heating system.	34
Fig. 4.6 : Traversing the pitot tube holding device.	35
Fig. 4.7 : Location of the pitot tube for measurement of velocity.	36
Fig. 4.8 : Location of the pressure tappings.	36
Fig. 4.9 : Location of thermocouples.	37
Fig.4.10 : Location of thermocouples for the outlet bulk temperature.	37
Fig. 5.1 : Variation of wall and bulk temperatures along axial distance for the tube with perforated rectangular strip insert having porosity, $R_p = 1.1\%$ .	54
Fig. 5.2 : Variation of wall and bulk temperatures along axial distance for the tube with perforated rectangular strip insert having porosity, $R_p = 2.5\%$ .	54
Fig. 5.3 : Variation of wall and bulk temperatures along axial distance for the tube with perforated rectangular strip insert having porosity, $R_p = 4.4\%$ .	55
Fig. 5.4 : Variation of wall and bulk temperatures along axial distance for the tube with perforated rectangular strip insert having porosity, $R_p = 6.8\%$ .	55



- Fig.5.5 : Variation of wall and bulk temperatures along axial distance for 56  
the tube with perforated rectangular strip insert having porosity,  
 $R_p = 13.3\%$ .
- Fig.5.6 : Variation of wall and bulk temperatures along axial distance for 56  
the tube with perforated rectangular strip insert having porosity,  
 $R_p = 17.4\%$ .
- Fig.5.7 : Variation of wall and bulk temperatures along axial distance for 57  
the tube with perforated rectangular strip insert having porosity,  
 $R_p = 22.0\%$ .
- Fig. 5.8 : Variation of wall and bulk temperatures along axial distance for 57  
the tube with perforated rectangular strip insert having porosity,  
 $R_p = 27.1\%$ .
- Fig 5.9 : Variation of wall and bulk temperatures along axial distance for 58  
the tube with perforated rectangular strip insert having porosity,  
 $R_p = 39.0\%$ .
- Fig.5.10 : Variation of wall and bulk temperatures along axial distance for 58  
the tube with rectangular strip insert.
- Fig.5.11 : Variation of wall and bulk temperatures along axial distance for 59  
the plain tube.
- Fig.5.11 (a) : Variation of wall and bulk temperatures along axial distance for 59  
different porosity of inserts at Reynolds number around 30,925.
- Fig.5.11 (b): : Variation of wall temperatures with different porosity ( $R_p$  from 0 60  
%-39 %) of inserts for axial distance of  $X/L = 0.57$  and at  
Reynolds number around 30,925.
- Fig.5.12 : Variation of the average wall temperatures for different porosity of 60  
rectangular strip inserts at different Reynolds numbers.
- Fig.5.13 : Variation of the average fluid bulk temperatures for different 61  
porosity of rectangular strip inserts at different Reynolds numbers.
- Fig.5.14 : Variation of dimensionless temperature differences along axial 61  
distance for the tube with perforated rectangular strip insert  
having porosity,  $R_p = 1.1\%$ .
- Fig.5.15 : Variation of dimensionless temperature differences along axial 62

- distance for the tube with perforated rectangular strip insert having porosity,  $R_p = 2.5\%$ .
- Fig. 5.16 : Variation of dimensionless temperature differences along axial distance for the tube with perforated rectangular strip insert having porosity,  $R_p = 4.4\%$ . 62
- Fig. 5.17 : Variation of dimensionless temperature differences along axial distance for the tube with perforated rectangular strip insert having porosity,  $R_p = 6.8\%$ . 63
- Fig. 5.18 : Variation of dimensionless temperature differences along axial distance for the tube with perforated rectangular strip insert having porosity,  $R_p = 13.3\%$ . 63
- Fig. 5.19 : Variation of dimensionless temperature differences along axial distance for the tube with perforated rectangular strip insert having porosity,  $R_p = 17.4\%$ . 64
- Fig. 5.20 : Variation of dimensionless temperature differences along axial distance for the tube with perforated rectangular strip insert having porosity,  $R_p = 22.0\%$ . 64
- Fig. 5.21 : Variation of dimensionless temperature differences along axial distance for the tube with perforated rectangular strip insert having porosity,  $R_p = 27.1\%$ . 65
- Fig. 5.22 : Variation of dimensionless temperature differences along axial distance for the tube with perforated rectangular strip insert having porosity,  $R_p = 39\%$ . 65
- Fig. 5.23 : Variation of dimensionless temperature differences along axial distance for the tube with rectangular strip insert. 66
- Fig. 5.24 : Variation of dimensionless temperature differences along axial distance for the plain tube. 66
- Fig. 5.24 (a) : Variation of dimensionless temperature differences along axial distance for different porosity of inserts at Reynolds number around 30,925. 67
- Fig. 5.24 (b) : Variation of dimensionless temperature differences with different porosity ( $R_p$  from 0 %-39 %) of inserts for axial distance of  $X/L =$  67

0.57 and at Reynolds number around 30,925.

- Fig.5.25 : Variation of the local heat transfer coefficient along axial distance 68  
for the tube with insert having porosity,  $R_p = 1.1\%$  at different  
Reynolds numbers.
- Fig.5.26 : Variation of the local heat transfer coefficient along axial distance 68  
for the tube with insert having porosity,  $R_p = 2.5\%$  at different  
Reynolds numbers.
- Fig.5.27 : Variation of the local heat transfer coefficient along axial distance 69  
for the tube with insert having porosity,  $R_p = 4.4\%$  at different  
Reynolds numbers.
- Fig.5.28 : Variation of the local heat transfer coefficient along axial distance 69  
for the tube with insert having porosity,  $R_p = 6.8\%$  at different  
Reynolds numbers.
- Fig.5.29 : Variation of the local heat transfer coefficient along axial distance 70  
for the tube with insert having porosity,  $R_p = 13.3\%$  at different  
Reynolds numbers.
- Fig.5.30 : Variation of the local heat transfer coefficient along axial distance 70  
for the tube with insert having porosity,  $R_p = 17.4\%$  at different  
Reynolds numbers.
- Fig.5.31 : Variation of the local heat transfer coefficient along axial distance 71  
for the tube with insert having porosity,  $R_p = 22.0\%$  at different  
Reynolds numbers.
- Fig.5.32 : Variation of the local heat transfer coefficient along axial distance 71  
for the tube with insert having porosity,  $R_p = 27.1\%$  at different  
Reynolds numbers.
- Fig.5.33 : Variation of the local heat transfer coefficient along axial distance 72  
for the tube with insert having porosity,  $R_p = 39.0\%$  at different  
Reynolds numbers.
- Fig.5.34 : Variation of the local heat transfer coefficient along axial distance 72  
for the tube with rectangular strip insert at different Reynolds  
numbers.

Fig.5.35	:	Variation of the local heat transfer coefficient along axial distance for the plain tube at different Reynolds numbers.	73
Fig.5.35 (a)	:	Variation of local heat transfer coefficient along axial distance for different porosity of inserts at Reynolds number around 30,925.	73
Fig.5.35 (b)	:	Variation of local heat transfer coefficient with different porosity ( $R_p$ from 0 %-39 %) of inserts for axial distance of $X/L = 0.57$ and at Reynolds number around 30,925.	74
Fig.5.36	:	Variation of the average heat transfer coefficient for different porosity of rectangular strip inserts at different Reynolds numbers.	74
Fig.5.36 (a)	:	Variation of average heat transfer coefficient with different porosity ( $R_p$ from 0 %-39 %) of inserts for different Reynolds numbers (considering constant Reynolds numbers for all inserts).	75
Fig.5.37	:	Variation of the average heat transfer coefficient for different inserts (perforated and unperforated) at different Reynolds numbers.	75
Fig. 5.38	:	Variation of the local Nusselt number along axial distance for the tube with insert having porosity, $R_p = 1.1$ % at different Reynolds numbers.	76
Fig.5.39	:	Variation of the local Nusselt number along axial distance for the tube with insert having porosity, $R_p = 2.5$ % at different Reynolds numbers.	76
Fig.5.40	:	Variation of the local Nusselt number along axial distance for the tube with insert having porosity, $R_p = 4.4$ % at different Reynolds numbers.	77
Fig.5.41	:	Variation of the local Nusselt number along axial distance for the tube with insert having porosity, $R_p = 6.8$ % at different Reynolds numbers.	77
Fig.5.42	:	Variation of the local Nusselt number along axial distance for the tube with insert having porosity, $R_p = 13.3$ % at different Reynolds numbers.	78
Fig.5.43	:	Variation of the local Nusselt number along axial distance for the tube with insert having porosity, $R_p = 17.4$ % at different	78

Reynolds numbers.

- Fig. 5.44 : Variation of the local Nusselt number along axial distance for the tube with insert having porosity,  $R_p = 22.0\%$  at different Reynolds numbers. 79
- Fig. 5.45 : Variation of the local Nusselt number along axial distance for the tube with insert having porosity,  $R_p = 27.1\%$  at different Reynolds numbers. 79
- Fig. 5.46 : Variation of the local Nusselt number along axial distance for the tube with insert having porosity,  $R_p = 39.0\%$  at different Reynolds numbers. 80
- Fig. 5.47 : Variation of the local Nusselt number along axial distance for the tube with rectangular strip insert at different Reynolds numbers. 80
- Fig. 5.48 : Variation of the local Nusselt number along axial distance for the plain tube at different Reynolds numbers. 81
- Fig. 5.48 (a) : Variation of local Nusselt number along axial distance for different porosity of inserts at Reynolds number around 30,925. 81
- Fig. 5.48 (b) : Variation of local Nusselt number with different porosity ( $R_p$  from 0 %-39 %) of inserts for axial distance of  $X/L = 0.57$  and at Reynolds number around 30,925. 82
- Fig. 5.49 : Variation of the average Nusselt number for different porosity of rectangular strip inserts at different Reynolds numbers. 82
- Fig. 5.50 : Variation of the heat transfer rate for different porosity of rectangular strip inserts at different Reynolds numbers. 83
- Fig. 5.51 : Variation of the heat transfer rate with the blower power at porosity,  $R_p = 4.4\%$ . 83
- Fig. 5.52 : Variation of the pressure drop along axial distance for insert having porosity,  $R_p = 1.1\%$  at different Reynolds numbers. 84
- Fig. 5.53 : Variation of the pressure drop along axial distance for insert having porosity,  $R_p = 2.5\%$  at different Reynolds numbers. 84
- Fig. 5.54 : Variation of the pressure drop along axial distance for insert having porosity,  $R_p = 4.4\%$  at different Reynolds numbers. 85
- Fig. 5.55 : Variation of the pressure drop along axial distance for insert 85

- having porosity,  $R_p = 6.8\%$  at different Reynolds numbers.
- Fig. 5.56 : Variation of the pressure drop along axial distance for insert 86  
having porosity,  $R_p = 13.3\%$  at different Reynolds numbers.
- Fig. 5.57 : Variation of the pressure drop along axial distance for insert 86  
having porosity,  $R_p = 17.4\%$  at different Reynolds numbers.
- Fig. 5.58 : Variation of the pressure drop along axial distance for insert 87  
having porosity,  $R_p = 22.0\%$  at different Reynolds numbers.
- Fig. 5.59 : Variation of the pressure drop along axial distance for insert 87  
having porosity,  $R_p = 27.1\%$  at different Reynolds numbers.
- Fig. 5.60 : Variation of the pressure drop along axial distance for insert 88  
having porosity,  $R_p = 39.0\%$  at different Reynolds numbers.
- Fig. 5.61 : Variation of the pressure drop along axial distance for the tube 88  
with rectangular strip insert at different Reynolds numbers.
- Fig. 5.62 : Variation of the pressure drop along axial distance for the plain 89  
tube at different Reynolds numbers.
- Fig. 5.62 (a) Variation of the pressure drop along axial distance for different 89  
porosity of inserts at Reynolds number around 30,925.
- Fig. 5.62 (b) Variation of the pressure drop with different porosity ( $R_p$  from 0 90  
%-39 %) of inserts for axial distance of  $X/L = 0.57$  and at  
Reynolds number around 30,925.
- Fig. 5.63 : Variation of the total pressure drop for different porosity of 90  
rectangular strip inserts at different Reynolds numbers.
- Fig. 5.64 : Variation of the blower power required for different porosity of 91  
rectangular strip inserts at different Reynolds numbers.
- Fig. 5.65 : Variation of the blower power required for different inserts 91  
(perforated and unperforated) at different Reynolds numbers.
- Fig. 5.66 : Variation of the friction factor along axial distance for insert 92  
having porosity,  $R_p = 1.1\%$  at different Reynolds numbers.
- Fig. 5.67 : Variation of the friction factor along axial distance for insert 92  
having porosity,  $R_p = 2.5\%$  at different Reynolds numbers.
- Fig. 5.68 : Variation of the friction factor along axial distance for insert 93  
having porosity,  $R_p = 4.4\%$  at different Reynolds numbers.

- Fig. 5.69 : Variation of the friction factor along axial distance for insert 93  
having porosity,  $R_p = 6.8\%$  at different Reynolds numbers.
- Fig. 5.70 : Variation of the friction factor along axial distance for insert 94  
having porosity,  $R_p = 13.3\%$  at different Reynolds numbers.
- Fig. 5.71 : Variation of the friction factor along axial distance for insert 94  
having porosity,  $R_p = 17.4\%$  at different Reynolds numbers.
- Fig. 5.72 : Variation of the friction factor along axial distance for insert 95  
having porosity,  $R_p = 22.0\%$  at different Reynolds numbers.
- Fig. 5.73 : Variation of the friction factor along axial distance for insert 95  
having porosity,  $R_p = 27.1\%$  at different Reynolds numbers.
- Fig. 5.74 : Variation of the friction factor along axial distance for insert 96  
having porosity,  $R_p = 39.0\%$  at different Reynolds numbers.
- Fig. 5.75 : Variation of the friction factor along axial distance for the tube 96  
with rectangular strip at different Reynolds numbers.
- Fig. 5.76 : Variation of the friction factor along axial distance for the plain 97  
tube at different Reynolds numbers.
- Fig. 5.76 (a) : Variation of the friction factor along axial distance for different 97  
porosity of inserts at Reynolds number around 30,925.
- Fig. 5.76 (b) : Variation of the friction factor with different porosity ( $R_p$  from 0 98  
%-39 %) of inserts for axial distance of  $X/L = 0.57$  and at  
Reynolds number around 30,925.
- Fig. 5.77 : Variation of the average friction factor for different porosity of 98  
rectangular strip inserts at different Reynolds numbers.
- Fig. 5.78 : Variation of the heat transfer effectiveness for different porosity of 99  
rectangular strip inserts at different Reynolds numbers.
- Fig. 5.79 : Variation of  $C$  with different porosity of the rectangular strip 99  
inserts,  $R_p$ .
- Fig. 5.80 : Variation of  $m$  with different porosity of the rectangular strip 100  
inserts,  $R_p$ .
- Fig. 5.81 : Variation of the experimental data with the predicted data for 100  
different porosity of rectangular strip inserts ( $R_p$  from 0 % to 39  
%).

Fig. 5.82	: Variation of the experimental Nusselt numbers with the predicted Nusselt numbers for different porosity of rectangular strip inserts ( $R_p$ from 0 % to 39 %).	101
Fig. 5.83	: Variation of performance parameter, (R) with blower power for different porosity of rectangular strip inserts ( $R_p$ from 1.1 % to 39 %) and unperforated rectangular strip insert.	101
Table 4.1	Uncertainties in measurands	29
Table 4.2	Uncertainties in calculated quantities	29
TableB.1	Experimental data of fluid flow through plain tube	B-3
TableB.2	Experimental data of heat transfer for plain tube	B-5
TableB.3	Experimental data of fluid flow through tube with perforated rectangular strip insert.	B-8
TableB.4	Experimental data of heat transfer through tube with perforated rectangular strip insert.	B-9



## NOMENCLATURE

---

---

$A_{xs}$	Cross sectional area of the plain tube ( $m^2$ )
$A_{xp}$	Cross- sectional area of the tube with perforated rectangular strip ( $m^2$ )
$b$	Atmospheric pressure (mm of Hg)
$B$	Bias limit of uncertainty
$C_p$	Specific heat of air ( $kJ/kg^\circ C$ ) at constant pressure.
$d$	Velocity head at inlet section (cm of water)
$d_p$	Pore diameter of the strip (mm)
$D_h$	Hydraulic diameter (m)
$D_i$	Inside diameter of tube (m)
$f_s$	Fanning friction factor for the plain tube
$f_p$	Fanning friction factor for the tube with perforated rectangular strip insert
$h$	Surface heat transfer co-efficient ( $W/m^2^\circ C$ )
$k$	Thermal conductivity of air ( $W/m^\circ C$ )
$L$	Length of the tube (m)
$L_p$	Length of the strip (m)
$m$	Mass flow rate of the air (kg/s)
$\Delta P$	Pressure drop along the axial length ( $N/m^2$ )
$P_m$	Blower power (W)
$P$	Precision limit of uncertainty
$R_p$	Porosity of the rectangular strip insert (ratio of total pores area in a strip to total strip area)
$Q$	Total heat transfer rate (W)
$Q_x$	Heat conduction through gasket
$q$	Heat flux ( $W/m^2$ )
$R$	Performance parameter
$T_\infty$	Room temperature ( $^\circ C$ )
$T_i$	Inlet temperature of air ( $^\circ C$ )
$T_b$	Bulk tempaure of the fluid ( $^\circ C$ )
$T_o$	Outlet bulk temperature of air ( $^\circ C$ )

$T_w$	Wall temperature of the tube ( $^{\circ}\text{C}$ )
$T_{wi}$	Inlet wall temperature
$T_{wo}$	Outlet wall temperature
$t$	Thickness of strip insert
$U$	uncertainty in the measurands
$V$	Mean velocity of air in the test section (m/s)
$V_i$	Mean velocity of air at the inlet section (m/s)
$X$	Axial distance(m)
$W$	Total limit of uncertainty
$W_s$	Wetted perimeter of the plain tube (m)
$W_p$	Width of the strip insert (m)

### **Greek Letters**

$T_{\infty}$	Ambient temperature
$\varepsilon$	Effectiveness of the heat exchanger
$\mu$	Kinematics viscosity ( $\text{m}^2/\text{s}$ )
$\rho$	Density of air ( $\text{kg}/\text{m}^3$ )

### **Subscripts**

$p$	perforated tube
$s$	plain tube
$x$	local

### **Dimensionless Numbers**

Nusselt number,  $Nu = hD_i/k$

Prandtl number,  $Pr = \mu C_p/k$

Reynolds number,  $Re = \rho VD/\mu$

## ACKNOWLEDGEMENT

The author would like to mention with gratitude Almighty Allah's continual kindness without which no work would reach its goal. The author is highly grateful and obliged to his honorable supervisor, Dr. M. A. Rashid Sarkar, Professor, Department of Mechanical Engineering, Bangladesh University of Engineering and Technology (BUET), Dhaka, for his continuous guidance, constant support, supervision, inspiration, advice, infinite patience and enthusiastic encouragement throughout this research work.

The author is also grateful to Dr. Abu Rayhan Md. Ali, Professor and Head, Department of Mechanical Engineering, BUET, Dhaka, for his moral support, advice, help and permission to use different laboratories of the department at various stages of this work.

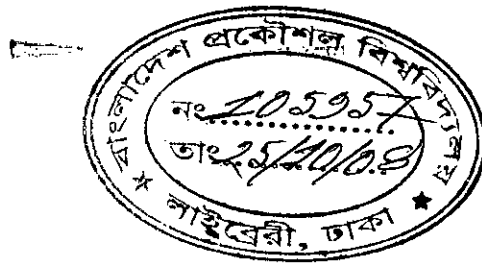
The author thanks the members of the Board of Examination namely Associate Professor Dr. Bodius Salam, and Professor Dr. Md. Ashraful Islam for their contribution in various ways in respect of this thesis.

The author is thankful to Mr. M. M. Sarwar, Foreman Instructor, Welding and Sheet metal Shop and Mr. Md. Anisur Rahman, Asstt. Foreman Instructor, Welding, Sheet Metal, Foundry and Pattern Shop, BUET, for their cordial co-operation and help in making the rectangular mild steel stripes. The author is also thankful to Mr. Rokon Uddin, and Mr. Aminul Islam Lab.Assistant, Department of Mechanical Engineering, BUET, Dhaka, for his help and co-operation during the experiment.

Finally, the author likes to express his sincere thanks to all other teachers and members of the Mechanical Engineering Department, BUET, Welding Shop of BUET, for their cooperation and help in the successful completion of the work.

## ABSTRACT

An experimental investigation was carried out for turbulent flow heat transfer in a circular tube with perforated rectangular strip inserts. Mild steel perforated rectangular strips with holes of different diameters were used as inserts in this experiment. Heat transfer and pressure drop characteristics were obtained in the tube for the turbulent flow. The flow of air through the tube was varied by using the flow control valve. Heat transfer and pressure drop data were taken for Reynolds numbers ranging from  $1.5 \times 10^4$  to  $4.7 \times 10^4$ . Air velocity, temperatures, tube wall temperatures, pressure drops were measured for the plain tube as well as for the tube with perforated rectangular strip inserts. Heat transfer coefficients, heat transfer rate, Nusselt numbers, friction factor, blower power and heat transfer effectiveness were calculated using measured variables for the plain tube as well as for the tube with inserts. Heat transfer rate was found to be increased up to 1.85 times with corresponding increase in friction factor and blower power for the tube with perforated rectangular strip inserts. For the comparable Reynolds number, the heat transfer coefficient for the tube with perforated rectangular strip inserts was found to be increased up to 2.80 times than that of the plain tube. The friction factor for the tube with perforated rectangular strip inserts was found to be increased up to 1.8 times compared to that of the plain tube. Whereas, the required blower power for the tube with perforated rectangular strip inserts was found to be increased up to 1.45 times than that of the plain tube. It was also found that the heat transfer effectiveness for the tube with perforated rectangular strip inserts was increased up to 2.45 times compared to that of the plain tube. With the experimental data, a correlation was developed for prediction of the heat transfer in the turbulent flow for the tube with perforated rectangular strip inserts.



## CHAPTER-1 INTRODUCTION

### 1.1 General:

The internal inserts are used to modify the flow characteristics of the fluid to enhance the heat transfer rate. Turbulent flow indicates that the motion of the fluid is chaotic in nature involving crosswise mixing of the mainstream. In the turbulent flow, the fluid properties such as instantaneous velocity, temperature and pressure are subjected to fluctuations. These fluctuations increase the heat transfer rate. Turbulent flow heat transfer in tubes with inserts has found wide engineering applications in heating or cooling of viscous fluids in the process industries, refrigeration and air conditioning system, internal cooling of gas turbine blades, thermal regenerators, gas cooled reactors, aerospace engineering, automobiles, cooling of modern electronic equipments and heat transfer in compact heat exchangers and so on. However, the insert devices may be used to upgrade the performance of an existing heat exchanger.

Energy and material saving considerations as well as economic incentives have led to comprehensive efforts to design high performance heat exchanger. The efficiency and economic competitiveness of many industrial processes depend, to a great extent, on the performance of heat exchangers. Improvement in performance of the heat exchanger may result in the reduction of its size and subsequently its costs. For a heat exchanger of fixed size, improvement may allow for either an increase of heat transfer rate or a decrease of temperature differences. The latter allows for more efficient utilization of thermodynamic availability. In practice, an enhanced surface must provide the desired heat transfer rate and meet the required flow rate and pressure drop constraints.

### 1.2 The Enhancement Techniques:

The performance of heat exchange equipments may be substantially improved by using different augmentation techniques like finned surfaces, integral roughness and insert devices. All the techniques used to enhance the heat transfer rate can be

conveniently divided into three major classes: passive, active, and a combination of these techniques. Passive techniques require no direct application of external power. These employ special surface finish or fluid additives for heat transfer enhancement. In active techniques, external promoters are used. One method of active techniques is providing rectangular strip inserts. Several options are available for enhancing heat transfer associated with internal flows. Enhancement may be achieved by increasing the convection coefficient,  $h$  and/or by increasing the convection surface area. For example,  $h$  may be increased by introducing strip inserts to enhance turbulence. These cause a intensive mixing of the flow along the tube length.

Strip inserts are inexpensive to manufacture. Extensive studies have been made both experimentally and analytically with tubes having internal inserts in laminar and turbulent flows. The employment of different types of porous materials in forced convection heat transfer has been extensively studied also. A comprehensive survey in this regard is chronologically given in the Chapter-2. The analysis for laminar and turbulent flow is based on momentum and energy conservation in the flowing fluid

The potential of perforated inserts enhanced the rate of heat transfer at constant heat flux was studied experimentally by Pavel and Mohamad [37]. It was found that the porosity and diameter of the pipe have a positive influence upon heat transfer and negative impact on pressure drop. Heat transfer in turbulent flow through tube with perforated twisted-tape inserts was studied experimentally by Ahamed [45]. It was found that the perforated twisted-tape-inserts caused an increased of heat transfer rate at the cost of increased pumping power .

So far very few research work has been reported in literature on heat transfer in turbulent flow through tube with perforated rectangular strip inserts. The perforated rectangular strip inserts may be a good candidate for heat transfer enhancement in a heat exchanger.

### **1.3 Objectives:**

The study was the following objectives:

- (a) To modify the test section of the existing experimental facility for studying turbulent heat transfer and fluid flow characteristics in a tube with perforated rectangular strip inserts.
- (b) To analyze the heat transfer and pressure drop phenomena and to compare the results with the data of plain tube giving an idea of augmentation of heat transfer and increase of pressure drop.
- (c) To compare the results of this experiment with those of previous works.
- (d) To develop a correlation, which may be recommended for prediction of heat transfer for similar cases.

## CHAPTER-2

### LITERATURE SURVEY

The compact and efficient heat exchangers are very much essential in industrial applications. In the last decade, significant effort has been made to increase the rate of heat transfer in order to improve overall performance of heat exchangers. A high performance heat exchanger of a fixed size can give an increased heat transfer rate. It might also cause a decrease in temperature differences between the process fluids enabling efficient utilization of thermodynamic availability.

Many researcher's have been studying the subject from the beginning of twentieth century. The performance can be improved by using various augmentation techniques such as finned surfaces, integral roughness and insert devices. To determine the characteristics of heat transfer in the tubes, Sieder and Tate [1] derived an empirical correlation for turbulent flow of forced convection heat transfer through circular as well as non-circular tubes at constant wall temperature. The correlation showed that higher heat transfer occurred in finned tubes than the plain tube.

Heat transfer in turbulent flow with turbulence promoters have been studied by Gunter and Shaw [2]. They have shown that higher heat transfer coefficient occurred in the turbulent flow than the flow in the plain tube. Experimental data for pressure drop and heat transfer coefficient for air in internally finned tubes have been reported by Hiding and Coogan [3]. It was shown that higher heat transfer coefficient occurred in the turbulent flow than the plain tube.

Smithberg and Landis [4] developed a semi empirical model for friction factor, which was based on adding the momentum losses for spiralling flow and induced fluid mixing by inserting tapes in the flow. They have shown that the model reasonably predicted their data for tapes having  $\infty \geq$  twist ratio  $(y) \geq 3.62$ . Their developed model was the first semi empirical model for turbulent flow heat transfer with a twisted tape insert.



Thomas [5] tested displaced wires for turbulent flow of water in an annulus. He concluded that the most favorable ( $St/f$ ) performance was obtained when the wires were axially spaced in pairs separated approximately nine wire diameters, followed by a second pair separated approximately 75 wire diameter from the first pair. The enhancement was provided by an increased velocity gradient at the surface and by the interaction of the cylinder wake with the fluid in the boundary layer.

Lopina and Bergles [6] attempted to account for the increased speed of the flow (caused by the spiral flow) and the centrifugal buoyancy effect using a superposition model. Cox et al. [7] used several kinds of enhanced tubes to improve the performance of a horizontal tube multiple effect plant for saline water conversion. Overall heat transfer coefficients (condensation inside and spray film evaporation outside) were reported for tube internally enhanced with circumferential V groups. No heat transfer enhancement was obtained with a knurled surface.

Heat transfer and friction correlations were developed by Webb et al. [8] for turbulent flow in tubes having a repeated-rib roughness. The friction correlation and the heat-momentum transfer analogy were based on law of the wall similarity. These correlations were found to be better than the other methods, especially in accounting for the effect of Prandtl numbers. They shown that these correlations were especially applicable to ribs of rectangular cross-section whose thicknesses were small relative to the rib spacing.

Prince [9] obtained 200% increase in heat transfer coefficient with internal circumferential ribs; however the outside (spray- film evaporation) was also enhanced. Hu and Chang [10] analyzed fully developed laminar flow in internally finned tubes by assuming constant and uniform heat flux in the tube surface. By using 22 fins , extended to about 80 % of the tube radius, it was shown that enhancement of heat transfer was 20 times higher than that of the unfinned tubes.

Date [11] developed a numerical model for predictions of heat transfer for twisted tape insert in fully developed laminar flow at constant temperature with constant properties. His analysis for loosely fitting tape with helix angle  $34.9^\circ$  and Prandtl number,  $Pr = 1$  showed that the Nusselt number increased with increasing Reynolds number, contrary to

laminar flow in plain tubes, which is independent of Re and Pr. Mergerlin et al. [12] found that bristle brushes provided enhancement ratio ( $h/h_p$ ) as high as 8.5, where, heat transfer co-efficient,  $h$  for inserted tubes and  $h_p$  for plain tube, where, the pressure drop were increased a factor of 28.

The first analytical study to predict the performance of tubes with straight internal fin in turbulent air flow was conducted by Patankar et al. [13].

The mixing length in the turbulent model was set up so that just one constant was required for experimental data. Gee and Webb [14] have shown the effect of helix angle ( $\alpha$ ) on Stanton number (St) and friction factor (f) for single-phase forced convection in a circular tube containing a two-dimensional rib roughness. The experiment was run by using air as working fluid and the three-helix angles ( $\alpha = 30^\circ, 45^\circ$  and  $70^\circ$ ) all having a rib pitch-to-height ratio of 15. Their investigation indicated that helical rib-roughness showed greater heat transfer per unit friction than traverse rib-roughness. As  $\alpha$  increased, the friction factor dropped faster than the Stanton number. They observed that the maximum  $St/f$  occurs at  $\alpha = 45^\circ$ .

Uttarwar and Raja Rao [15] carried out an experimental investigation on isothermal pressure drop and convective heat transfer to Servotherm medium grade oil in laminar flow in one plain tube and seven wire coil-inserted tubes of different pitch of wire coil. Their investigation has indicated that, when compared with a plain tube at constant pumping power and constant basic geometry, an improvement as high as 350 % has been obtained in heat transfer capacity and a reduction in heat exchanger area of about 70 to 80 percent might be achieved using wire coil-inserted tubes. Plessis and Kroger [16] conducted experiments to develop a correlation for thermally developing laminar flow in a plain tube with a twisted tape insert.

Garimella et al. [17] conducted a survey of heat transfer and pressure-drop augmentation for turbulent flow in spirally enhanced tubes. A geometric parameter known as severity ( $\phi = e^2/pD$ ) was used to characterize Nusselt number and friction factor enhancements. An increased in  $e$  or a decreased in  $p$  or  $D$ , keeping other dimensions constant, yield a geometry that departed further from that of a plain tube. Three functions were defined,

namely, heat transfer enhancement ( $e_h = Nu_f/Nu_s$ ), friction-factor enhancement ( $e_f = f_f/f_s$ ), and enhancement efficiency ( $\xi = e_h/e_f$ ), and the dependence of each of these functions on severity was investigated. Severity was found to be a good correlating parameter for data for over 60 different tubes from many previous studies. They showed that in turbulent flow, the friction factor increased was usually much larger than the corresponding increased in heat transfer.

Friction and Nusselt number data were generated and semi-empirically evaluated by Gupte and Date [18] for twisted tape generated helical flow in annuli. Results were obtained for radius ratios of 0.41 and 0.61 and twist ratios of  $\infty$ , 5.302, 5.038, and 2.659. The experimental results showed that for the same twist ratio ( $y$ ), the increase in pressure drop exceeds the increase in heat transfer irrespective of the radius ratios ( $r^*$ ). For  $y = 5.302$ ,  $r^* = 0.41$  and at the same Reynolds number based on hydraulic diameter, the increase in pressure drop and heat transfer coefficient over an empty annulus were 90 % and 60 % respectively. At lower twist ratios both the percentages are even greater. Again the semi-analytical expressions developed predict the Nusselt numbers with good agreement for  $y = \infty$  and  $y = 5.302$  and 5.038.

Zhuo et al. [19] found that the Smithberg and Landis friction model under predicted their friction data ( $y = 3, 4.25, 5.25$ ) by approximately 15%. Although much work have been done on twisted tapes, papers by Manglik and Bergles [20, 21] presented an updated understanding of the heat transfer and friction characteristics for both laminar and turbulent flow. The papers provided correlations valid for developed laminar flow through the turbulent regime, including the transition regime for constant wall temperature boundary condition. In the laminar flow regime, they showed that entrance length and buoyancy forces influence the laminar flow Nusselt number; these effects were controlled by the magnitude of the Graetz number ( $Gz$ ) and the Rayleigh number ( $Ra$ ) respectively.

Heat transfer and pressure drop characteristics in annuli with spirally fluted inner tubes, for the laminar, transition, and turbulent flow regimes were studied by Garimella and Christensen [22]. Heat transfer in fluted-tube annuli for the Reynolds numbers range  $700 < Re < 40,000$  was investigated in that study. They found that the Nusselt numbers in

spirally fluted annuli were between 4 and 20 times higher than the corresponding smooth-annulus values in laminar flow due to the induced swirl flow. For turbulent flow, the enhancement was between 1.1 and 4.0. The fluted annulus Nusselt number increased with an increase in flute depth, and with a decrease in flute pitch and annulus radius ratio. Turbulent behavior was exhibited for Re values as low as 700. A Nusselt number correlation was developed in terms of the fluted annulus friction factor and geometric parameters. This correlation predicted 84 % of data fell within  $\pm 20$  %, of the total 642 data points.

Agarwal and Raja Rao [23] experimentally determined isothermal and non-isothermal friction factors and mean Nusselt numbers for uniform wall temperature during heating and cooling of Servotherm oil ( $Pr = 195 \sim 375$ ) in a circular tube ( $Re = 70 \sim 4000$ ) with twisted tape inserts (twist ratio,  $y = 2.41 \sim 4.84$ ). Isothermal friction factors were found to be 3.13-9.71 times higher than that of the plain tubes. The Nusselt numbers were found to be 2.28-5.35 and 1.21-3.70 times higher than that of the plain tubes in forced convection based on constant flow rate and constant pumping power, respectively, for the minimum twist ratio.

Huq [24] studied experimentally the steady state turbulent flow heat transfer performance of circular tubes having six integral internal longitudinal fins and found an abrupt pressure fluctuation near the entrance region of the tubes. He found that the heat transfer coefficient based on inside diameter and nominal area was 1.98 to 2.12 times higher than that of the smooth tube. Based on inside diameter and nominal area, heat transfer rate for the finned tube exceeded by 97 % to 112 % than that of the smooth tube values for Reynolds numbers range from  $2.66 \times 10^4$  to  $7.86 \times 10^4$ . Friction factor based on inside diameter for finned tube was in the range of 3.2 to 4.5 times higher than that of the smooth tube values. Their study indicated that significant enhancement of heat transfer was possible by using internal fins without scarfing much additional pumping power.

Dutta and Han [25] studied heat transfer in a two-pass square channel with rib-roughened surfaces. The ribs were placed in a staggered half-V fashion and experiments were conducted for three orientation angles  $0^\circ$ ,  $45^\circ$ , and  $90^\circ$ . They found that staggered half-V ribs showed a higher heat transfer coefficient compared to continuous ribs for both  $60^\circ$

and  $90^\circ$  ribs under conditions of rotation.

Uddin [26] studied pressure drop characteristics and heat transfer performance of air through an internal rectangular finned tube. He observed that the heat transfer coefficient based on inside diameter and nominal area was in the range of 1.5 to 1.75 times higher than that of the plain tube. When heat transfer co-efficient was compared with a plain tube at constant pumping power an improvement of 4 % was obtained.

Buyruk et al. [27] studied numerically and experimentally the laminar flow and heat transfer characteristics of a cylinder in cross flow. Calculations were carried out for Reynolds numbers of 120 and 390 and blockage ratios between 0.18 and 0.47. The results were compared with experimental value. They found that increasing blockage caused the separation point to move downstream and experimental separation point locations did not always agree well with the flow predictions. Increasing blockage increased the heat transfer rate from the cylinder, increasing Reynolds number caused the point of separation to move upstream and the overall heat transfer to increase. They also showed that the agreement between measured and numerically predicted heat transfer distributions was generally satisfactory except for the rear of the cylinder because of the difficulty of predicting accurately the separation point.

Mamun [28] experimentally investigated the heat transfer characteristics of steady state turbulent fluid flow through an internally in-line segmented and non-segmented finned (of rectangular cross-section) tube at constant pumping power. The results indicated that for the same Reynolds number, friction factor of in-line finned tube was 2.0 to 3.5 times higher than that of the plain tube. Friction factor of in-line segmented finned tube was 1.72 to 2.5 times higher than that of the plain tube. Pumping power of an in-line finned tube was 2.44 to 3.41 times higher than that of the plain tube. Whereas, pumping power of an in-line segmented finned tube was 2.21 to 2.34 times higher than that of the plain tube for the same Reynolds number. Heat transfer for the in-line finned tube was 1.7 to 1.8 times higher than that of the plain tube for the same Reynolds number. Heat transfer for the in-line segmented finned tube was 1.77 to 1.9 times higher than that of the plain tube for same Reynolds number. For the same Reynolds number, heat transfer and convective heat transfer coefficient for in-line finned tube and in-line segmented finned

tube were found similar but for in-line segmented finned tube, pressure drop was less than that of in-line finned tube.

Hsieh and Huang [29] studied experimentally plain tubes and tubes with square and rectangular as well as crossed-strip inserts using water as working fluid. Their experiment showed that transition from laminar to turbulent flow occurred at lower Reynolds number for using insert of aspect ratio 1. Aspect ratio means the ratio of base to height of a strip.

Aloke [30] studied experimentally heat transfer performance of a T-section internal fin in a circular tube. He found that for finned tube, friction factor was 3.0 to 4.0 times and pumping power was 3.5 to 4.5 times higher than those of plain tube for the Reynolds numbers range from  $2.0 \times 10^4$  to  $5.0 \times 10^4$ . Heat transfer coefficient for finned tube was about 1.5 to 2.0 times higher than that of the plain tube within the same Reynolds numbers.

Liu and Jensen [31] performed a parametric study on turbulent flow and heat transfer in internally finned tubes. A comprehensive numerical study on the effect of rectangular fins on Nusselt numbers and friction factors in internally finned tubes was conducted over a wide range of geometric conditions. Nusselt numbers and friction factors increased with an increased of the number of fins and helix angle. Larger helix angles generated stronger circumferential velocities, which enhanced fluid mixing between the solid walls and the core flow. Increased fin height produced larger Nusselt numbers and friction factors, but the increased was moderate at smaller helix angles ( $\gamma < 20^\circ$ ). When  $\gamma > 20^\circ$ , both heat transfer and pressure drop increased greatly within the same fin-height variation range. In addition, the performance of three fin profiles i.e. rectangular, triangular, and semicircular with the same fin heights, widths, and helix angles were compared for Reynolds numbers between 10,000 and 70,000. With a large number of shorter fins, the rectangular and triangular fin profiles behaved similarly; for some geometric conditions the round crest fin had lower friction factors and Nusselt numbers (17 % and 10 %, respectively) than the rectangular fin. However, when the number of fins was large, the round crest fin could have larger friction factors (about 16 %).

Saha and Dutta [32] studied laminar swirl flow through a tube fitted with twisted tape where a large Prandtl number viscous fluid was used as working fluid. On the basis of constant pumping power and constant heat duty, short length twisted-tapes placed at inlet showed better performance than the full-length twisted tapes.

Heat transfer enhancement was investigated in a coaxial-pipe heat exchanger using dimples in the inner tube by Chen et al. [33]. Experimental investigations of six dimpled tubes used as heat transfer augmentation devices were carried out. They obtained that all dimpled tubes increased the tube-side heat transfer coefficient significantly above the smooth tube values. It was shown that the augmentation was 1.25-2.37 times at constant Reynolds number, and 1.15-1.84 times at constant pumping power. Friction factor ranged from 1.08 to 2.35 times those for the smooth tube. Based on either constant Reynolds number or constant pumping power, the best dimpled tube was tube 4 (whose additional heat transfer surface area,  $a = 4307.6 \text{ mm}^2$ , inside diameter,  $d_i = 16.6 \text{ mm}$ , wall thickness,  $\delta = 1.22 \text{ mm}$ , length,  $L = 1500 \text{ mm}$ , depth of dimple,  $e = 1.3 \text{ mm}$ , diameter of dimple,  $\phi = 3.5 \text{ mm}$ , pitch of dimple,  $p = 10.0$ ), which had the largest dimple depth-to-tube inside diameter ratio, dimple depth-to-pitch ratio, dimple depth-to-dimple diameter ratio, and number of dimple columns  $N$ . They developed a correlation based on the results of that work appeared to be sufficiently accurate for predicting the heat transfer coefficients and friction factors.

Saha and Langile [34] experimentally studied the friction factors and Nusselt numbers for longitudinal strips (full length, short length but regularly spaced) in laminar flow under constant wall heat flux. They found that short length strip up to a limited value (0.3) of 1 and regularly spaced strip elements for  $2.5 < y < 5$  and  $2.5 < s < 5$  perform better than the full length strips. They also developed a correlation. The friction factor reduced by 8-58 percent and Nusselt number reduced by 2-40 percent for short length twisted tape inserts compared to full length twisted tapes inserts.

Mohammad [35] numerically investigated the heat transfer augmentation for flow in a pipe or a channel partially or fully filled with perforated material placed at the core of the channel. It was shown that partially filling the channel with perforated substrates could reduce the thermal entrance length by 50% and increase the rate of heat transfer from the walls. Although the perforated materials contributed to the pressure drop along the

channel, an optimum thickness of about 60 % of the channel height was found to offer a substantial increase in the Nusselt number at the expense of reasonable pressure drop.

Hsieh et al. [36] studied experimentally turbulent heat transfer and flow characteristics in a horizontal circular tube with strip-type inserts (longitudinal, LS and cross, CS inserts) using air as working fluid. They conducted that the hydrodynamic entry length with a tube insert was found to be shorter than that of a bare tube. Friction factor increased for tubes with inserts as compared to bare tube values were typically between 1.1 and 1.5 for  $6500 < Re < 19500$ . They also developed a correlation for friction factors by using measuring data and compared with those existing data for bare tubes.

Pavel and Mohamad [37] experimentally investigated the potential of perforated inserts to enhance the rate of heat transfer at constant heat flux where the fluid was air. They found that the porosity and diameter of the pipe have a positive influence upon heat transfer and negative impact on pressure drop. The highest increase in the Nusselt number of approximately 5.28 times (compared to smooth tube) was obtained by fully filling the pipe at the expense of the highest pressure drop of 64.8 Pa. In comparison with fully filling the pipe, a partial filling has the advantages of a same increase in the Nusselt and a smaller increase in the pressure drop.

An experimental study was performed on heat transfer and friction factor characteristics for a helical tape insert in a circular tube using hot air as the test fluid by Eiamsa-ard et al. [38]. They obtained that the increased in heat transfer and friction factor were strongly influenced by swirling motion induced by the helical. As the Reynolds number increased, the swirling flow was stronger which in turn results in an increased in the heat transfer and friction factor while it decreased at low Reynolds number.

Sahiti et al. [39] demonstrated a considerable enhancement of heat transfer by using small cylindrical pins on surfaces of heat exchangers. They found that the pin height to its diameter ratio influenced the pin efficiency and the heat transfer rate of pins. Pin fins a good compromise between the pin efficiency and the pin heat transfer rate and was achieved if the ratio of pin height to pin diameter was of the order of 15.



Islam [40] studied the heat transfer in turbulent flow through tube with wire-coil inserts of varying pitches,  $p = 12$  mm, 24 mm, 40 mm, and 50 mm with corresponding helix angles of,  $\alpha = 10.01^\circ$ ,  $20.35^\circ$ ,  $35.45^\circ$ , and  $46.44^\circ$  respectively. He observed that the heat transfer coefficient was increased with corresponding increased in friction factor and pumping power. The heat transfer coefficient for the tube with wire-coil inserts varied from 1.2 to 2.0 folds than that of the smooth tube for the comparable Reynolds number. Whereas, the friction factor for the tube with wire-coil inserts varied from 1.5 to 4.0 folds than that of the smooth tube and the pumping power was increased up to 2.5 times than that of the smooth tube. The heat transfer effectiveness for the tube with wire-coil inserts increased up to 2 folds in comparison to the smooth tube.

Abedin [41] studied experimentally the pressure drop and convective heat transfer in a tube with wire coil inserts of varying pitch in turbulent flow at low Reynolds number. He fabricated four sets of wire coil insert for different geometries (pitch,  $p = 12$  mm, 24 mm, 40 mm and 50 mm with corresponding helix angles,  $\alpha = 10.01^\circ$ ,  $20.35^\circ$ ,  $35.45^\circ$ ,  $46.44^\circ$  respectively). The Reynolds number was chosen based on inlet diameter of the tube and was varied in the range of  $6,000 \leq Re \leq 22,000$ . He observed that the heat transfer coefficient was increased with corresponding increased in friction factor and pumping power. The heat transfer coefficient increased by 2 folds in a coil inserted tube than that of the smooth tube. The friction factor and pumping power were found to be increased by 3.5 folds and 3 folds respectively, compared to that of the smooth tube at comparable Reynolds number. The effectiveness at constant wall temperature for the wire coil inserted tube increased as much as 1.25 folds than that of the smooth tube. He also proposed a correlation for the prediction of heat transfer for tubes with wire coil inserts.

Garcia et al.[42] studied the enhancement of heat transfer with wire-coil inserts in laminar-transition-turbulent regimes at different Prandtl numbers. In the turbulent flow wire-coils caused higher pressure drops. But in the laminar region tube with wire coil behaved like plain tube and transition took place at low Reynolds number ( $Re = 700$ ). At constant pumping power, wire coil insert showed an increase of heat transfer rate at Reynolds number below 30,000 over the plain tube.

Ahmed et al. [43] studied the heat transfer for turbulent flow through a circular tube with twisted tape inserts having different twist ratios. They found higher heat transfer rate in the entrance region for lower twist ratio. They found the average heat transfer rate 3 times higher than that of the plain tube.

Sarkar et al. [44] studied the heat transfer in turbulent flow through tube with longitudinal strip inserts. They found that the heat transfer co-efficient for the tube with longitudinal strip insert higher than that of the plain tube. For comparable Reynolds number, average heat transfer co-efficient increased up to 1.4 times, up to 2 times and up to 3 times than that of the plain tube for the tube with Y-shaped, X-shaped and star-shaped longitudinal inserts respectively.

Ahamed [45] studied the heat transfer in turbulent flow through tube with perforated twisted-tape inserts. The study revealed that the perforated twisted-tape-inserts caused an increased of heat transfer rate at the cost of increased pumping power. For comparable Reynolds number, the average heat transfer coefficient for the tube with perforated twisted tape inserts increased up to 5.5 times than that of the plain tube. The heat transfer rate for the tube with perforated twisted tape inserts up to 1.8 times than that of the plain tube for the comparable Reynolds number. Whereas, the pumping power required for the tube with perforated twisted tape inserts varied from 1.2 to 2.25 folds than that of the plain tube. At constant pumping power, the performance parameter, R increased up to 400% for the tube with perforated twisted tape inserts compared to that of the plain tube.

## CHAPTER-3

### THEORY

#### 3.1 General:

To analyze the heat transfer characteristics, some basic heat transfer parameters and thermal boundary conditions are to be defined. In this chapter, the basic heat transfer parameters and thermal boundary conditions, which were involved with the present work were briefly discussed. The mathematical equations needed to calculate the variables namely the hydraulic diameter and wetted perimeter of the test section, Reynolds number, pressure drop, friction factor, heat transfer rate, bulk temperature, heat transfer coefficient, Nusselt number, blower power, and effectiveness on the basis of plain tube and tube with perforated rectangular strip inserts and performance parameter (on the basis of constant blower power) are summarized here.

Perforated rectangular strip insert is a turbulence creator, not like fin. It acts as an agitator. Tube will convect more heat to the fluid. The insert has an area perpendicular to the flow is to be neglected. Tube area is assumed for the flow because the flow within the tube is very complicated and can not be measured.

#### 3.2 Hydraulic Diameter ( $D_h$ ):

For turbulent flow heat transfer, the friction factor in a tube is dependent upon the Reynolds number and the relative roughness of the tube surface. Both these terms are applied to flow through conduits of various internal geometries. Here, the knowledge of hydraulic diameter is important and it can be defined as the ratio of four times the cross sectional area to the wetted perimeter of the conduit in the test section. For plain tube, hydraulic diameter ( $D_h$ ) can be expressed as,

$$D_h = \frac{4 \times \pi D_i^2 / 4}{\pi D_i} \quad (3.1)$$

$$\Rightarrow D_h = D_i$$

Where,  $D_i$  is the inside diameter of the tube.

But hydraulic diameter for tube with perforated rectangular strip inserts is different for

different porosity of inserts. It is not constant throughout the length of the inserts. To make it comparable with other studies, especially for perforated inserts, inside diameter of tube is considered rather than the hydraulic diameter in defining Reynolds number and other parameters.

### 3.3 Reynolds Number (Re):

The behavior of the fluid for heat transfer characteristics depends on flow geometry and Reynolds number. The Reynolds number represents the ratio of the inertia to viscous force. This result implies that viscous forces are dominant for small Reynolds numbers and inertia forces are dominant for large Reynolds numbers. The Reynolds number is used as the criterion to determine whether the flow is laminar or turbulent. As the Reynolds number is increased, the inertia forces become dominant and small disturbances in the fluid may be amplified to cause the transition from laminar to turbulent. Mathematically, Reynolds number, here is defined as

$$R_e = \frac{\rho V D_i}{\mu} \quad (3.2)$$

(Based on inside diameter of the tube)

### 3.4 Pressure Drop ( $\Delta P$ ) and Fanning Friction Factor (f):

When air passes through a tube, pressure drop will occur in the tube due to the frictional forces. Pressure drop is the hydraulic loss due to the surface over which the fluid is moving. Pressure drop is a term used to describe the decrease in pressure from one point in a pipe or a tube to another point in the down stream. Higher pressure drop requires higher blower power for the flow of the fluid over the surface. For rough surface the drop of pressure is high. From the pressure drop, friction factor can be calculated.

Pressure drop at any axial location x is given by the following equation

$$\Delta P = P_i - P(x) \quad (3.3)$$

Where,

$\Delta P$  = Pressure drop ( $N/m^2$ )

$P_i$  = Pressure at inlet ( $N/m^2$ )

$P(x)$  = Pressure at any axial location, x ( $N/m^2$ )

The fanning friction factor is a dimensionless number used in fluid flow calculations.

Generally in the chemical and process industries fanning friction factor is used to determine the friction characteristics. Sometimes the fanning friction factor is called skin friction. The friction factor (fanning) based on inside diameter is given by,

$$f = \frac{(-\Delta P / x) D_i}{2\rho V^2} \quad (3.4)$$

Where,

$f$  = Fanning friction factor over a length  $x$  from the inlet

$x$  = Axial distance (m)

$\rho$  = Density of fluid ( $\text{kg/m}^3$ )

$V$  = Velocity of fluid in the tube (m/s)

$D_i$  = Inside diameter of the tube (m)

### 3.5 Porosity ( $R_p$ ):

Porosity is a measure of the void spaces in a material, and is measured as a fraction, between 0–1, or as a percentage between 0–100%. Porosity increases with the increase of pores diameter or with the decrease of central distance between the two adjacent pores. Higher porosity causes higher flow rate of fluid and lower porosity causes lower flow rate of fluid. Porosity of the strip inserts can be defined as,

Porosity,

$$R_p = \frac{\text{Total pores area}}{\text{Total strip area}}$$

$$= \frac{\frac{\pi}{4} D_p^2}{L_p \times W_p}$$

Where,  $D_p$  = Pore diameter (mm)

$L_p$  = Length of the strip (m)

$W_p$  = Width of the strip (m)

### 3.6 Heat Transfer Rate (Q):

Heat transfer is the passage of thermal energy from a hot body to a cold body. When a physical body, e.g. an object or fluid, is at a different temperature than its surroundings or another body, transfer of thermal energy, also known as heat transfer, occurs in such a way that the body and the surroundings reach thermal equilibrium. Heat transfer rate

means the transfer of energy per unit time. Cold fluid will absorb heat from the tube surface when it passes through the heated tube. When the temperature of the cold fluid is  $T_i$ , its bulk outlet temperature is  $T_o$ , and the mass flow rate is  $m$ , then the total heat transfer rate ( $Q$ ) to the fluid can be defined as,

$$Q = mC_p(T_o - T_i) \quad (3.5)$$

For plain tube of length,  $L$  heat transfer rate per unit area to the air will be

$$q_s = mC_p(T_o - T_i)/(W_s L) \quad (3.6)$$

Where,  $W_s$  is the wetted perimeter of the plain tube.

For tube, with perforated rectangular strip inserts of same length, heat transfer rate to the fluid will be (basis of tube inside diameter)

$$q_p = mC_p(T_o - T_i)/(\pi D_i L) \quad (3.7)$$

Where, the wetted perimeter of the tube with perforated rectangular strip inserts was taken same as that of the plain tube. In these experiments, the rate of energy supplied to the tube was kept constant. But time of supply of energy was varied. Here ideally thermal boundary conditions for constant heat flux are applicable.

### 3.7 Bulk Fluid Temperature ( $T_{bx}$ ):

The mean or bulk temperature of the fluid at a given cross section is defined in terms of the thermal energy transported by the fluid as it moves past the cross section. The rate at which this transport occurs may be obtained by integrating the product of the mass flux ( $\rho u$ ) and the internal energy per unit mass ( $c_p T$ ) over the cross section. The bulk temperature is the representative of the total energy of the flow at any particular location.

The local bulk temperature,  $T_b(x)$  at any location,  $x$  for the plain tube can be expressed as:

$$\begin{aligned} mC_p \times \{T_b(x) - T_i\} &= q_s W_s X \\ \Rightarrow T_b(x) &= T_i + \frac{q_s W_s X}{mC_p} \end{aligned} \quad (3.8)$$

Similarly, the local bulk temperature for the tube with perforated rectangular strip inserts at any location,  $x$  can be written as:

$$T_b(x) = T_i + \frac{q_p W_s X}{mC_p} \quad (3.9)$$

### 3.8 Heat Transfer Coefficient (h):

Heat transfer coefficient is, in general, a complicated function of the surface and fluid properties, the fluid flow rate and flow description, and geometry. For turbulent flow heat transfer, the heat transfer coefficient is higher than the laminar flow heat transfer under the similar flow field. It shows the effect of replacing a plain tube by a tube with perforated rectangular strip inserts. The local heat transfer coefficient for the plain tube and the tube with perforated rectangular strip inserts at any axial location,  $x$  can be defined as:

$$h(x) = \frac{q}{T_w(x) - T_b(x)} \quad (3.10)$$

In this experiment, eight thermocouples were set at eight different locations in the test section. To measure the average heat transfer coefficient for the plain tube and the tube with perforated rectangular strip inserts, it can be expressed as follows:

$$h = \frac{\sum_1^8 h(x)}{8.0} \quad (3.11)$$

For convenience in engineering applications, the average value of heat transfer coefficient ( $h$ ) is considered instead of its local values.

### 3.9 Nusselt Number (Nu):

It is an important criteria to analyze the heat transfer characteristics of a flow. The Nusselt number is a dimensionless number that measures the enhancement of heat transfer from a surface that occurs in a real situation, compared to the heat transferred if just conduction occurred. Typically it is used to measure the enhancement of heat transfer when convection takes place. The increase in the value of Nusselt number implies enhancement of heat transfer by convection. For plain tube and tube with perforated rectangular strip inserts, local Nusselt number at location,  $x$  can be defined as:

$$Nu(x) = \frac{h(x)D_i}{k} \quad (3.12)$$

(Based on inside diameter of the plain tube)

To calculate the average Nusselt number ( $Nu$ ) for the plain tube and the tube with perforated rectangular strip inserts, it can be expressed as follows:

$$Nu = \frac{\sum_1^8 Nu(x)}{8.0} \quad (3.13)$$

For convenience in engineering applications, the average value of Nusselt number (Nu) is considered instead of its local values.

### 3.10 Blower Power ( $P_m$ ):

As the tube with perforated rectangular strip inserts creates resistance to flow of the air through the tube, so the pressure drop will be increased in comparison to the flow without the insert. Required blower power also will be higher than that of the tube without the insert to cause flow of the air through the tube. It depends on the pressure drop, the mass flow rate and the density of the air which passes through the tube. Mathematically, blower power,  $P_m$  can be defined as:

$$P_m = \frac{\Delta P \times m}{\rho_b} \quad (3.14)$$

Where,

$P_m$  = Blower power(Watt)

$\Delta P$  = Pressure drop ( $N/m^2$ )

$\rho_b$  = Density of air at bulk temperature ( $kg/m^3$ )

$m$  = mass flow rate of air through the tube ( $kg/s$ )

### 3.11 Effectiveness ( $\epsilon$ ):

Effectiveness is the measure of performance of heat exchanger. The wall temperature to be considered constant and same through out the entire heated section. Effectiveness of the heat exchanger ( $\epsilon$ ) can be defined as:

$$\begin{aligned} \text{Effectiveness, } \epsilon &= \frac{\text{Actual heat transfer}}{\text{Maximum possible heat transfer}} \\ &= \frac{m \times C_p (T_o - T_i)}{m \times C_p (T_{wav} - T_i)} \\ \Rightarrow \epsilon &= \frac{(T_o - T_i)}{(T_{wav} - T_i)} \end{aligned} \quad (3.15)$$

Where,

$T_o$  = Outlet bulk temperature of the air ( $^{\circ}C$ )



$T_i$  = Inlet temperature of the air ( $^{\circ}$  C)

$T_{wav}$  = Average wall temperature of the test section of the tube ( $^{\circ}$  C)

### 3.12 Performance Parameter (R):

The performance of the present experiment can also be evaluated on the basis of constant blower power. The performance parameter on this basis is indicated as R . In this context, the performance parameter (R) is defined as the ratio of Nusselt number for the perforated rectangular strip inserts ( $Nu_p$ ) to the Nusselt number of the plain tube ( $Nu_s$ ) at constant blower power. Mathematically,

$$R = \frac{Nu_p}{Nu_s} \quad (3.16)$$

Generally, the blower power can be defined as

$$\begin{aligned} P_m &= (-\Delta P / \rho)m \\ &= \frac{4f_i L}{D_i} \frac{V^2}{2} A_x V \rho \end{aligned} \quad (3.17)$$

For equal blower power in plain tube ( $P_{ms}$ ) and tube with perforated rectangular strip inserts ( $P_{mp}$ ) it can be written as:

$$P_{ms} = P_{mp}$$

Therefore,

$$A_{xs} f_s V_s^3 = A_{xp} f_p V_p^3 \quad (3.18)$$

$$\left( \frac{V_p}{V_s} \right)^3 = \frac{A_{xs} f_s}{A_{xp} f_p} \quad (3.19)$$

Equating the velocity ratio by Reynolds number ratio for fixed tube diameter, equation (3.19) becomes,

$$\begin{aligned} \left( \frac{Re_p}{Re_s} \right)^3 &= \frac{A_{xs} f_s}{A_{xp} f_p} \\ Re_p &= Re_s \cdot \left( \frac{A_{xs} f_s}{A_{xp} f_p} \right)^{1/3} \end{aligned}$$

To measure  $A_{xp}$  is very complicated at every cross- section and there is a little change occurs due to the presence of insert, so it can be assumed as  $A_{xp} \approx A_{xs}$  . Then the equation will becomes

$$\text{Re}_p = \text{Re}_s \cdot \left( \frac{f_s}{f_p} \right)^{1/3} \quad (3.20)$$

$\text{Re}_p$  is the equivalent Reynolds number for the tube with perforated rectangular strip inserts at constant blower power (same as plain tube). Putting this  $\text{Re}_p$  in the final correlation developed for Nusselt number equation (5.5),  $\text{Nu}_p$  is to be found. Then from equation (3.16), performance parameter,  $R$  can be obtained for the different inserts.

## CHAPTER-4

### EXPERIMENTAL FACILITY AND PROCEDURE

#### 4.1 General:

The experimental facility and procedure of collecting the different measuring data for the plain tube and the tube with perforated rectangular strip inserts are described in this chapter. The uncertainty estimates of the measuring items are also described in this chapter.

#### 4.2 Experimental Facility:

The experimental facility consists of an inlet section, a test section, an air supply system (electric blower) and a heating arrangement. The schematic diagram of the experimental facility is shown in figure 4.1. The dimensions of the experimental facility are shown in figure 4.2a. All the layers of insulation over the tube surface are shown in figure 4.2b.

##### 4.2.1 Test Section:

The most important part of the experimental facility was the test section. A cross-sectional view of the tube, with perforated rectangular strip insert is shown in the figure 4.3a. The isometric view of the perforated rectangular strip insert is also shown in the figure 4.3b. The semi cylindrical plain tube made of two halves were clamped together by flanges at the ends having 70 mm inside diameter and 1500 mm length. The mild steel perforated rectangular strips of different pore diameters were in turn inserted at  $45^{\circ}$  angles within the plain tube. The length of the strip was 1500 mm and the width was 58 mm. The strip was inserted axially in one half of the tube, and then the two halves of the plain tube were clamped together. In order to prevent leakage, the putting was pressed into the joint of the tube. Then the plain tube in the test section was covered with mica sheet to isolate electrically. A layer of glass fiber tape was put on the mica sheet. Nichrome wire (of resistance 1.2 ohm/m) used as an electric heater was spirally wound uniformly with spacing of 16 mm around the tube. Then mica sheet, glass fiber tape,

heat insulating tape, and asbestos tape were sequentially put over the Nichrome wire heater coil. These protected the radial heat losses. The test section was installed in the experimental facility with the help of the bolted flanges with gaskets of asbestos (of thickness 3.5 mm) to prevent the heat flow in the longitudinal direction and to prevent leakage of air.

In the similar way, nine test specimens were made with nine different perforated rectangular strips. The pore diameter varied from 2 mm to 12 mm. The distance between two adjacent holes was axially 15 mm and transverse wise 18 mm (figure 4.3c). Porosity of the rectangular strips was calculated by dividing the total pores area in a strip to the strip area (including holes). Porosity of the different inserts varied from 1.1 % to 39 %.

#### **4.2.2 Inlet Section:**

The unheated inlet section (533 mm long) cast and machined was of aluminum with the same inside diameter as the test section i.e. 70 mm. The pipe shaped inlet section (figure 4.4) was made integral to avoid any flow disturbances at upstream of the test section to get fully developed flow in the test section as well. The shape of the entrance part of the inlet section was made, as per suggestions of Owner and Pankhurst [46] to avoid separation and stratification of the flow.

#### **4.2.3 Air Supply System:**

Air was induced by an electrically driven centrifugal blower, which was fitted down stream of the test section so that any disturbance produced by the blower would not affect the flow in the test section. Air entered through the inlet section containing traversing pitot tube and it passed successively through the heated test section and diffuser system. A 12° diffuser made of mild steel plate was fitted to the suction side of the blower. It was used for minimizing head loss at the suction side. To isolate the vibration of the blower, a flexible duct was installed between the inlet section of the blower and the gate valve as shown in the figure 4.1. The gate valve was of butterfly

type and was used to control the flow rate of air. It was fitted ahead of the flexible duct to control the flow rate of air through the tube.

#### **4.2.4 Heating Arrangement:**

An electric heater (made of Nichrome wire) was used to heat the test section at constant heat flux. Power was supplied to heater by a regulated alternating current source with a 5 kVA variable voltage transformer through a magnetic contactor and a temperature controller. Huq [24], Uddin [26], Mamun [28], Aloke [30], Islam [40] and Ahamed [45] all used a regulated alternating current source with a 5 kVA variable voltage transformer through a magnetic contactor and a temperature controller for power supplied to heater. The temperature controller was used to sense the outlet air temperature by providing signal for switching the heater off or on automatically. It was used to control the outlet air temperature at a specified limit. This was also used to protect excessive heating of the experimental facility. The nichrome wire for heating was wound uniformly around the test section as shown in the figure 4.2a. Electric heat input to Nichrome wire was kept constant for all the experiments. The electric power supplied to the test section was determined by measuring the current and voltage applied to the heating element multiplying by a power factor of 0.8. The voltage was measured with a voltmeter and current by an a.c. ammeter. Figure 4.5 shows the electric circuit diagram for the heating system of the test section. The specifications of the electric heater, temperature controller and blower are given in Appendix-A.

### **4.3 Measurement Systems:**

For performing the experiment three measuring systems namely flow measuring system, pressure measuring system and temperature measuring system were involved apart from the electric power measurement as mentioned above.

#### **4.3.1 Flow Measuring System:**

Flow of air through the test section was measured at the inlet section with the help of a traversing pitot tube. The traversing pitot tube was fitted at a distance of  $4D_i$  from the

inlet according to Owner and Pankhurst [46] where,  $D_i$  was the inlet diameter of the tube. In this experiment, High Speed Diesel oil of specific gravity 0.855 was used as a manometric fluid. A schematic diagram of the traversing pitot tube is shown in figure 4.6. Arithmetic mean method (given in Appendix-C) was applied to determine the position of the traversing pitot tube for determination of mean velocity of air. Uddin [26], Mamun [28], Alope [30], Islam [40] and Ahamed [45] all applied arithmetic mean method to determine the position of the traversing pitot tube for determination of mean velocity of air. The different positions of pitot tube for measuring the velocity head are shown in figure 4.7.

#### **4.3.2 Pressure Measuring System:**

Static pressure varied at different axial locations along the tube. The static pressure tapings were made at the inlet of the test section as well as at eight equally spaced axial locations of the test section as shown in the figure 4.8. Huq [24], Uddin [26], Mamun [28], Alope [30], Islam [40] and Ahamed [45] all used static pressure tapings for measurement of static pressure at the inlet of the test section as well as at eight equally spaced axial locations of the test section. Pressure tapings for measurement of static pressure were fitted carefully so that it just touches the inner surface of the test section. Epoxy glue was used for proper fixing of the static pressure tapings. U-tube manometers at an inclination of  $30^\circ$  were attached with the pressure tapings. Water was used as the manometric fluid in this experiment. The friction factors were determined from the measurement of pressure drops across the axial locations of the test section for plain tube as well as the tube with perforated rectangular strip inserts.

#### **4.3.3 Temperature Measuring System:**

The temperatures at the different axial locations of the test section and the air inlet temperature were measured with the help of K-type thermocouples connected with the Rotary selector switch. Eight thermocouples were fitted at eight equally spaced axial locations of the test section to measure the tube wall temperatures. Uddin [26], Mamun [28], Alope [30], Islam [40] and Ahamed [45] all used eight thermocouples at eight

equally spaced axial locations of the test section to measure the tube wall temperatures. Axial locations of the thermocouples are shown in the figure 4.9. Air inlet temperature was determined by thermocouple positioned at the tube centerline, in the inlet section. Air outlet bulk temperature was measured by traversing the thermocouple at the exit of the test section. Arithmetic mean method (given in Appendix-C) was applied to determine the position of the traversing thermocouple for determination of the mean outlet bulk temperature of the air. Mamun [28], Aloke [30], Islam [40] and Ahamed [45] all applied arithmetic mean method to determine the position of the traversing thermocouple for determination of the mean outlet bulk temperature of the air. The different positions of the thermocouple for outlet bulk temperature are shown in the figure 4.10.

#### **4.4 Experimental Procedures:**

At first the electric heater was switched on and allowed to heat for about five minutes and then the blower was switched on. The electric power was adjusted (if necessary) with the help of a regulatory transformer or variac. The flow of air through the test section was set to a desired value and kept constant with the help of the flow control valve. First the variations in wall temperatures at all locations were observed until constant values were attained at all the eight locations. Then the bulk outlet air temperature was monitored. Steady state condition was attained when the outlet air temperature did not fluctuate over 30 minutes time. At the steady state condition, thermocouple readings were recorded with the help of selector switch and at the same time, manometer readings were recorded from the inclined tube manometers.

After each experimental run, the air flow rate was changed with the help of the flow control valve thereby changing the Reynolds number. At that time, electrical power supply was kept constant. After waiting for steady state condition, different data were recorded in the similar way.

#### 4.5 Uncertainty Analysis:

Almost all engineers in the real world at same stage deal with data derived from experiments or tests. These experimental data were processed to generate results. The connection between primary measurements and the results was always a mathematical function of some kind i.e. if R was a result and  $X_1$ ,  $X_2$ , and  $X_3$  were the primary measurements of them. Uncertainty in calculating R was

$$R = f(X_1, X_2, X_3 \dots \dots \dots) \dots \dots \dots (4.1)$$

In the experiment, it was necessary to calculate the uncertainty in the results from the estimates of uncertainty in the measurands. This calculation process is called “propagation of uncertainty”. According to Kline and McClintock [47], the uncertainty in R resulting from the uncertainties in  $X_1$ ,  $X_2$ , and  $X_3$  ..... the following equation was used

$$W_R = \left[ \left( \frac{\partial R}{\partial X_1} w_{x1} \right)^2 + \left( \frac{\partial R}{\partial X_2} w_{x2} \right)^2 + \dots \dots \dots \left( \frac{\partial R}{\partial X_m} w_{xm} \right)^2 \right]^{\frac{1}{2}} \dots \dots \dots (4.2)$$

Where,  $w_{x1}$ ,  $w_{x2}$ ,  $w_{x3}$ -----are the uncertainties in the individual variable  $X_1$ ,  $X_2$ , and  $X_3$  -----.

In this experiment primary measurands were  $T_\infty$ , d, b, A,  $T_0$ ,  $T_i$ ,  $\Delta P$ ,  $D_i$  and X. The results of uncertainty analysis of the primary measurements are presented in Table 4.1, while the uncertainties of the calculated quantities are presented in Table 4.2.



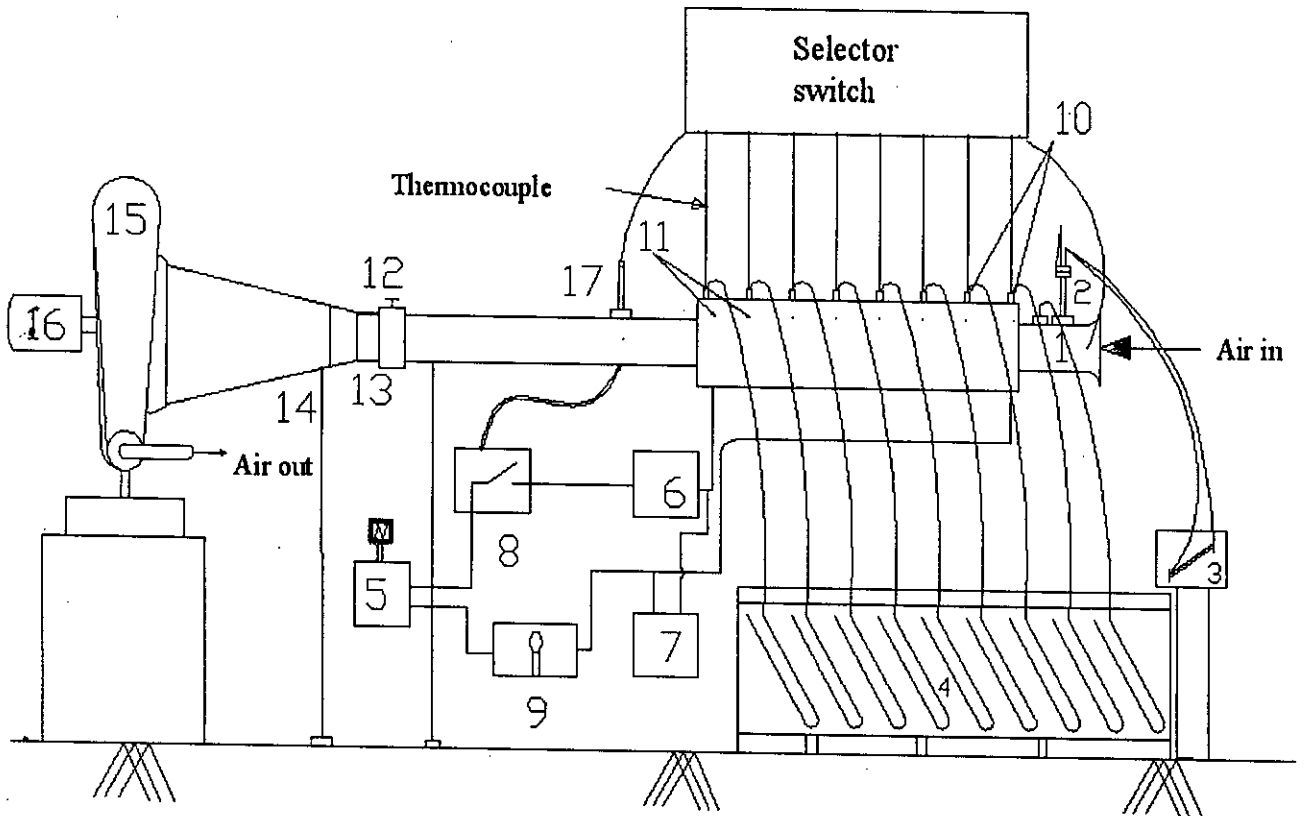
**Table 4.1: Uncertainties in measurands.**

Items measured	Precision limit, P (%)	Bias limit, B (%)	Total limit, W (%)
$T_{\infty}$	1.5	0.02	1.5
b	0.01	0.012	0.016
d	1.00	3.0	3.185
A	0.00	0.52	0.520
$T_o$	1.55	0.02	1.55
$T_i$	1.5	0.02	1.50
$\Delta P$	5.0	3.00	5.83
$D_i$	0.00	0.02	0.02
$X_{T_o}$	0.00	0.02	0.020

**Table 4.2: Uncertainties in calculated quantities:**

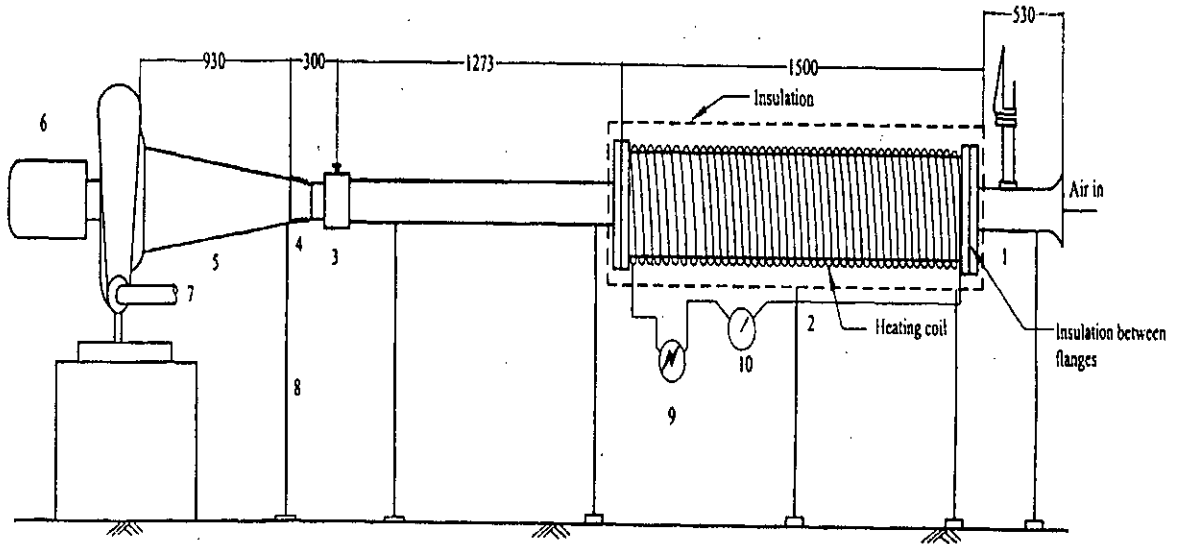
Quantity	Total uncertainty (%)
V	1.59
Q	7.80
$f_i$	1.2

The calculation of the above values is given in Appendix - D.



- |                                 |                           |                             |
|---------------------------------|---------------------------|-----------------------------|
| 1. Inlet section                | 6. Ammeter                | 12. Flow control valve      |
| 2. Traversing pitot tube        | 7. Voltmeter              | 13. Flexible pipe           |
| 3. Inclined tube manometer      | 8. Temperature controller | 14. Diffuser                |
| 4. U-tube manometer             | 9. Heater on off lamp     | 15. Blower                  |
| 5. Variable voltage Transformer | 10. Pressure tapplings    | 16. Motor                   |
|                                 | 11. Thermocouples         | 17. Traversing thermocouple |

Figure 4.1: Schematic diagram of the experimental facility.



\*All dimensions are in mm.

- |                       |                    |                          |            |
|-----------------------|--------------------|--------------------------|------------|
| 1. Inlet section      | 4. Flexible duct   | 7. Air outlet            | 10. Variac |
| 2. Test section       | 5. Diffuser        | 8. Supports              |            |
| 3. Flow control valve | 6. Electric blower | 9. Electric power supply |            |

Figure 4.2a: Schematic diagram of the experimental facility with dimensions

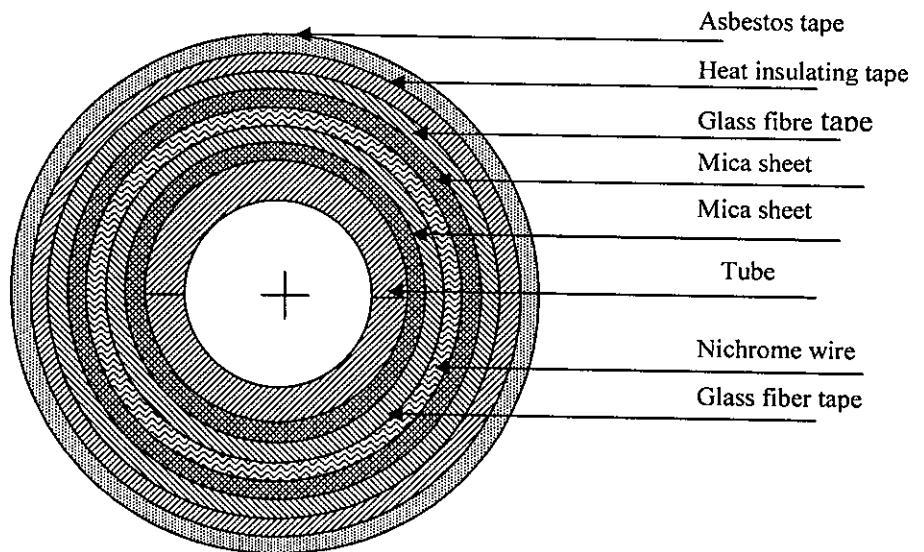


Figure 4.2b: X- section of the test section with insulations.

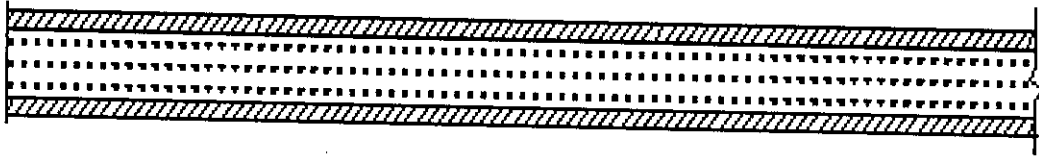


Figure 4.3a: X- section of the test section with perforated rectangular strip insert.

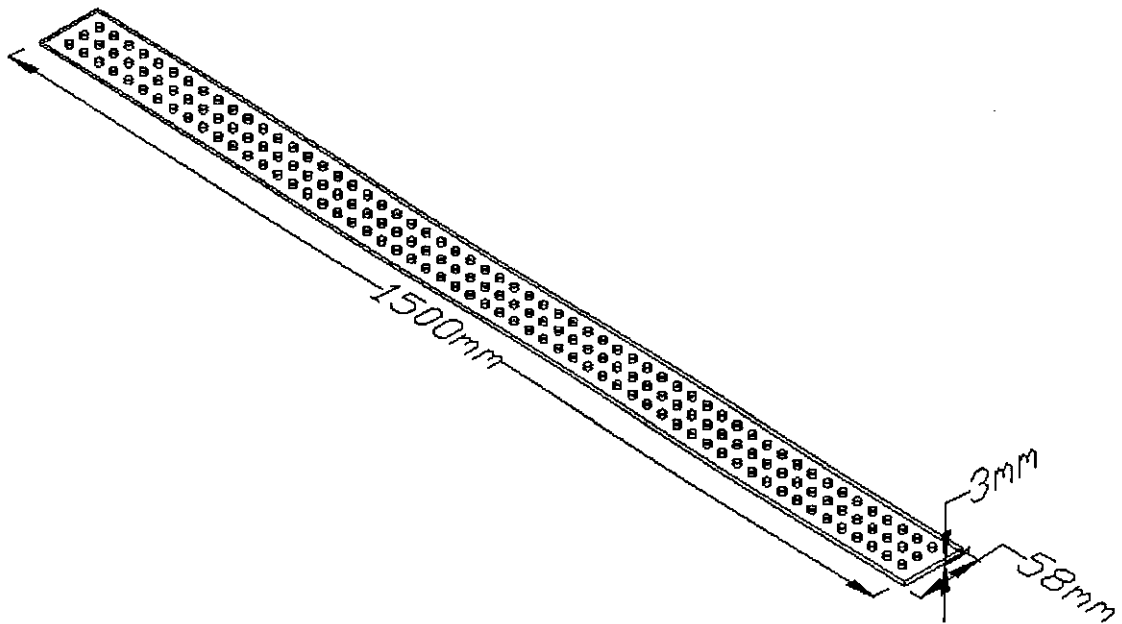


Figure 4.3b: Isometric view of the perforated rectangular strip insert with dimensions.

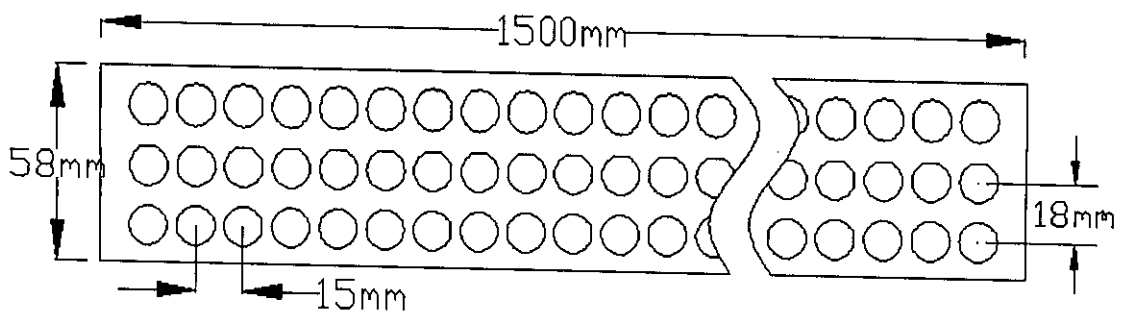
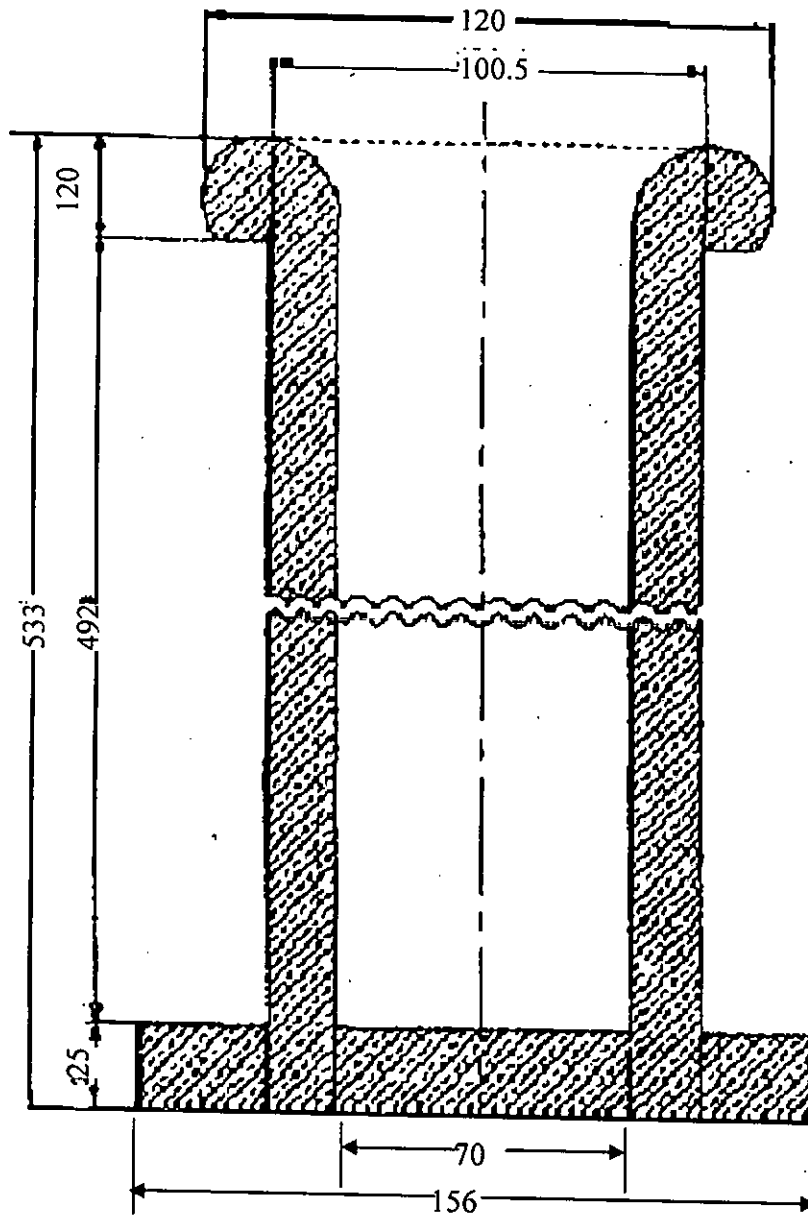


Figure 4.3c: Schematic diagram of the hole position in the strip with dimensions.



\* All dimensions are in mm  
 Figure 4.4: Shaped inlet section

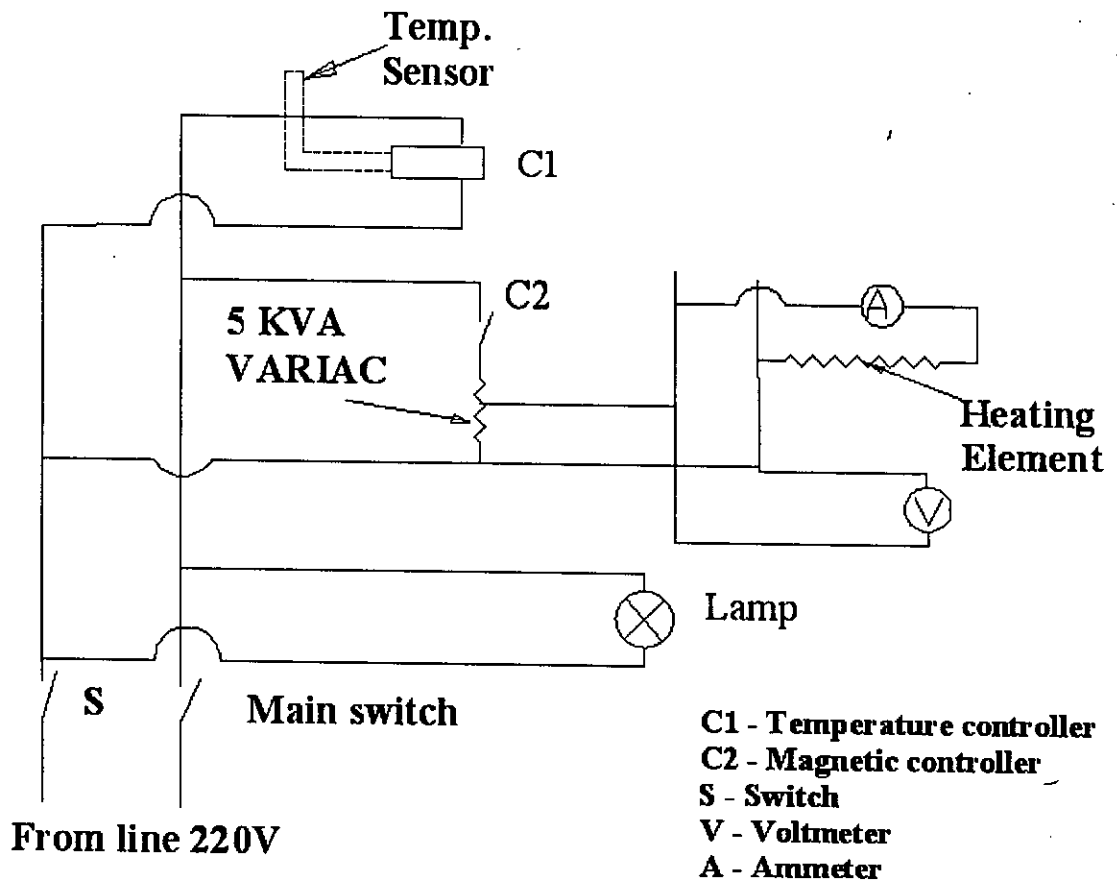


Figure 4.5: Electrical circuit diagram for the heating system.

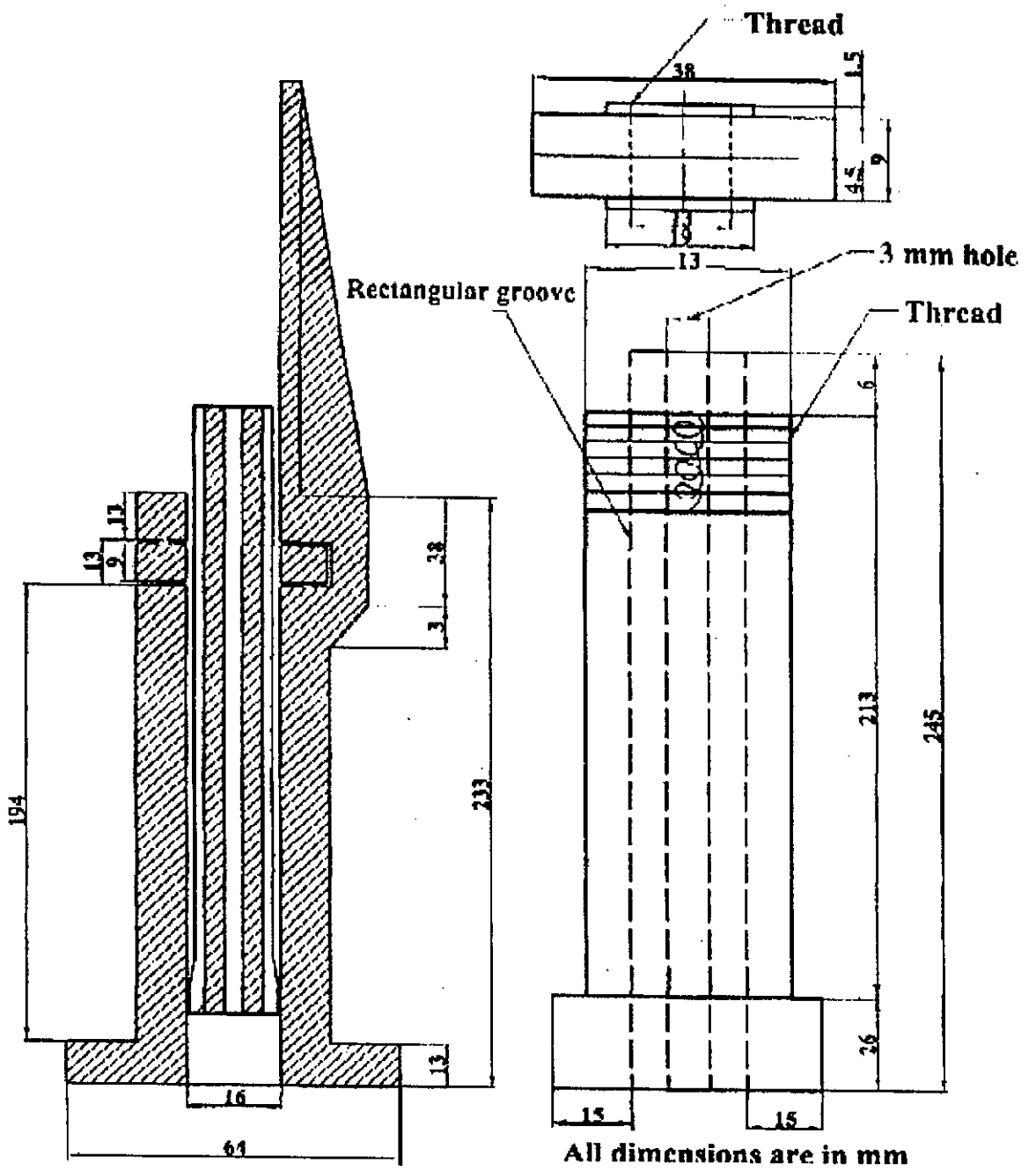


Figure 4.6: Traversing the pitot tube holding device.

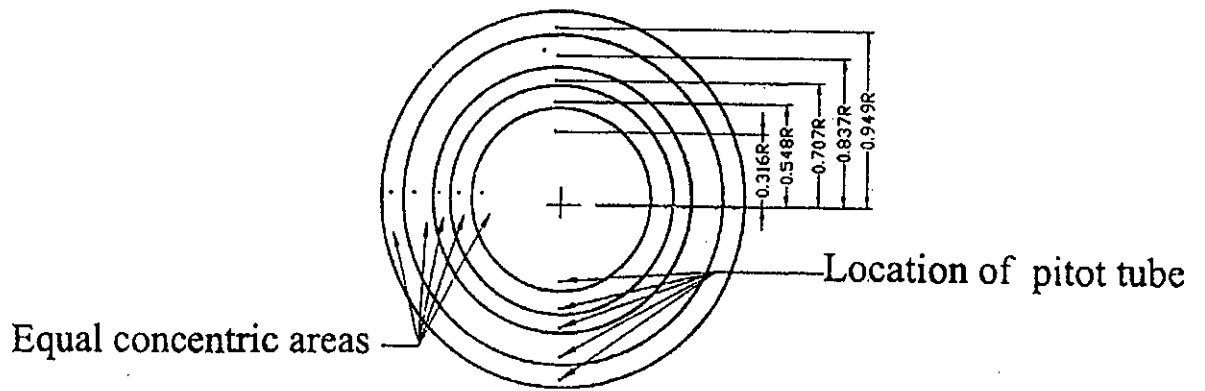


Figure 4.7: Location of the pitot tube for measurement of velocity.

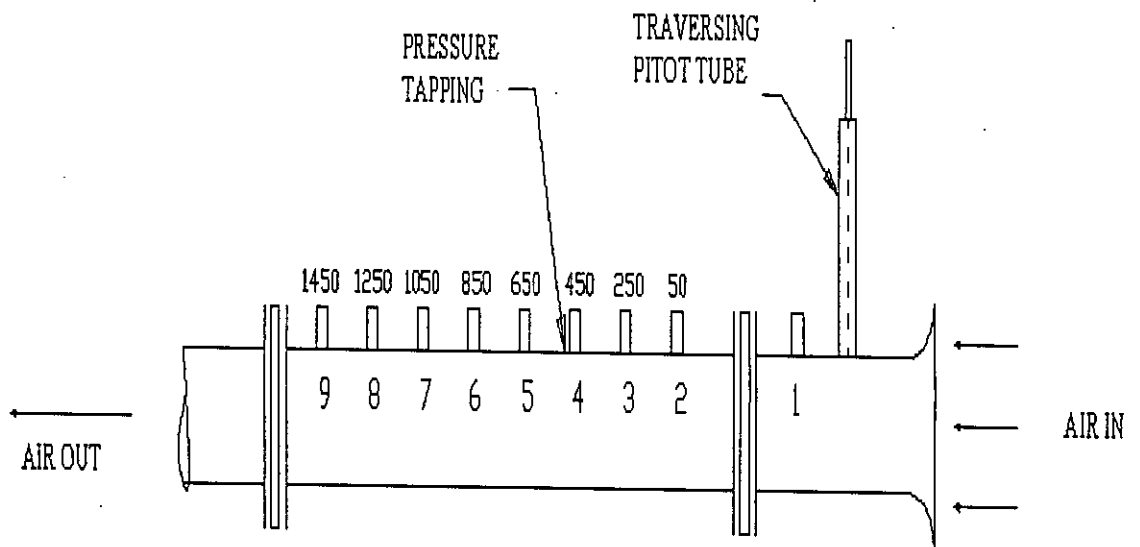
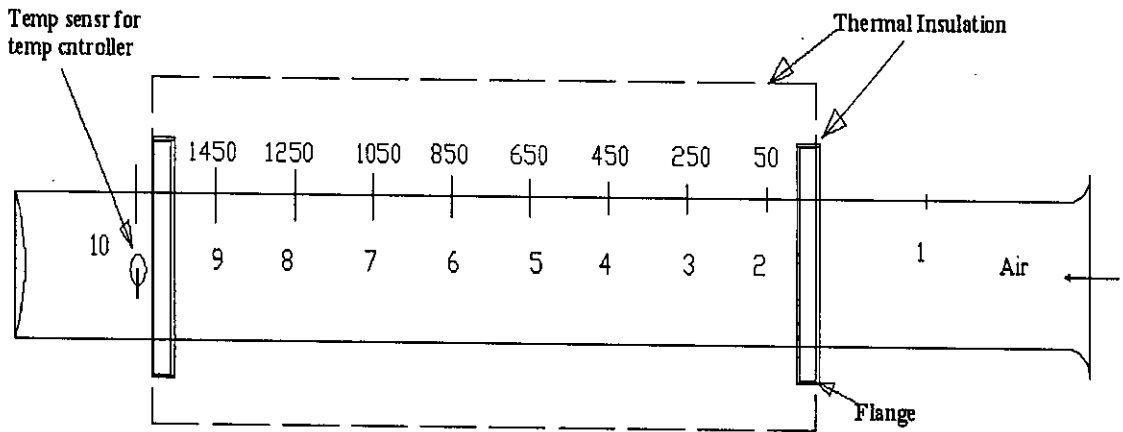


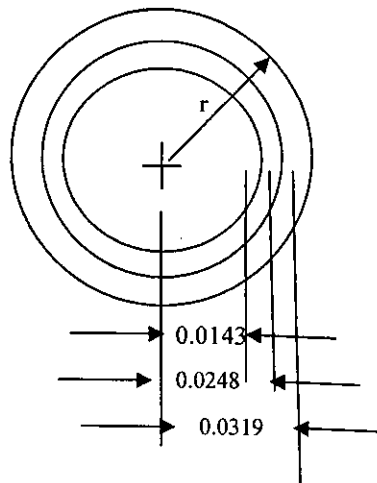
Figure 4.8: Location of the pressure tapings.





2-9 – Tube Wall Temperature  
 1- Inlet air Temperature and 10- Outlet air Temperature

Figure 4.9: Location of thermocouples.



\* All dimensions are in m

Figure 4.10: Location of thermocouples for the outlet bulk temperature.

## CHAPTER- 5

### RESULTS AND DISCUSSION

#### 5.1 General :

In this experimental study the friction factors and heat transfer characteristics in turbulent flow through a tube with and without perforated rectangular strip inserts were analyzed. Nine mild steel rectangular strips of different pore diameters were used. The diameter of the pores were 2 mm, 3 mm, 4 mm, 5 mm, 7 mm, 8 mm, 9 mm, 10 mm and 12 mm and hence porosity of the rectangular strip inserts varied from 1.1 % to 39 %. Porosity of insert,  $R_p = 0$  indicated the rectangular strip without perforation and  $R_p = \infty$  indicated the plain tube. The central distance between the two adjacent pores was fixed as 15 mm ( axially) and 18 mm ( transverse wise). All the necessary variables were calculated from the taken data . These data and performance characteristic graphs were presented and analyzed in this chapter.

In the present work, in order to make easy comparison and analysis some assumptions were made. These assumptions occurred limitations in the actual results. These were:

- i. Inside diameter of the tube ( $D_i$ ) was used instead of hydraulic diameter ( $D_h$ ) in defining  $Re$ ,  $Nu$  and friction factor.
- ii. All the fluid properties were calculated at fluid mean bulk temperature instead of film temperature and at atmospheric pressure instead of local pressure in the test section which was slightly less than the atmospheric pressure.
- iii.  $T_b$  was assumed to vary linearly along the length of the test section whereas,  $T_w$  varied non-linearly along the length of the test section.
- iv. Calculated blower power did not indicate the total blower power required to run the blower for the flow. It was the power required to cause flow of the fluid through the test section only.
- v. It was assumed that the heat was transferred only by forced convection from inside wall of the tube to the fluid. But there has been some conduction heat transfer through the strip from the wall due to the contact of the strip with the wall. Heat was also conducted through the ends of the test section to the

adjacent section.

## **5.2 Temperature Distribution :**

The local wall and bulk fluid temperatures at different axial locations for plain tube, tube with unperforated and tube with perforated rectangular strip inserts at different Reynolds numbers are shown in figures 5.1-5.11. The variation of tube wall temperatures along axial distance for different porosity of inserts at Reynolds number around 30,925 is shown in figure 5.11(a). The variation of tube wall temperatures with different porosity ( $R_p$  from 0 %-39 %) of inserts for axial distance of  $X/L = 0.57$  and at Reynolds number around 30,925 is shown in figure 5.11(b). The average wall and average fluid bulk temperatures for plain tube, tube with unperforated and tube with perforated rectangular strip inserts at different Reynolds numbers are shown in figures 5.12-5.13.

The variation of dimensionless temperature differences along axial distance for plain tube, tube with unperforated and tube with perforated rectangular strip inserts at different Reynolds numbers are shown in figures 5.14-5.24. The variation of dimensionless temperature differences along axial distance for different porosity of inserts at Reynolds number around 30,925 is shown in figure 5.24(a). The variation of dimensionless temperature differences with different porosity ( $R_p$  from 0 %-39 %) of inserts for axial distance of  $X/L = 0.57$  and at Reynolds number around 30,925 is shown in figure 5.24(b).

### **5.2.1 Effect of Reynolds Numbers and Porosity of the Rectangular Strip on Local and Average Tube Wall and Fluid Bulk Temperatures:**

Variation of tube wall and fluid bulk temperatures along the axial locations in the test section with perforated rectangular strip inserts at different Reynolds numbers are presented in figures 5.1-5.9. Figure 5.10 shows the variation of tube wall and fluid bulk temperatures along the axial locations for the unperforated rectangular strip insert at different Reynolds numbers. Figure 5.11 shows the variation of tube wall and fluid bulk temperatures along the axial locations for the plain tube at different Reynolds numbers. The axial position of any point is non-dimensionalized by the total length of

the test section (L). The wall temperatures were recorded directly during the experiment. But the local fluid bulk temperatures were calculated using the equation (3.8). Considering uniform heat flux, the variation of the fluid bulk temperature was assumed linear throughout the test section. From the figures 5.1-5.11, it was observed that the wall temperature increased along the axial position for a given Reynolds number and reached its maximum at  $X/L = 0.577$ . Then the tube wall temperature dropped slightly at the downstream due to end effect. It might be noted that for both cases the wall temperatures were lower at the entry and the exit partly because of the conduction losses(end effect). For both the cases the wall temperatures decreased with the increase in Reynolds number.

Higher Reynolds number indicated higher flow rate of fluid and it was possible to take away more heat from the tube wall. Wall temperatures in the tube with perforated rectangular strip inserts at any location was lower than that of the plain tube for a given Reynolds number. As the plain tube had lower wetted perimeter and less contact area with the working fluid compared to the inserted tube, so, its ability to transfer heat was low.

The calculated bulk fluid temperatures based on average 'q' along the axial locations of the tube with and without perforated rectangular strip inserts at different Reynolds numbers increased linearly. Because air passed through the heated tube along the length and took away heat from the tube wall. So, it increased along the tube length for both cases (plain tube and tube with inserts). At lower Reynolds number, the bulk fluid temperature was higher. The reason was that at lower Reynolds number there was less velocity of air, which provided much time for sufficient heating of air in the test section as well as the inserts. Thus the bulk fluid temperature was higher at a particular location at lower Reynolds number. But at higher Reynolds number, faster moving of air got insufficient time for being heated.

Figure 5.11(a) shows the variation of tube wall temperatures along axial distance for different porosity of inserts at Reynolds number around 30,925. Figure 5.11(a) showed that the wall temperature was higher in the plain tube than that of the tube with

inserts for any axial location of the test section. At porosity,  $R_p = 4.4\%$ , the wall temperature was lower than that of the tube with other inserts. Tube with unperforated rectangular strip insert was higher wall temperature than that of the tube with perforated rectangular strip inserts.

Figure 5.11(b) shows the variation of tube wall temperature with different porosity ( $R_p$  from 0 %-39 %) of inserts for axial distance of  $X/L = 0.57$  and at Reynolds number around 30,925. Figure 5.11(b) showed that the wall temperature for the tube with porosity of 4.4 % was lower than that of the tube with other inserts. Wall temperature lower indicated the heat transfer rate was higher. After porosity,  $R_p = 4.4\%$ , the wall temperature increased with the increase of porosity. The figure 5.11(b) also showed that the wall temperature was higher at the lower porosity of 4.4 %.

Figures 5.12-5.13 show the variation of average wall and average fluid bulk temperatures for different porosity of rectangular strip inserts at different Reynolds numbers. From the figure 5.12, it was clear that the wall temperature for the plain tube was higher than that of the tube with inserts. The wall temperature for the tube with unperforated rectangular strip insert was also higher than that of the tube with perforated rectangular strip inserts. At porosity,  $R_p = 4.4\%$  the wall temperature was lower than that of the tube with other inserts. It was also clear from the figure 5.13 that the bulk fluid temperature of the plain tube was lower than that of the tube with inserts. And the bulk fluid temperature of the unperforated rectangular strip insert was also lower than that of the tube with perforated rectangular strip inserts.

### **5.2.2 Effect of Reynolds Numbers and Porosity of the Rectangular Strip on Dimensionless Temperature Differences:**

Figures 5.14-5.23 show the variation in dimensionless temperature differences (wall and bulk) along the axial distance for the tube with perforated and unperforated rectangular strip inserts. Figure 5.24 also shows the variation in dimensionless temperature differences along axial distance for the plain tube. From the figures 5.14-5.24, it was clear that the plain tube had the highest temperature difference. Keeping the other parameters fixed, the smallest temperature difference indicated the highest

heat transfer coefficient as constant heat flux condition was assumed throughout the test section. The blockage of the flow due to the presence of the inserts increased the flow velocity and improved the intensive mixing of the fluid. So, the temperature difference for the inserts was lower than that of the plain tube.

Figure 5.24(a) shows the variation of dimensionless temperature differences along axial distance for different porosity of inserts at Reynolds number around 30,925. Figure 5.24(a) showed that the dimensionless temperature difference was higher in the plain tube than that of the tube with inserts for any axial location of the tube. At porosity,  $R_p = 4.4\%$ , the dimensionless temperature difference was lower than that of the tube with other inserts. Tube with unperforated rectangular strip insert was higher dimensionless temperature difference than that of the tube with perforated rectangular strip inserts.

Figure 5.24(b) shows the variation of dimensionless temperature difference with different porosity ( $R_p$  from 0 %-39 %) of inserts for axial distance of  $X/L = 0.57$  and at Reynolds number around 30,925. Figure 5.24(b) showed that the dimensionless temperature difference for the tube with porosity of 4.4 % was lower than that of the tube with other inserts. Dimensionless temperature difference lower indicated more heat was taken away from the tube surface. After porosity,  $R_p = 4.4\%$ , the dimensionless temperature difference was higher for the tube with porosity of other inserts. The figure 5.24(b) also showed that the dimensionless temperature difference was higher at the lower porosity of 4.4 %.

### **5.3 Heat Transfer Characteristics:**

In this section, the variation of heat transfer coefficient, Nusselt number along the axial distance of the test section, average heat transfer coefficient, average Nusselt number and heat transfer rate at different Reynolds numbers were calculated and analyzed. A comparison of these parameters for plain tube and tube with perforated and unperforated rectangular strip inserts are discussed below:

### 5.3.1 Effect of Reynolds Numbers and Porosity of the Rectangular Strip on Heat Transfer Coefficient:

Figures 5.25-5.34 show the variation of local heat transfer coefficient ( $h_x$ ) along the axial distance of the tube with perforated and unperforated rectangular strip inserts at different Reynolds numbers. Figure 5.35 shows the variation of local heat transfer coefficient along axial distance for the plain tube at different Reynolds numbers. The figures 5.25-5.35 indicated that the local heat transfer coefficient was high at the entrance region due to the development of thermal boundary layer with the entrance section at the leading edge. Then it gradually decreased up to a certain location. Again from the figures 5.25-5.35, it was clear that at higher Reynolds number the local heat transfer coefficient was higher. This was expected because a higher flow rate result in increment of local heat transfer from the tube surface.

Figure 5.35(a) shows the variation of local heat transfer coefficient along axial distance for different porosity of inserts at Reynolds number around 30,925. Figure 5.35(a) showed that the local heat transfer coefficient was lower in the plain tube than that of the tube with inserts for any axial location of the test section. At porosity,  $R_p = 4.4\%$ , the local heat transfer coefficient was higher than that of the tube with other inserts. The local heat transfer coefficient for the tube with unperforated rectangular strip insert was lower than that of the tube with perforated rectangular strip inserts.

Figure 5.35(b) shows the variation of local heat transfer coefficient with different porosity ( $R_p$  from 0 %-39 %) of inserts for axial distance of  $X/L = 0.57$  and at Reynolds number around 30,925. Figure 5.35(b) showed that the local heat transfer coefficient for the tube with porosity of 4.4 % was higher than that of the tube with other inserts. After porosity,  $R_p = 4.4\%$ , the heat transfer coefficient decreased with the increase of porosity. The figure 5.35(b) also showed that the heat transfer coefficient was lower at the lower porosity of 4.4 %.

Variation of average heat transfer coefficient for plain tube and tube with perforated and unperforated rectangular strip inserts at different Reynolds numbers are shown in figure 5.36. The figure 5.36 showed that average heat transfer coefficient increased

with the increase in Reynolds number for the plain tube and the tube with inserts. At higher Reynolds number, mixing of the fluid occurred and more heat is taken away from the tube surface and hence the heat transfer coefficient increased. Again from the figure 5.36, it could be noted that the average heat transfer coefficient depends on porosity of rectangular strip inserts. The average heat transfer coefficient was maximum for the porosity,  $R_p = 4.4\%$  of rectangular strip insert. For porosity,  $R_p = 4.4\%$ , the heat transfer coefficient increased up to 2.80 times compared to that of the plain tube. The higher and lower porosity than the porosity of 4.4%, the heat transfer coefficient decreased. Because area decreased with the increase of porosity. Lower porosity caused less fluid pass through the hole. At high speed fluid could not pass through the small hole.

Figure 5.36(a) shows the variation of average heat transfer coefficient with different porosity ( $R_p$  from 0 %-39 %) of inserts for different comparable Reynolds numbers. Figure 5.36(a) showed that the average heat transfer coefficient for the tube with porosity of 4.4% was higher than that of the tube with other inserts. After porosity,  $R_p = 4.4\%$ , the heat transfer coefficient gradually decreased with the increase of porosity. The figure 5.36(a) also showed that the heat transfer coefficient gradually increased with the increase of porosity up to 4.4%.

### **5.3.2 Effect of Reynolds Numbers and Porosity of the Rectangular Strip on Nusselt Number :**

Figures 5.38-5.47 show the variation of local Nusselt number ( $Nu_x$ ), based on local heat transfer coefficient ( $h_x$ ), along axial distance of the tube with perforated and unperforated rectangular strip inserts at different Reynolds numbers. The figures 5.38-5.47 indicated that the local Nusselt numbers were large at the entry of the test section as observed in the local heat transfer coefficients in the figures 5.25-5.34. Figure 5.48 shows the variation of local Nusselt number ( $Nu_x$ ) along axial distance for the plain tube at different Reynolds numbers.

The figure 5.48 indicated that the local Nusselt number was large at the entrance region of the test section as observed in the local heat transfer coefficient in the figure 5.35.



Then it gradually decreased up to a certain point. Again from the figure 5.48, it was clear that at higher Reynolds number the local Nusselt number was higher. This was expected because a higher flow rate result in increment of local heat transfer from the tube surface.

Figure 5.48(a) shows the variation of local Nusselt number along axial distance for different porosity of inserts at Reynolds number around 30,925. Figure 5.48(a) showed that the local Nusselt number was lower in the plain tube than that of the tube with inserts for any axial location of the test section. At porosity,  $R_p = 4.4\%$ , the local Nusselt number was higher than that of the tube with other inserts. The local Nusselt number for the tube with unperforated rectangular strip insert was lower than that of the tube with perforated rectangular strip inserts.

Figure 5.48(b) shows the variation of local Nusselt number with different porosity ( $R_p$  from 0 %-39 %) of inserts for axial distance of  $X/L = 0.57$  and at Reynolds number around 30,925. Figure 5.48(b) showed that the local Nusselt number for the tube with porosity of 4.4 % was higher than that of the tube with other inserts. After porosity,  $R_p = 4.4\%$ , the local Nusselt number decreased with the increase of porosity. The figure 5.48(b) also showed that the Nusselt number was lower at the lower porosity of 4.4 %.

Figure 5.49 shows the variation of average Nusselt number with porosity of the rectangular strip inserts at different Reynolds numbers. Average Nusselt number increased with the increase in Reynolds number. Again from the figure 5.49, it was clear that the average Nusselt number also depend on porosity of rectangular strip inserts. Average Nusselt number was maximum for porosity of rectangular strip insert,  $R_p = 4.4\%$ . For porosity,  $R_p = 4.4\%$ , the average Nusselt number varied from 2.5 to 2.80 folds in comparison to the plain tube. The higher and lower porosity than the porosity of 4.4 %, the Nusselt number decreased. So, tube with perforated rectangular strip inserts was advantageous over the plain tube.

### **5.3.3 Effect of Reynolds Numbers and Porosity of the Rectangular Strip on Heat Transfer Rate :**

Figure 5.50 shows the variation of heat transfer rate for porosity of rectangular strip inserts at different Reynolds numbers. The figure 5.50 indicated that the heat transfer rate increased with the increase in Reynolds number for all the cases. At higher Reynolds number, there was intensive mixing of air, which increased the heat transfer rate. The figure 5.50 also indicated that the heat transfer rate was higher for the perforated rectangular strip inserts than that of the plain tube. Perforated rectangular strip inserts created swirl flow and turbulence in the test section. Heat transfer rate for the tube with perforated rectangular strip inserts increased up to 1.85 folds in comparison to that of the plain tube.

Again from the figure 5.50, it could be noted that the heat transfer rate depend on the porosity of rectangular strip inserts. Heat transfer rate was maximum when the porosity of rectangular strip insert was 4.4 %. It decreased with the increase of porosity as well as decrease of porosity of the rectangular strip inserts. Higher porosity caused less turbulence. Hence the heat transfer rate was decreased with the strip of higher porosity. Lower porosity failed to produce the necessary turbulence. At the comparable Reynolds number, tube with porosity of 4.4 % showed higher heat transfer rate than that of the porosity of other rectangular strip inserts within the range of porosity,  $R_p=1.1\%$  to  $39\%$ . So, it was more useful than the plain tube.

Increasing the flow rate, the heat transfer rate was increased with the increase of blower power required. Relation of the blower power with the increase of the heat transfer rate was shown in the figure 5.51. Figure 5.51 showed that at the same blower power, heat transfer rate was higher for perforated rectangular strip insert than that of the plain tube. The figure 5.51 also showed that  $Q_p/Q_s$  was always greater than unity at the same blower power. So, the use of perforated rectangular strip inserts for heat transfer enhancement was advantageous over the plain tube.

### **5.4 Fluid Flow Characteristics :**

Variation of pressure drop and friction factor along the axial distance of the test section

for different Reynolds numbers for plain tube and tube with perforated and unperforated rectangular strip inserts were analyzed. Variation of blower power required for all the cases were also analyzed. A comparison of these parameters for plain tube and the tube with perforated and unperforated rectangular strip inserts are discussed.

#### **5.4.1 Effect of Reynolds Numbers and Porosity of the Rectangular Strip on Pressure Drop:**

Figures 5.52-5.61 represent the variation of pressure drop along axial distance for the tube with perforated and unperforated rectangular strip inserts at different Reynolds numbers. Figure 5.62 shows the variation of pressure drop along axial distance for the plain tube at different Reynolds numbers. As the blower was set at the suction side of the test section, the pressure inside the tube was always negative. The pressure drop occurred along the axial direction of the tube due to the frictional forces of the tube surface.

Figure 5.62(a) shows the variation of the pressure drop along axial distance for different porosity of inserts at Reynolds number around 30,925. Figure 5.62(a) showed that the local pressure drop was lower in the plain tube than that of the tube with inserts for any axial location of the test section. At porosity,  $R_p = 13.3\%$ , the local pressure drop was higher than that of the tube with other inserts. The local pressure drop for the tube with unperforated rectangular strip insert was higher than that of the tube with perforated rectangular strip inserts but slightly less than the porosity of,  $R_p = 13.3\%$ .

Figure 5.62(b) shows the variation of the pressure drop with different porosity ( $R_p$  from 0 %-39 %) of inserts for axial distance of  $X/L = 0.57$  and at Reynolds number around 30,925. Figure 5.62(b) showed that the local pressure drop was lower for the tube with porosity of 1.1 %, but for the tube with porosity of 4.4 % the pressure drop was not significantly high. The pressure drop increased up to the increase of porosity,  $R_p = 13.3\%$  and then the pressure drop decreased with the increase of porosity.

Figure 5.63 shows the variation of total pressure drop with Reynolds number for plain tube and tube with perforated and unperforated rectangular strip inserts. It was clear from the figure 5.63 that at lower Reynolds number, change of pressure drop was comparatively high, and at higher Reynolds number, it was low. This might be explained by the fact that at lower values of Reynolds number, corresponding to lower flow rate, air could pass all the pores and touches the strip and created high frictional forces. At a given Reynolds number, pressure drop in the strip inserts was higher than that of the plain tube. The increase in the pressure drop was due to the presence of small vortices, turbulence, secondary flow and swirl for the tube with the inserts than that of the plain tube.

#### **5.4.2 Effect of Reynolds Numbers and Porosity of the Rectangular Strip on Friction Factor (f):**

Figures 5.66–5.75 show the nature of friction factor with dimensionless distance for both the tube with perforated and unperforated rectangular strip inserts at different Reynolds numbers. Figure 5.76 shows the nature of friction factor with dimensionless distance for the plain tube at different Reynolds numbers. From the figures 5.66-5.76, it could be noted that the friction factor was high near the entrance region, then sharply fell up to a certain limit and then finally it was almost constant. At the entrance region friction factor was high for settings of asbestos gasket between the inlet section and the test section and the blockage created by the inserts.

Figure 5.76(a) shows the variation of the friction factor along axial distance for different porosity of inserts at Reynolds number around 30,925. Figure 5.76(a) showed that the friction factor was lower in the plain tube than that of the tube with inserts for any axial location of the test section. At porosity,  $R_p = 13.3\%$ , the friction factor was higher than that of the tube with other inserts. The friction factor for the tube with unperforated rectangular strip insert was higher than that of the tube with perforated rectangular strip inserts but slightly less than the porosity of,  $R_p = 13.3\%$ .

Figure 5.76(b) shows the variation of the friction factor with different porosity ( $R_p$  from 0 %-39 %) of inserts for axial distance of  $X/L = 0.57$  and at Reynolds number

around 30,925. Figure 5.76(b) showed that the friction factor was lower for the tube with porosity of 1.1 %, but for the tube with porosity of 4.4 % the friction factor was not significantly high. The friction factor increased up to the increase of porosity,  $R_p = 13.3\%$  and then the friction factor decreased with the increase of porosity.

Figure 5.77 shows the variation of average friction factor with Reynolds number for plain tube and the tube with perforated and unperforated rectangular strip inserts. From the figure 5.77, it could be shown that the average friction factor for the tube with perforated and unperforated strip inserts was higher than that of the plain tube for the comparable Reynolds number. It was also clear from the figure 5.77 that the increase of Reynolds number the average friction factor decreased. In this experimental study, it was observed that the average friction factor for the tube with perforated rectangular strip inserts varied from 1.08 to 1.80 folds than that of the plain tube. The presence of small vortices for different inserts might be responsible for increase of the friction factor.

#### **5.5 Blower Power ( $P_m$ ):**

The figure 5.64 represents the variation of blower power with Reynolds number for both the plain tube and the tube with perforated and unperforated rectangular strip inserts. For all the inserted tubes blower power increased as the Reynolds number increased. From the figure 5.64, it could be noted that the required blower power for the tube with perforated and unperforated rectangular strip inserts was higher than that of the plain tube for the comparable Reynolds number. The presence of small vortices, turbulence and increased surface area was responsible for higher pressure drop and blower power. The required blower power for the tube with perforated rectangular strip inserts increased up to 1.45 times than that of the plain tube.

#### **5.6 Effectiveness ( $\epsilon$ ):**

For performance analysis, effectiveness is the measure of heat exchanger performance where wall temperature should be considered as constant. Considering constant wall temperature throughout the test section, the heat transfer effectiveness for both the plain tube and the tube with perforated and unperforated rectangular strip inserts were

calculated using equation (3.15). Figure 5.78 shows the variation of heat transfer effectiveness for the plain tube and the tube with perforated and unperforated rectangular strip inserts at different Reynolds numbers.

From the figure 5.78, it was observed that the heat transfer effectiveness increased with the increase in Reynolds number up to a certain limit ( $Re \sim 15,000-22,000$ ), after that it decreased slightly. And finally, the heat transfer effectiveness increased slightly with the increase in Reynolds number. From the figure 5.78, it was also clear that the heat transfer effectiveness was higher for the tube with perforated rectangular strip inserts than that of the plain tube. The heat transfer effectiveness for the tube with perforated rectangular strip inserts varied from 1.50 to 2.45 folds than that of the plain tube.

#### **5.7 Performance Parameter (R):**

On the basis of constant blower power, performance parameter was calculated for different Reynolds numbers and porosity of rectangular strip inserts. Variation of performance parameter, (R) with blower power for different porosity of rectangular strip inserts at different Reynolds numbers is shown in figure 5.83. Performance of the heat exchanger with perforated rectangular strip inserts increased with the increase in Reynolds number up to a certain limit ( $Re \sim 21,000 -27,000$ ) after that it decreased slightly up to the Reynolds number of 31,000. And after that it increased slightly up to the Reynolds number of 37,000. And then, it decreased slightly up to 40,000 and then finally, the performance parameter increased with the increase in Reynolds number. For the rectangular strip inserts, maximum value of performance parameter, R was 2.10.

#### **5.8 Comparison of the Results with the Previous Results:**

Results of the tube with the perforated rectangular strip inserts were compared with that of the tube without perforation. Figure 5.37 shows the variation of average heat transfer coefficient for different inserts like perforated rectangular strip insert (porosity,  $R_p = 4.4\%$ ), longitudinal strip insert and wire-coil inserts. From the figure 5.37, it was observed that the heat transfer coefficient for the perforated rectangular strip insert was approximately 1.38 times higher than that of the longitudinal strip (Y-shaped) insert by

Sarkar et al.[44]. Heat transfer coefficient for the tube with perforated rectangular strip insert was 1.45 times higher than that of the wire-coil-inserts by Islam [40].

Figure 5.50 showed that the tube with the rectangular strip inserts with or without perforation gave higher heat transfer rate than that of the plain tube. Heat transfer rate for the tube with perforated rectangular strip insert increased up to 1.44 times in comparison to that of the tube without perforation. So, the tube with perforated rectangular strip insert was advantageous over the tube without perforation.

From the figure 5.49, it was shown that the average Nusselt number for the tube with perforated rectangular strip insert increased up to 1.83 times compared to that of the rectangular strip inset without perforation. Figure 5.36 showed that the average heat transfer coefficient for the tube with perforated rectangular strip insert increased up to 1.83 times compared to that of the tube without perforation. Figure 5.64 showed that the required blower power for the tube with perforated rectangular strip insert generally was not significantly different from that of unperforated rectangular strip insert.

Figure 5.65 shows the variation of blower power required for different inserts like perforated rectangular strip insert, perforated twisted tape insert, and wire-coil – inserts. From the figure 5.65, it was observed that the blower power required for the perforated rectangular strip insert was 2.15 times lower than that of the perforated twisted tape insert by Ahamed [45]. And the blower power required for the perforated rectangular strip insert was 1.40 times lower than that of the wire-coil-inserts by Islam [40].

It was shown from the figure 5.78 that the tube with perforated rectangular strip inserts had higher effectiveness than that of the tube without perforation. It was also shown from the figure 5.82 that the tube with perforated rectangular strip inserts had higher performance than that of the tube without perforation. But the performance of the tube with porosity of 13.3 % was slightly less than the unperforated rectangular strip insert.

So, from the figures it was observed that the tube with perforated rectangular strip inserts had better heat transfer augmentation than the tube with rectangular strip insert without perforation.

### 5.9 Data Reduction :

In the present work seven sets of data were taken carefully for each porosity. For nine inserts, total  $(9 \times 7) = 63$  sets of data were taken. And without perforation seven sets of data were also taken.

From the figure 5.49, it was evident that the Nusselt number for the plain tube and the tube with the rectangular strip insert (perforation and without perforation) was a function of Reynolds number and porosity of the strip inserts. These might be correlated by the following Colburn equation :

$$\begin{aligned} Nu &= C Re^m Pr^{0.33} \\ \Rightarrow \frac{Nu}{Pr^{0.33}} &= C Re^m \end{aligned} \quad (5.1)$$

$$\Rightarrow \ln\left(\frac{Nu}{Pr^{0.33}}\right) = \ln(C Re^m)$$

$$\Rightarrow \ln\left(\frac{Nu}{Pr^{0.33}}\right) = \ln C + m \ln Re$$

This equation was similar to the straight line equation,  $y = mx + c$ . Where, the term  $\ln C$  was the intercept and  $m$  was the slope of the graph. The independent variable was  $\ln(Re)$  and the dependent variable was  $\ln(Nu/Pr^{0.33})$ . The slopes of the straight lines,  $m$  and the intercepts  $\ln C$  were obtained on  $\ln(Nu/P^{0.33})$  Vs  $\ln(Re)$  for different porosity of rectangular strip inserts ranges from 0 % to 39 %. It was found that  $C$  and  $m$  were different for different porosity of inserts ( $R_p$ ). The coefficient  $C$  was plotted against  $R_p$  in figure 5.79 and the variation of  $C$  with  $R_p$  was represented by

$$\begin{aligned} C &= 1.364 \cdot 10^7 \cdot (R_p)^9 - 1.725 \cdot 10^7 \cdot (R_p)^8 + 8.696 \cdot 10^6 \cdot (R_p)^7 - 2.24 \cdot 10^6 \cdot (R_p)^6 + \\ & 3.127 \cdot 10^5 \cdot (R_p)^5 - 2.281 \cdot 10^4 \cdot (R_p)^4 + 744.8 \cdot (R_p)^3 - 6.312 \cdot (R_p)^2 - 0.03467 \cdot (R_p) + 0.003407 \end{aligned} \quad (5.2)$$

From the figure 5.80, it was also possible to correlate  $m$  with  $R_p$ . The variation of  $m$  with  $R_p$  was represented by



$$m = -1.9 \cdot 10^8 \cdot (R_p)^9 + 2.334 \cdot 10^8 \cdot (R_p)^8 - 1.124 \cdot 10^8 \cdot (R_p)^7 + 2.68 \cdot 10^7 \cdot (R_p)^6 - 3.215 \cdot 10^6 \cdot (R_p)^5 + 1.56 \cdot 10^5 \cdot (R_p)^4 + 2051 \cdot (R_p)^3 - 390.8 \cdot (R_p)^2 + 8.571 \cdot (R_p) + 0.9758 \quad (5.3)$$

Then the final correlation was obtained for the Nusselt number for the tube with perforated and unperforated rectangular strip inserts as follows :

$$\text{Nu} = \{ 1.364 \cdot 10^7 \cdot (R_p)^9 - 1.725 \cdot 10^7 \cdot (R_p)^8 + 8.696 \cdot 10^6 \cdot (R_p)^7 - 2.24 \cdot 10^6 \cdot (R_p)^6 + 3.127 \cdot 10^5 \cdot (R_p)^5 - 2.281 \cdot 10^4 \cdot (R_p)^4 + 744.8 \cdot (R_p)^3 - 6.312 \cdot (R_p)^2 - 0.03467 \cdot (R_p) + 0.003407 \} \text{Re}^{\{-1.9 \cdot 10^8 \cdot (R_p)^9 + 2.334 \cdot 10^8 \cdot (R_p)^8 - 1.124 \cdot 10^8 \cdot (R_p)^7 + 2.68 \cdot 10^7 \cdot (R_p)^6 - 3.215 \cdot 10^6 \cdot (R_p)^5 + 1.56 \cdot 10^5 \cdot (R_p)^4 + 2051 \cdot (R_p)^3 - 390.8 \cdot (R_p)^2 + 8.571 \cdot (R_p) + 0.9758 \} \cdot \text{Pr}^{0.33} \quad (5.4)$$

But a simplified form of the correlation could be developed from the figure 5.81, for different porosity of rectangular strip inserts ranges from 0 % to 39 %. From the figure a straight line equation was obtained as follows:

$$\ln(\text{Nu}/\text{Pr}^{0.33}) = 1.0174 \ln(\text{Re}) - 5.5756$$

From the graph, slope,  $m = 1.0174 \approx 1.02$  and  $\ln C = -5.7754$

Then,  $C = 0.003102 \approx 0.003$

So, the correlation could be written as:

$$\text{Nu} = 0.003 \text{Re}^{1.02} \text{Pr}^{0.33} \quad (5.5)$$

Figure 5.82 shows the variation of the experimental Nusselt numbers with the predicted Nusselt numbers for different porosity of rectangular strip inserts ( $R_p$  from 0 % to 39 %). It was clear from the figure 5.82 that the total data fell within 33 % to -30 % of the predicted correlation with r.m.s. value of error 16.60 %, whereas 80 % of data fell within + 22 % to -19 % of the predicted correlation.

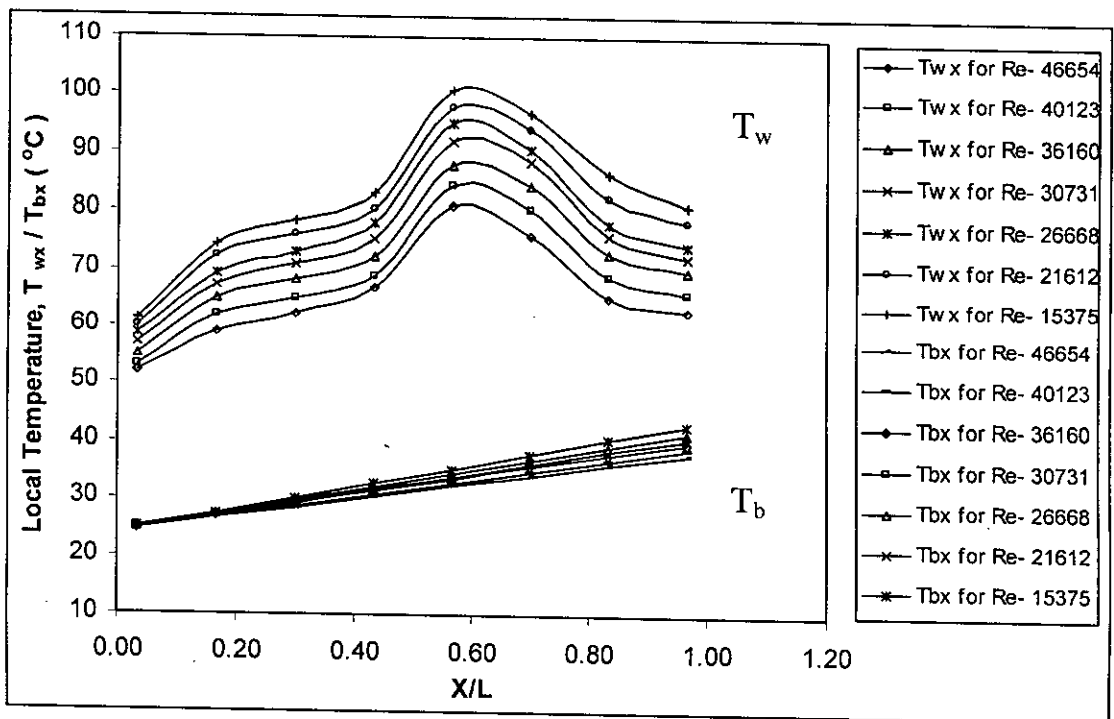


Figure 5.1: Variation of wall and bulk temperatures along axial distance for the tube with perforated rectangular strip insert having porosity,  $R_p = 1.1\%$ .

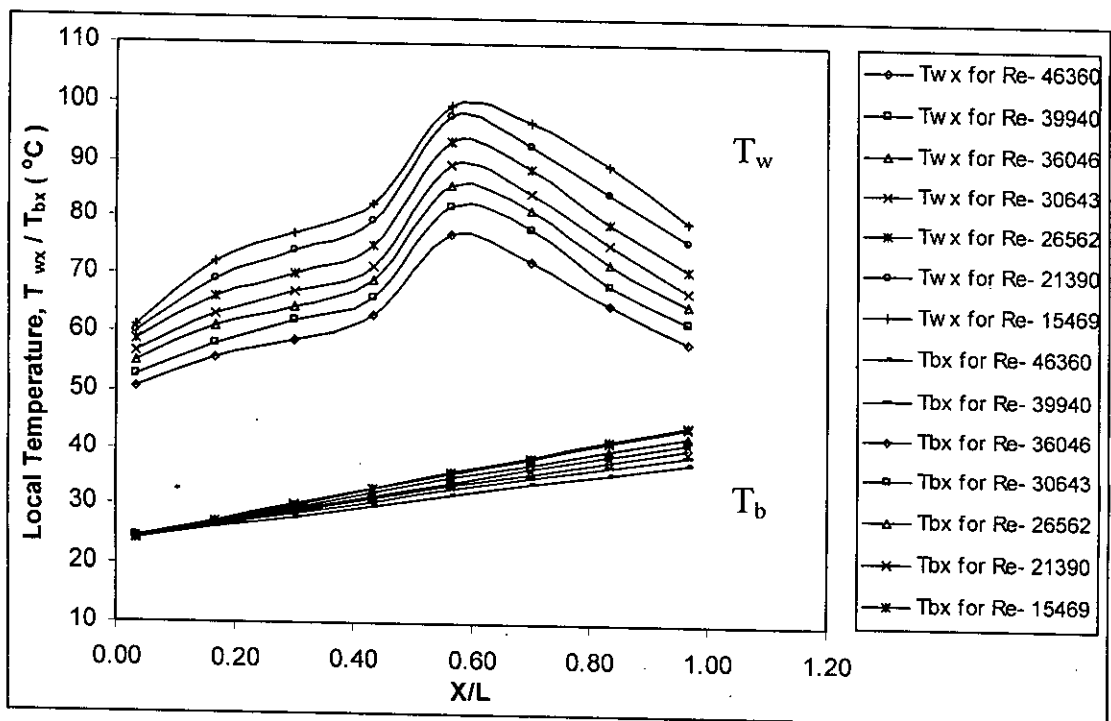


Figure 5.2: Variation of wall and bulk temperatures along axial distance for the tube with perforated rectangular strip insert having porosity,  $R_p = 2.5\%$ .

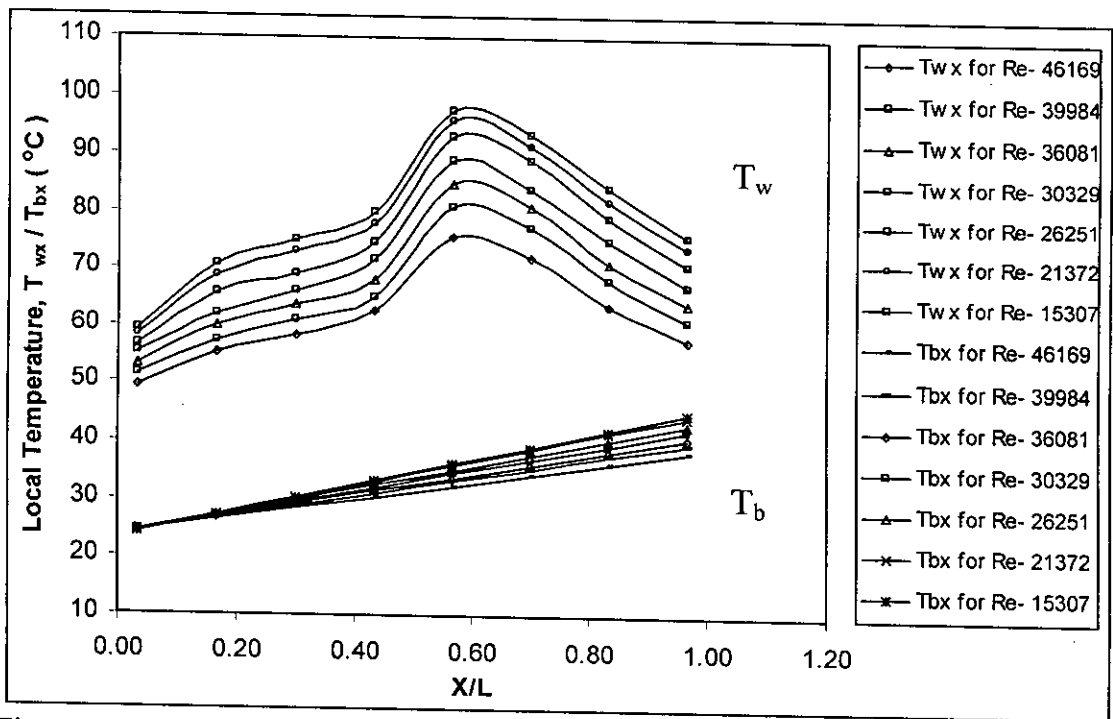


Figure 5.3: Variation of wall and bulk temperatures along axial distance for the tube with perforated rectangular strip insert having porosity,  $R_p = 4.4\%$ .

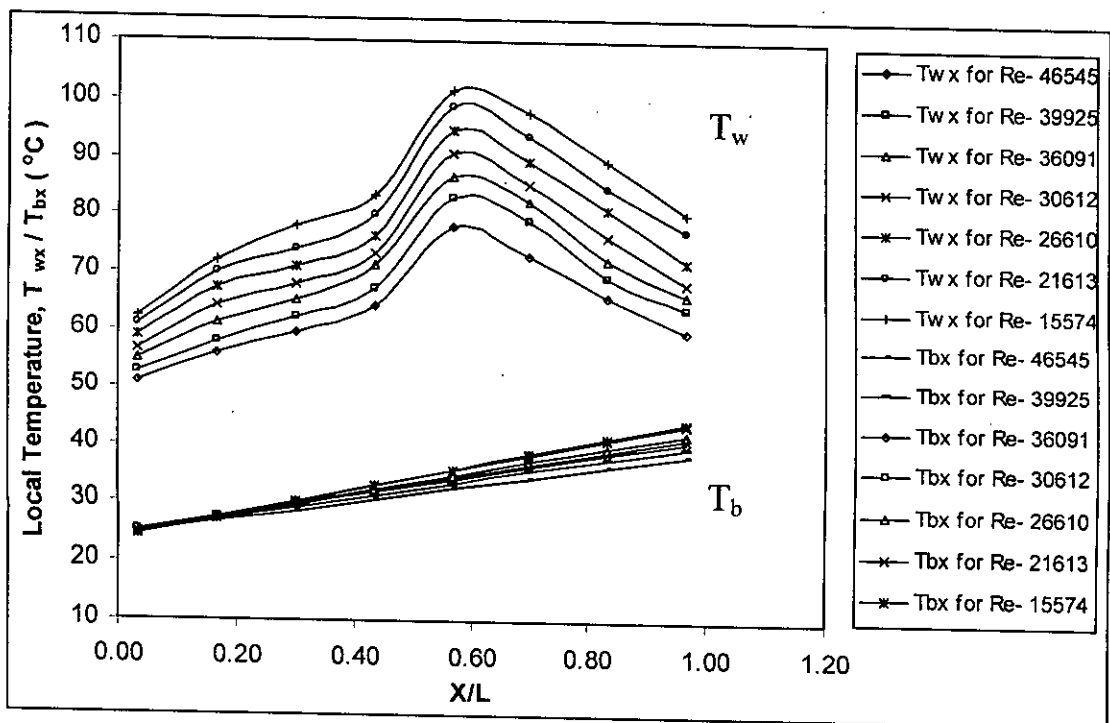


Figure 5.4: Variation of wall and bulk temperatures along axial distance for the tube with perforated rectangular strip insert having porosity,  $R_p = 6.8\%$ .

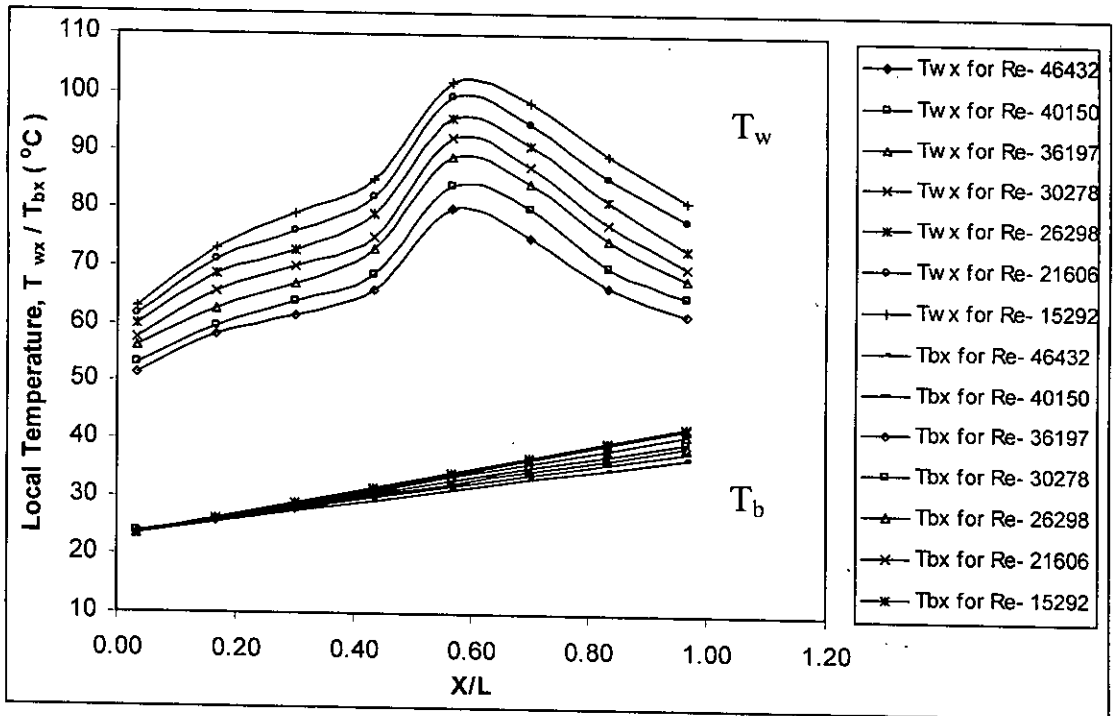


Figure 5.5: Variation of wall and bulk temperatures along axial distance for the tube with perforated rectangular strip insert having porosity,  $R_p=13.3\%$ .

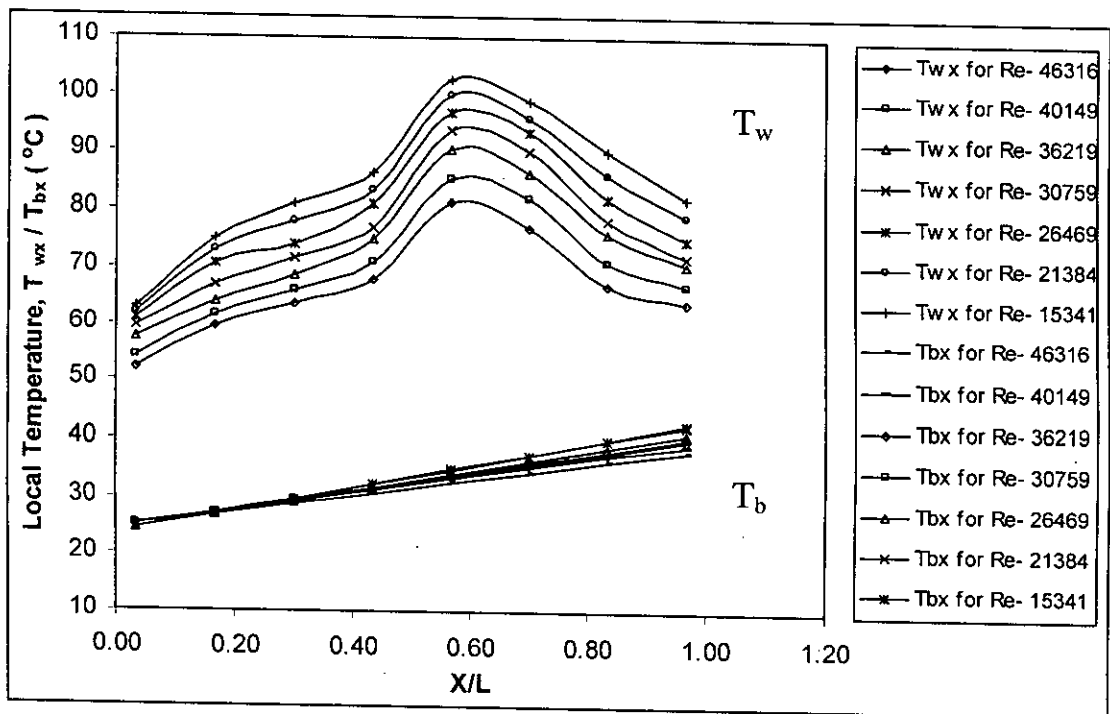


Figure 5.6: Variation of wall and bulk temperatures along axial distance for the tube with perforated rectangular strip insert having porosity,  $R_p=17.4\%$ .

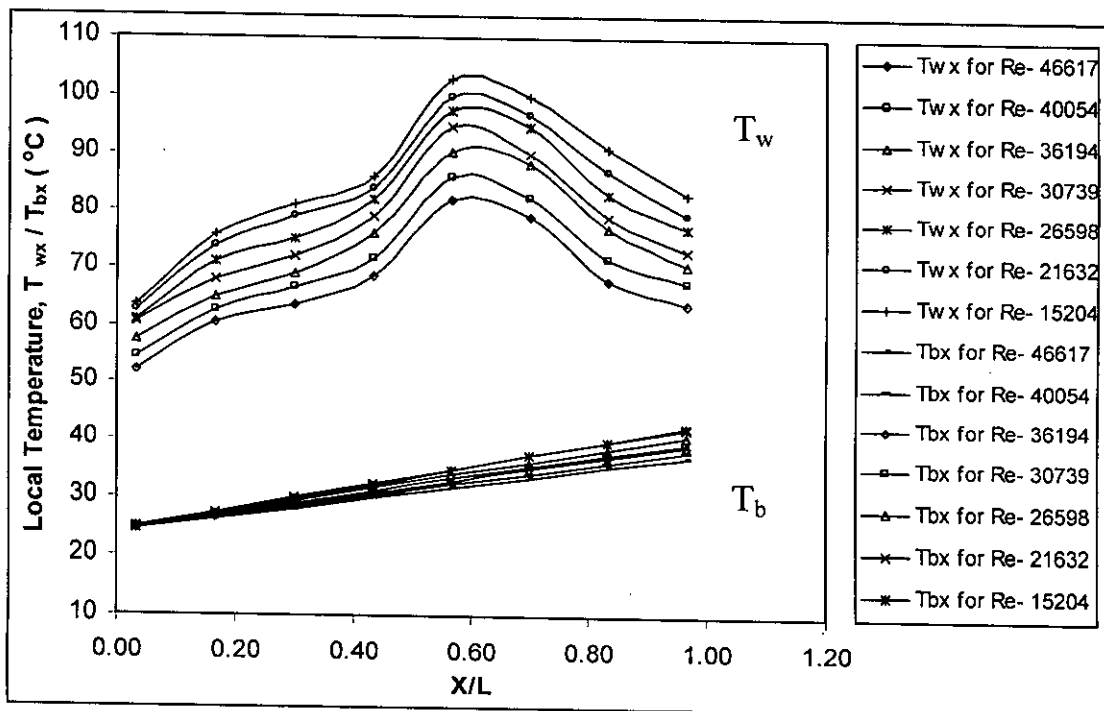


Figure 5.7: Variation of wall and bulk temperatures along axial distance for the tube with perforated rectangular strip insert having porosity,  $R_p=22\%$ .

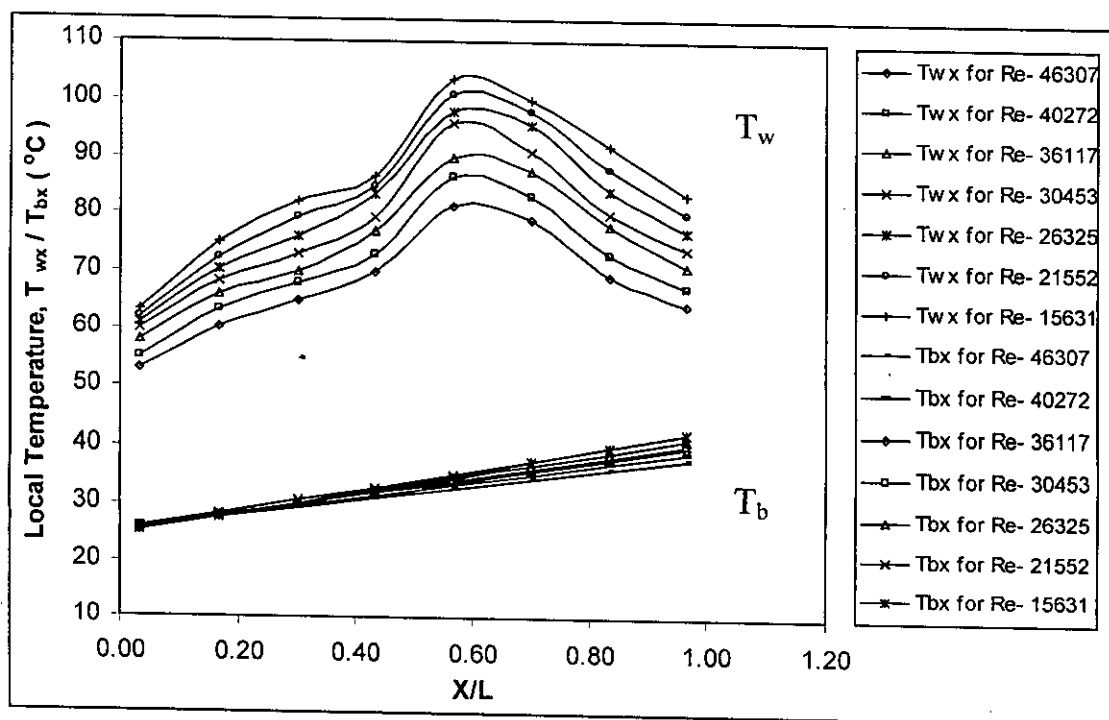


Figure 5.8: Variation of wall and bulk temperatures along axial distance for the tube with perforated rectangular strip insert having porosity,  $R_p=27.1\%$ .

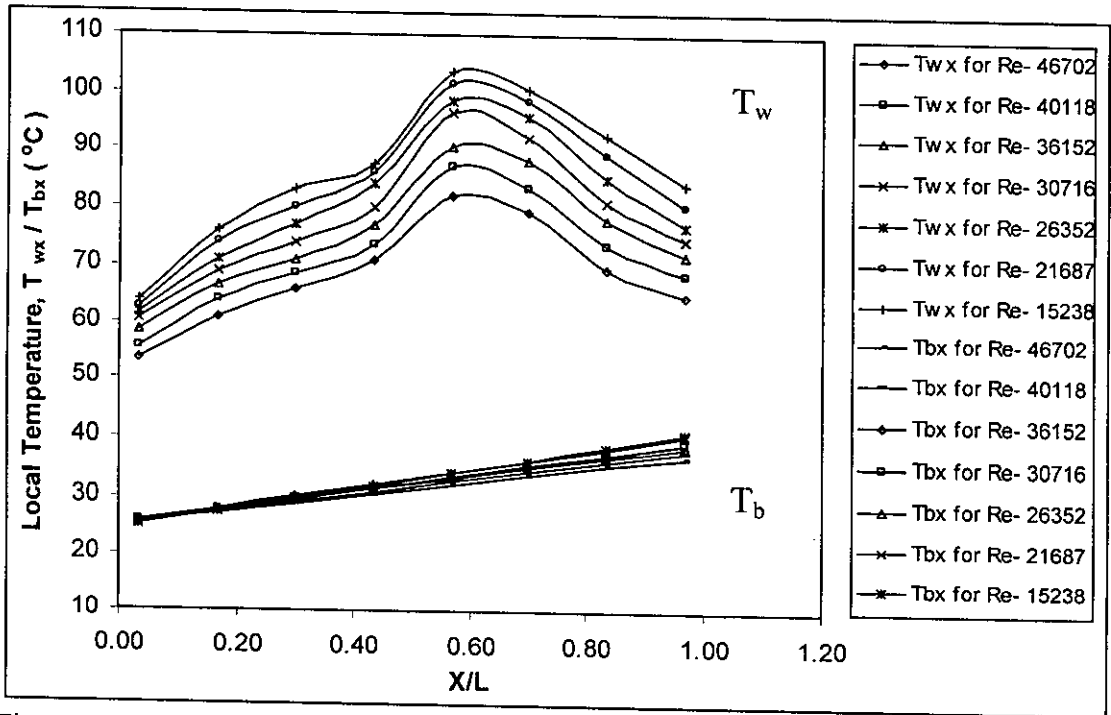


Figure 5.9: Variation of wall and bulk temperatures along axial distance for the tube with perforated rectangular strip insert having porosity,  $R_p = 39\%$ .

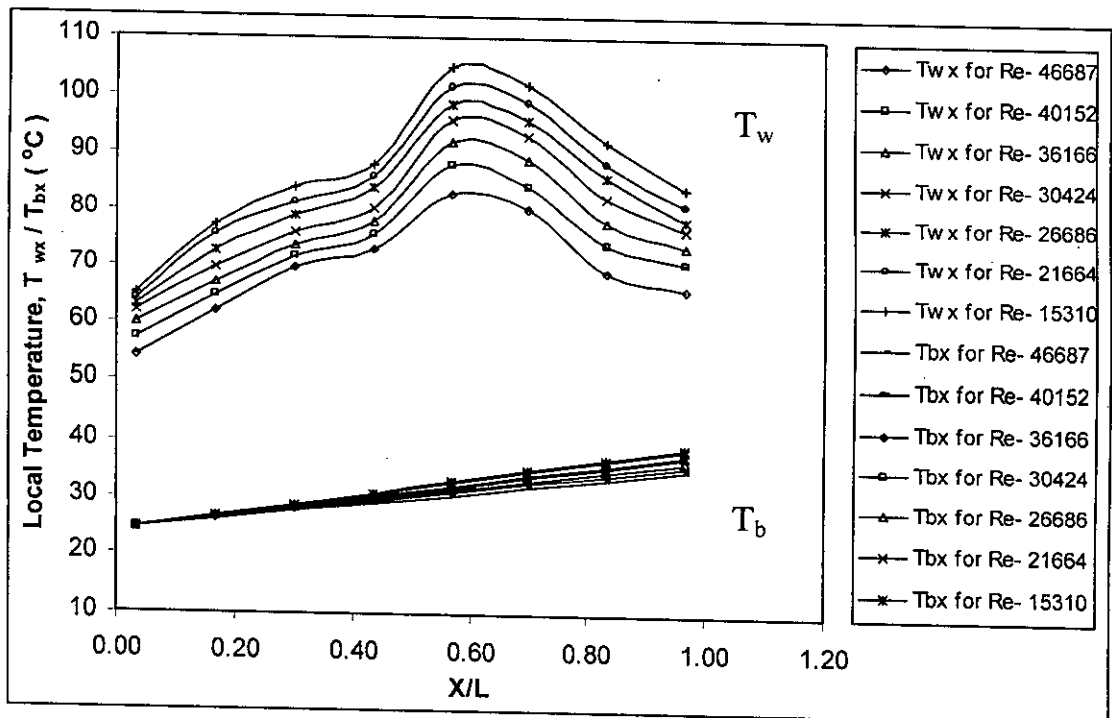


Figure 5.10: Variation of wall and bulk temperatures along axial distance for the tube with rectangular strip insert having porosity,  $R_p = 0$ .

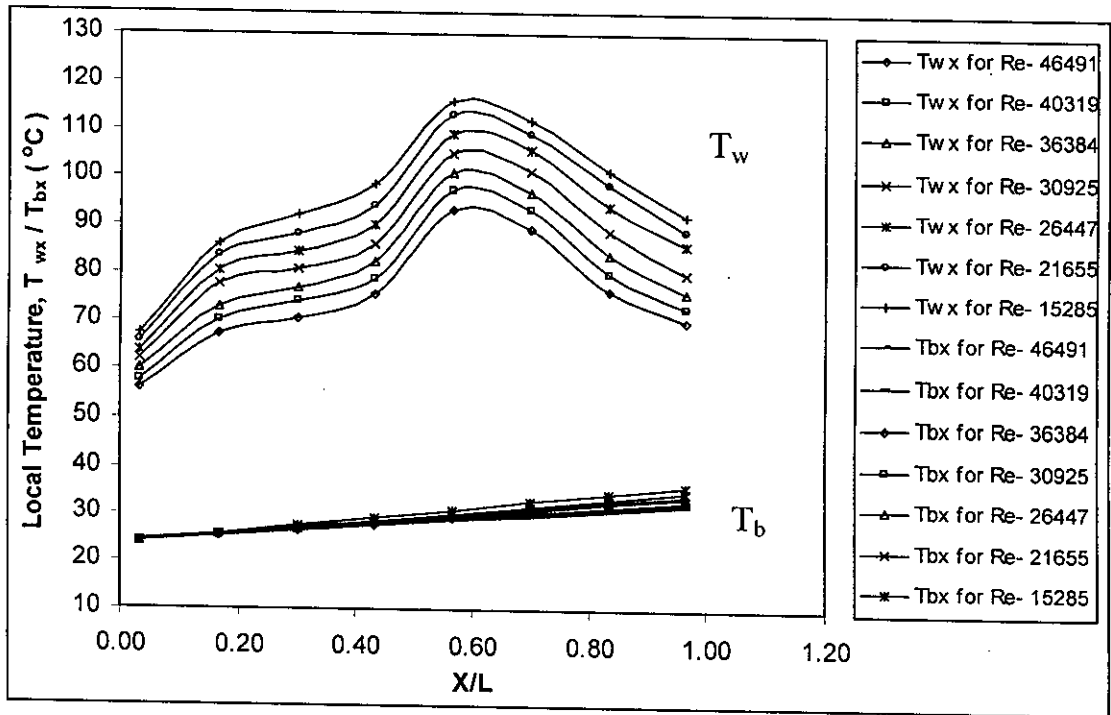


Figure 5.11: Variation of wall and bulk temperatures along axial distance for the plain tube.

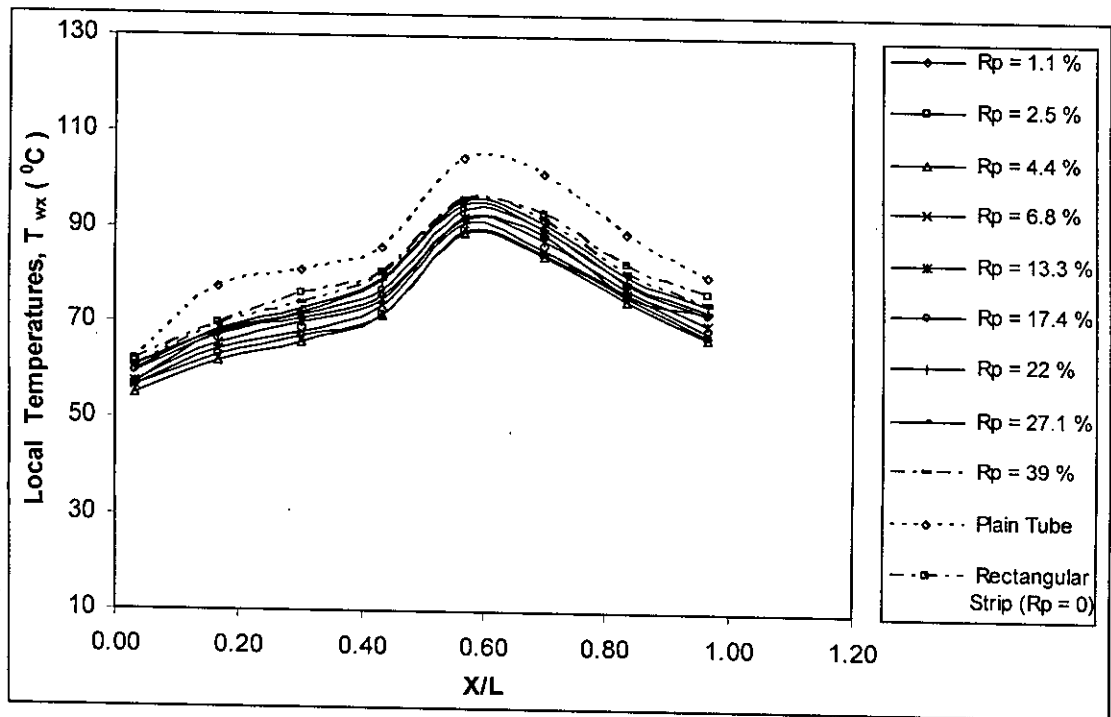


Figure 5.11(a): Variation of wall temperatures along axial distance for different porosity of inserts at Reynolds number around 30,925.

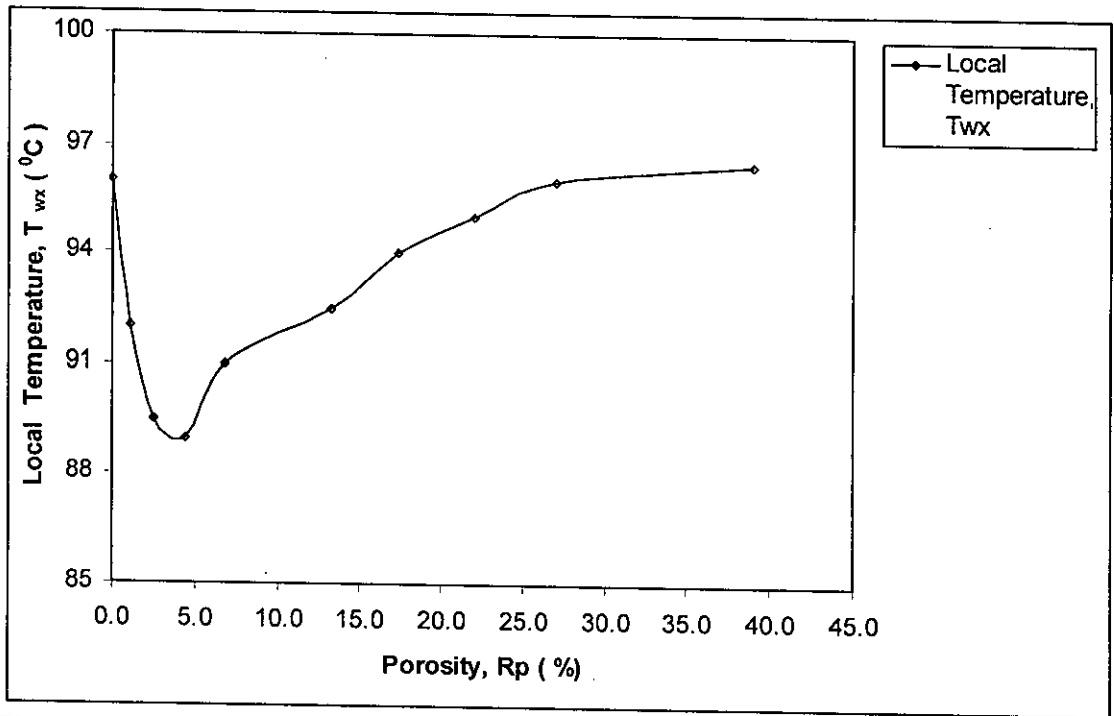


Figure 5.11(b): Variation of wall temperatures with different porosity ( $R_p$  from 0 %-39 %) of inserts for axial distance of  $X/L = 0.57$  and at Reynolds number around 30,925.

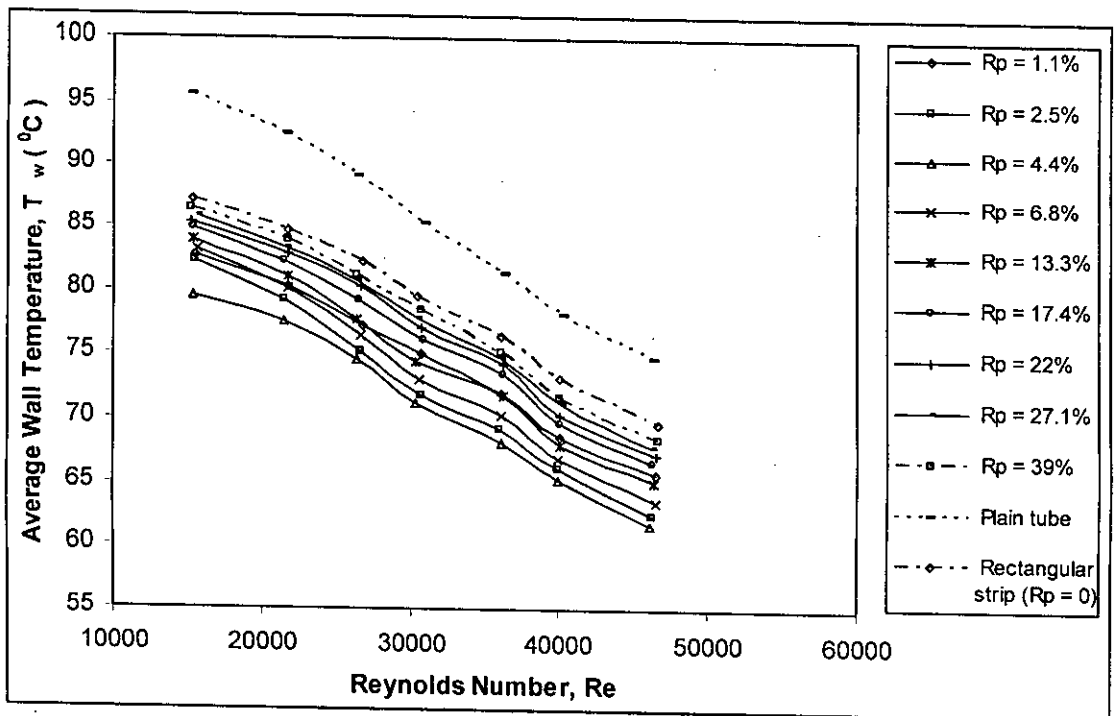


Figure 5.12: Variation of the average wall temperatures for different porosity of rectangular strip inserts at different Reynolds numbers.



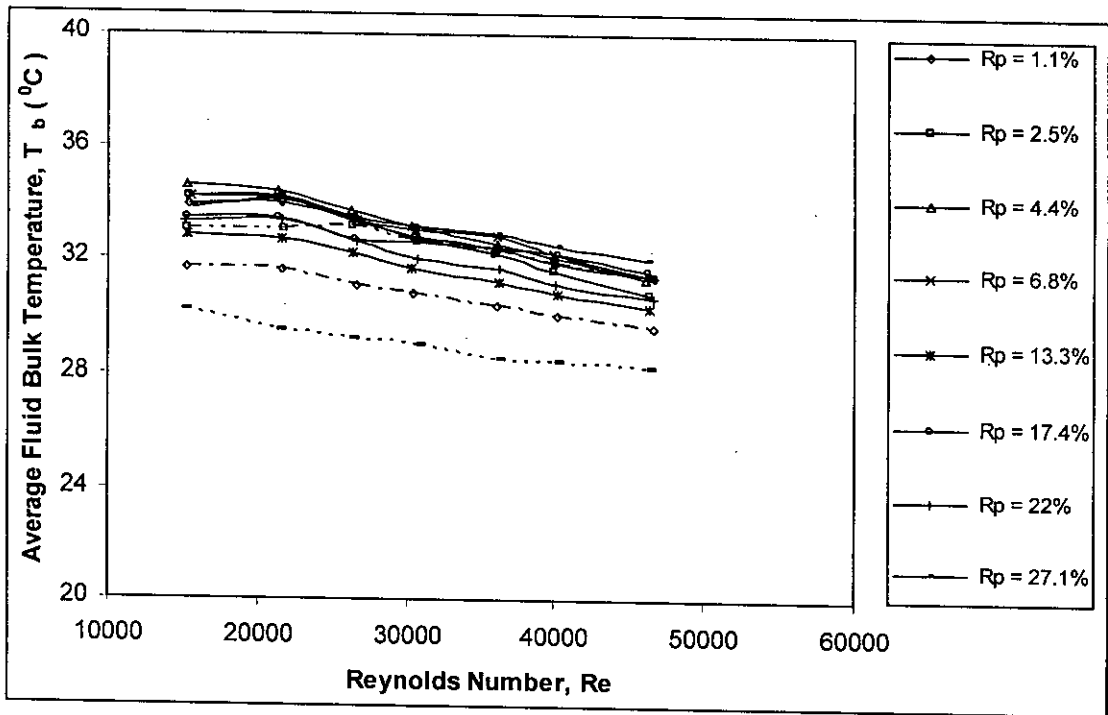


Figure 5.13: Variation of the average fluid bulk temperatures for different porosity of rectangular strip inserts at different Reynolds numbers.

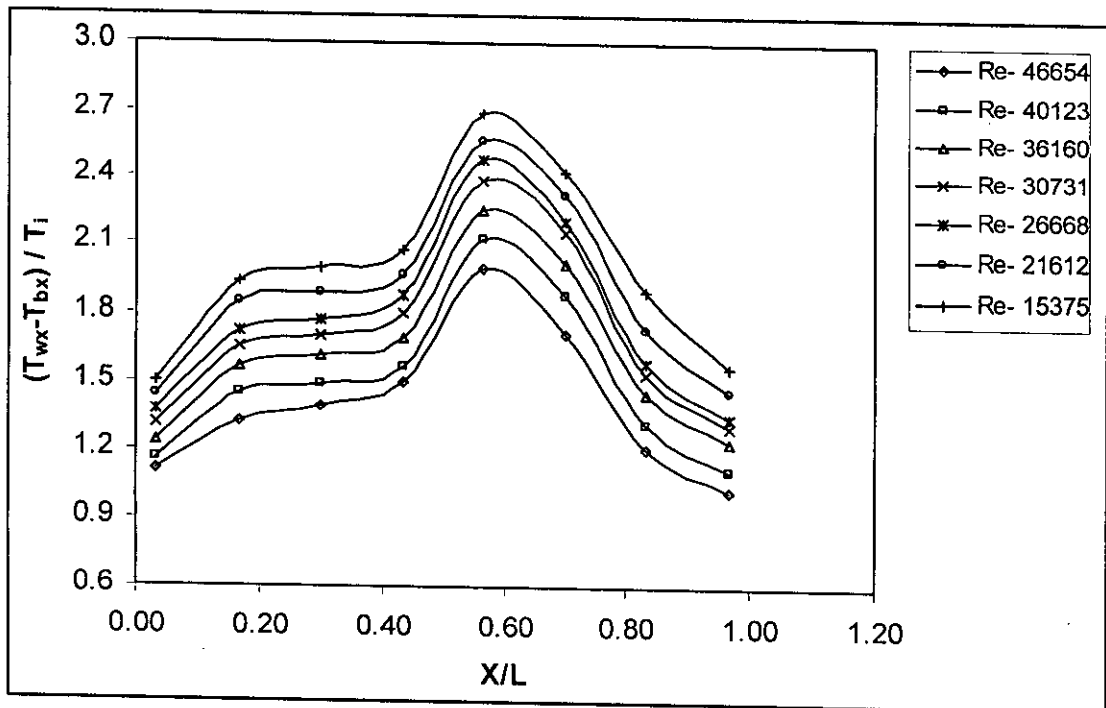


Figure 5.14: Variation of dimensionless temperature differences along axial distance for the tube with perforated rectangular strip insert having porosity,  $R_p = 1.1\%$ .

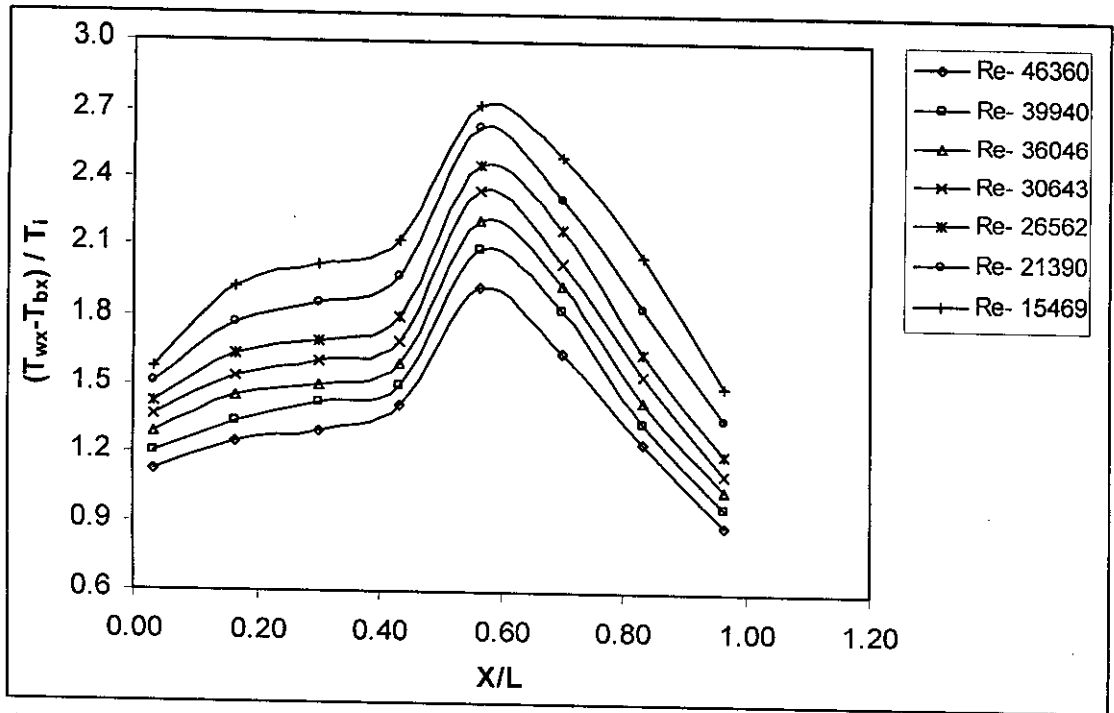


Figure: 5.15: Variation of dimensionless temperature differences along axial distance for the tube with perforated rectangular strip insert having porosity,  $R_p = 2.5\%$ .

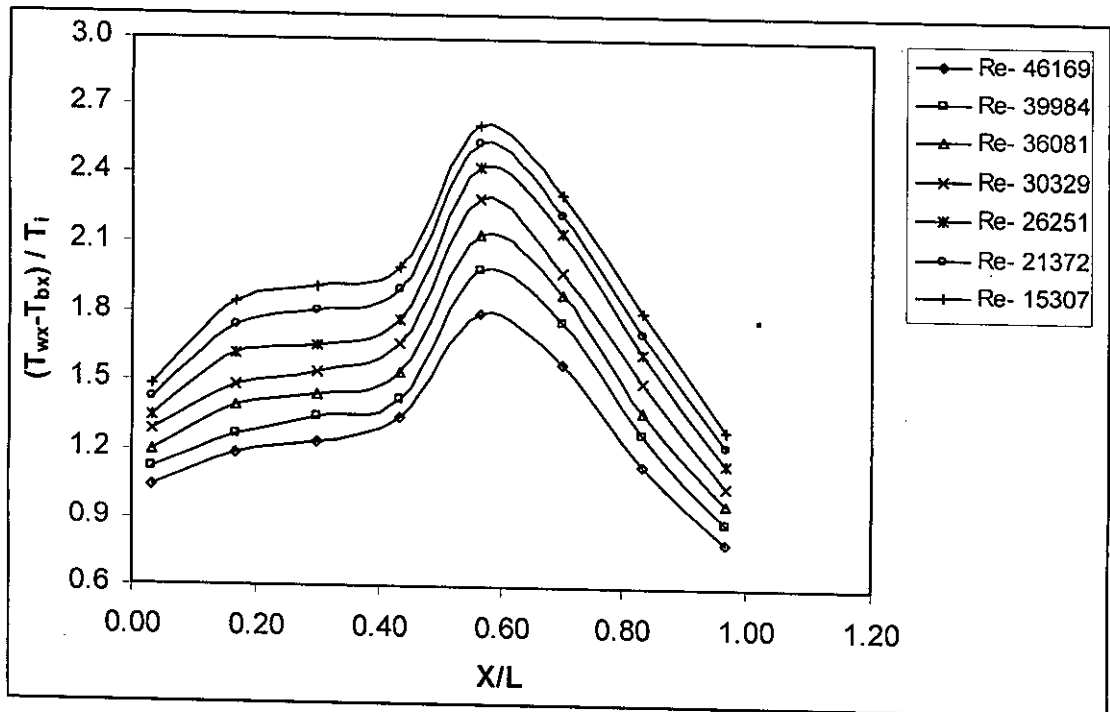


Figure: 5.16: Variation of dimensionless temperature differences along axial distance for the tube with perforated rectangular strip insert having porosity,  $R_p = 4.4\%$ .

105957

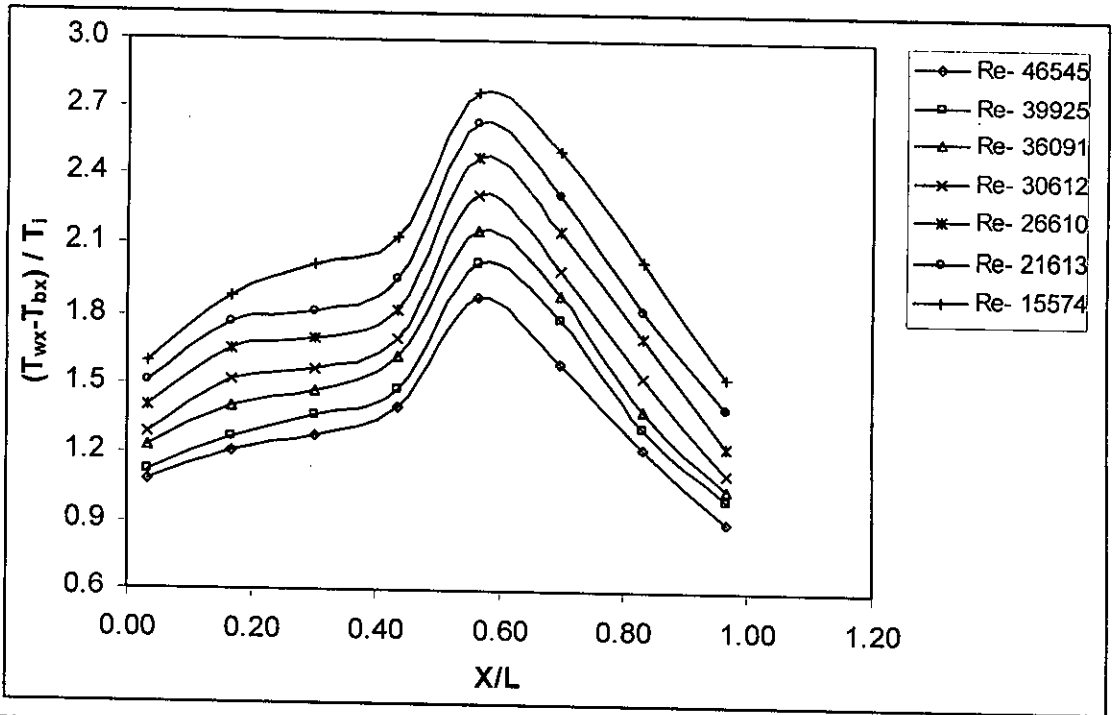


Figure 5.17: Variation of dimensionless temperature differences along axial distance for the tube with perforated rectangular strip insert having porosity,  $R_p = 6.8\%$ .

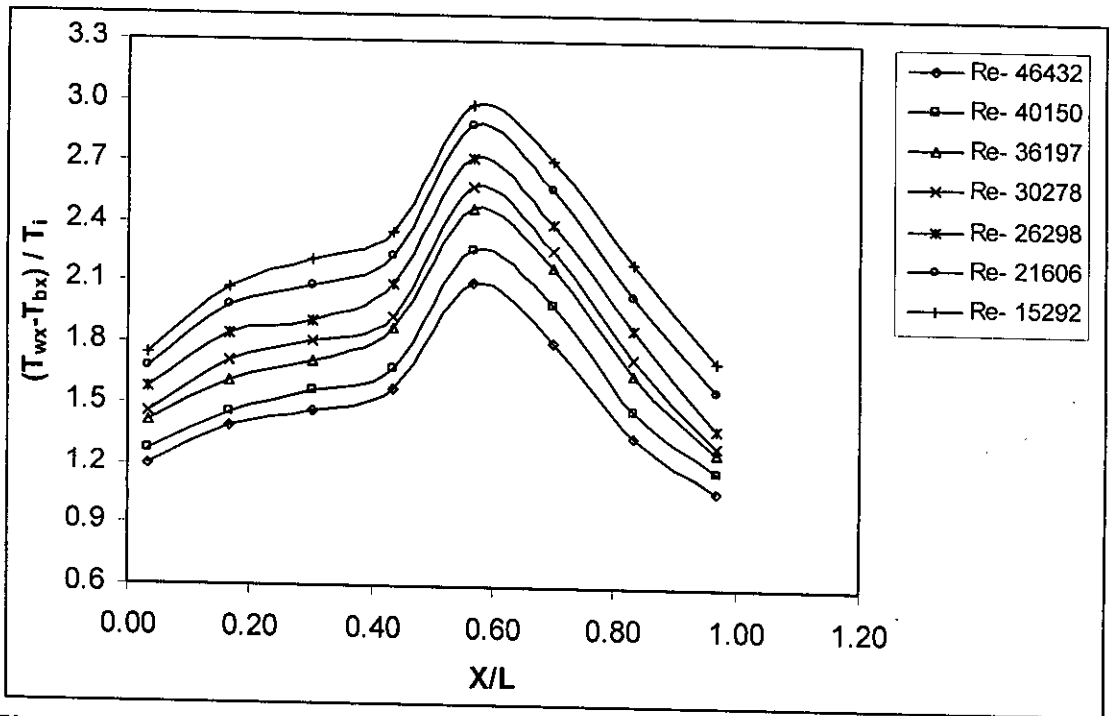


Figure 5.18: Variation of dimensionless temperature differences along axial distance for the tube with perforated rectangular strip insert having porosity,  $R_p = 13.3\%$ .

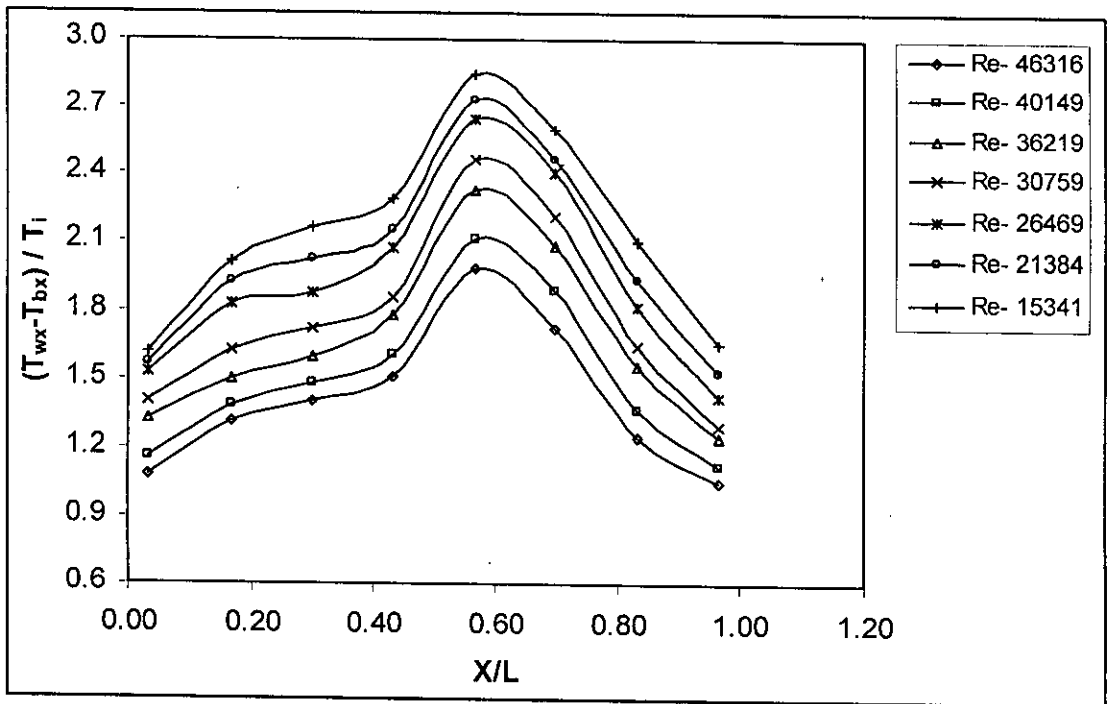


Figure 5.19: Variation of dimensionless temperature differences along axial distance for the tube with perforated rectangular strip insert having porosity,  $R_p = 17.4\%$ .

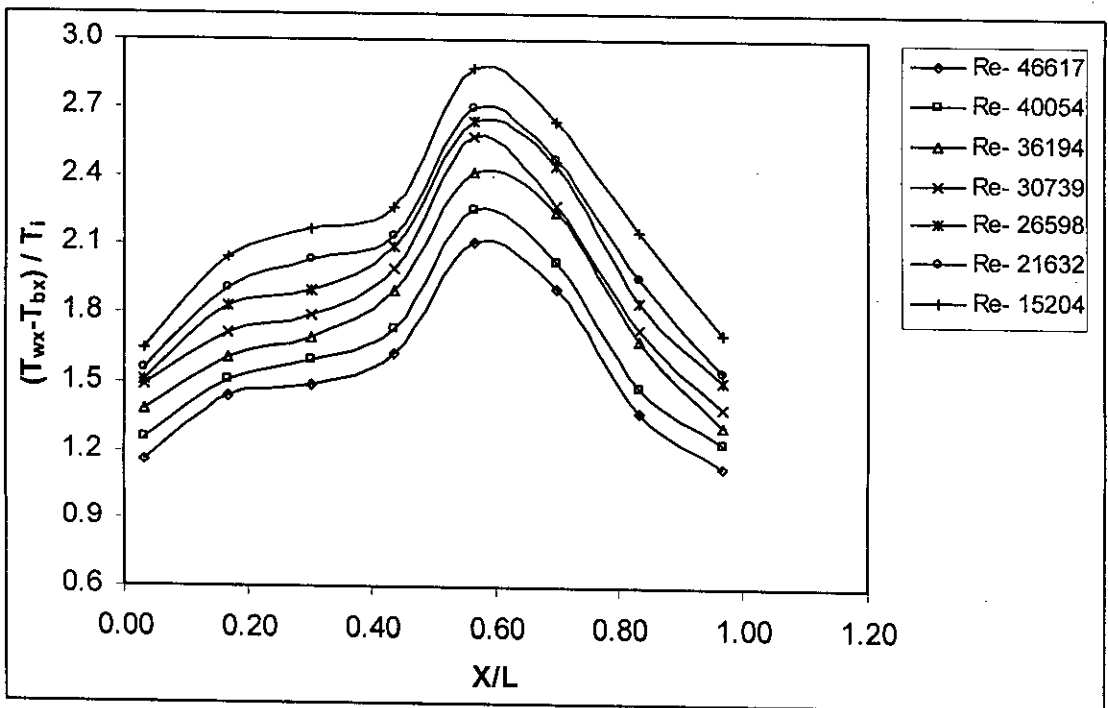


Figure 5.20: Variation of dimensionless temperature differences along axial distance for the tube with perforated rectangular strip insert having porosity,  $R_p = 22\%$ .

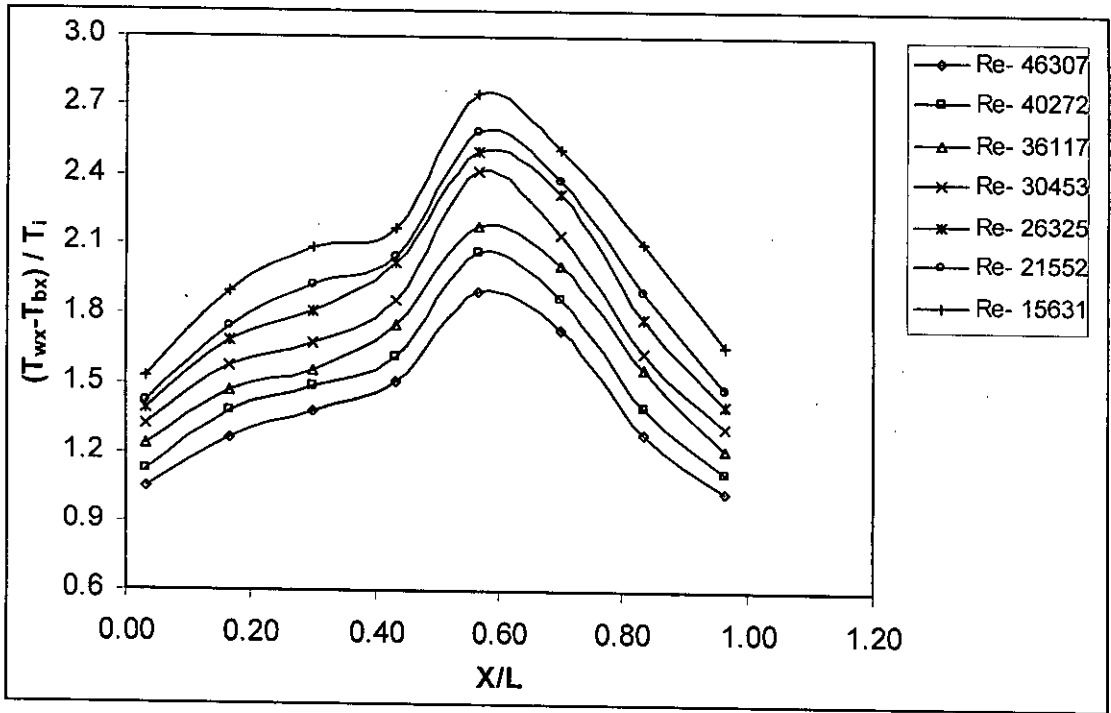


Figure 5.21: Variation of dimensionless temperature differences along axial distance for the tube with perforated rectangular strip insert having porosity,  $R_p = 27.1\%$ .

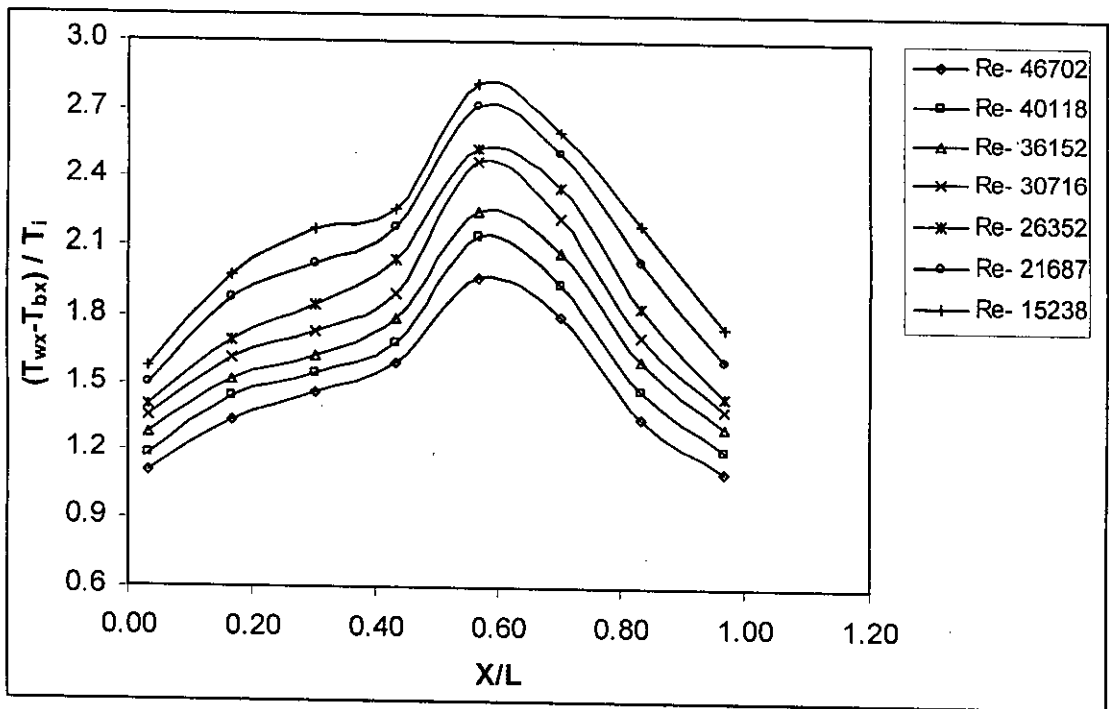


Figure 5.22: Variation of dimensionless temperature differences along axial distance for the tube with perforated rectangular strip insert having porosity,  $R_p = 39\%$ .

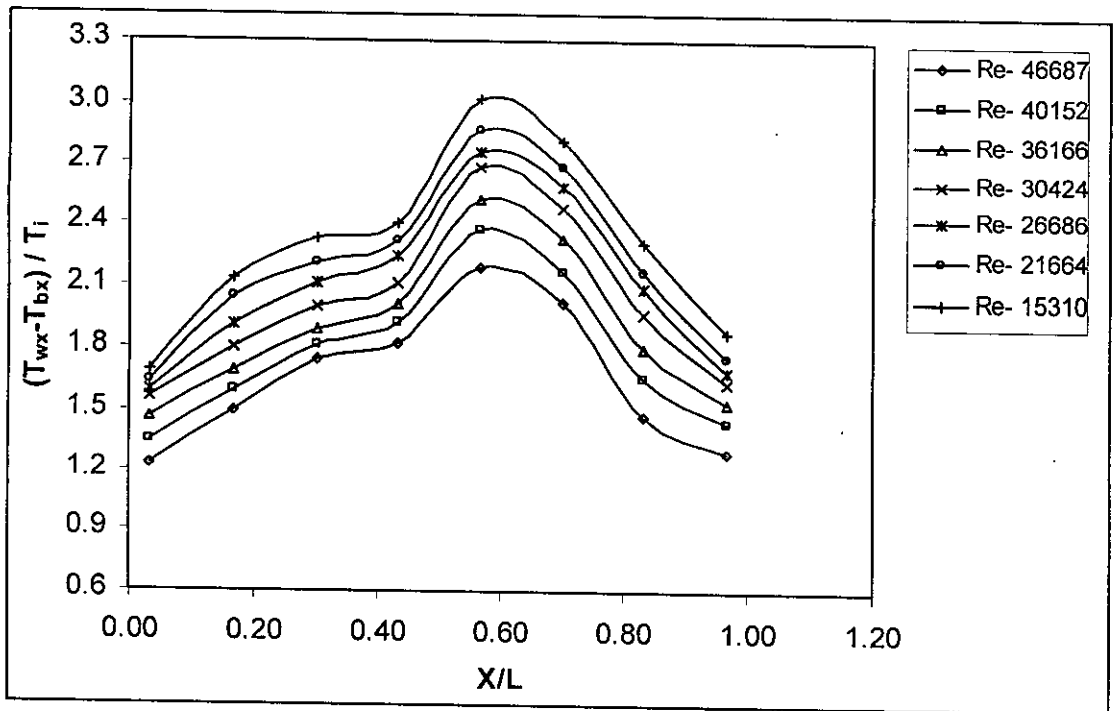


Figure: 5.23: Variation of dimensionless temperature differences along axial distance for the tube with rectangular strip insert having porosity,  $R_p = 0$ .

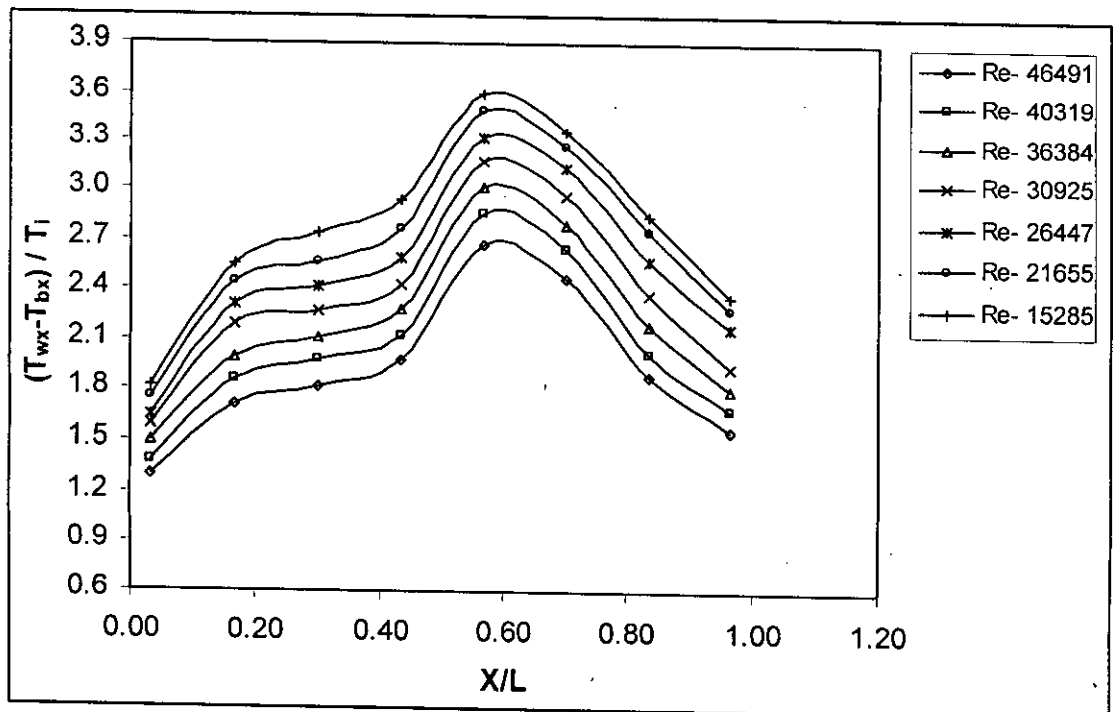


Figure: 5.24: Variation of dimensionless temperature differences along axial distance for the plain tube.

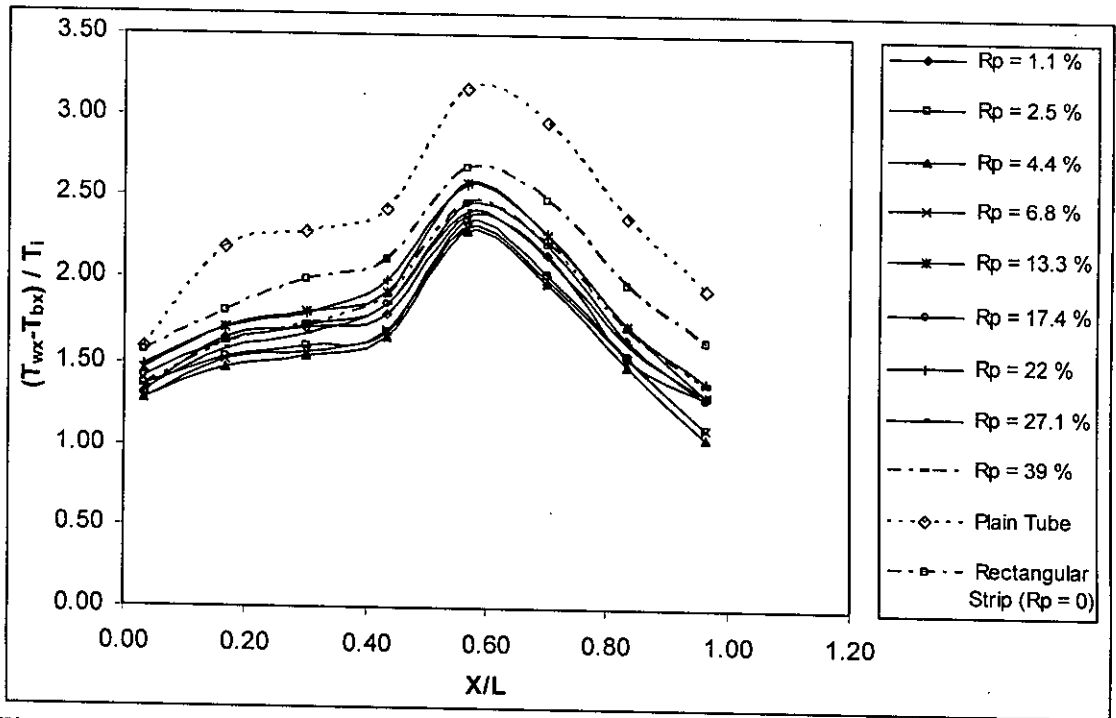


Figure 5.24 (a): Variation of dimensionless temperature differences along axial distance for different porosity of inserts at Reynolds number around 30,925.

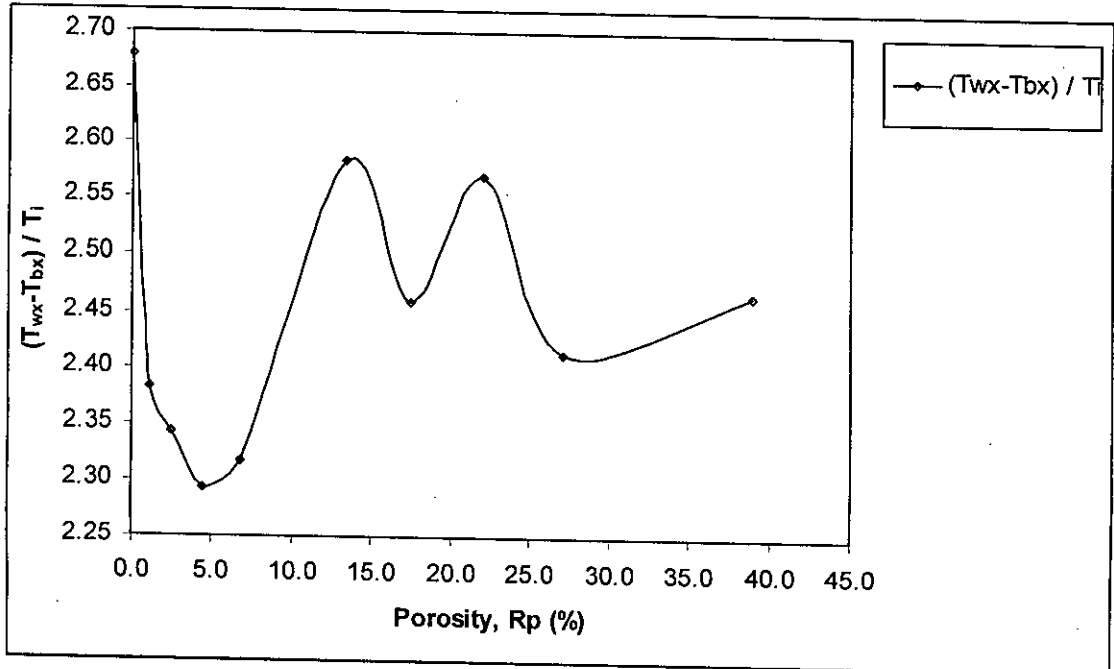


Figure 5.24(b): Variation of dimensionless temperature differences with different porosity ( $R_p$  from 0 %-39 %) of inserts for axial distance of  $X/L = 0.57$  and at Reynolds number around 30,925.

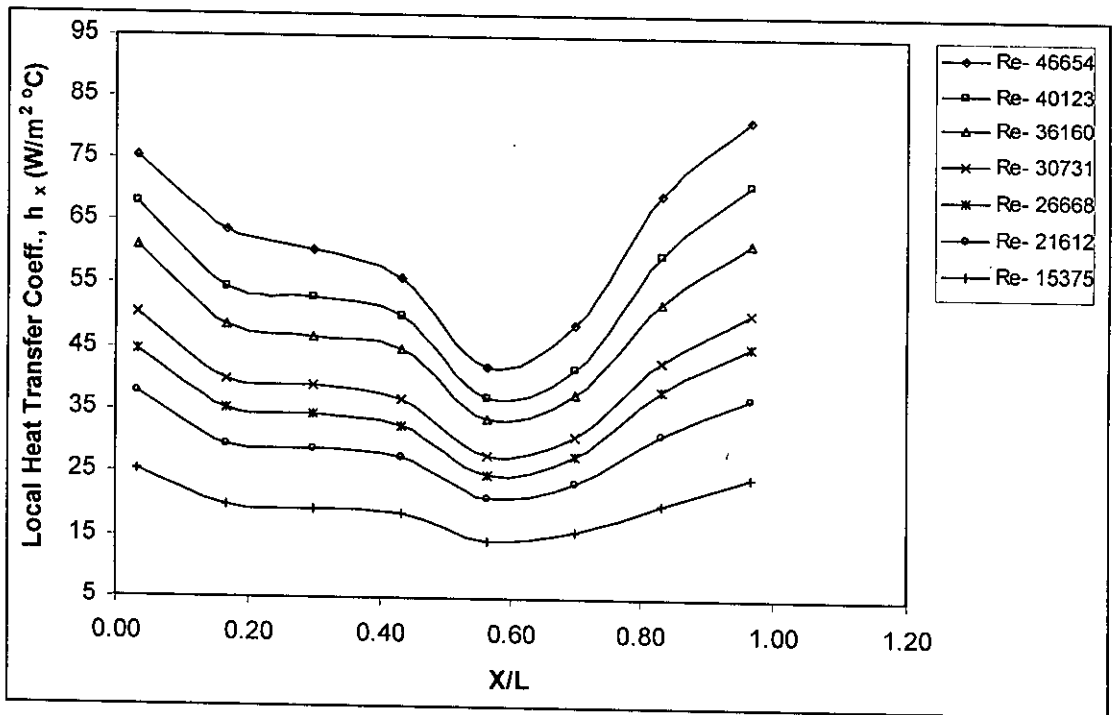


Figure 5.25: Variation of the local heat transfer coefficient along axial distance for the tube with insert having porosity,  $R_p = 1.1\%$  at different Reynolds numbers.

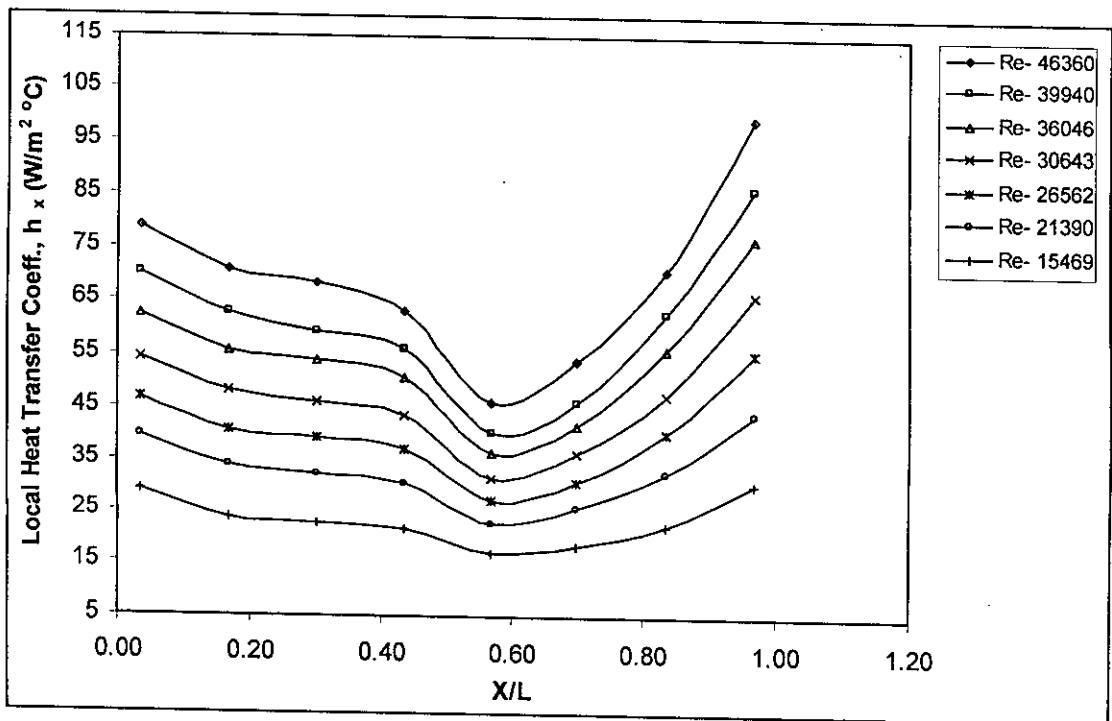


Figure 5.26: Variation of the local heat transfer coefficient along axial distance for the tube with insert having porosity,  $R_p = 2.5\%$  at different Reynolds numbers.



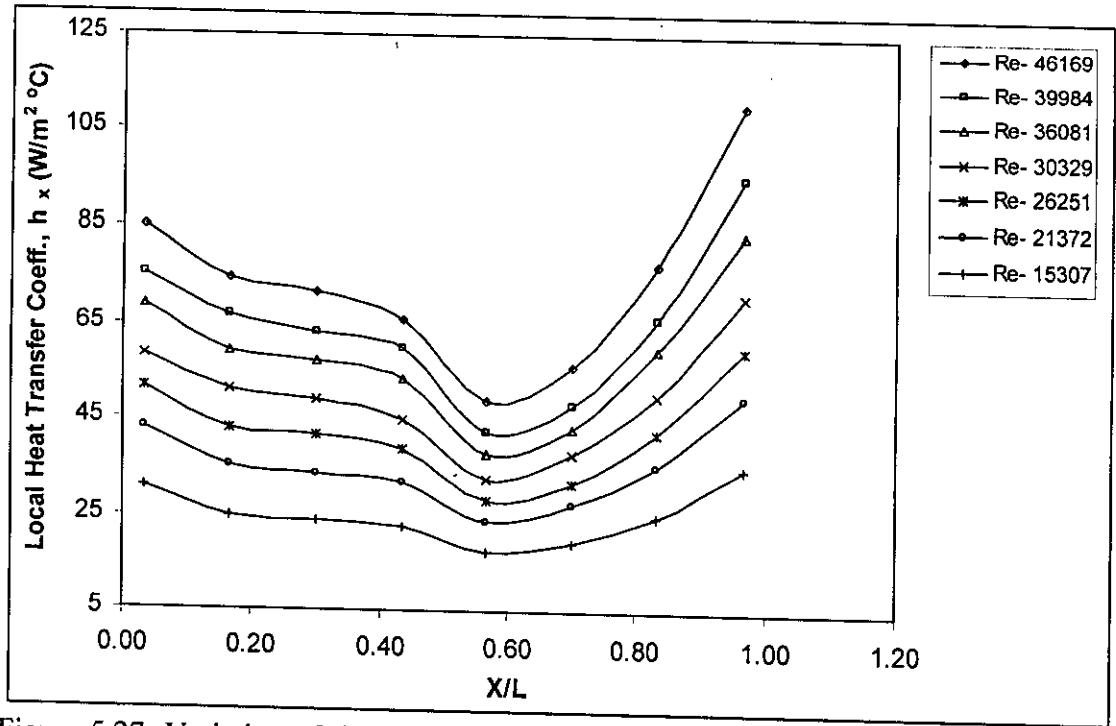


Figure 5.27: Variation of the local heat transfer coefficient along axial distance for the tube with insert having porosity,  $R_p = 4.4\%$  at different Reynolds numbers.

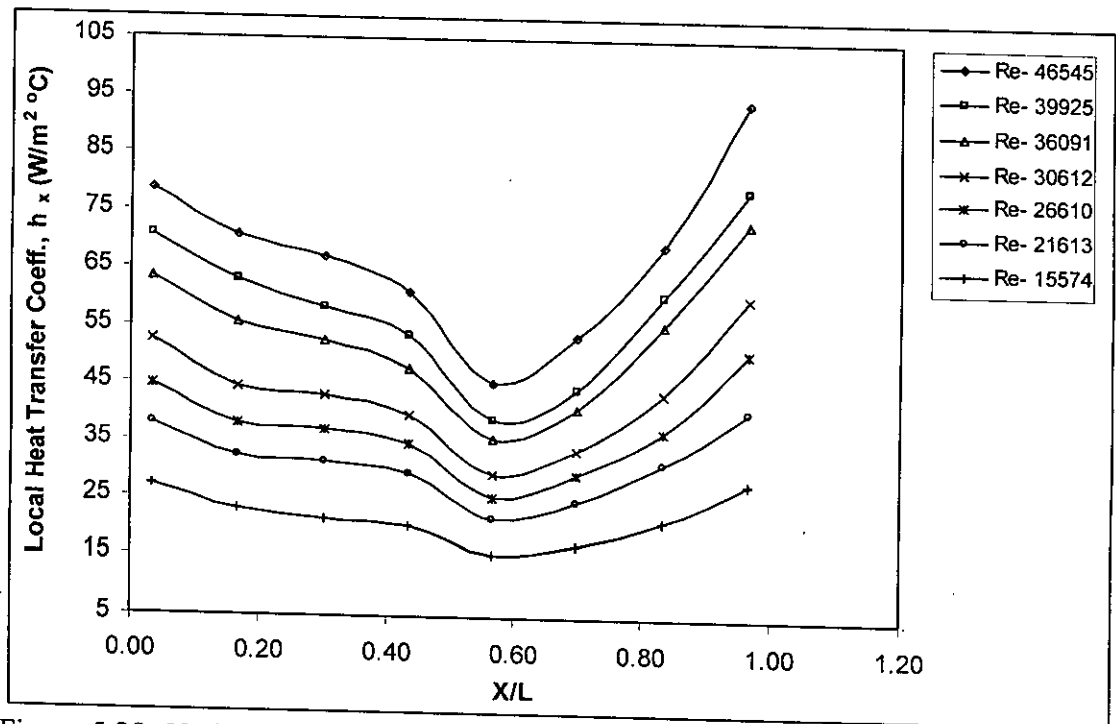


Figure 5.28: Variation of the local heat transfer coefficient along axial distance for the tube with insert having porosity,  $R_p = 6.8\%$  at different Reynolds numbers.

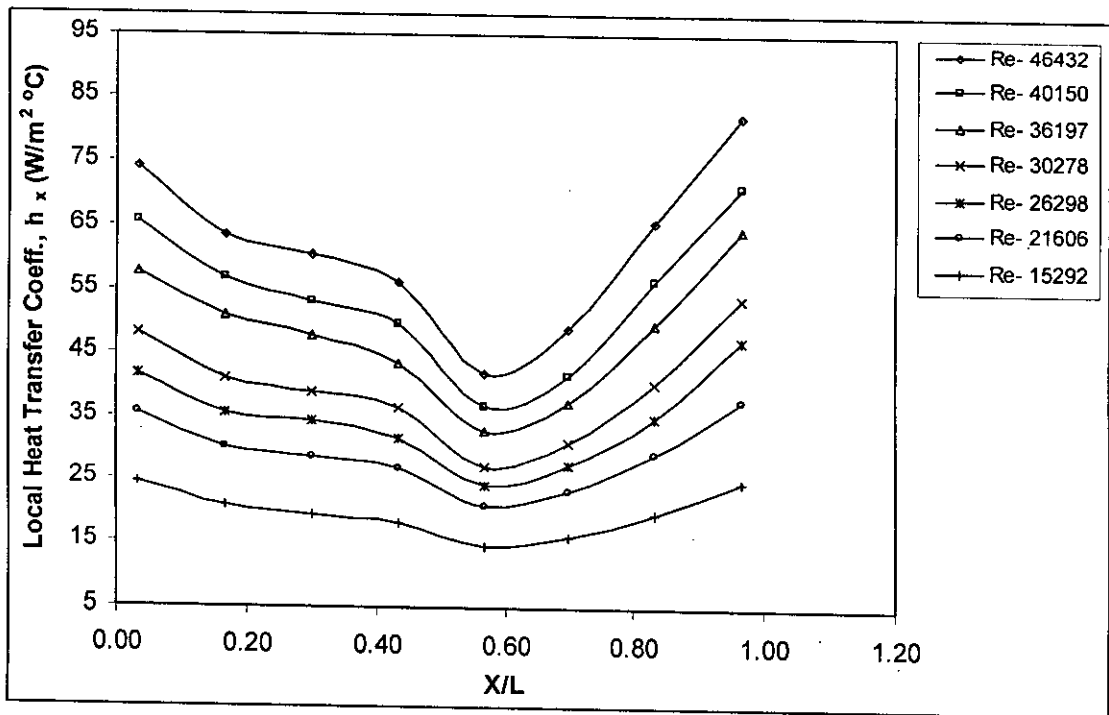


Figure 5.29: Variation of the local heat transfer coefficient along axial distance for the tube with insert having porosity,  $R_p = 13.3\%$  at different Reynolds numbers.

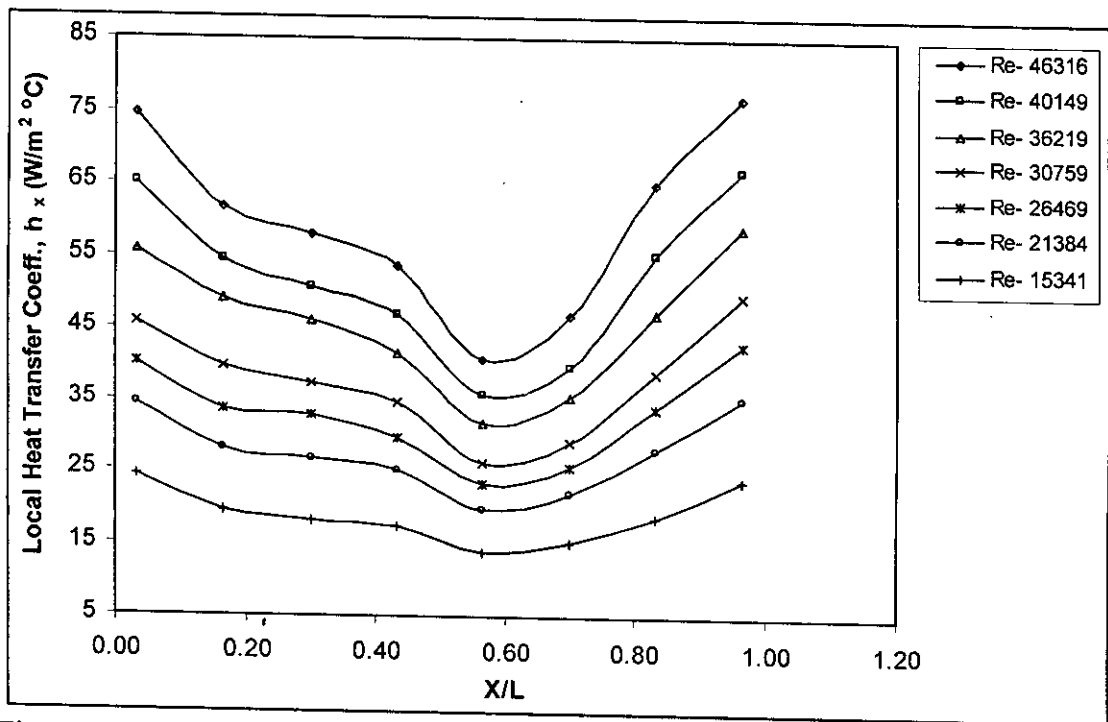


Figure 5.30: Variation of the local heat transfer coefficient along axial distance for the tube with insert having porosity,  $R_p = 17.4\%$  at different Reynolds numbers.

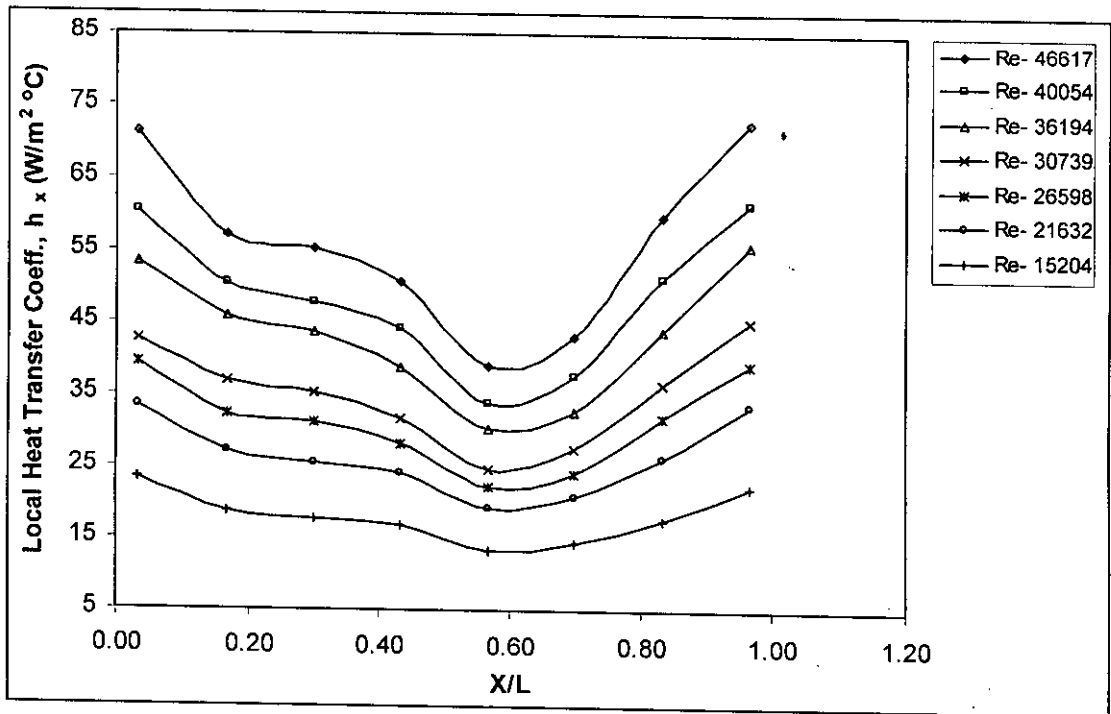


Figure 5.31: Variation of the local heat transfer coefficient along axial distance for the tube with insert having porosity,  $R_p = 22\%$  at different Reynolds numbers.

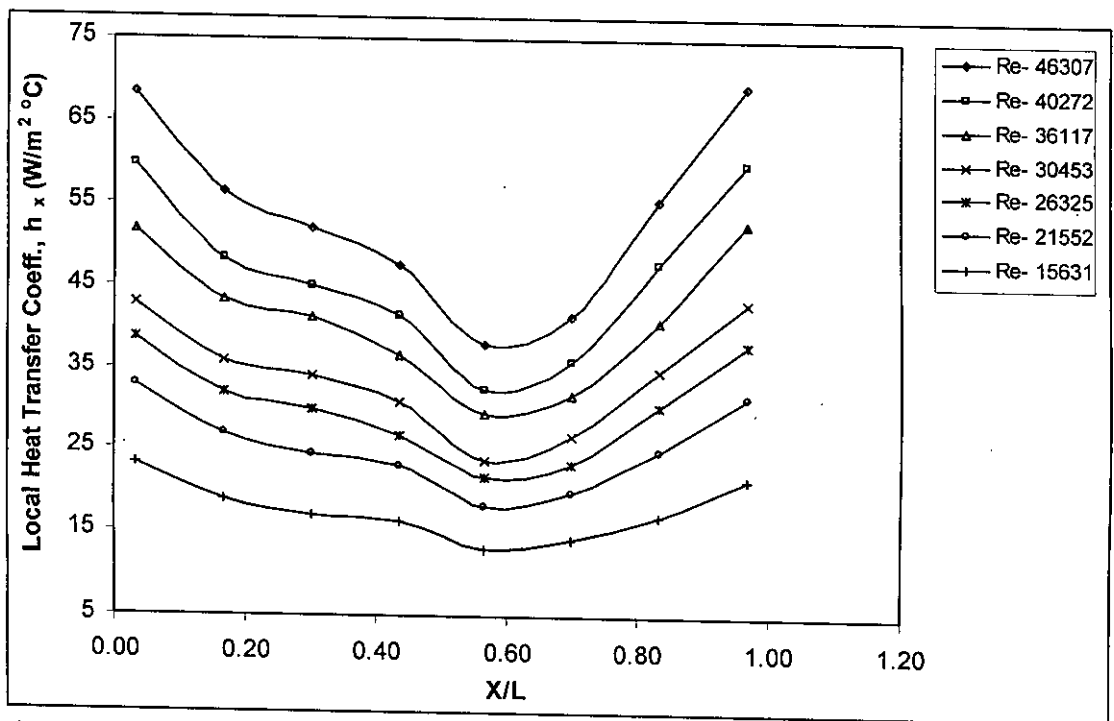


Figure 5.32: Variation of the local heat transfer coefficient along axial distance for the tube with insert having porosity,  $R_p = 27.1\%$  at different Reynolds numbers.

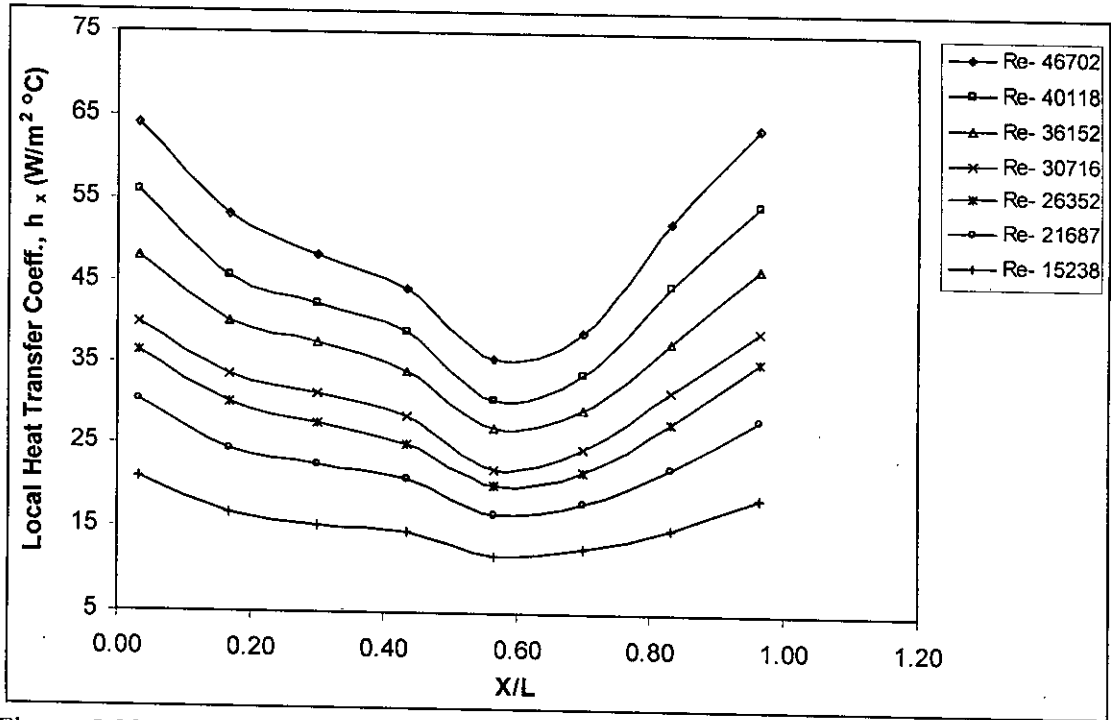


Figure 5.33: Variation of the local heat transfer coefficient along axial distance for the tube with insert having porosity,  $R_p = 39\%$  at different Reynolds numbers.

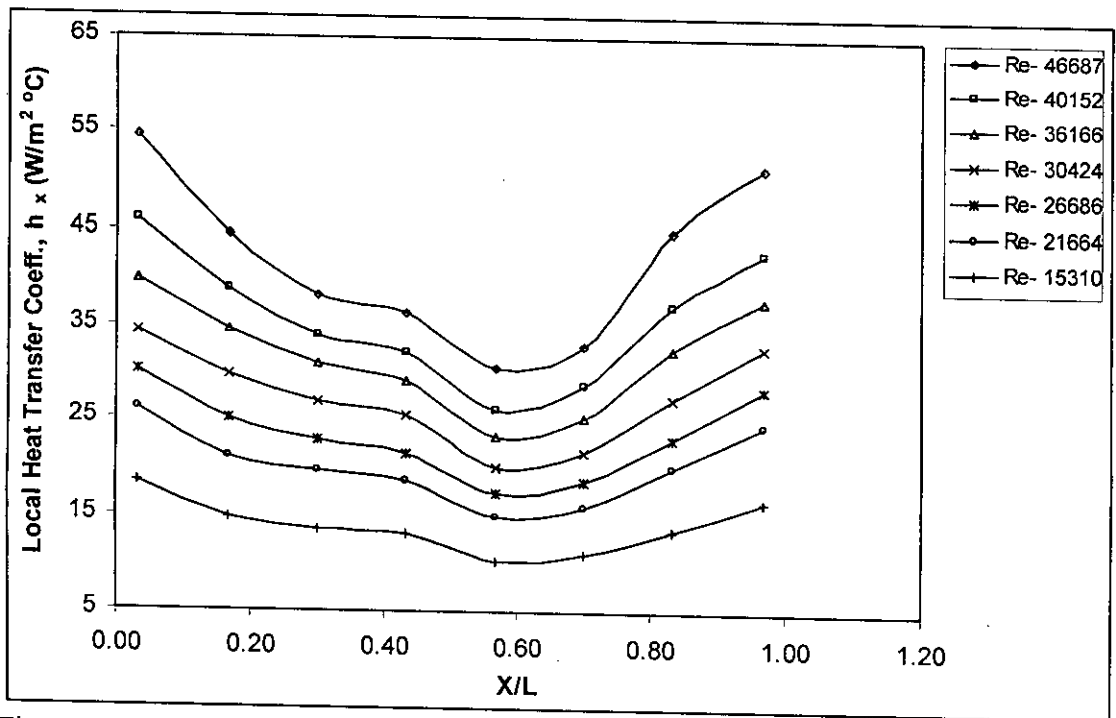


Figure 5.34: Variation of the local heat transfer coefficient along axial distance for the tube with rectangular strip insert having porosity,  $R_p = 0$  at different Reynolds numbers.

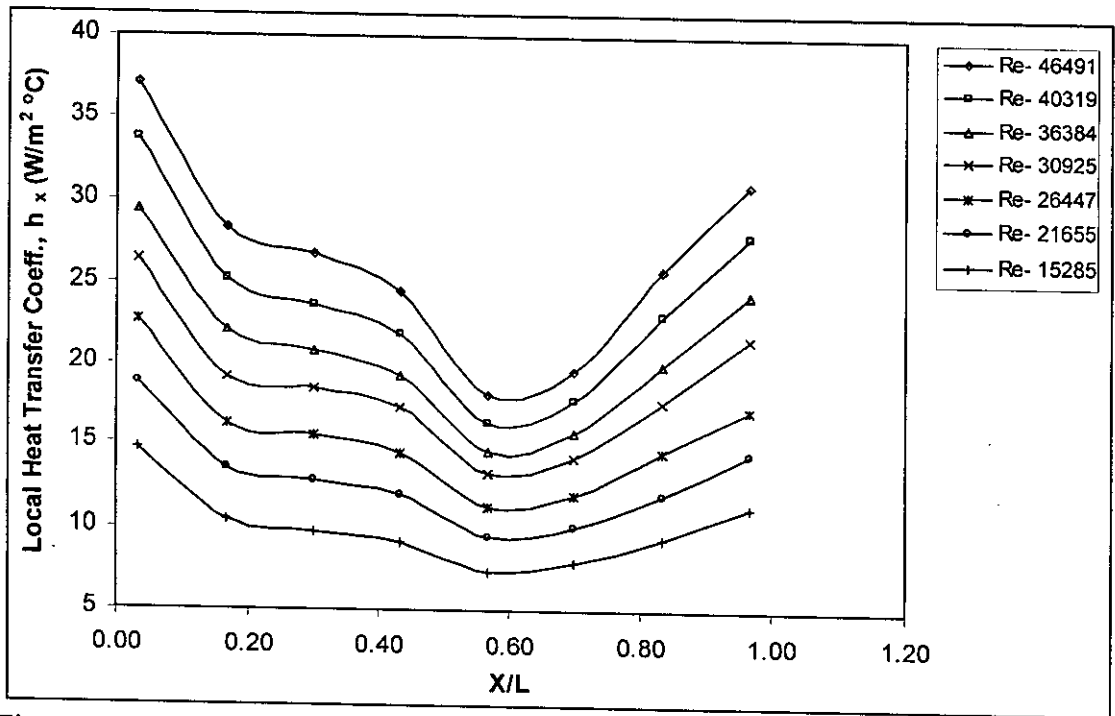


Figure 5.35: Variation of the local heat transfer coefficient along axial distance for the plain tube at different Reynolds numbers.

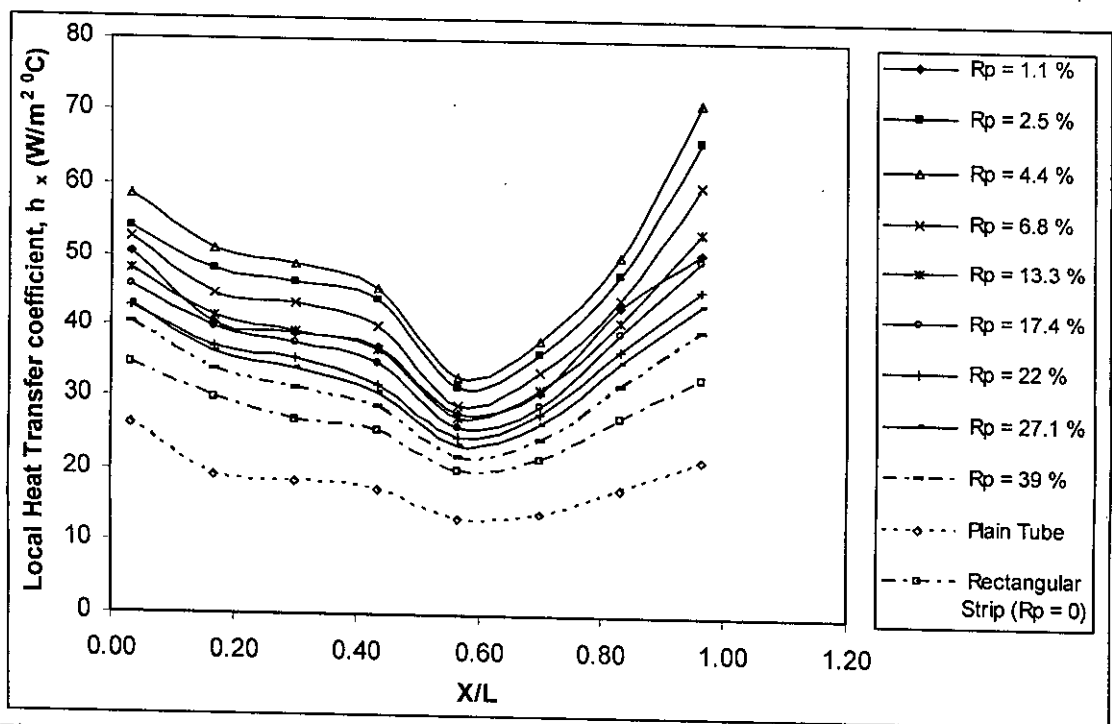


Figure 5.35(a): Variation of local heat transfer coefficient along axial distance for different porosity of inserts at Reynolds number around 30,925.

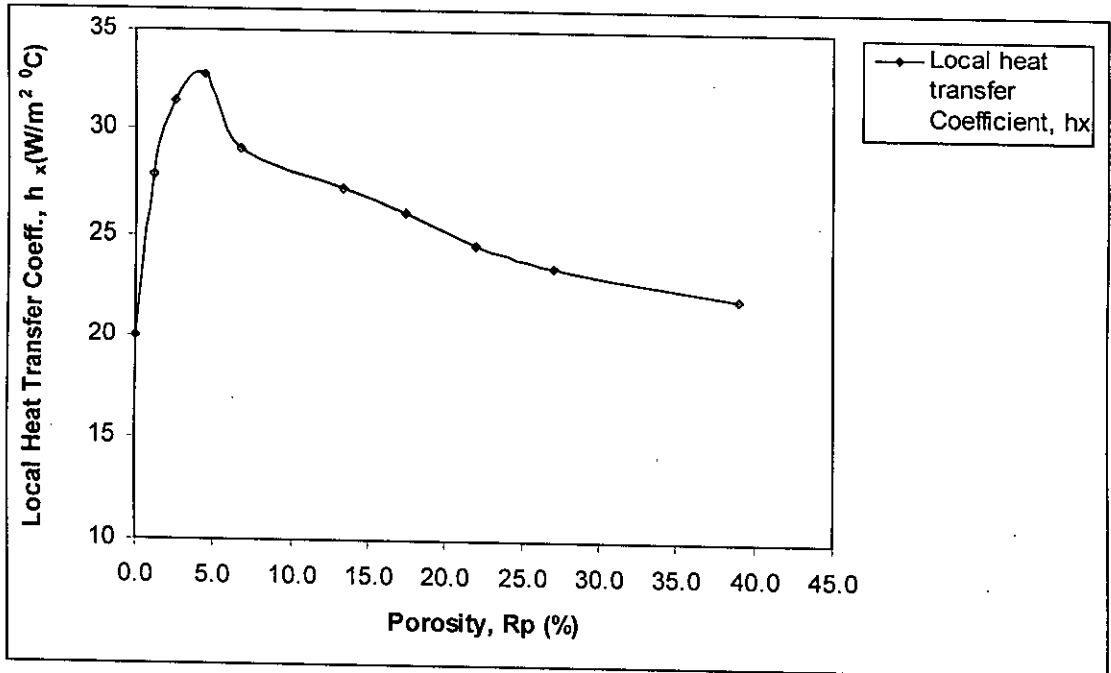


Figure 5.35(b): Variation of local heat transfer coefficient with different porosity ( $R_p$  from 0 %-39 %) of inserts for axial distance of  $X/L = 0.57$  and at Reynolds number around 30,925.

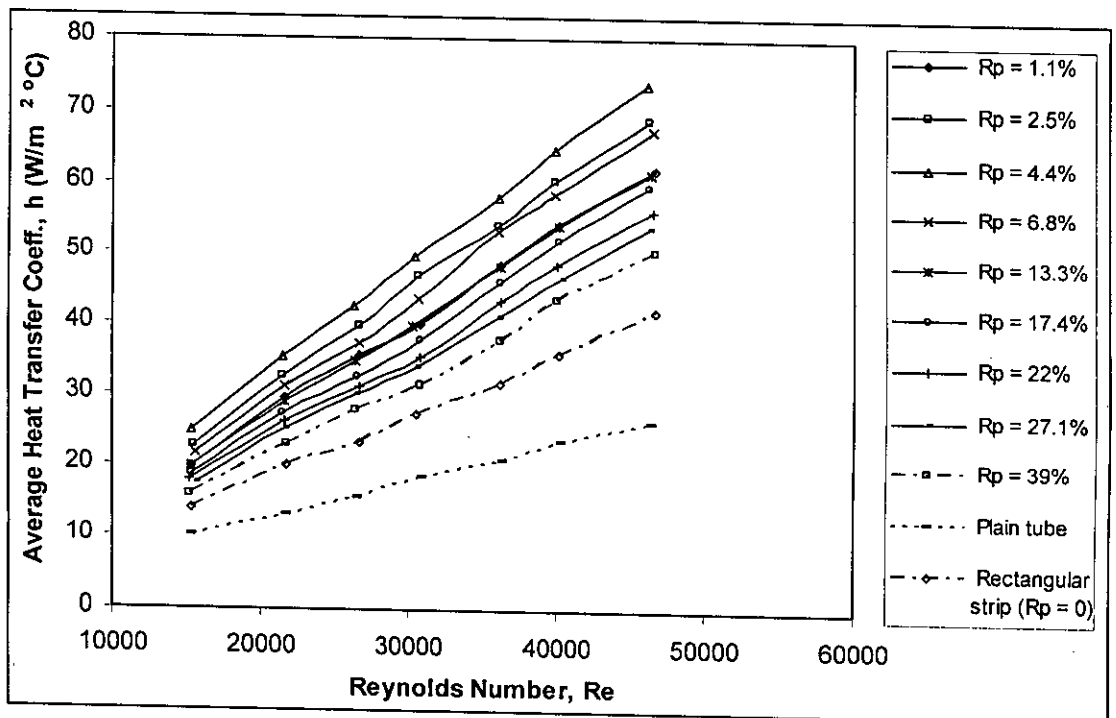


Figure 5.36: Variation of the average heat transfer coefficient for different porosity of rectangular strip inserts at different Reynolds numbers.

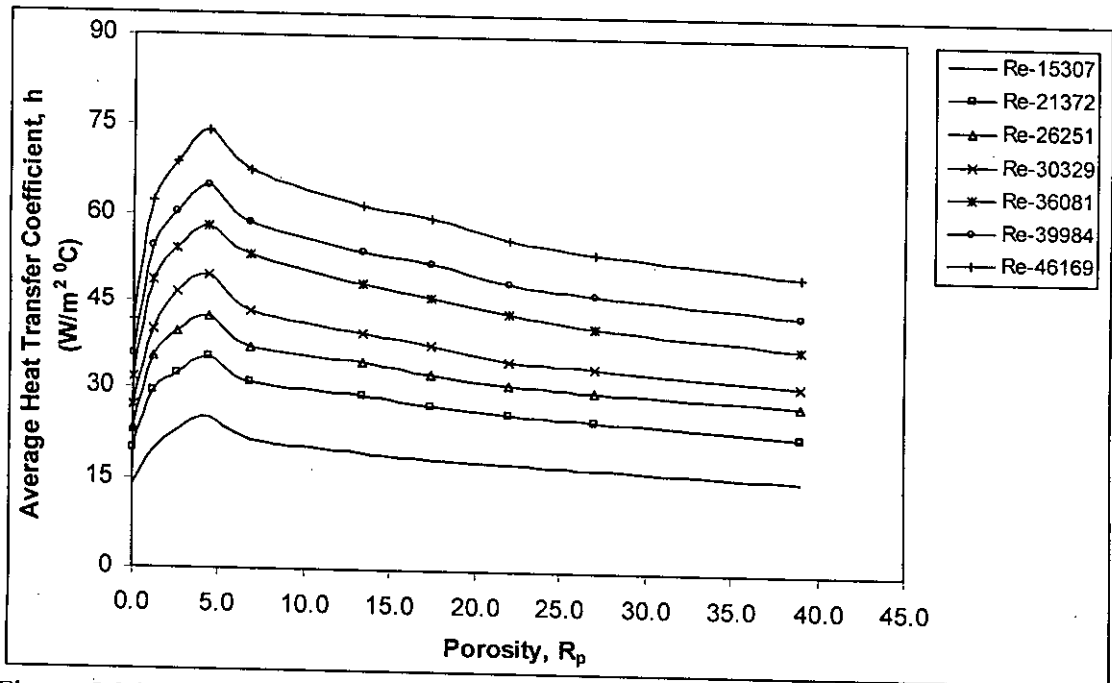


Figure 5.36(a): Variation of average heat transfer coefficient with different porosity ( $R_p$  from 0 %-39 %) of inserts for different Reynolds numbers (considering constant Reynolds numbers for all inserts).

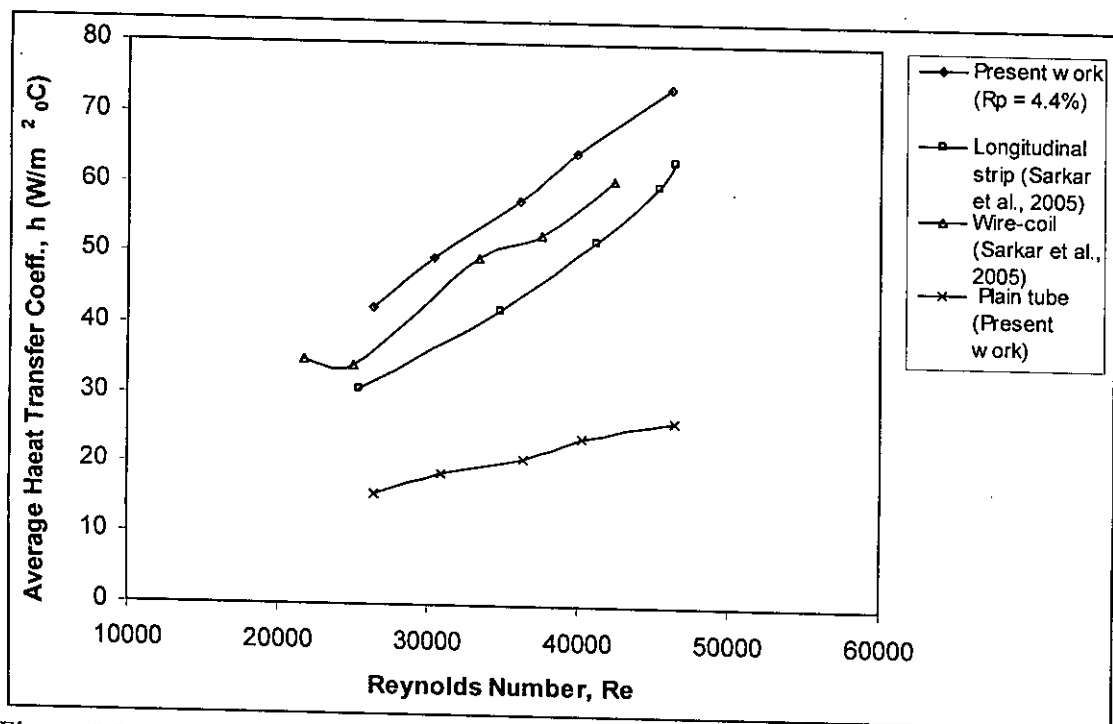


Figure 5.37: Variation of the average heat transfer coefficient for different inserts (perforated and unperforated) at different Reynolds numbers.

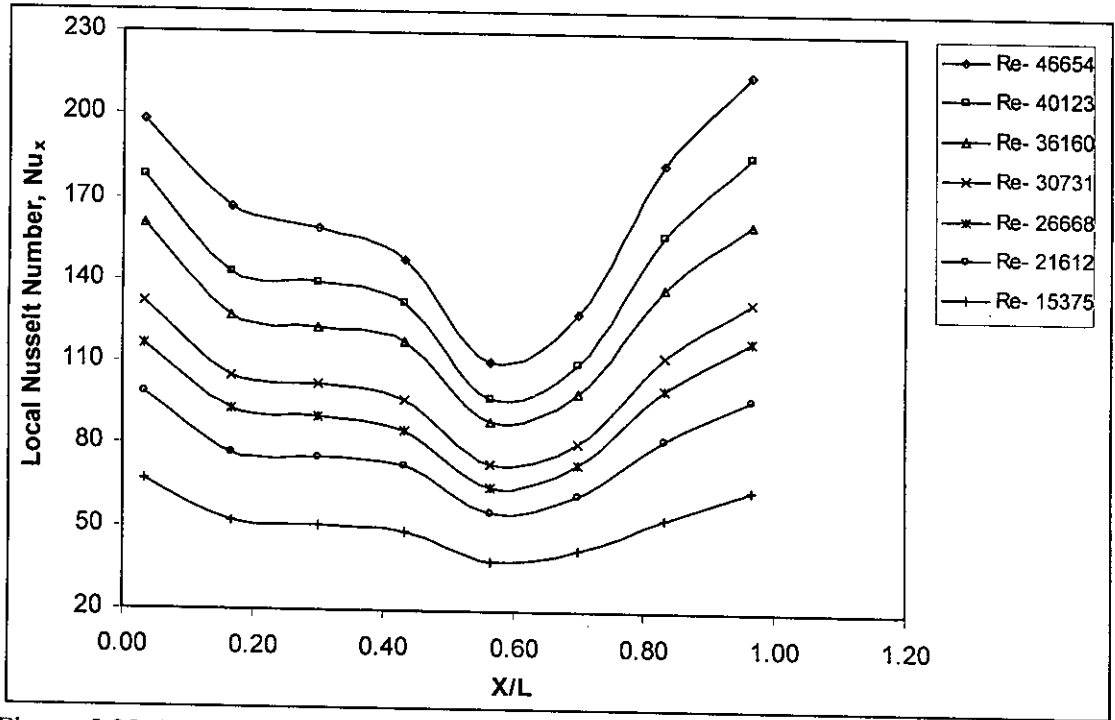


Figure 5.38: Variation of the local Nusselt number along axial distance for the tube with insert having porosity,  $R_p = 1.1\%$  at different Reynolds numbers.

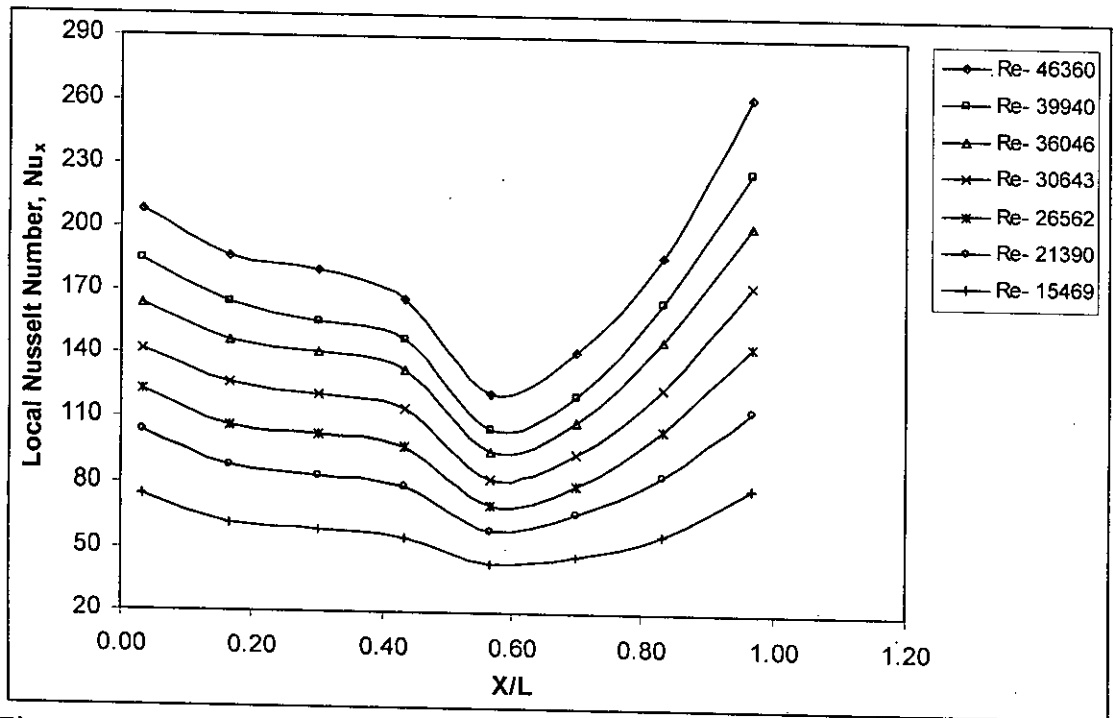


Figure 5.39: Variation of the local Nusselt number along axial distance for the tube with insert having porosity,  $R_p = 2.5\%$  at different Reynolds numbers.



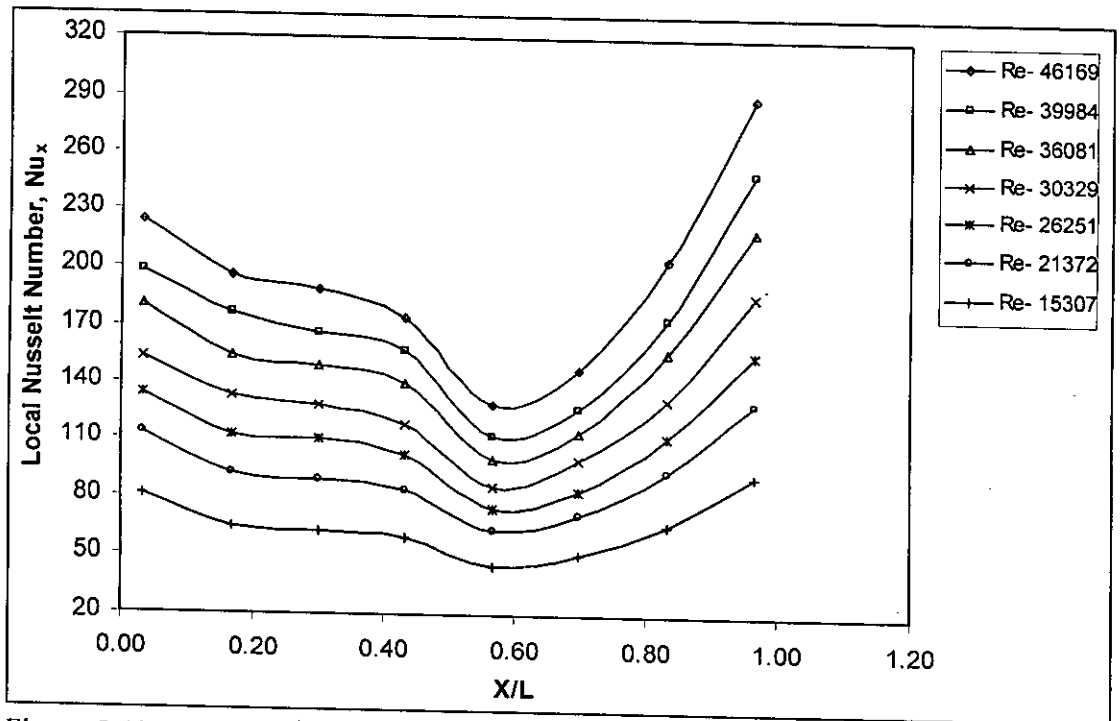


Figure 5.40: Variation of the local Nusselt number along axial distance for the tube with insert having porosity,  $R_p = 4.4\%$  at different Reynolds numbers.

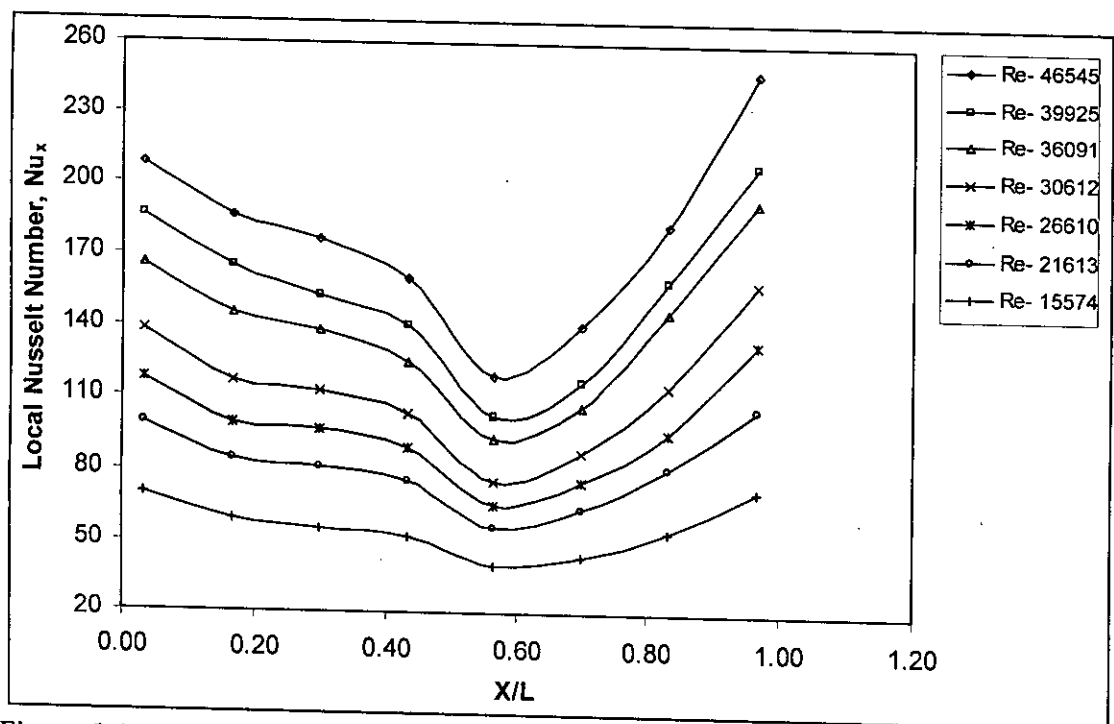


Figure 5.41: Variation of the local Nusselt number along axial distance for the tube with insert having porosity,  $R_p = 6.8\%$  at different Reynolds numbers.

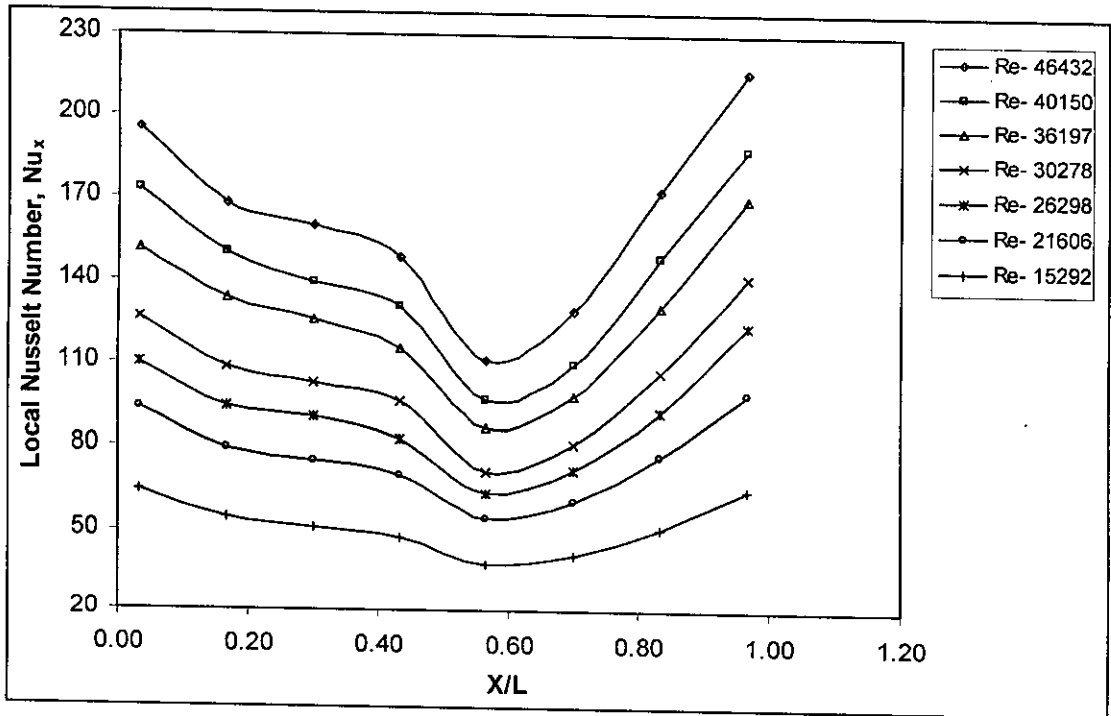


Figure 5.42: Variation of the local Nusselt number along axial distance for the tube with insert having porosity,  $R_p = 13.3\%$  at different Reynolds numbers.

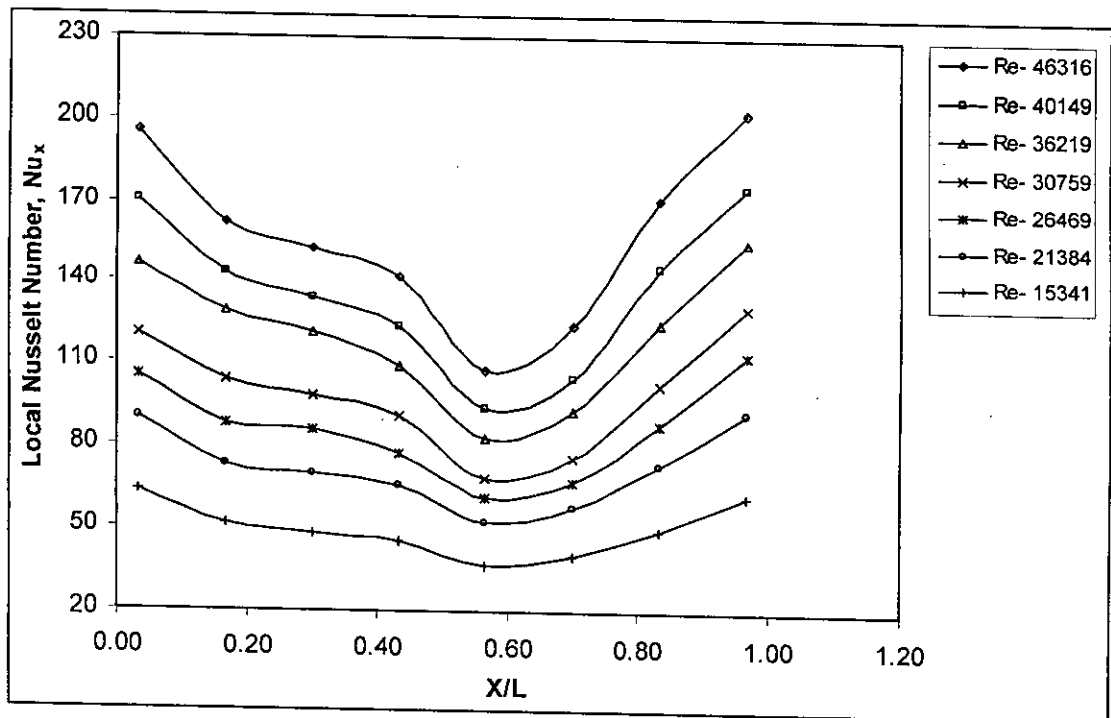


Figure 5.43: Variation of the local Nusselt number along axial distance for the tube with insert having porosity,  $R_p = 17.4\%$  at different Reynolds numbers.

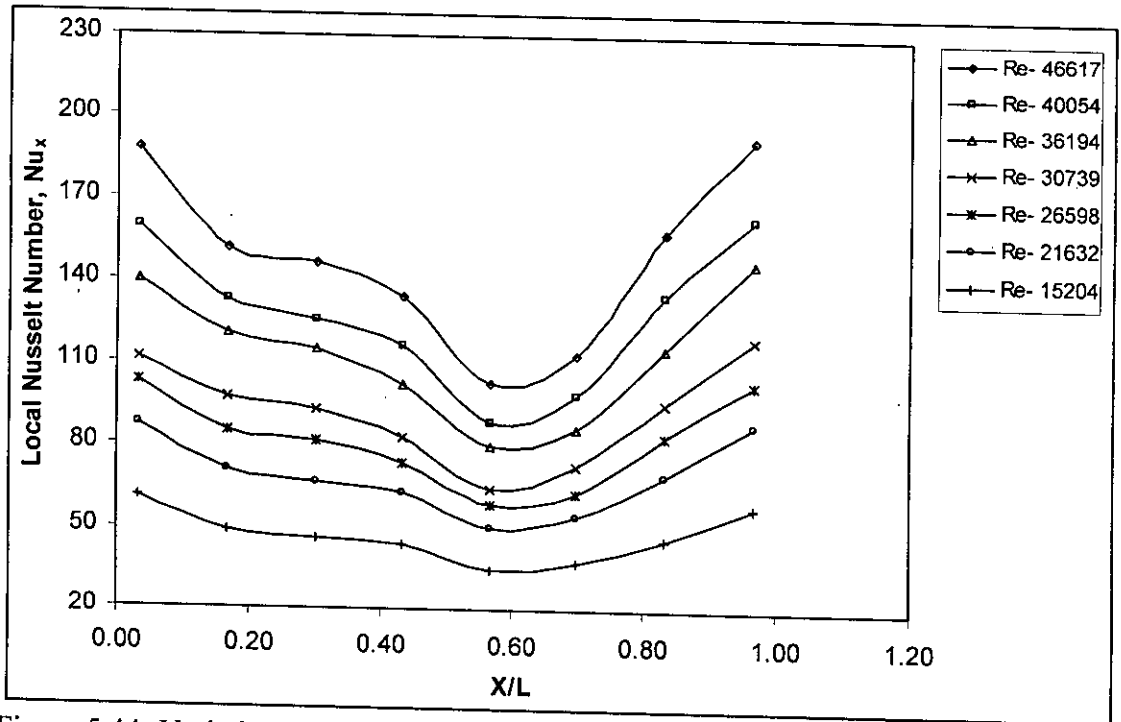


Figure 5.44: Variation of the local Nusselt number along axial distance for the tube with insert having porosity,  $R_p = 22\%$  at different Reynolds numbers.

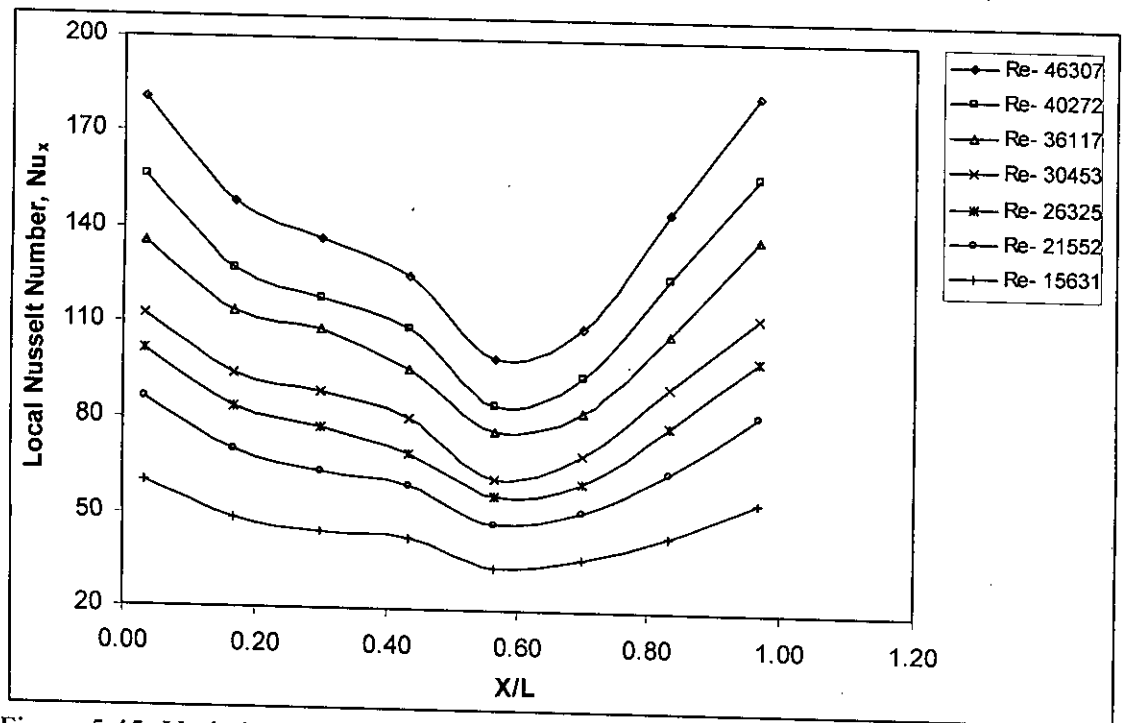


Figure 5.45: Variation of the local Nusselt number along axial distance for the tube with insert having porosity,  $R_p = 27.1\%$  at different Reynolds numbers.

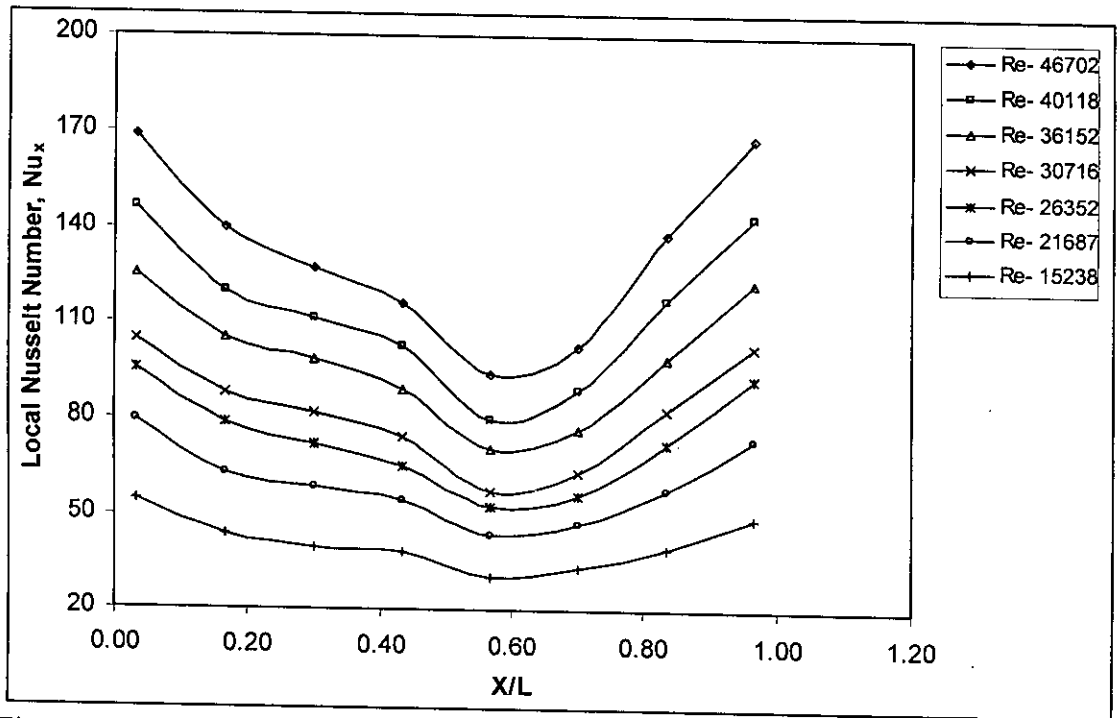


Figure 5.46: Variation of the local Nusselt number along axial distance for the tube with insert having porosity,  $R_p = 39\%$  at different Reynolds numbers.

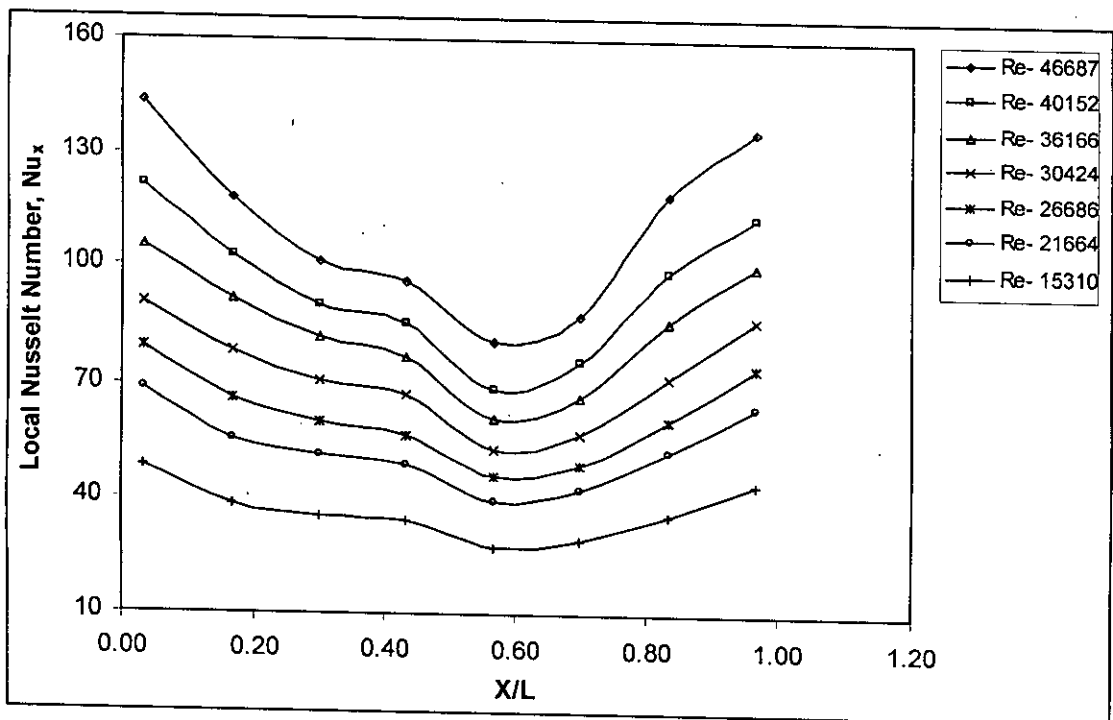


Figure 5.47: Variation of the local Nusselt number along axial distance for the tube with rectangular strip insert having porosity,  $R_p = 0$  at different Reynolds numbers.

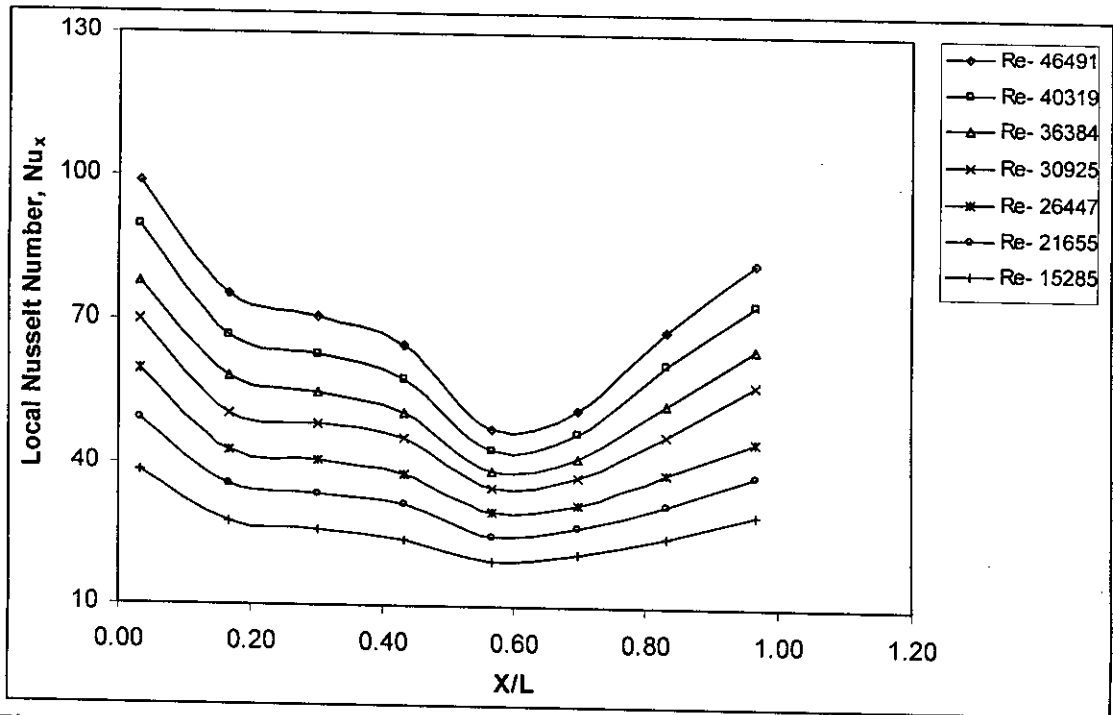


Figure 5.48: Variation of the local Nusselt number along axial distance for the plain tube at different Reynolds numbers.

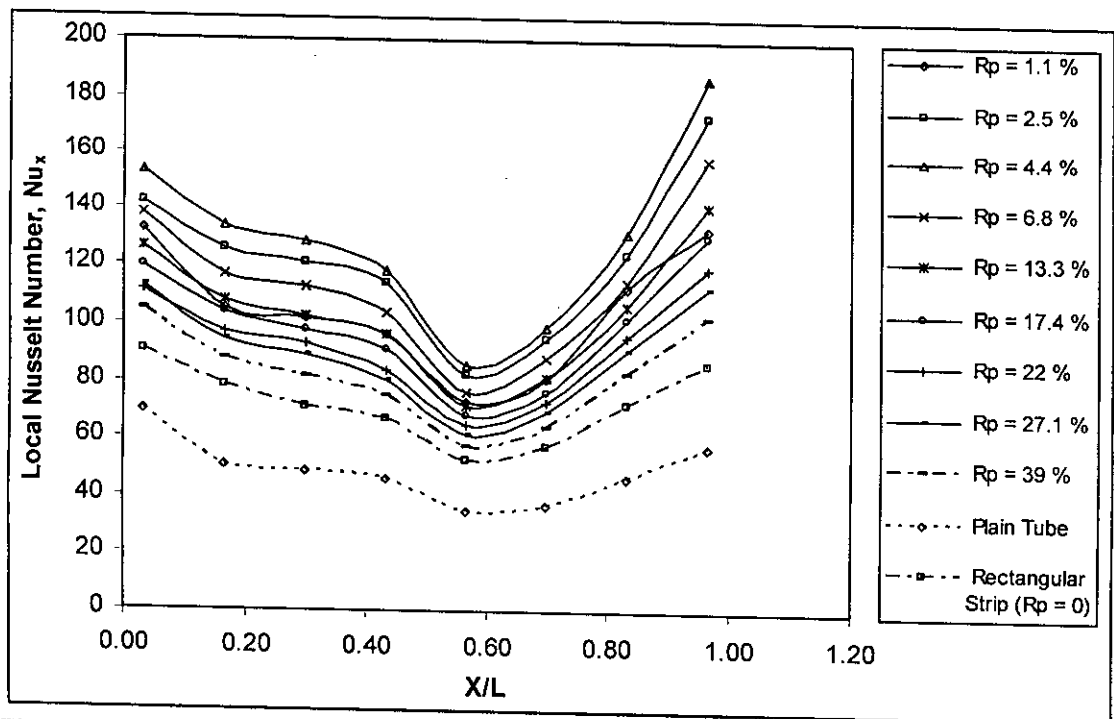


Figure 5.48(a): Variation of local Nusselt number along axial distance for different porosity of inserts at Reynolds number around 30,925.

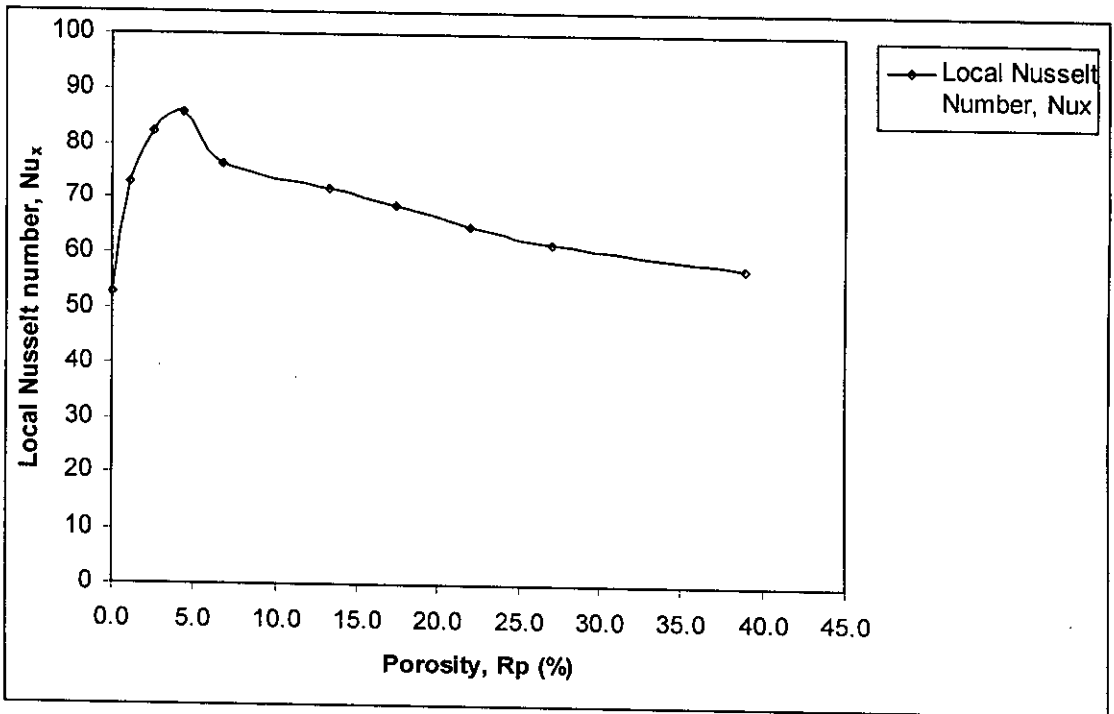


Figure 5.48(b): Variation of local Nusselt number with different porosity ( $R_p$  from 0 %-39 %) of inserts for axial distance of  $X/L = 0.57$  and at Reynolds number around 30,925.

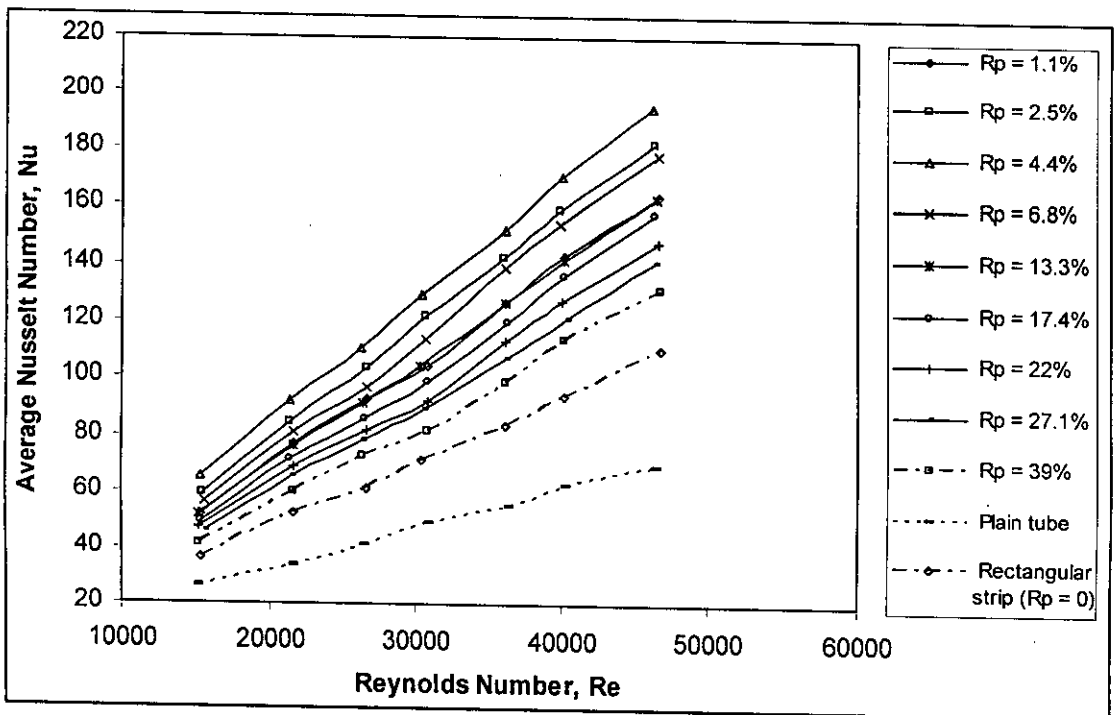


Figure 5.49: Variation of the average Nusselt number for different porosity of rectangular strip inserts at different Reynolds numbers.

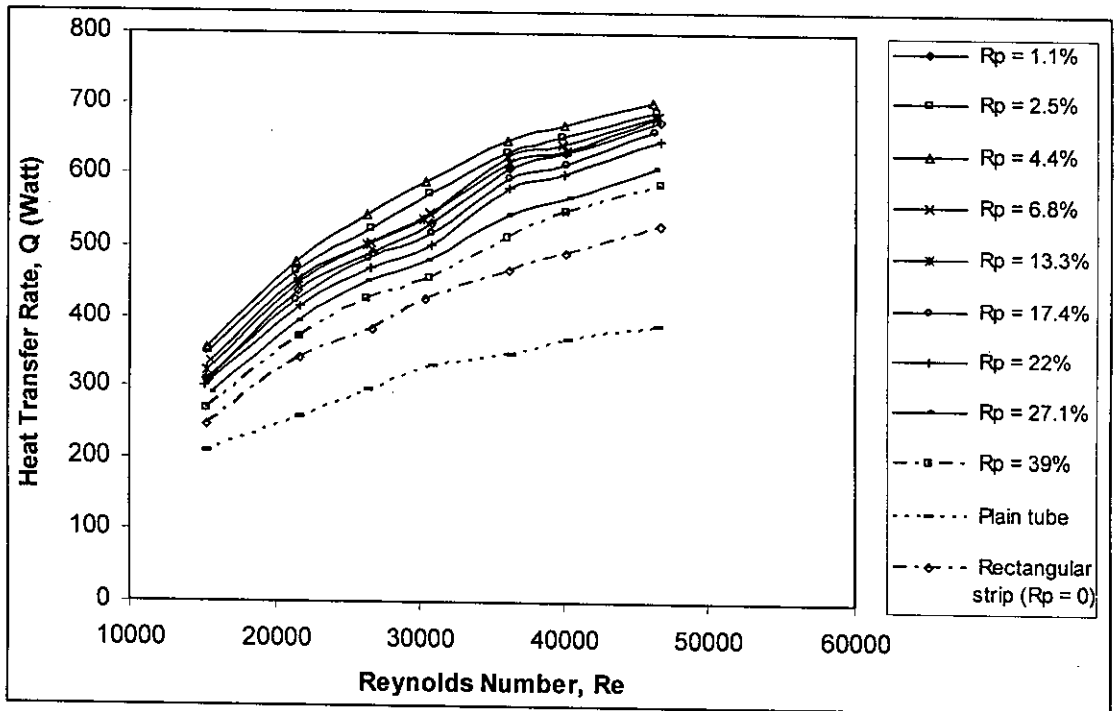


Figure 5.50: Variation of the heat transfer rate for different porosity of rectangular strip inserts at different Reynolds numbers.

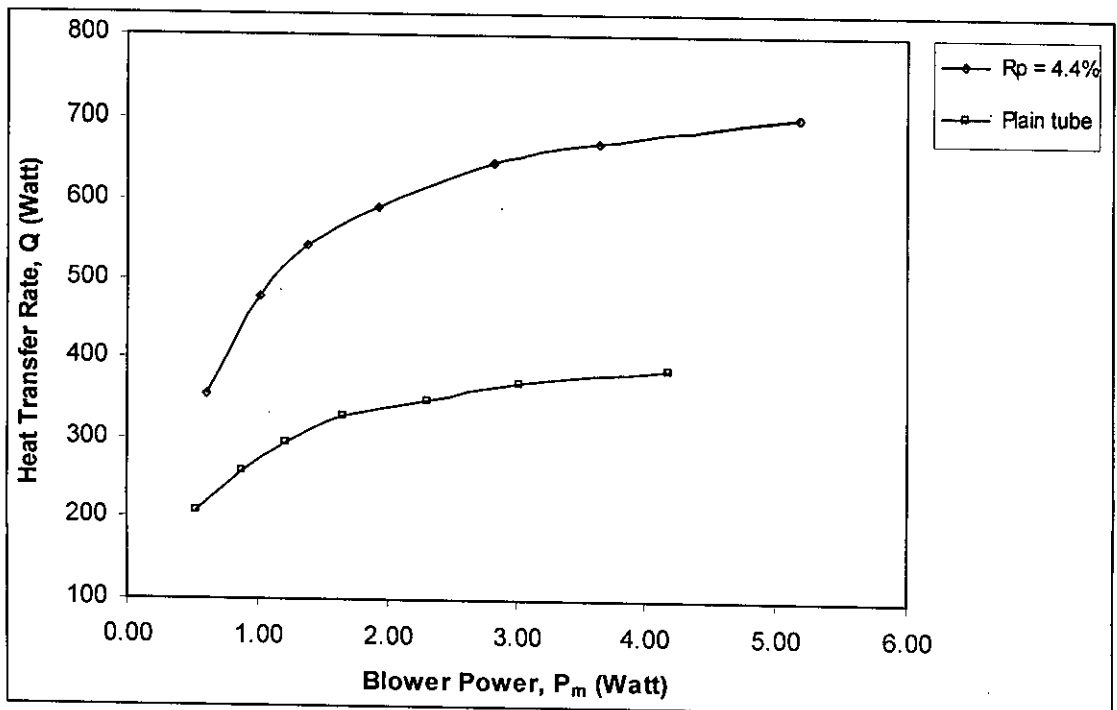


Figure 5.51: Variation of the heat transfer rate with the blower power at porosity,  $R_p = 4.4\%$ .

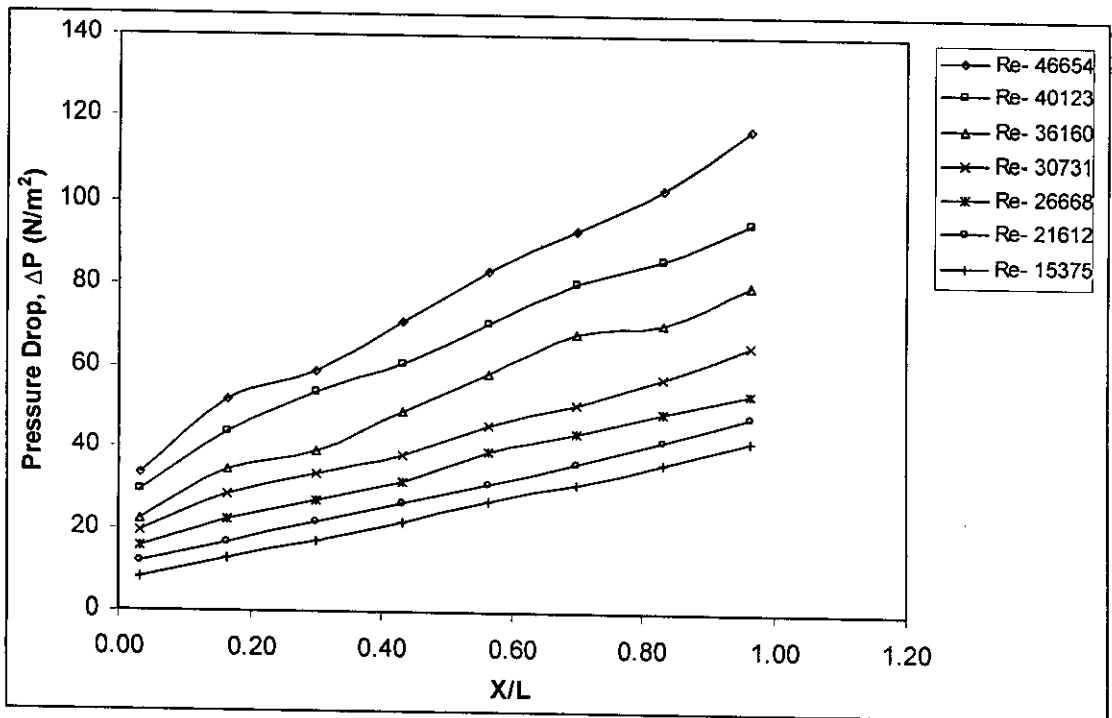


Figure 5.52: Variation of the pressure drop along axial distance for insert having porosity,  $R_p = 1.1\%$  at different Reynolds numbers.

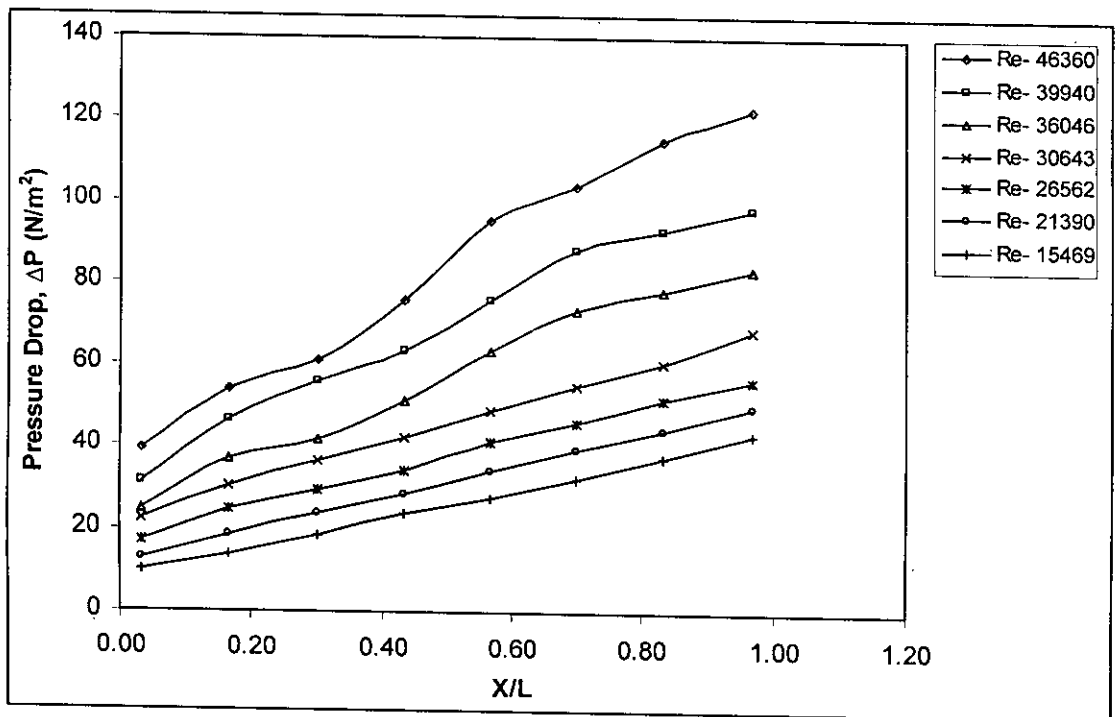


Figure 5.53: Variation of the pressure drop along axial distance for insert having porosity,  $R_p = 2.5\%$  at different Reynolds numbers.

22



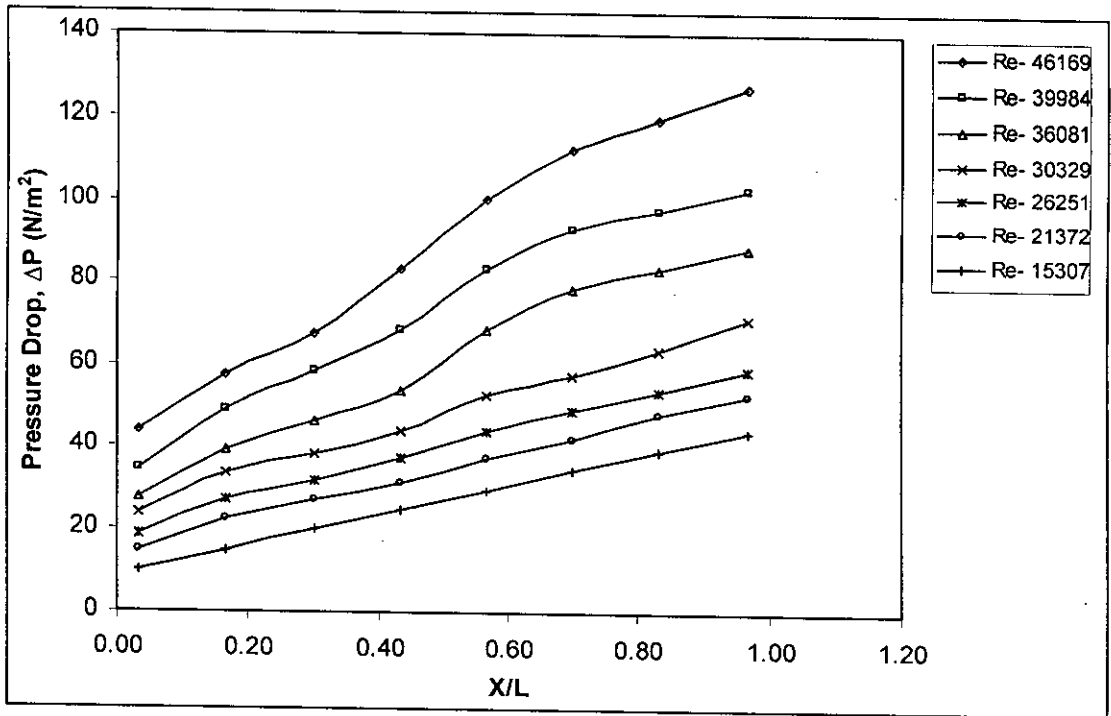


Figure 5.54: Variation of the pressure drop along axial distance for insert having porosity,  $R_p = 4.4\%$  at different Reynolds numbers.

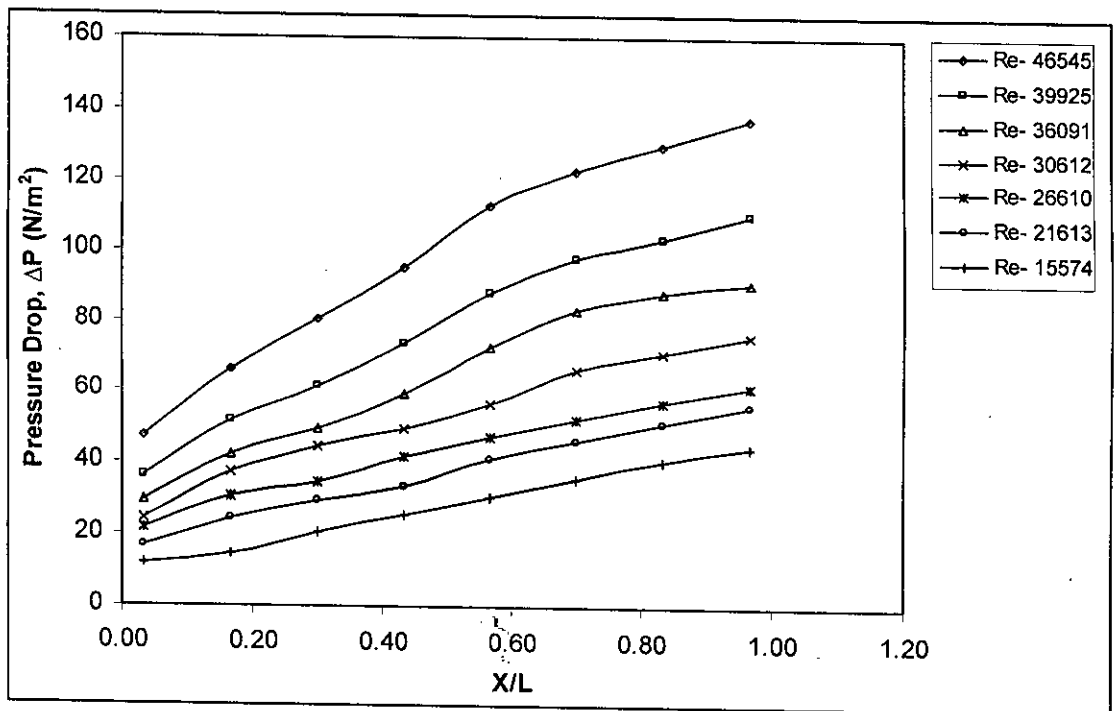


Figure 5.55: Variation of the pressure drop along axial distance for insert having porosity,  $R_p = 6.8\%$  at different Reynolds numbers.

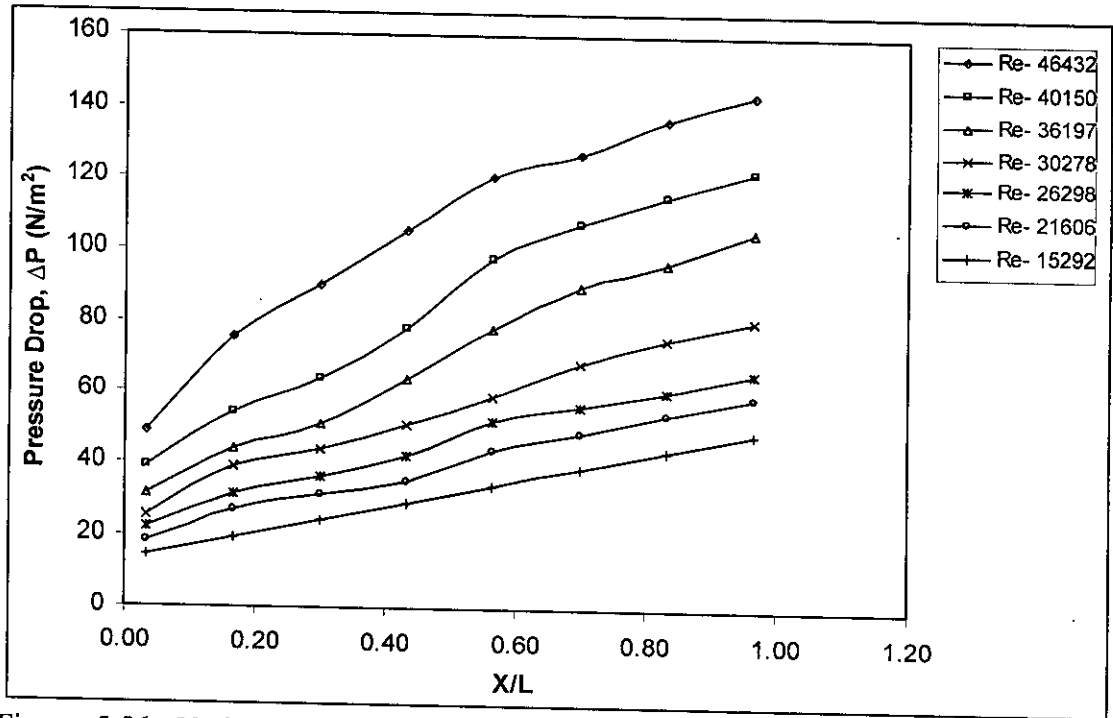


Figure 5.56: Variation of the pressure drop along axial distance for insert having porosity,  $R_p = 13.3\%$  at different Reynolds numbers.

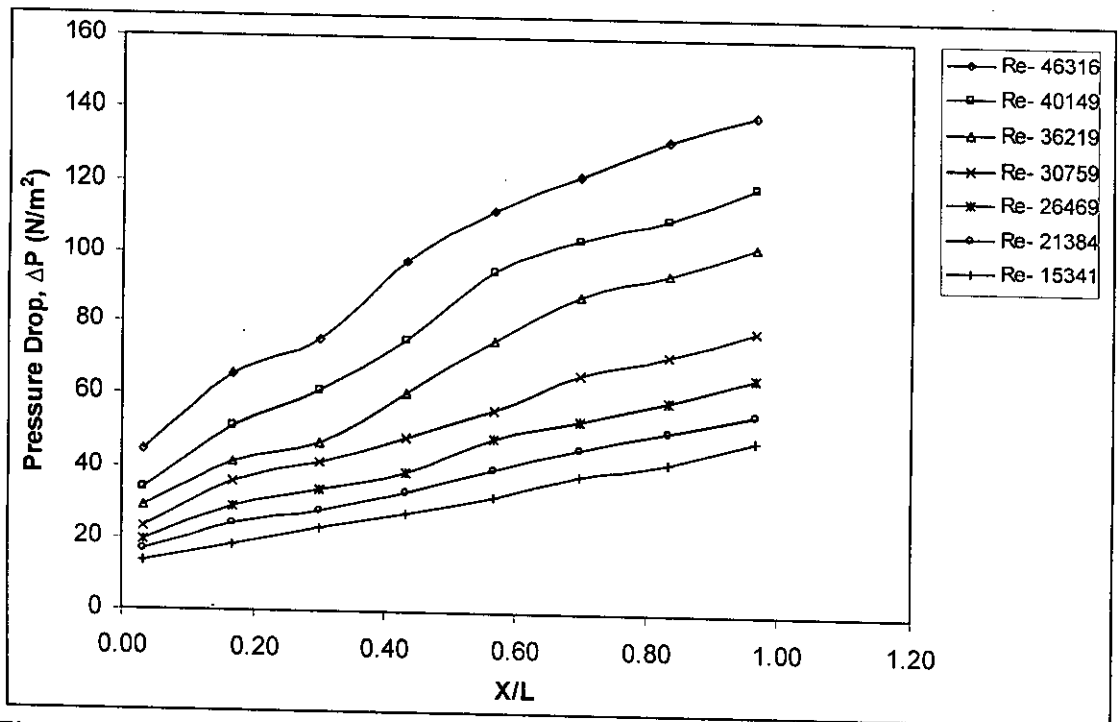


Figure 5.57: Variation of the pressure drop along axial distance for insert having porosity,  $R_p = 17.4\%$  at different Reynolds numbers.

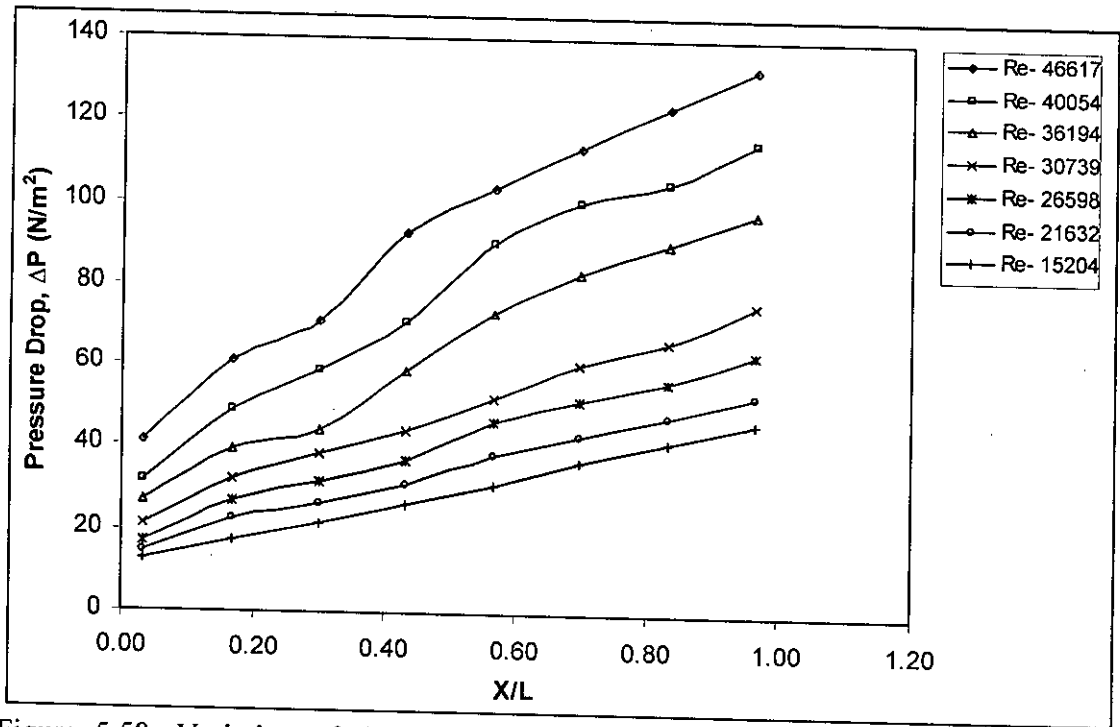


Figure 5.58: Variation of the pressure drop along axial distance for insert having porosity,  $R_p = 22\%$  at different Reynolds numbers.

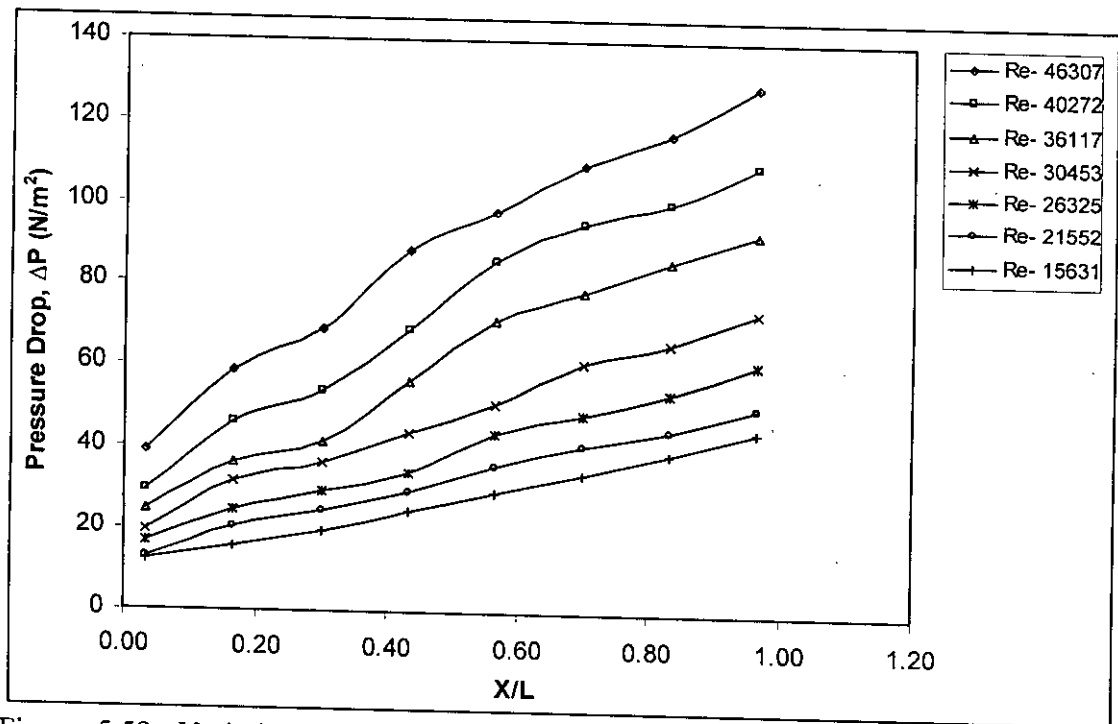


Figure 5.59: Variation of the pressure drop along axial distance for insert having porosity,  $R_p = 27.1\%$  at different Reynolds numbers.

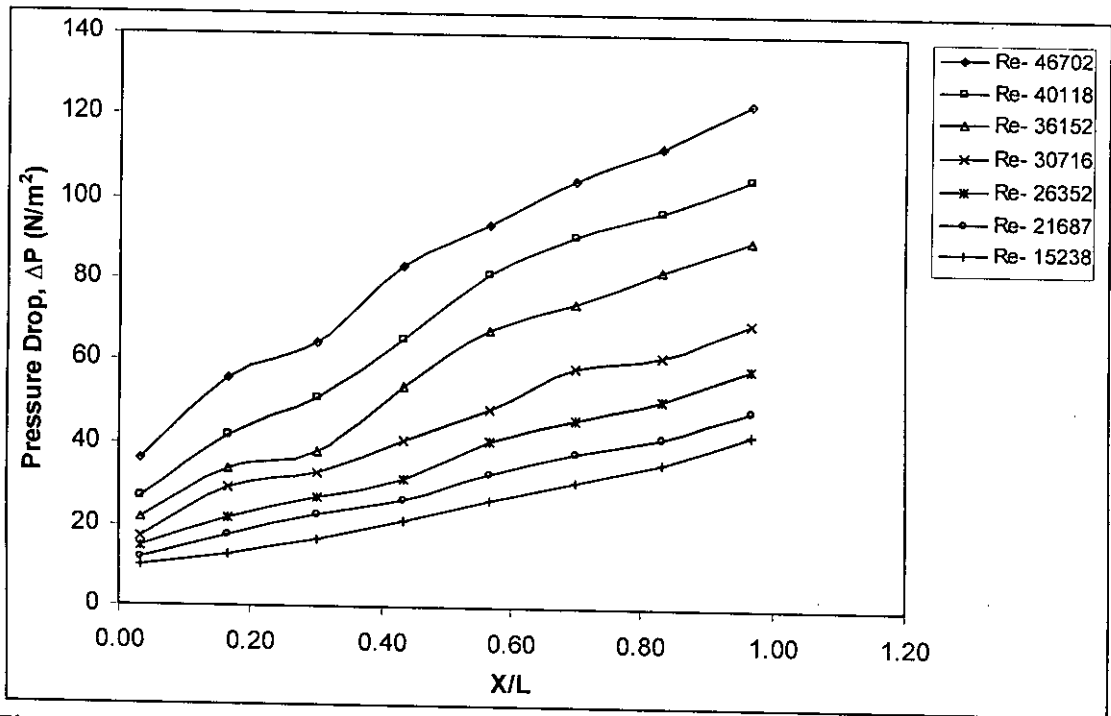


Figure 5.60: Variation of the pressure drop along axial distance for insert having porosity,  $R_p = 39\%$  at different Reynolds numbers.

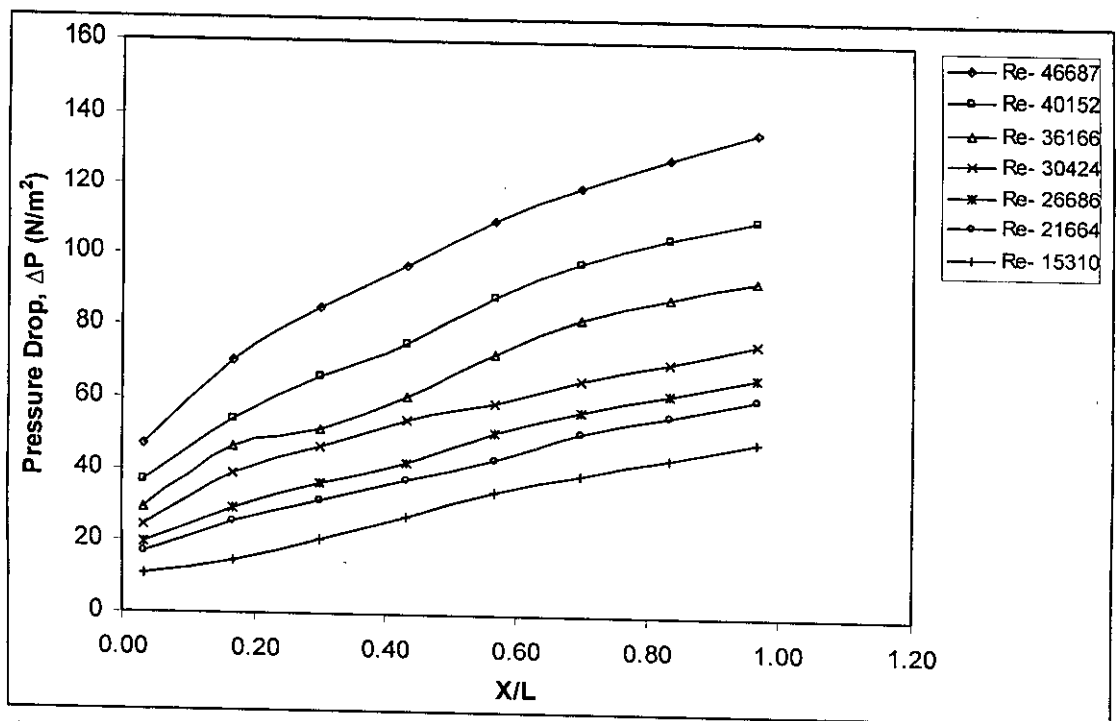


Figure 5.61: Variation of the pressure drop along axial distance for the tube with rectangular strip insert having porosity,  $R_p = 0$  at different Reynolds numbers.

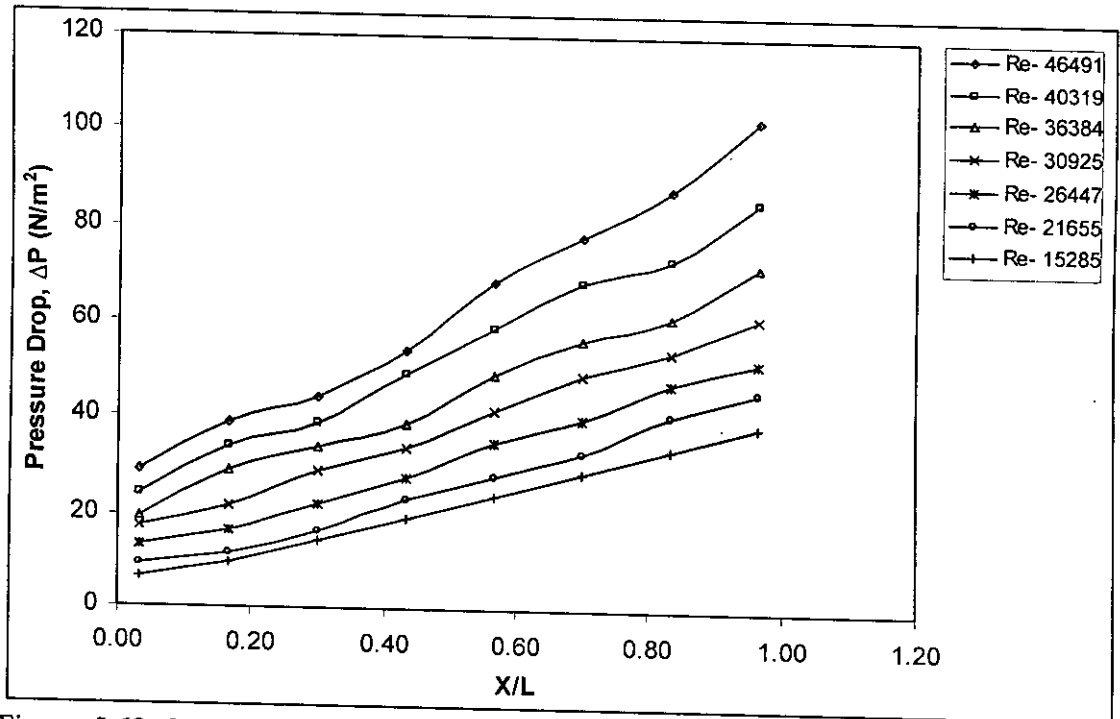


Figure 5.62: Variation of the pressure drop along axial distance for the plain tube at different Reynolds numbers.

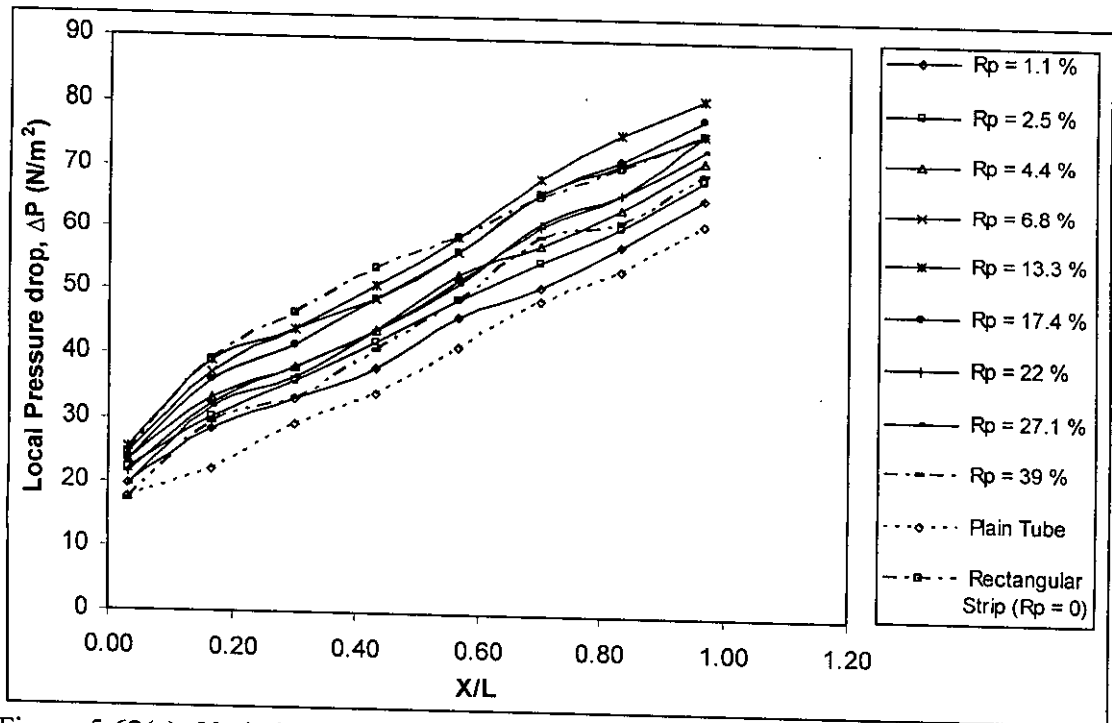


Figure 5.62(a): Variation of the pressure drop along axial distance for different porosity of inserts at Reynolds number around 30,925.

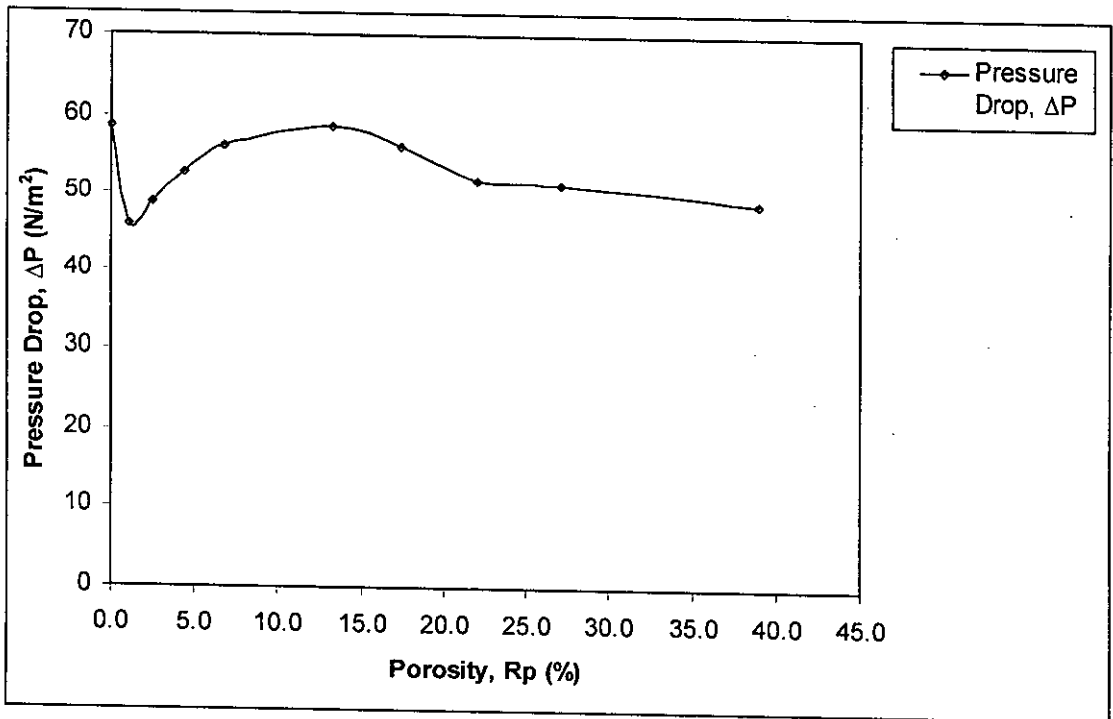


Figure 5.62(b): Variation of the pressure drop with different porosity ( $R_p$  from 0 %-39 %) of inserts for axial distance of  $X/L = 0.57$  and at Reynolds number around 30,925.

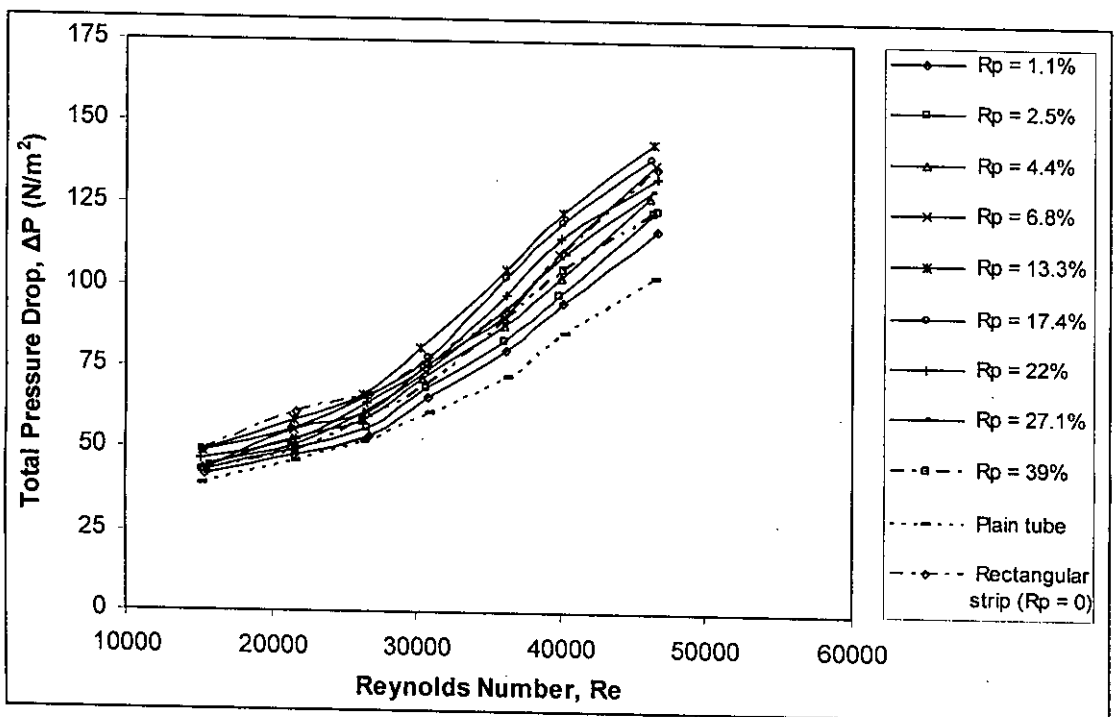


Figure 5.63: Variation of the total pressure drop for different porosity of rectangular strip inserts at different Reynolds numbers.

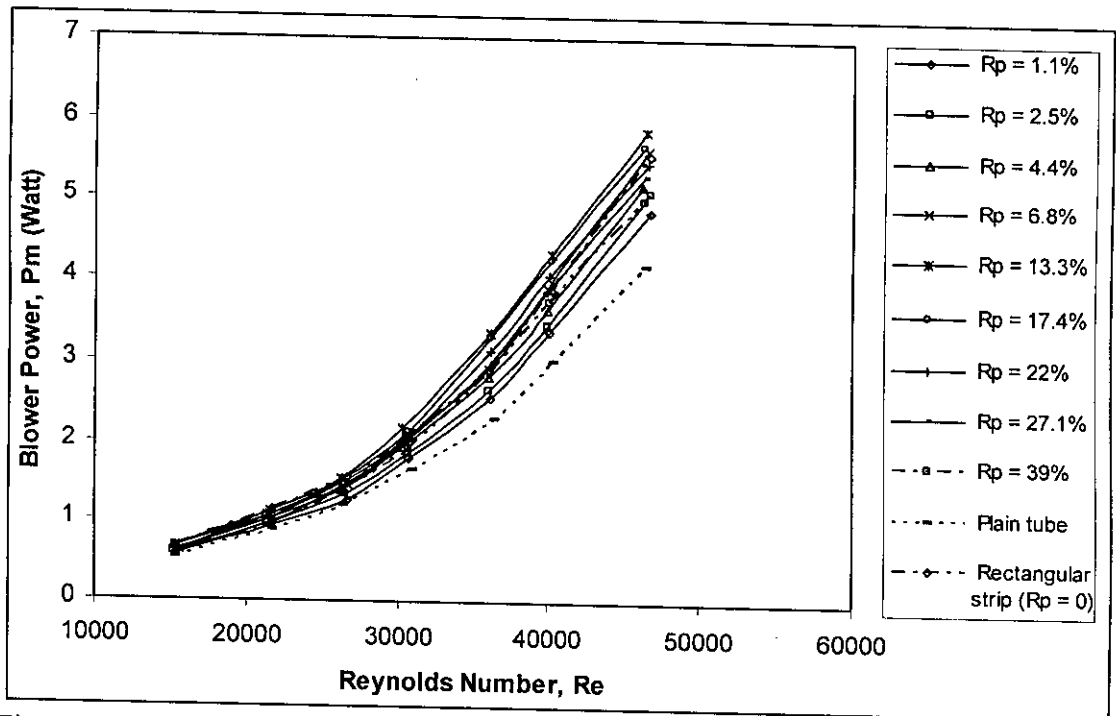


Figure 5.64: Variation of the blower power required for different porosity of rectangular strip inserts at different Reynolds numbers.

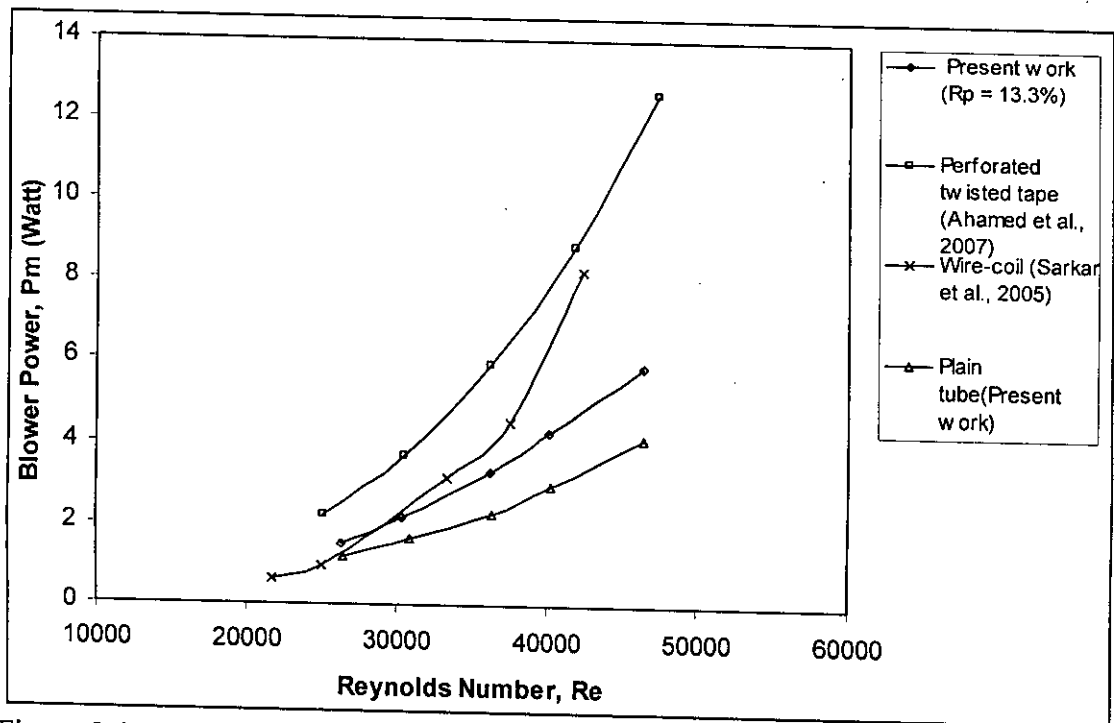


Figure 5.65: Variation of the blower power required for different inserts (perforated and unperforated) at different Reynolds numbers.

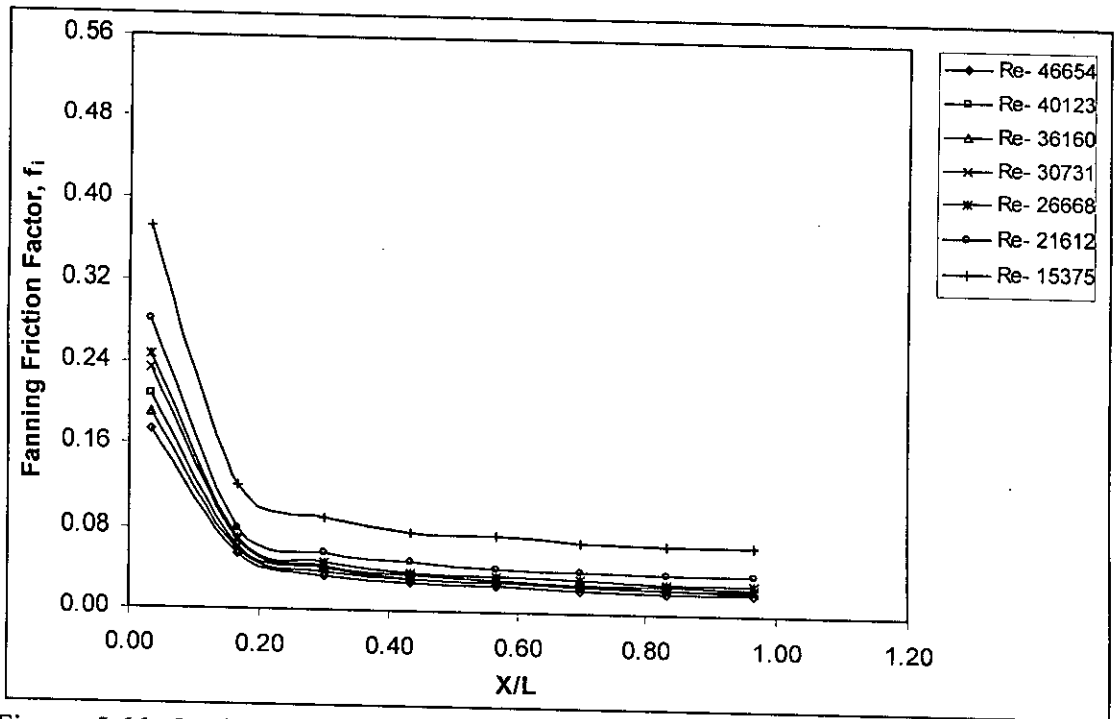


Figure 5.66: Variation of the friction factor along axial distance for insert having porosity,  $R_p = 1.1\%$  at different Reynolds numbers.

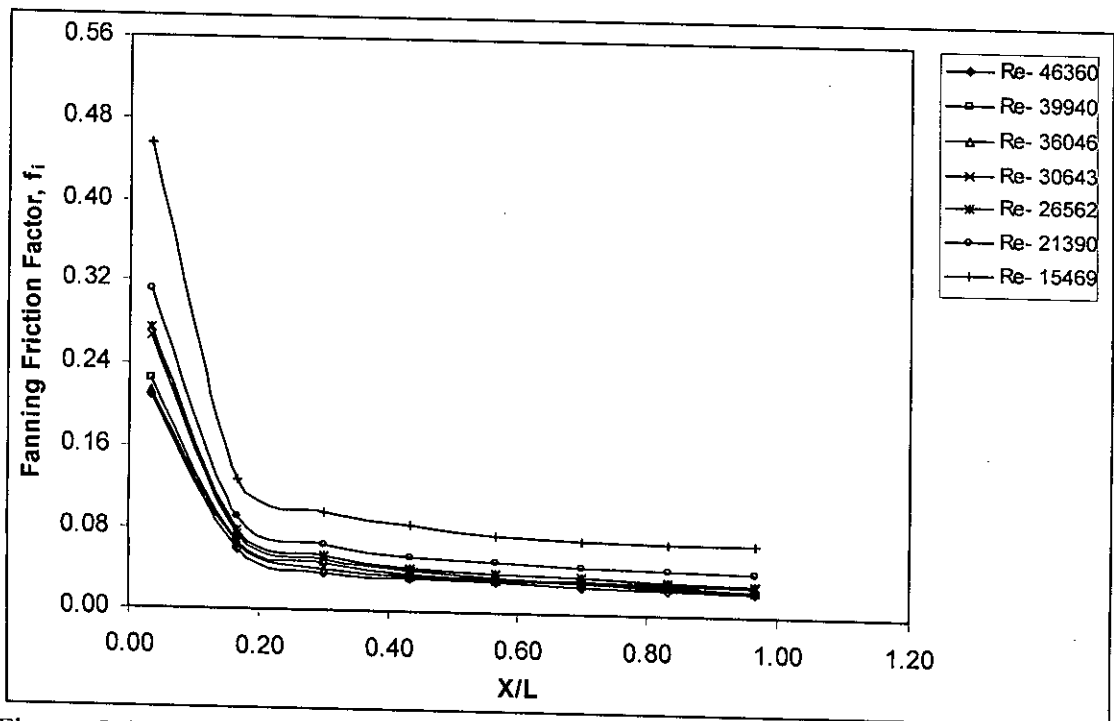


Figure 5.67: Variation of the friction factor along axial distance for insert having porosity,  $R_p = 2.5\%$  at different Reynolds numbers.



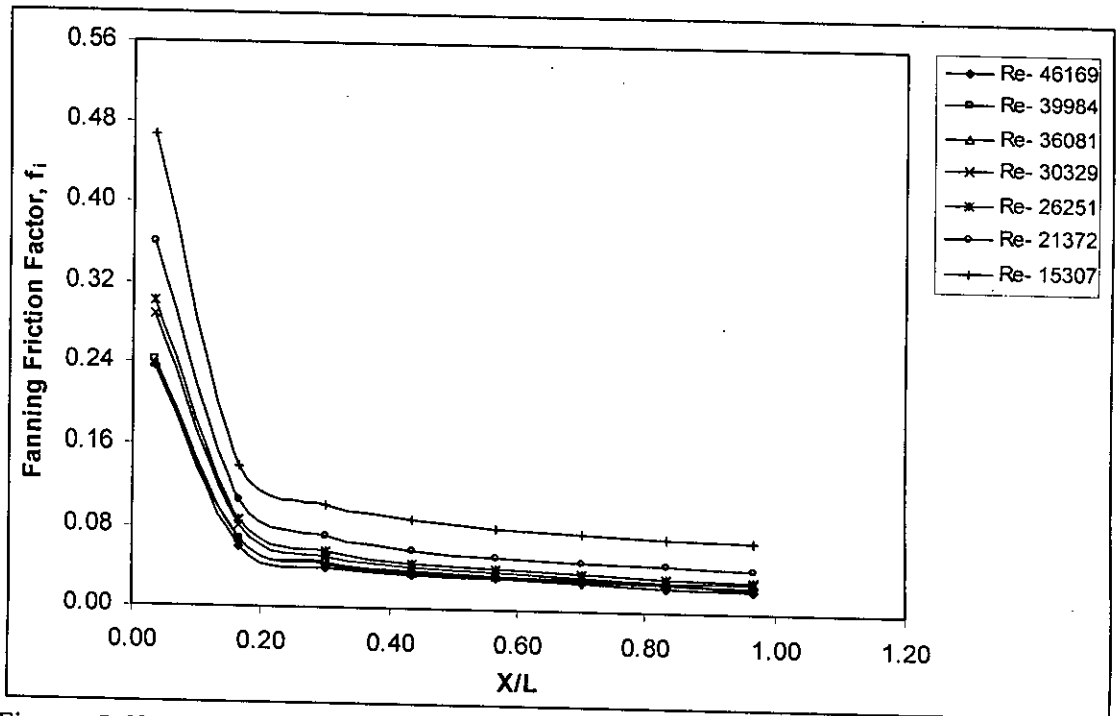


Figure 5.68: Variation of the friction factor along axial distance for insert having porosity,  $R_p = 4.4\%$  at different Reynolds numbers.

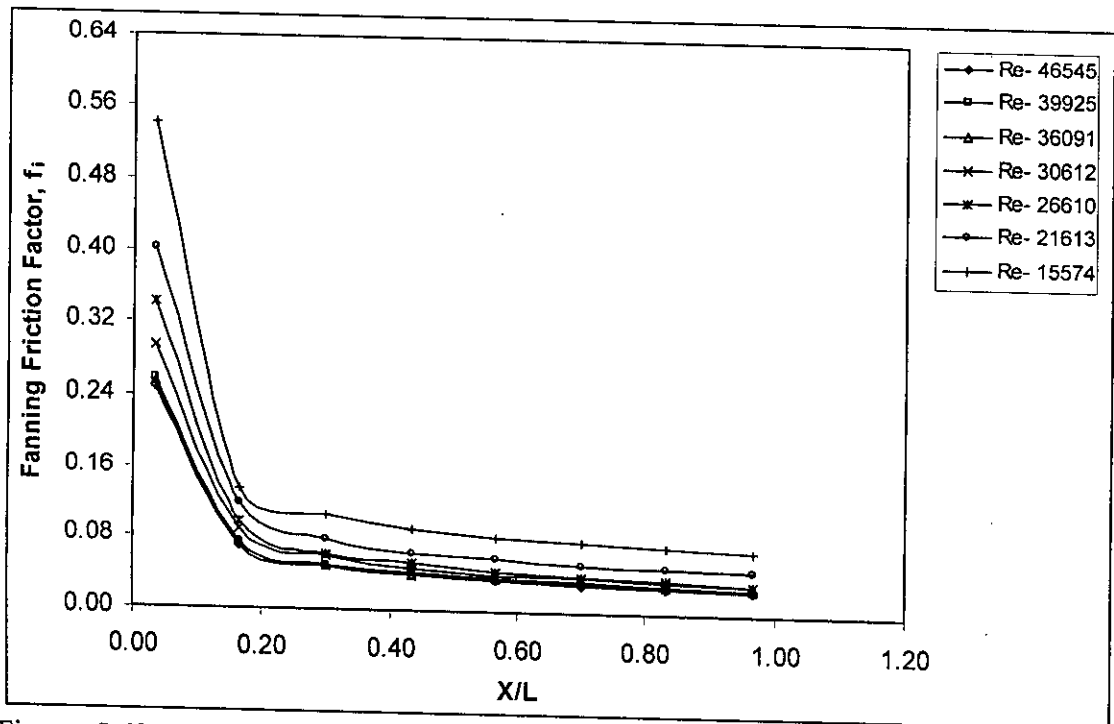


Figure 5.69: Variation of the friction factor along axial distance for insert having porosity,  $R_p = 6.8\%$  at different Reynolds numbers.

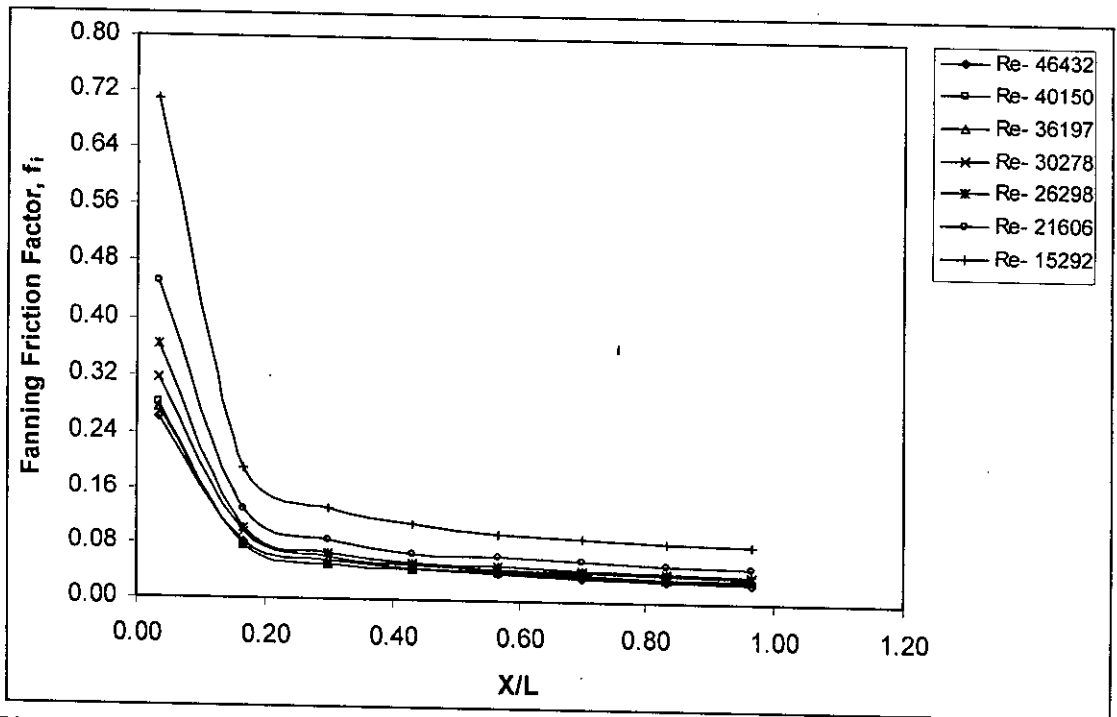


Figure 5.70: Variation of the friction factor along axial distance for insert having porosity,  $R_p = 13.3\%$  at different Reynolds numbers.

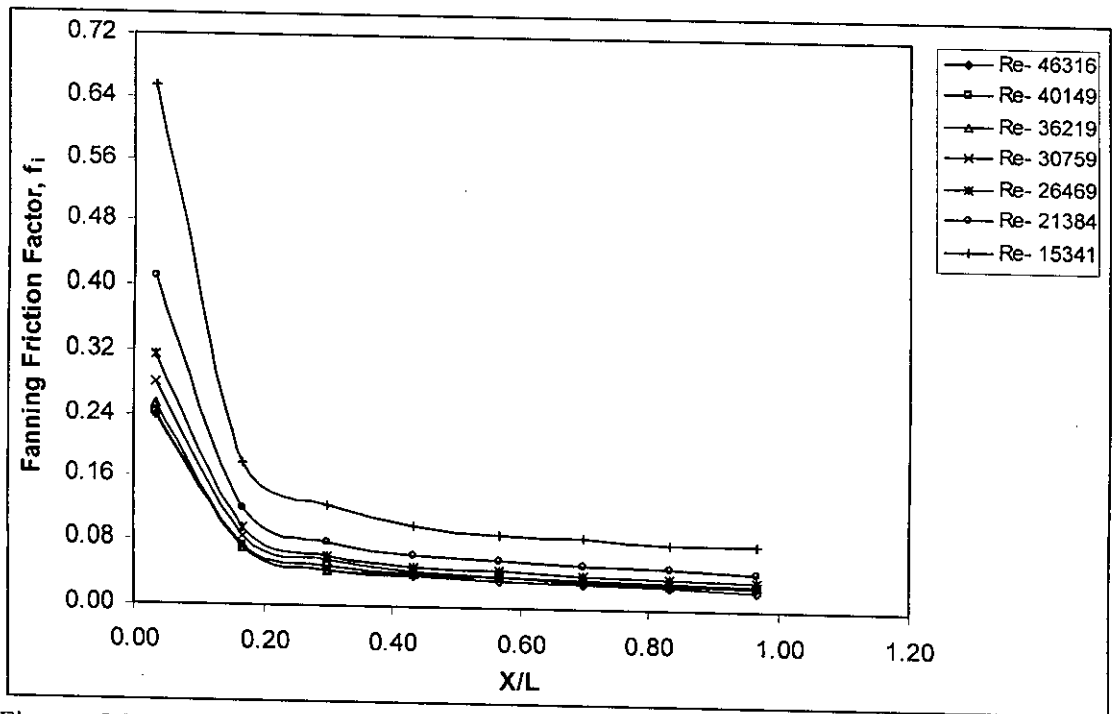


Figure 5.71: Variation of the friction factor along axial distance for insert having porosity,  $R_p = 17.4\%$  at different Reynolds numbers.

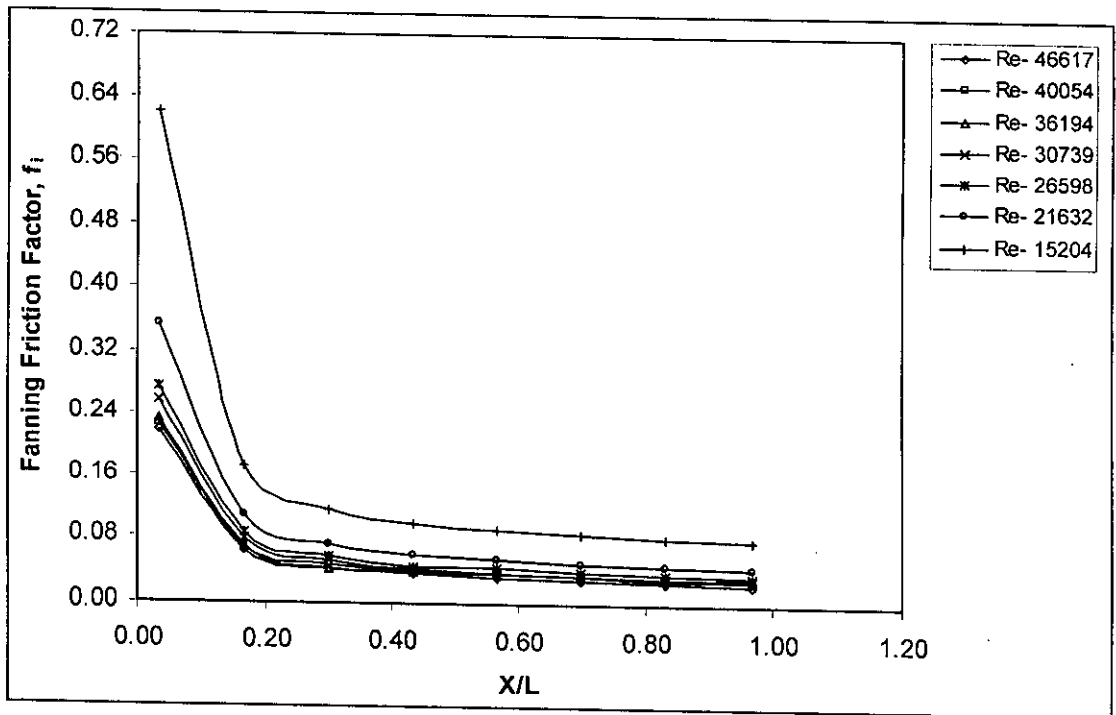


Figure 5.72: Variation of the friction factor along axial distance for insert having porosity,  $R_p = 22\%$  at different Reynolds numbers.

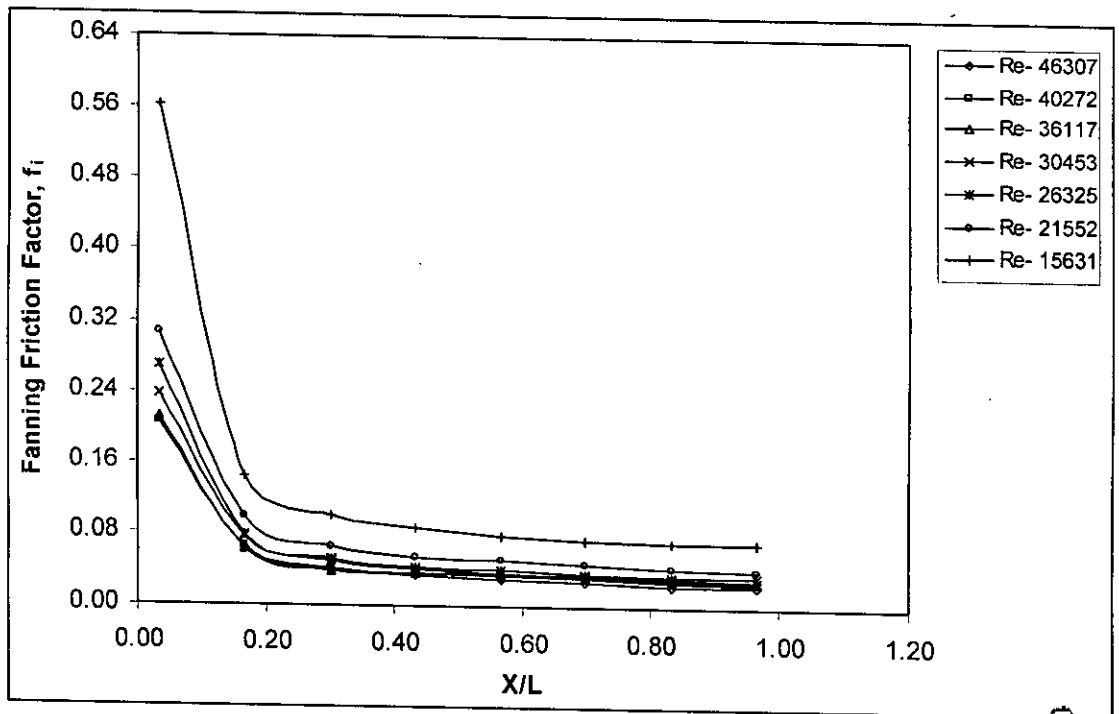


Figure 5.73: Variation of the friction factor along axial distance for insert having porosity,  $R_p = 27.1\%$  at different Reynolds numbers.

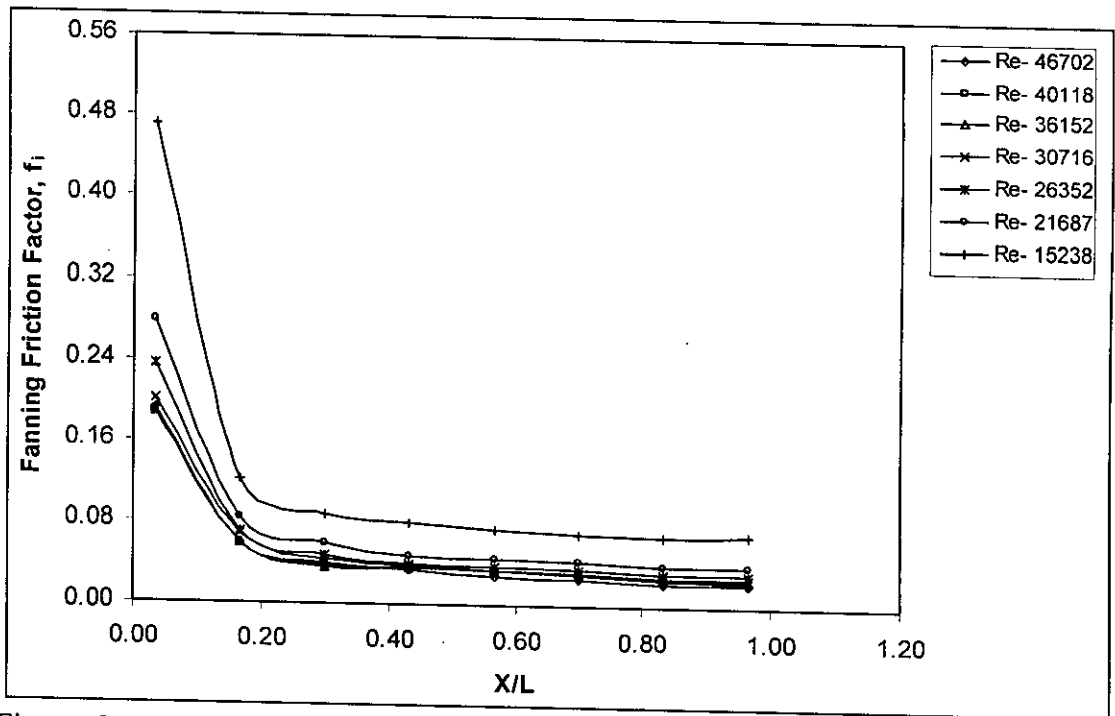


Figure 5.74: Variation of the friction factor along axial distance for insert having porosity,  $R_p = 39\%$  at different Reynolds numbers.

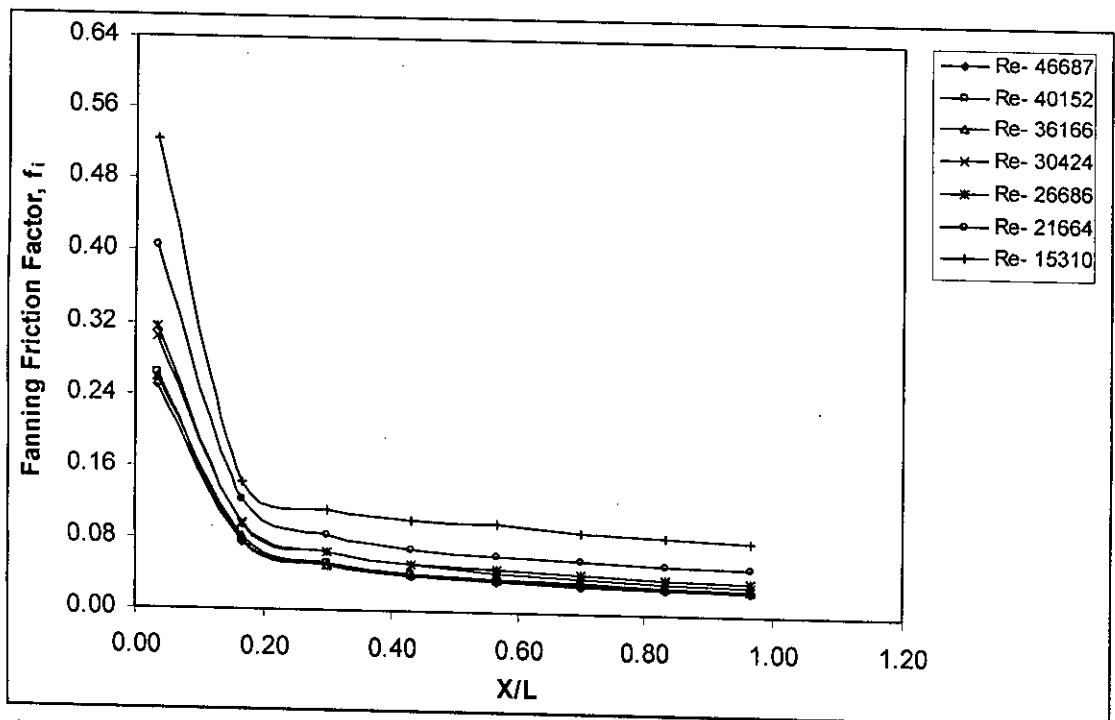


Figure 5.75: Variation of the friction factor along axial distance for the tube with rectangular strip insert having porosity,  $R_p = 0$  at different Reynolds numbers.

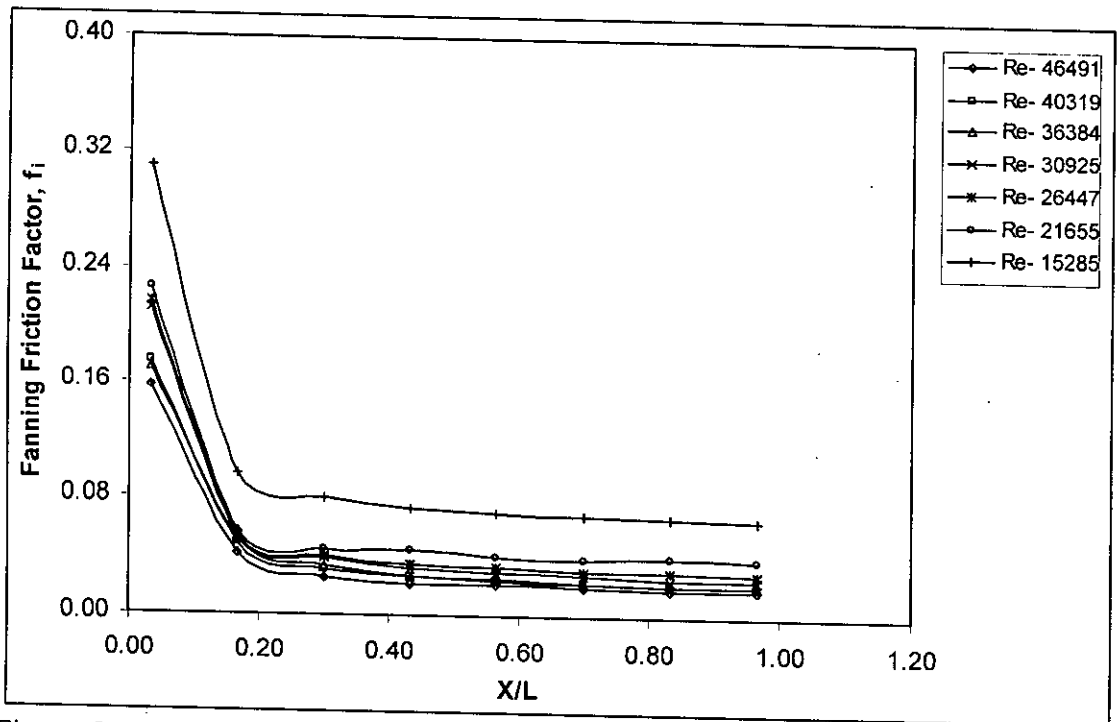


Figure 5.76: Variation of the friction factor along axial distance for the plain tube at different Reynolds numbers.

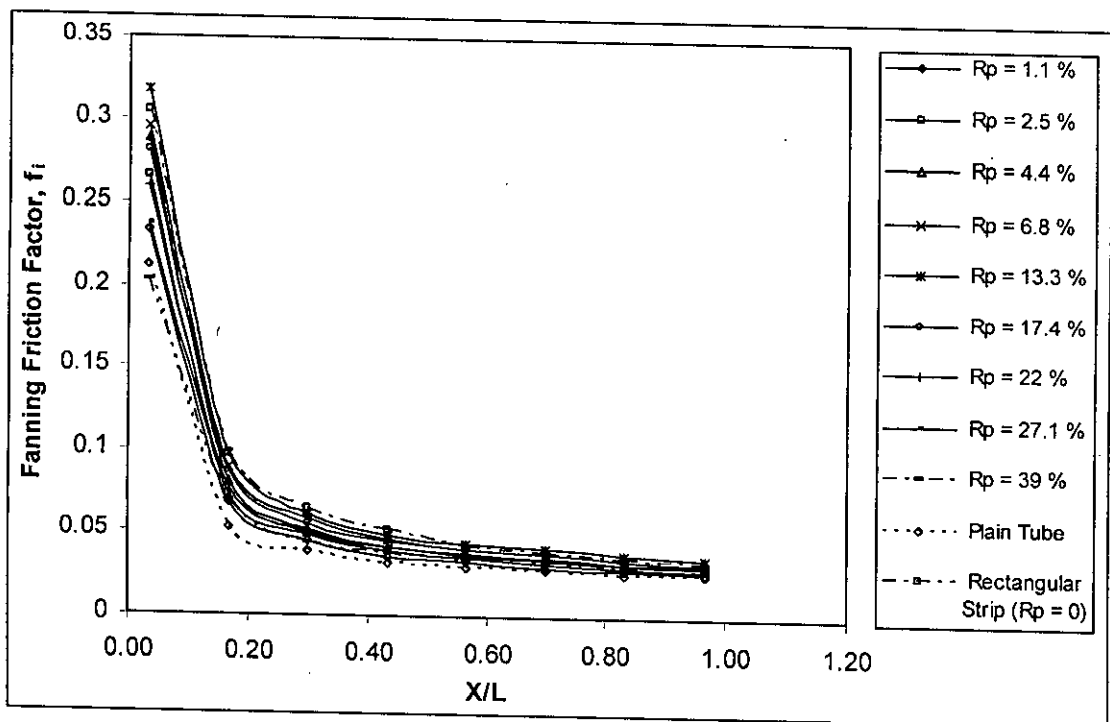


Figure 5.76(a): Variation of the friction factor along axial distance for different porosity of inserts at Reynolds number around 30,925.

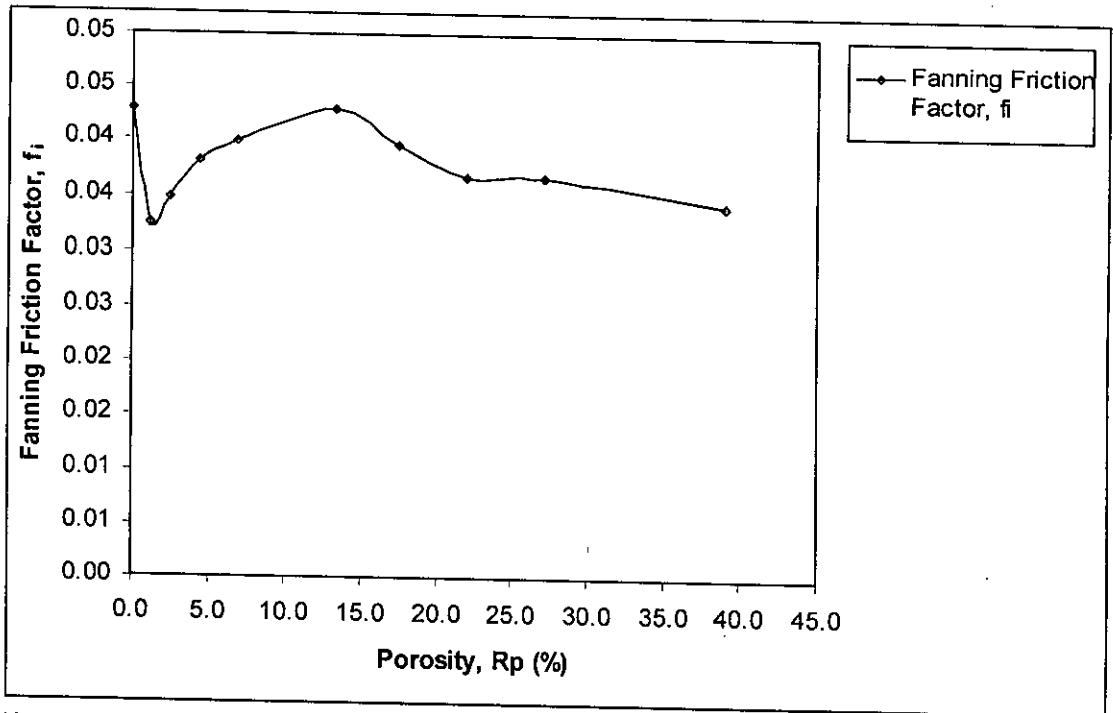


Figure 5.76(b): Variation of the friction factor with different porosity ( $R_p$  from 0 %-39 %) of inserts for axial distance of  $X/L = 0.57$  and at Reynolds number around 30,925.

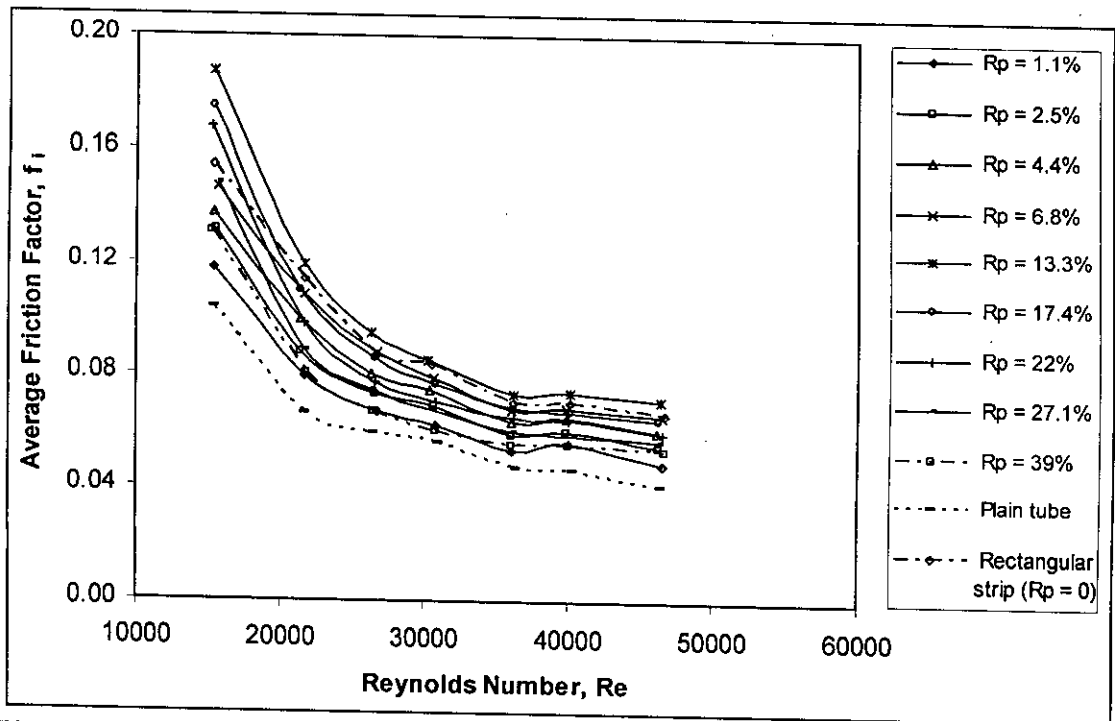


Figure 5.77: Variation of the average friction factor for different porosity of rectangular strip inserts at different Reynolds numbers.

Handwritten signature or mark.

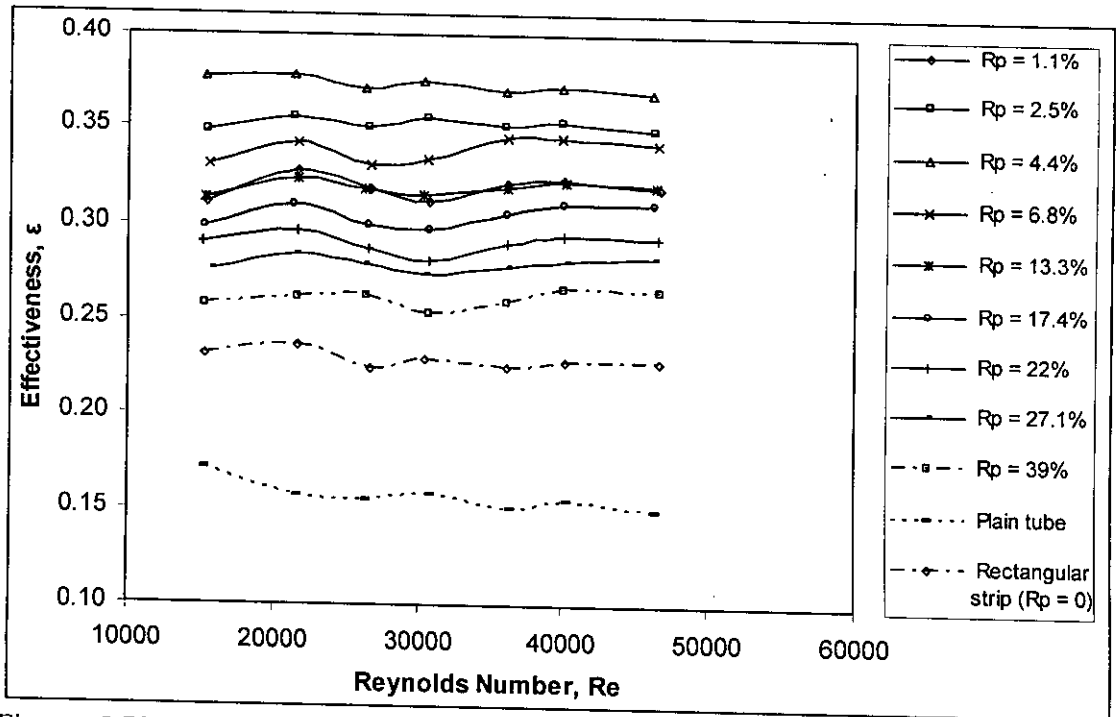


Figure 5.78: Variation of the heat transfer effectiveness for different porosity of rectangular strip inserts at different Reynolds numbers.

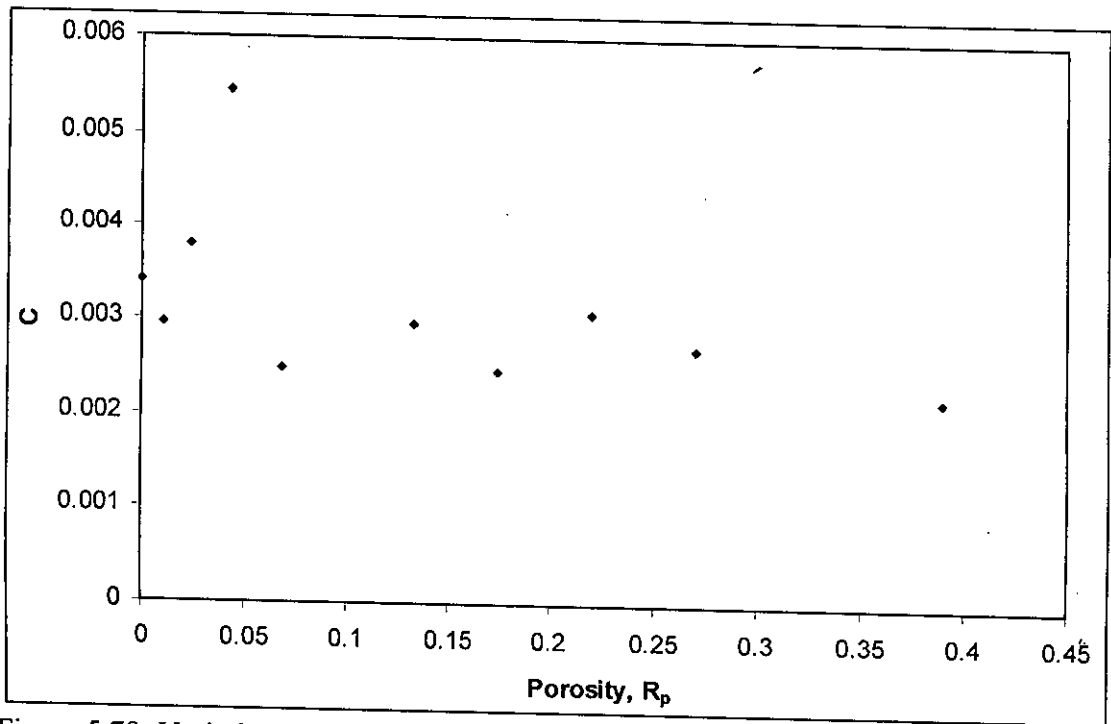


Figure 5.79: Variation of  $C$  with different porosity of the rectangular strip inserts,  $R_p$ .

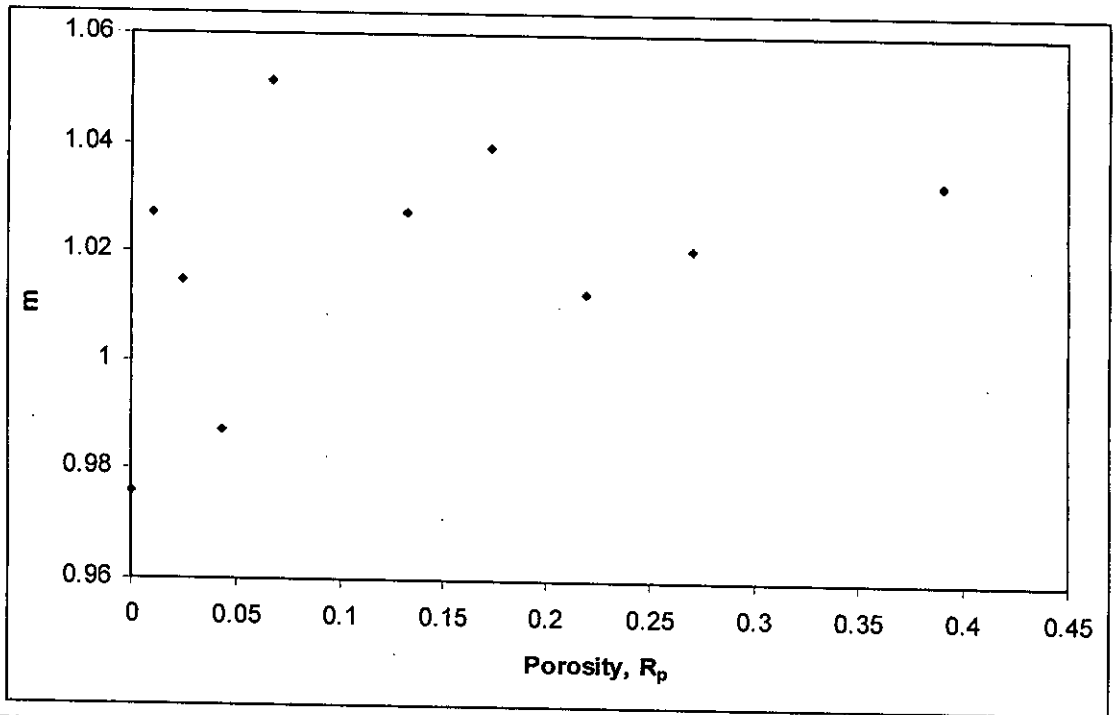


Figure 5.80: Variation of  $m$  with different porosity of the rectangular strip inserts,  $R_p$ .

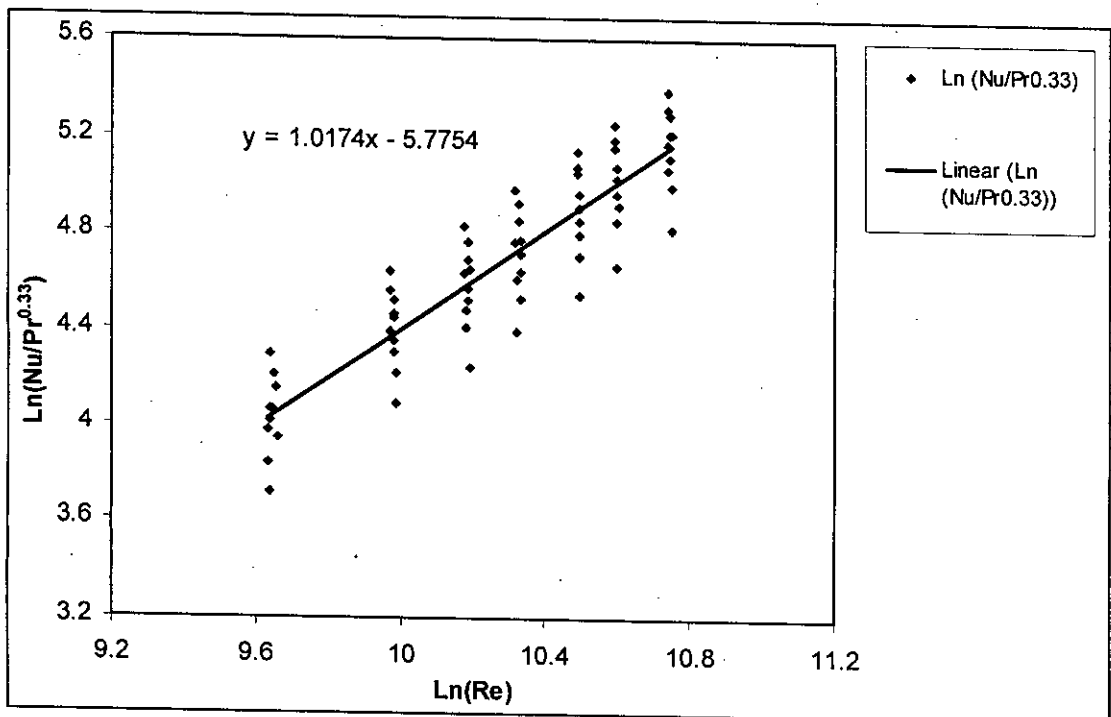


Figure 5.81: Variation of the experimental data with the predicted data for different porosity of rectangular strip inserts ( $R_p$  from 0 % to 39 %).



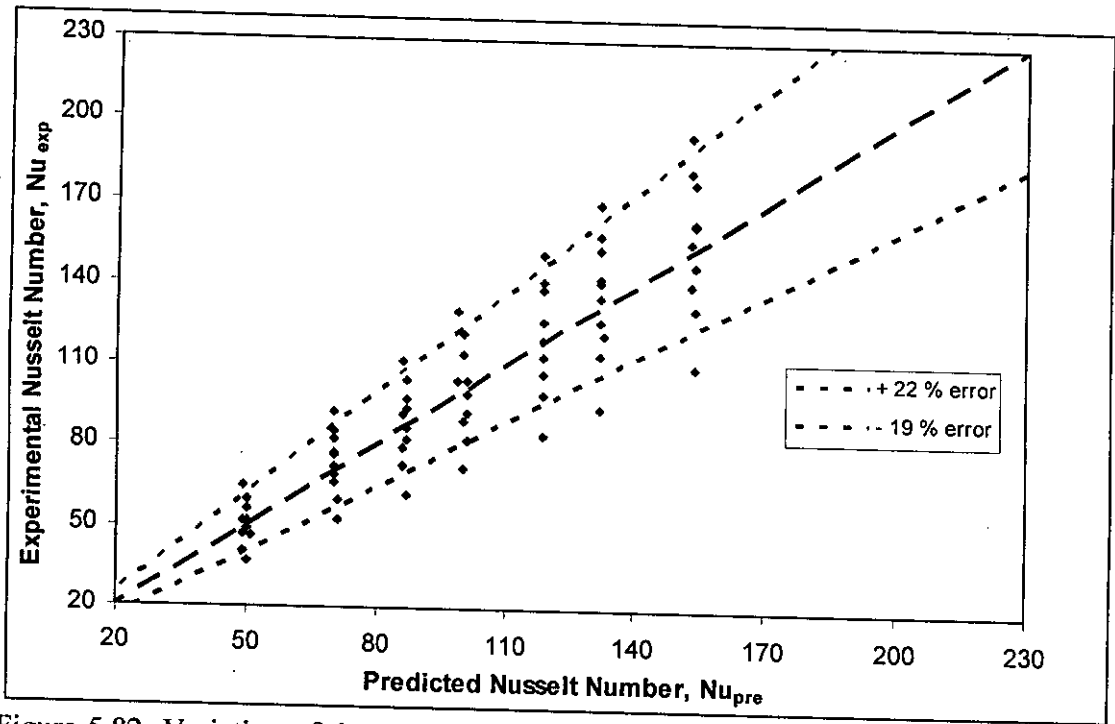


Figure 5.82: Variation of the experimental Nusselt numbers with the predicted Nusselt numbers for different porosity of rectangular strip inserts ( $R_p$  from 0 % to 39 %).

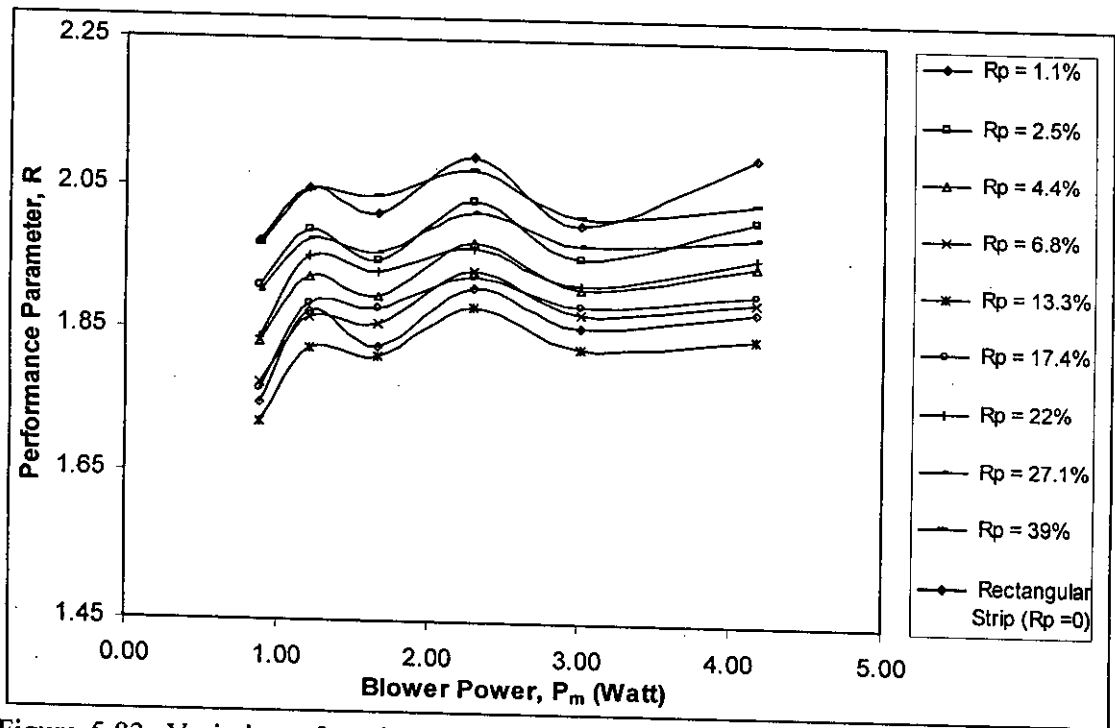


Figure 5.83: Variation of performance parameter, ( $R$ ) with blower power for different porosity of rectangular strip inserts ( $R_p$  from 0 % to 39 %).

## CHAPTER-6 CONCLUSION AND RECOMMENDATION

An experimental investigation was carried out for turbulent flow heat transfer in a circular tube with perforated rectangular strip inserts. The study revealed that the perforated rectangular strip inserts caused an increase of heat transfer. The conclusions of the present study were given below:

- The average heat transfer coefficient for the tube with perforated rectangular strip inserts varied from 1.55 to 2.80 folds compared to that of the plain tube. The average heat transfer coefficient was maximum for the tube with porosity of,  $R_p = 4.4\%$ , and varied from 2.5 to 2.80 folds compared to that of the plain tube.
- Nusselt numbers were high in the entrance and exit regions of the test section. From the entrance region it decreased gradually upto the dimensionless distance of  $x/L = 0.57$  and then increased gradually up to the exit region of the test section.
- The heat transfer rate for the tube with perforated rectangular strip inserts increased up to 1.85 times than that of the plain tube. The heat transfer rate was maximum for the tube with porosity of,  $R_p = 4.4\%$ , and varied from 1.70 to 1.85 folds compared to that of the plain tube.
- The heat transfer effectiveness for the tube with perforated rectangular strip inserts varied from 1.5 to 2.45 folds compared to that of the plain tube. And the heat transfer effectiveness was maximum for the tube with porosity of,  $R_p = 4.4\%$ .
- At constant blower power, performance parameter,  $R$  increased up to 210 % for the tube with perforated rectangular strip inserts compared to that of the plain tube.

- Heat transfer rate,  $Q$  for the tube with the perforated rectangular strip inserts was 1.45 times higher than that of the rectangular strip insert.
- The average friction factor for the tube with perforated rectangular strip inserts varied from 1.08 to 1.80 folds compared to that of the plain tube.
- The power consumed by the blower for the tube with perforated rectangular strip inserts varied from 1.05 to 1.45 folds compared to that of the plain tube. The power consumed by the blower was maximum for the tube with porosity of,  $R_p = 13.3 \%$ , and varied from 1.25 to 1.45 folds compared to that of the plain tube.
- The following correlation is proposed for prediction of heat transfer, based

on the results of the present work:

$$Nu = C Re^m Pr^{0.33}$$

For the range of porosity 0 % to 39 % a simplified form of this correlation can be reformed as:

$$Nu = 0.003 Re^{1.02} Pr^{0.33}$$

The present work will serve as the basis of further work concerning the optimization of perforated insert for application in heat exchangers. This will encourage the development of simple and cheap method to build heat exchangers with perforated insert for industrial applications.

### **Recommendations for Future Work:**

The following recommendations are made:

- The experiment may be conducted by using various geometries of inserts.
- The experiment may be conducted by using perforated cross strip of different pore diameters to compare the results with those of cross strip insert.
- The experiment may be conducted by using perforated Y-shaped strip of different pore diameters to compare the results with those of Y-shaped strip insert.

## REFERENCES

- [1] Sieder, E.N. and Tate, C. E., "Heat Transfer and Pressure Drop of Liquids in Tubes," *Ind. Engg Chemicals*, Vol. 28, p 1429, 1936.
- [2] Gunter, A. Y. and Shaw, W. A., "Heat Transfer, Pressure Drops and Fouling Rates of Liquids for Continuous and Non-continuous Longitudinal Fins," *Transactions of ASME*, Vol.64, pp. 795-802, 1942.
- [3] Hiding, W. E. and Coogan, C. H. Jr., "Heat Transfer and Pressure Drop Measurement in Internal Finned Tubes," *Symposium on Air Cooled Heat Exchanger*, ASME, National Heat Transfer Conference, Cleveland, Ohio, Pp.57-85, 1964.
- [4] Smithberg, E., and Landis, F., "Friction and Forced Convection Heat Transfer Characteristics in Tubes with Twisted Tape Swirl Generators," *Journal of Heat Transfer*, Vol. 87, pp 39-49, 1964.
- [5] Thomas, D. G., "Enhancement of Forced Convection Mass Transfer Coefficient using Detached Turbulence Promoters," *Industrial Engineering and Chemical Process Design Developments*, Vol. 6, pp. 385-390, 1967.
- [6] Lopina, R. F. and Bergles, A.E., "Heat Transfer and Pressure Drop in Tape Generated Swirl Flow of Single-phase Water," *Journal of Heat Transfer*, Vol. 91, pp. 434 - 442, 1969.
- [7] Cox, R. B., Matta, G. A., Pascale, A. S. and Stromberg, K. G., "Second Report on Horizontal Tubes Multiple-effect Perforated Pilot Plant Test and Design," *off Saline Water Res. Dev. Rep. No. 592 DSW*, Washington, DC, May, 1970.
- [8] Webb, B. L., Eckert, E. R. G., and Goldstein, R. J., "Heat Transfer and Friction in Tubes with Repeated Rib Roughness," *International Journal of Heat and Mass Transfer* 14, 601- 617, 1971.
- [9] Prince, W. J., "Enhanced Tubes for Horizontal Evaporation Desalination Process," *MS thesis in Engineering University of California, Loss Angles*, 1971.
- [10] Hu, M. H. and Chang, Y. P., "Optimization of Finned Tubes for Heat Transfer in Laminar Flow," *Journal of Heat Transfer*, Vol. 95, pp. 332-338, 1973.
- [11] Date, A.W., "Prediction of Fully-Developed Flow in a Tube Containing a Twisted Tape," *International Journal of Heat Mass Transfer*, Vol. 17, pp. 845-859, 1974.
- [12] Mergerlin, F. E., Murphy, R. W. and Bergles, A. E., "Augmentation of Heat Transfer in Tubes by Means of Mesh and Brush Inserts," *Journal of Heat Transfer*, Vol. 96, pp. 145-151, 1974.
- [13] Patankar, S.V., Ivanovic, M. and Sparrow, E.M., "Analysis of Turbulent Flow and Heat Transfer in Internally Finned Tubes and Annuli," *Journal of Heat Transfer*, Vol.101, pp. 29-37, 1979.
- [14] Gee, D. L., and Webb, R.L., "Forced Convection Heat Transfer in Helically Rib Roughened Tubes," *International Journal of Heat and Mass Transfer*, Vol. 23, 1127-1136, 1980.
- [15] Uttawar, S. B., and Raja Rao, M., "Augmentation of Laminar Flow Heat Transfer in Tubes by Means of Wire Coil Inserts," *Journal of Heat*

- Transfer, Vol. 105, pp 930-935, 1985.
- [16] Plessis, J.P. and Kroger, D.G., "Heat Transfer Correlation for Thermally Developing Laminar flow in a Plain Tube with a Twisted- Tape Insert," *International Journal of Heat and Mass Transfer*, Vol. 30, No. 3, pp. 509-515, 1987.
- [17] Garimella, S., Chandrachud, V., Christensen, R.N. and Richards, D.E., "Investigation of Heat Transfer and Pressure Drop Augmentation for Turbulent Flow in Spirally Enhanced Tubes," *ASHRAE Transactions*, Vol. 94, Part 2, pp. 1119-1131, 1988.
- [18] Gupte, N. S. and Date, A.W., "Friction and Heat Transfer Characteristics of Helical Turbulent Air Flow in Annuli," *Journal of Heat Transfer*, Vol. 111, pp. 337-344, 1989.
- [19] Zhuo, N., Ma, Q. L., Zhang, Z. Y., Sun, J. Q. and He, J., " Friction and Heat Transfer Characteristics in a loose Fitting Twisted Tape insert," in *Multiphase Flow and Heat Transfer, Second International Symposium*, Hemisphere Publishing corp., New York, Vol.1, pp. 657-661, 1992.
- [20] Manglik, R. M. and Bergles, A.E., "Heat Transfer and Pressure Drop Correlations for Twisted-Tape-Inserts in Isothermal Tubes: Part 1- Laminar Flows," *Journal of Heat Transfer*, Vol.115, pp. 881-889, 1993a.
- [21] Manglik, R. M. and Bergles, A.E., "Heat Transfer and Pressure Drop Correlations for Twisted-Tape Inserts in Isothermal Tubes: Part 2- Transition and Turbulent Flows," *Journal of Heat Transfer*, Vol. 115, pp.890-896, 1993b.
- [22] Garimella, S. and Christensen, R. N., "Heat Transfer and Pressure Drop Characteristics of Spirally Fluted Annuli: Part II-Heat transfer," *ASME Journal of Heat Transfer*, Vol.117, pp.61-68, 1995.
- [23] Agarwal, S. K. and Raja Rao, M., "Heat Transfer Augmentation for the Flow of a Viscous Liquid in Circular Tubes using Twisted Tape Inserts," *International Journal of Heat and Mass Transfer*, Vol. 39, pp. 3547-3557, 1996.
- [24] Huq, M., "An Experimental Study of Heat Transfer in an Internally Finned Tube," M.Sc. Thesis, Dept. of Mech. Engg., BUET, Dhaka, 1989.
- [25] Dutta, S and Han, J.C., "Local Heat Transfer in Rotating Smooth & Ribbed Two-Pass Square Channels with Three Channel Orientations," *Journal of Heat Transfer*, Vol. 118, pp. 578-584, 1996.
- [26] Uddin, J.M., "Study of Pressure Drop Characteristics and Heat Transfer Performance in an Internally Finned Tube," M.Sc. Thesis, Dept. of Mech. Engg., BUET, Dhaka, 1998.
- [27] Buyruk, E., Johnson, M.W. and Owen, I., " Numerical and Experimental Study of Flow and Heat Transfer Around a Tube in Cross-Flow at low Reynolds Number," *International Journal of Heat and fluid flow* Vol. 19, pp. 223-232, 1998.
- [28] Mamun, A. H. M., "Pressure Drop and Heat Transfer in an Internally Finned Tube," M.Sc.Thesis, Dept. of Mechanical Engg., BUET, Dhaka, 1999.
- [29] Hsieh, S. S. and Huang, I. W., "Heat transfer and Pressure Drop of Laminar Flow in Horizontal Tubes With/Without Longitudinal Inserts," *Journal of Heat Transfer*, Vol. 122, pp. 465-476, 2000.

- [30] Aloke Kumar Mozumder, "Heat Transfer Performance of Internally Finned Tube," M. Sc. Thesis, Dept. of Mech. Engg., BUET, Dhaka, 2001.
- [31] Liu, X. and Jensen, M. K., "Geometry Effects on Turbulent Flow and Heat Transfer in Internally Finned Tubes," *Journal of Heat Transfer*, Vol. 123, pp. 1035-1043, 2001.
- [32] Saha, S. K and Dutta, A., "Thermohydraulic Study of Laminar Swirl Flow through a Circular Tube Fitted with Twisted Tapes," *ASME, Journal of Heat Transfer*, Vol. 123, pp 417-425, 2001.
- [33] Chen, J., Steinhagen, H.M. and Duffy, G.G., "Heat Transfer Enhancement in Dimpled Tubes," *Applied Thermal Engineering*, Vol. 21, pp. 535-547, 2001.
- [34] Saha, S. K and Langille, P., "Heat Transfer and Pressure Drop characteristics of Laminar Flow Through a Circular Tube with Longitudinal Strip Inserts Under Uniform Wall Heat Flux," *ASME, Journal of Heat Transfer*, Vol.124, pp. 421-430, 2002.
- [35] Mohamad, A. A., "Heat Transfer Enhancement in Heat Exchangers Fitted with Perforated Media. Part1: Constant Wall Temperature," *International Journal of Heat and Mass Transfer*, Vol.42, pp.385-395, 2003.
- [36] Hsieh, S. S., Wu, F. Y. and Tsai, H. H, "Turbulent Heat Transfer and Flow Characteristics in a Horizontal Circular Tube with Strip-Type Inserts: Part I. Fluid mechanics," *International Journal of Heat and Mass Transfer*, Vol. 46, pp. 823-835, 2003.
- [37] Pavel, B. I. and Mohamad, A. A., "Experimental Investigation of the Potential of Metallic perforated Inserts in Enhancing Forced Convective Heat Transfer," *Journal of Heat Transfer*, Vol. 126, pp.540-545, 2004.
- [38] Eiamsa-ard, S., Ploychay, Y., Sripattanapipat, S. And Promvong, P., "An Experimental Study of Heat Transfer and Friction Factor Characteristics in a Circular Tube Fitted with a Helical Tape," *Proceedings of the 18<sup>th</sup> Conference of Mechanical Engineering Network of Thailand*, October 2004, Khon Kaen.
- [39] Sahiti, N., Durst, F. and Dewan, A., "Heat Transfer Enhancement by Pin Elements," *International Journal of Heat and Mass Transfer*, Vol. 48, pp.4738-4747, 2005.
- [40] Islam, M. Z., "Heat Transfer in Turbulent Flow through Tube with Wire-Coil-Inserts," M. Sc. Thesis, Dept. of Mech. Engg., BUET, Dhaka, 2004.
- [41] Abedin, M.Z., "Heat Transfer in Turbulent Flow through Tube with Wire-Coil-Inserts at low Reynolds number," M. Engg. Thesis, Dept. of Mech. Engg., BUET, Dhaka, 2004.
- [42] Garcia, A., Vicente, P. G. and Viedma, A., "Experimental Study of Heat Transfer Enhancement with Wire-Coil-Inserts in Laminar-Transition-Turbulent Regimes at Different Prandtl Numbers," *International Journal of Heat and Mass Transfer*, Vol. 48, pp. 4640-4651, 2005.
- [43] Ahmed, M., Deju, L., Sarkar, M. A. R., and Islam, S. M. N., "Heat Transfer in Turbulent Flow through a Circular Tube with Twisted Tape Inserts," *Proceedings of ICME-Dhaka, TH-08*, 2005.
- [44] Sarkar, M. A. R, Hasan, A. B. M. Toufique, Ehsan, M., Talukdar, M. M. Alam and Huq, A. M. A., "Heat Transfer in Turbulent Flow through Tube with Longitudinal Strip Inserts," *Proceedings of ICME-Dhaka, TH-46*, 2005.

- [45] Ahamed, J. U., "Heat Transfer in Turbulent Flow through Tube with Perforated Twisted Tape Insert." M. Sc. Thesis, Dept. of Mech. Engg., BUET, Dhaka, 2007.
- [46] Owner, E. and Pankhurst, R. C., "The Measurement of Air flow.," Fifth Edition (in SI units), Pergamon Press, 1977.
- [47] Kline, S. J. and McClintock, F. A., " Describing Uncertainties in Single-Sample Experiments," Mechanical Engineering, 75, January, pp.3-8, 1953.



**APPENDIX-A**  
**SPECIFICATION OF EQUIPMENT**

**1. Blower:**

Capacity	:	30 m <sup>3</sup> /min.
Pressure	:	125 mm of water
H.P	:	3
Phase	:	3
Current	:	4.1 Amp
Voltage	:	380 V

**2. Temperature Controller:**

Range	:	0-200°C
Input voltage	:	220V

**3. Electric Heating System:**

Heat Resistance	:	5.8 Ohm
Maximum Voltage	:	115 Volts
Maximum Current	:	18A
Power	:	1.980 kW

**4. Rotary Selector Switches: OMEGA**

Insulator Resistance	:	2 MΩ or less
Contact Resistance	:	0004 Ω or less
Continuous use Temperature	:	110 °Centigrade

**APPENDIX-B**  
**SAMPLE CALCULATION**

**For Plain Tube:**

Internal diameter of the tube,  $D_i = 70 \text{ mm}$ .

Cross sectional area,  $A_x = \pi D_i^2 / 4 = 3.85 \times 10^{-3} \text{ m}^2$

Perimeter,  $W_s = \pi D_i = 0.2199 \text{ m}$

**Determination of Mean Velocity, V:**

$$\Delta P = \frac{1}{2} \rho V^2 \quad [\text{From Bernoulli's equation}] \quad (\text{B.1})$$

If V was m/s,  $\rho$  was  $\text{kg/m}^3$ ,  $\Delta P$  was  $\text{N/m}^2$  and d was the velocity head expressed in cm of water, then

$$\begin{aligned} \Delta P &= \gamma_{\text{water}} \times d \\ &= 98.1 \times d \text{ N/m}^2 \end{aligned} \quad (\text{B.2})$$

**Standard Atmospheric Properties at the Sea Level are:**

Pressure = 760 mm of Hg.

Temperature = 15 °C

Density = 1.225  $\text{Kg/m}^3$

For any temperature  $T_\infty$  °C and pressure b mm of Hg, the value of the density in  $\text{Kg/m}^3$  was calculated as –

$$\rho_2 = \frac{P_2 T_1}{P_1 T_2} \rho_1 = \frac{b}{760} \times \frac{(273 + 15)}{(273 + T_\infty)} \times 1.225 \quad (\text{B.3})$$

From equation (B.1), (B.2) and (B.3) ---

$$V = C\sqrt{d}$$

$$\text{Where, } C = 20.558 \sqrt{\left(\frac{273 + T_{\infty}}{b}\right)} \quad (\text{B.4})$$

**Room Condition:**

Temperature,  $T_{\infty} = 24^{\circ}\text{C}$

Pressure,  $b = 761 \text{ mm of Hg}$

Therefore,

$$C = 20.558 \sqrt{\left(\frac{273 + 24}{761}\right)}$$

$$= 12.84$$

The experiment was conducted using a manometric fluid of sp.gr = 0.855 but it was recommended to perform with a fluid of sp.gr = 0.834. For this reason a correction was needed which was as follows-

$$\omega d = \omega_1 d_1$$

$$\Rightarrow d = 0.8765 \times 2.54 d_1 \text{ cm} \quad [d_1 \text{ is in inch of water}]$$

$$\Rightarrow d = 2.2263 d_1 \text{ cm}$$

Measurement of mean velocity of 11 points was as follows –

$$\text{Mean inlet velocity, } V_i = C \frac{\sqrt{2.2263} (\sqrt{d_1} + \sqrt{d_2} + \dots + \sqrt{d_{11}})}{11}$$

$$= 10.36 \text{ m/s}$$

Mass flow rate,  $m = \rho A_x V_i$

$$= 1.191524 \times 3.85 \times 10^{-3} \times 10.36$$

$$= 0.047499 \text{ Kg/s}$$

[Density of air at room temperature =  $1.191524 \text{ Kg/m}^3$ ]

In the test section, the velocity of air would be

$$V = \frac{m}{\rho_b A_x} \quad [\text{Density at bulk mean temperature}]$$

$$= \frac{0.047499}{1.167892 \times 3.85 \times 10^{-3}}$$

$$= 10.568 \text{ m/s}$$

**Reynolds Number:**

Now,  $Re = \frac{\rho_b V D_i}{\mu}$

$$= 46491 \quad [\text{Fluid properties were calculated at its bulk temp.}]$$

**Friction Factor:**

Local friction factor based on inside diameter was given by –

$$F_i = \frac{(-\Delta P/x)D_i}{2\rho_b V^2} \quad [\text{Where } \Delta P \text{ was in N/m}^2] \quad (B5)$$

$$= 0.00027 \times (\Delta P/x) \quad [\rho_b \text{ of air at } 28.25^\circ\text{C was } 1.167892 \text{ kg/m}^3]$$

Table B.1: Experimental data of fluid flow through plain tube

Axial distance, x (mm)	Tapping Pressure(mm of water)	Tapping Pressure (N/m <sup>2</sup> )	Pressure drop, ΔP(N/m <sup>2</sup> )	Friction factor, f <sub>i</sub>
0	6	58.658	-	-
50	9	87.987	29.329	0.157
250	10	97.763	39.105	0.042
450	10.5	102.652	43.994	0.026
650	11.5	112.428	53.770	0.022
850	13	127.092	68.434	0.022
1050	14	136.869	78.211	0.020
1250	15	146.645	87.987	0.019
1450	16.5	161.310	102.652	0.019

**Heat Transfer Calculation:**

Air inlet temperature,  $T_i = 24.2$  °C

Air outlet temperature,  $T_o = 32.3$  °C

Properties of air were calculated at fluid bulk temperature as-

$$C_p = 1005.875 \text{ J/kg } ^\circ\text{C}$$

$$k = 0.026441 \text{ W/m.k}$$

$$\mu = 1.858326 \times 10^{-5} \text{ Kg/m.s}$$

$$\rho = 1.167892 \text{ Kg/m}^3$$

Heat supplied by electrically,

Supplied Voltage,  $V = 80$  volts

Supplied current,  $I = 13.8$  amp

Constant heat supplied,  $Q_{in} = VICos\theta$

$$= 80 \times 13.8 \times 0.8 \text{ (assuming power factor, } \cos\theta = 0.8)$$

$$= 883 \text{ W}$$

Total heat taken by air,  $Q = mC_p(T_o - T_i)$

$$= 0.047499 \times 1005.875 \times (32.3 - 24.2)$$

$$= 387 \text{ W}$$

Heat taken per unit area,  $q_s = Q / (W_s \times L)$

$$= 387 / (0.2199 \times 1.5)$$

$$= 1173.20 \text{ W/m}^2$$

The local bulk temperature of the fluid was calculated according to the following way-

$$q = Q / W_s L = mC_p \Delta T / W_s L$$

$$\Delta T = q W_s L / (mC_p)$$

Now, fluid bulk temperature

$$T_{bx} = T_i + (\Delta T)_x$$

$$T_{bx} = T_i + \frac{q W_s x}{mC_p}$$

$$= 24.2 + 5.4 x \text{ } ^\circ\text{C}$$

Local convective heat transfer co-efficient was given by

$$h_x = \frac{q}{(T_w - T_b)_x} = \frac{1173.20}{(T_w - T_b)_x}$$

Local Nusselt Number,

$$\text{Nu}_x = \frac{h_x D_i}{k} = 2.65 h_x$$

Table B.2: Experimental data of heat transfer for plain tube.

Axial Distance, x(m)	Bulk Temperature, $T_{bx}$ ( $^\circ\text{C}$ )	Wall Temperature, $T_{wx}$ ( $^\circ\text{C}$ )	Local heat Transfer coeff., $h_x$ ( $\text{W}/\text{m}^2\text{ } ^\circ\text{C}$ )	Local Nusselt number, $\text{Nu}_x$	Average, $h$ ( $\text{W}/\text{m}^2\text{ } ^\circ\text{C}$ )	Average, $\text{Nu}$
0.05	24.47	56	37.21	98.51		
0.25	25.55	67	28.30	74.93		
0.45	26.63	70.5	26.74	70.80		
0.65	27.71	75.5	24.55	64.99	26.41	69.91
0.85	28.79	93.5	18.13	48.00		
1.05	29.87	89.5	19.67	52.09		
1.25	30.95	76.5	25.76	68.19		
1.45	32.03	70	30.90	81.80		

$$\text{Required blower power, } P_m = \frac{\Delta P}{\rho_b} \cdot m = 4.1749 \text{ W}$$

Heat transfer effectiveness of the heat exchanger was calculated as

$$\begin{aligned} \varepsilon &= \frac{(T_{bo} - T_{bi})}{(T_{wav} - T_{bi})} \\ \Rightarrow \varepsilon &= \frac{(32.03 - 24.47)}{(74.81 - 24.47)} \\ &= 0.150 \end{aligned}$$

Gasket was used in the entrance and exit of the test section. So, heat was conducted from the wall axially. But radial heat flow was to be neglected.

Inlet and outlet wall temperatures were,  $T_{wi} = 56^{\circ} \text{C}$  and  $T_{wo} = 70^{\circ} \text{C}$

Atmospheric Temperature,  $T_{\infty} = 24^{\circ} \text{C}$

Thermal conductivity for gasket,  $k = 0.166 \text{ W/mK}$

$$\begin{aligned} \text{Total heat conducted through gasket, } Q_x &= 0.166 * 22/7 * (.156^2 - .07^2) / 4 * \{(70 - 24) + (56 - 24)\} / (.0035) \\ &= 56.49 \text{ W} \end{aligned}$$

$$\text{Heat lost by conduction} = 56.49 / 387 = 14.5 \%$$

**For Tube with Perforated Rectangular Strip Insert:**

For porosity of rectangular strip,  $R_p = 1.1 \%$

Pore diameter,  $d_p = 2 \text{ mm}$ , No. of holes in a row was 100.

No. of row was 3. So, total hole in a row was 300. And thickness of the strip,  $t = 3 \text{ mm}$ ,

Width of the strip,  $W_p = 58 \text{ mm}$

Porosity,

$$\begin{aligned} R_p &= \frac{\text{Total pores area}}{\text{Total strip area}} \\ &= \frac{300 \times \pi \times .002^2}{4 \times 0.058 \times 1.5} \\ &= 0.011 \\ &= 1.1 \% \end{aligned}$$

Cross Sectional area of the tube with perforated rectangular strip insert  
(Based on inside diameter of the tube)

$$\begin{aligned} A_{xp} &= \frac{\pi \times D_i^2}{4} \\ &= \frac{\pi \times 0.07^2}{4} \\ &= 3.85 \times 10^{-3} \text{ m}^2 \end{aligned}$$

Cross Sectional area of the tube for different inserts was different for different porosity of inserts. So, cross sectional area of the plain tube was considered.

$$\text{Mean inlet velocity, } V_i = C \frac{\sqrt{2.2263} (\sqrt{d_1} + \sqrt{d_2} + \dots + \sqrt{d_{11}})}{11}$$

$$= 10.44 \text{ m/s}$$

$$\text{Mass flow rate, } m = \rho A_x V_i$$

$$= 1.191524 \times 3.85 \times 10^{-3} \times 10.44$$

$$= 0.047871 \text{ Kg/s}$$

[Density of air at room temperature = 1.191524 Kg/m<sup>3</sup>]

In the test section, the velocity of the air was calculated as

$$V = \frac{m}{\rho_b A_x}$$

$$= \frac{0.047871}{1.161882 \times 0.00385}$$

$$= 10.71 \text{ m/s}$$

**Reynolds Number:**

$$\text{Now, } R_e = \frac{\rho_b V D_i}{\mu}$$

$$= 46654 \quad [\text{Fluid properties were calculated at its bulk temp.}]$$

**Friction Factor:**

Local friction factor based on inside diameter was given by –

$$f_i = \frac{(-\Delta P/X) D_i}{2 \rho_b V^2} \quad [\text{Where } \Delta P \text{ was in N/m}^2] \quad (B5)$$

$$= 0.00026 \times (\Delta P/x) \quad [\rho_b \text{ of air at } 31.4^\circ \text{C was } 1.161613 \text{ kg/m}^3]$$



Table B.3: Experimental data of fluid flow through tube with perforated rectangular strip insert.

Axial distance, x (mm)	Tapping Pressure(mm of water)	Tapping Pressure, (N/m <sup>2</sup> )	Pressure drop, ΔP(N/m <sup>2</sup> )	Friction factor, f <sub>i</sub>
0	6.2	60.61		
50	9.6	93.85	33.24	0.175
250	11.5	112.43	51.81	0.054
450	12.25	119.76	59.15	0.035
650	13.5	131.98	71.37	0.029
850	14.75	144.20	83.59	0.026
1050	15.75	153.98	93.36	0.023
1250	16.75	163.75	103.14	0.022
1450	18.2	177.93	117.32	0.021

**Heat Transfer Calculation:**

Air inlet temperature,  $T_i = 24.4$  °C

Air outlet temperature,  $T_o = 38.4$  °C

Properties of air were calculated at fluid bulk temperature as-

$$C_p = 1005.99 \text{ J/kg } 0\text{C}$$

$$K = 0.02657352 \text{ W/m.k}$$

$$\mu = 1.866334 \times 10^{-5} \text{ Kg/m.s}$$

$$\rho = 1.161613 \text{ Kg/m}^3$$

$$\begin{aligned} \text{Total heat taken by air, } Q &= mC_p (T_o - T_i) \\ &= 0.047871 \times 1005.99 \times (38.4 - 24.4) \\ &= 674.21 \text{ W} \end{aligned}$$

$$\begin{aligned} \text{Heat taken per unit area, } q &= Q / (W_s \times L) \\ &= 674.21 / (.22 \times 1.5) \\ &= 2043.86 \text{ W/m}^2 \end{aligned}$$

The local bulk temperature of the fluid could be calculated according to the following way-

$$q = Q / W_s L = mC_p \Delta T / W_s L$$

$$\Delta T = q W_s L / (m C_p)$$

Now, fluid bulk temperature

$$T_{bx} = T_i + (\Delta T)_x$$

$$T_{bx} = T_i + \frac{q W_s x}{m C_p}$$

$$= 24.4 + 9.33 x \text{ } ^\circ\text{C}$$

Local convective heat transfer co-efficient was given by

$$h_x = \frac{q}{(T_w - T_b)_x} = \frac{2043.86}{(T_w - T_b)_x}$$

Local Nusselt Number on the basis of inside diameter,

$$Nu_x = \frac{h_x D_i}{k} = 2.63 h_x$$

Table B.4: Experimental data of heat transfer through the tube with perforated rectangular strip insert.

Axial Distance, x(m)	Bulk Temperature, $T_{bx}$ ( $^\circ\text{C}$ )	Wall Temperature, $T_{wx}$ ( $^\circ\text{C}$ )	Local heat Transfer coeff., $h_x$ ( $\text{W}/\text{m}^2\text{ } ^\circ\text{C}$ )	Local Nusselt number, $Nu_x$	Average, $h$ ( $\text{W}/\text{m}^2\text{ } ^\circ\text{C}$ )	Average, $Nu$
0.05	24.87	52	75.33	198.43		
0.25	26.73	59	63.34	166.86		
0.45	28.60	62.5	60.29	158.82		
0.65	30.47	67	55.95	147.37	62.10	163.58
0.85	32.33	81	42.00	110.63		
1.05	34.20	76	48.90	128.80		
1.25	36.07	65.5	69.44	182.92		
1.45	37.93	63	81.54	214.79		

$$\text{Required blower power, } P_m = \frac{\Delta P}{\rho_b} \cdot m = 4.83 \text{ W}$$

Heat transfer effectiveness of the heat exchanger was calculated as

$$\begin{aligned}\varepsilon &= \frac{(T_{bo} - T_{bi})}{(T_{wav} - T_{bi})} \\ \Rightarrow \varepsilon &= \frac{(37.93 - 24.87)}{(65.75 - 24.87)} \\ &= 0.32\end{aligned}$$

Gasket was used in the entrance and exit of the test section. Heat was conducted from the axially. Heat lost by convection was neglected.

Inlet and out let wall temperatures were  $T_{wi} = 52^{\circ} \text{C}$  and  $T_{wo} = 63^{\circ} \text{C}$

Atmospheric Temperature,  $T_{\infty} = 24^{\circ} \text{C}$

Thermal conductivity for gasket,  $k = 0.166 \text{ W/mK}$

$$\begin{aligned}\text{Total heat conducted through gasket, } Q_x &= 0.166 * 22/7 * (.156^2 - .07^2) / 4 * \{(63 - 24) + (52 - 24)\} / (.0035) \\ &= 48.527 \text{ W}\end{aligned}$$

$$\text{Heat lost by conduction} = 48.527 / 674.21 = 7 \%$$

### Constant Pumping Power Result:

Equivalent Reynolds number for the Tube with perforated rectangular strip insert on the basis of constant blower power, from equation (3.20)

$$\begin{aligned}Re_p &= Re_s \left( \frac{f_s}{f_p} \right)^{1/3} \\ \Rightarrow Re_p &= 46491 \times \left( \frac{0.041}{0.048} \right)^{1/3} \\ &= 44077\end{aligned}$$

This Reynolds number had the same pumping power. Using the correlation equation (5.5) for perforated rectangular strip insert,

$$\begin{aligned}Nu_p &= 0.003 \times 44074^{1.02} \times 0.7^{0.33} \\ &= 146.45\end{aligned}$$

For plain tube constant blower power,  $Nu_s = 69.91$

So, Performance parameter(R), Using equation (3.16)

$$\begin{aligned} R &= \frac{Nu_p}{Nu_s} \\ &= \frac{146.45}{69.91} \\ &= 2.09 \end{aligned}$$

**APPENDIX-C**

**DETERMINATION OF LOCATION OF MEASURING  
INSTRUMENTS**

**1. Location of Pitot Tube for Velocity Measurement:**

When fluid flowed through tube, velocity head varied from wall to center of the tube. To obtain the mean velocity, the tube diameter was divided into five equal concentric areas, and their centers were calculated by using arithmetic mean method. The locations of the traversing pitot tube are shown in Figure. 4.7. The locations were calculated as follows: Considering  $R$  is the radius of the whole tube and  $r_1$  is the radius of a circle of equal concentric areas.

$$\text{So, } \frac{1}{5} \pi R^2 = \pi r_1^2$$
$$\Rightarrow r_1 = 0.447R$$

And  $r_2$  is the radius of another concentric circle, then

$$\frac{1}{5} \pi R^2 = \pi r_2^2 - \pi r_1^2$$
$$\Rightarrow r_2 = 0.632R$$

Similarly,

$$r_3 = 0.774R, r_4 = 0.894R \text{ and } r_5 = 1R$$

Now, to find the center of these circles,

$$\pi r_{5-4}^2 = \frac{\pi R^2 + \pi(0.894R)^2}{2}$$

$$\Rightarrow r_{5-4} = 0.948R$$

$$\pi r_{4-3}^2 = \frac{\pi(0.894R)^2 + \pi(0.774R)^2}{2}$$

$$\Rightarrow r_{4-3} = 0.836R$$

Similarly,

$$r_{3-2} = 0.7065 R$$

$$r_{2-1} = 0.547 R$$

$$r_{1-0} = 0.316 R$$

## 2. Location of Thermocouple:

Temperature of the flowing fluid also changed with radial locations of the thermocouple. Tube diameter was divided into three equal concentric areas to determine the outlet temperature of the air. The arithmetic mean method was used to find out the centers of the areas. The locations of the thermocouples are shown in Figure 4.10. The arithmetic mean method was as follows:

$$D=0.07 \text{ m}$$

$$R_1 = 0.035 \text{ m}$$

$$A = \pi R_1^2 = 0.003848 \text{ m}^2$$

$$A/3 = A_1 = A_2 = A_3 = 0.0012828 \text{ m}^2$$

$$A_1 = \pi R_1^2 - \pi R_2^2$$

And  $A_2 = \pi R_2^2 - \pi R_3^2$

$$A_3 = \pi R_3^2$$

Now volume flow rate,

$$Q_1 = A_1 V \rho C_p (T_{b1} - T_i)$$

$$Q_2 = A_2 V \rho C_p (T_{b2} - T_i)$$

$$Q_3 = A_3 V \rho C_p (T_{b3} - T_i)$$

Now total

$$Q = Q_1 + Q_2 + Q_3 = A_1 V \rho C_p (T_{b1} + T_{b2} + T_{b3} - 3T_i)$$

$$\Rightarrow A V \rho C_p (T_{bavg} - T_i) = A_1 V \rho C_p (T_{b1} + T_{b2} + T_{b3} - 3T_i)$$

$$\Rightarrow 3A_1 (T_{bavg} - T_i) = A_1 (T_{b1} + T_{b2} + T_{b3} - 3T_i)$$

$$\Rightarrow T_{bavg} = \frac{T_{b1} + T_{b2} + T_{b3}}{3}$$

$$A_1 = \pi R_1^2 - \pi R_2^2$$

$$\Rightarrow 0.0012828 = \pi (0.035)^2 - \pi R_2^2$$

$$\Rightarrow R_2 = 0.0286 \text{ m}$$

$$A_2 = \pi R_2^2 - \pi R_3^2$$

$$\Rightarrow 0.0012828 = \pi (0.0286)^2 - \pi R_3^2$$

$$\Rightarrow R_3 = 0.02024 \text{ m}$$

Now for center,

$$\pi r_1^2 = \frac{\pi R_1^2 + \pi R_2^2}{2}$$

$$\Rightarrow r_1 = 0.0319 \text{ m}$$

Similarly,

$$\pi r_2^2 = \frac{\pi R_2^2 + \pi R_3^2}{2}$$

$$\Rightarrow r_2 = 0.02475 \text{ m and } r_3 = 0.0143 \text{ m}$$

$$r_1' = 0.035 - r_1 = 0.00304 \text{ m}$$

$$r_2' = 0.035 - r_2 = 0.01025 \text{ m}$$

$$r_3' = 0.035 - r_3 = 0.02068 \text{ m}$$

Mean outlet temperature was measured by traversing the thermocouple along the diameter of the tube at seven measuring points.

## APPENDIX-D

### UNCERTAINTY ANALYSIS

In this experiment there might be some inaccuracies in measuring the primary data. It needed a description of such inaccuracies. It was known that an appropriate idea for expressing inaccuracies was an "uncertainty" and the actual value should be provided by an "uncertainty analysis". An uncertainty was not the same as an error. The error in the measurement was the difference between the true value and the measured value. Since uncertainty could take on various values over a range, it was inherently a statistical variable.

A more precise method of estimating uncertainty in experimental results was presented by Kline and McClintock [47]. The method was based on a careful specification of the uncertainties in the various primary experimental measurements. When the plus or minus notation was used to designate the uncertainty, the person making this designation was stating the degree of accuracy with which he or she believed the measurement was made. We might note that this specification was in itself uncertain because the experimenter was naturally uncertain about the accuracy of these measurements.

To add a further specification of the uncertainty of a particular measurement, Kline and McClintock [47] proposed that the experimenter specified certain odds for the uncertainty.

It was important to note that the specification of such odds could only be made by the experimenter based on the total laboratory experience.

#### **1. Uncertainties in Measurands:**

As we could eliminate the uncertainties in the experiment so experimenters were advised to report the uncertainties in every measurand. For measuring the uncertainties following information should be considered:



- a. Precision limit, P: This is an estimate of the lack of repeatability caused by random errors and process unsteadiness. This element can be sampled with the available procedures and apparatus. It should be based on statistical estimates from samples whenever possible.
- b. Bias limit, B: The bias limit is an estimate of the magnitude of the fixed constant error. This element can not be sampled within available procedure and its existence is what mandates the need of cross-checks.
- c. Total uncertainty, W: The  $\pm 5$  interval about the nominal results is the band within which the experiment is 95% confident that the true value of the results lies. And it is calculated from the following way :

$$W = [P^2 + B^2]^{1/2} \quad (D-1)$$

## 2. Propagation of Uncertainties into Results:

In nearly all other experiments, it was necessary to compute the uncertainty in the results from the estimates of uncertainty in the measurands. This computation process was called "propagation of uncertainty".

According to Kline and McClintock (47), the propagation equation of a result R computed from m measurands  $x_1, x_2, \dots, x_m$  having absolute uncertainty  $W_R$  was given by the following equation:

$$W_R = \left[ \left( \frac{\delta R}{\delta X_1} w_{x1} \right)^2 + \left( \frac{\delta R}{\delta X_2} w_{x2} \right)^2 + \dots + \left( \frac{\delta R}{\delta X_m} w_{xm} \right)^2 \right]^{1/2} \quad [D-2]$$

## 3. Calculation of Uncertainties in the Present Experiment:

Primary measurands were  $T_\infty, b, d, A, T_o, T_i, \Delta P, D_i,$  and  $x$ . Results of these uncertainties was presented in the Tables 4.1 and 4.2. From these results, uncertainty in velocity, heat transfer rate and friction factor were calculated.

### Determination of Mean Velocity:

$$V = 20.558 \left( \frac{273 + T_\infty}{b} \right)^{1/2} \sqrt{d}$$

Room temperature,  $T_{\infty}=24 \pm 1.5\% \text{ }^{\circ}\text{C}$

Atmospheric pressure,  $b=761 \pm 0.016 \% \text{ mm of Hg}$

Velocity head,  $d= 0.65051 \pm 3.18\%$ . The uncertainties in these values were calculated as follows:

$$w_T = 0.36 \text{ }^{\circ}\text{C}$$

$$w_d = 0.020686 \text{ cm of fluid}$$

$$w_b = 0.12176 \text{ mm of Hg}$$

Now, change of velocity with respect to temperature,

$$\begin{aligned}\frac{\partial V}{\partial T} &= 20.558 \times \frac{1}{2} \left( \frac{273 + T_{\infty}}{b} \right)^{-1/2} \times \frac{1}{b} \sqrt{d} \\ \Rightarrow \frac{\partial V}{\partial T} &= 20.558 \times \frac{1}{2} \left( \frac{273 + 24}{761} \right)^{-1/2} \times \frac{1}{761} \sqrt{0.65051} \\ &= 0.017437\end{aligned}$$

Now, change of velocity with respect to manometric fluid head,

$$\begin{aligned}\frac{\partial V}{\partial d} &= 20.558 \times \frac{1}{2} \left( \frac{273 + T_{\infty}}{b} \right)^{1/2} \times d^{-1/2} \\ \Rightarrow \frac{\partial V}{\partial d} &= 20.558 \times \frac{1}{2} \left( \frac{273 + 24}{761} \right)^{1/2} \times 0.65051^{-1/2} \\ &= 7.96177\end{aligned}$$

Now, change of velocity with respect to atmospheric pressure,

$$\begin{aligned}\frac{\partial V}{\partial b} &= 20.558 \times \frac{1}{2} (273 + 24)^{1/2} \times b^{-3/2} \sqrt{d} \\ &= 0.006805798\end{aligned}$$

Thus, the uncertainty in the velocity was

$$\begin{aligned}W_v &= \left[ \left( \frac{\partial V}{\partial T} w_T \right)^2 + \left( \frac{\partial V}{\partial b} w_b \right)^2 + \left( \frac{\partial V}{\partial d} w_d \right)^2 \right]^{1/2} \\ &= 0.1648188\end{aligned}$$

Now,

$$\frac{W_v}{V} = \frac{0.1648188}{10.3584} = 1.59\%$$

Total Heat transfer rate,

$$Q = mC_p(T_o - T_i)$$

$$Q = \rho AVC_p(T_o - T_i)$$

$$A = 0.0038485 \pm 0.52 \% \text{ m}^2$$

$$V = 10.3584 \pm 1.59 \% \text{ m/s}$$

$$T_i = 24.2 \pm 1.5 \% \text{ } ^\circ\text{C}$$

$$T_o = 32.3 \pm 1.55 \% \text{ } ^\circ\text{C}$$

The uncertainties in these values were calculated as follows:

$$w_A = 0.00002$$

$$w_v = 0.16366$$

$$w_{T_i} = 0.363$$

$$w_{T_o} = 0.50065$$

Change of total heat transfer rate with respect to area

$$\frac{\partial Q}{\partial A} = \rho VC_p(T_o - T_i)$$

$$= 1.191524 \times 10.3584 \times 1005.875 \times (32.3 - 24.2)$$

$$= 100559.82$$

Change of total heat transfer rate with respect to velocity

$$\frac{\partial Q}{\partial V} = \rho AC_p(T_o - T_i)$$

$$= 1.191524 \times 0.0038485 \times 1005.875 \times (32.3 - 24.2)$$

$$= 37.3614$$

Change of total heat transfer rate with respect to outlet temperature

$$\frac{\partial Q}{\partial T_o} = \rho VC_p A$$

$$= 1.191524 \times 0.0038485 \times 1005.875 \times 10.3584$$

$$= 47.77833$$

Change of total heat transfer rate with respect to inlet temperature

$$\begin{aligned}\frac{\partial Q}{\partial T_i} &= \rho V C_p A \\ &= 1.191524 \times 0.0038485 \times 1005.875 \times 10.3584 \\ &= 47.77833\end{aligned}$$

Thus the total uncertainty in the total heat transfer rate was

$$\begin{aligned}W_Q &= \left[ \left( \frac{\partial Q}{\partial A} w_A \right)^2 + \left( \frac{\partial Q}{\partial V} w_V \right)^2 + \left( \frac{\partial V}{\partial T_o} w_{T_o} \right)^2 + \left( \frac{\partial V}{\partial T_i} w_{T_i} \right)^2 \right]^{1/2} \\ &= 30.239179 \text{ watt}\end{aligned}$$

Now,

$$\begin{aligned}\frac{W_Q}{Q_i} &= \frac{30.239179}{387} \\ &= 7.80 \%\end{aligned}$$

### Friction Factor:

Local friction factor (fanning) based on inside diameter was given by

$$f_i = \frac{(-\Delta P / x) D_i}{2 \rho_b V^2}$$

Where,

$$\Delta P = 29.329 \pm 5.83\% \text{ N/m}^2$$

$$x = 0.05 \pm 0.02\% \text{ m}$$

$$D_i = 0.07 \pm 0.02\% \text{ m}$$

$$V = 10.3584 \pm 1.59\% \text{ m/s}$$

$$\text{So, } W_{\Delta P} = 1.70988$$

$$W_x = 0.00001$$

$$W_{D_i} = 0.000014$$

$$W_V = 0.164698$$

Change of friction factor with respect to pressure drop

$$\frac{\partial f_i}{\partial \Delta P} = \frac{2D_i}{\rho_b V^2 x} = \frac{2 \times 0.07}{1.167892 \times 10.3584^2 \times 0.05} = 0.022344$$

Change of friction factor with respect to axial distance

$$\frac{\partial f_i}{\partial x} = \frac{-2D_i \Delta P}{\rho_b V^2 x^2} = \frac{-2 \times 0.07 \times 29.329}{1.167892 \times 10.3584^2 \times 0.05^2} = -13.1068$$

Change of friction factor with respect to inside diameter

$$\frac{\partial f_i}{\partial D_i} = \frac{2\Delta P}{\rho_b V^2 x} = \frac{-2 \times 29.328}{1.167892 \times 10.3584^2 \times 0.05} = 9.3620$$

Change of friction factor with respect to velocity

$$\frac{\partial f_i}{\partial V} = -2 \frac{2D_i \Delta P}{\rho_b V^3 x} = -2 \times \frac{2 \times 0.07 \times 29.329}{1.167892 \times 10.3584^3 \times 0.05} = .12653$$

Thus, the total uncertainty in the friction factor was

$$W_{f_i} = \left[ \left( \frac{\partial f_i}{\partial \Delta P} w_{\Delta P} \right)^2 + \left( \frac{\partial f_i}{\partial V} w_V \right)^2 + \left( \frac{\partial f_i}{\partial x} w_x \right)^2 + \left( \frac{\partial f_i}{\partial D_i} w_{D_i} \right)^2 \right]^{1/2}$$

$$= \left[ (0.022344 \times 1.70988)^2 + (.12653 \times .164698)^2 + (-13.1068 \times 0.00001)^2 + (9.3620 \times 0.00001)^2 \right]^{1/2}$$

$$= 0.0018939$$

$$\text{Now, } \frac{W_{f_i}}{f_i} = \frac{0.0018939}{0.157} = 1.2\%$$

**APPENDIX-E**  
**DATA TABLES**

**Plain Tube**  
**Local Wall Temperature,  $T_{wx}$  (° C)**

X/L	Re-46491	Re-40319	Re-36384	Re-30925	Re-26447	Re-21655	Re-15285
0.03	56	57.5	60	62	63.5	65.5	67
0.17	67	70	73	77.5	80.5	83.5	86
0.30	70.5	74	77	81	84.5	88	92
0.43	75.5	79	82.5	86	90	94	98.5
0.57	93.5	97.5	101	105	109	113	116
0.70	89.5	93.5	97	101.5	106	109	112
0.83	76.5	80	84	89	94	98.5	101.5
0.97	70	73	76	80	86	89	92

**Local Bulk Temperature,  $T_{bx}$  (° C)**

X/L	Re-46491	Re-40319	Re-36384	Re-30925	Re-26447	Re-21655	Re-15285
0.03	24.47	24.29	24.21	24.15	24.16	24.08	24.04
0.17	25.55	25.47	25.45	25.53	25.60	25.62	25.79
0.30	26.63	26.64	26.68	26.91	27.04	27.16	27.54
0.43	27.71	27.81	27.92	28.29	28.48	28.69	29.29
0.57	28.79	28.98	29.15	29.67	29.91	30.23	31.05
0.70	29.87	30.15	30.39	31.05	31.35	31.76	32.80
0.83	30.95	31.33	31.63	32.43	32.79	33.30	34.55
0.97	32.03	32.50	32.86	33.81	34.23	34.84	36.30

**Local Heat Transfer Coefficient,  $h_x$  ( $W/m^2 \cdot ^\circ C$ )**

X/L	Re-46491	Re-40319	Re-36384	Re-30925	Re-26447	Re-21655	Re-15285
0.03	37.21	33.24	29.36	26.39	22.68	18.87	14.65
0.17	28.30	25.36	22.10	19.22	16.25	13.50	10.45
0.30	26.74	23.81	20.88	18.47	15.53	12.85	9.77
0.43	24.55	22.00	19.25	17.31	14.50	11.97	9.10
0.57	18.13	16.35	14.62	13.26	11.28	9.44	7.41
0.70	19.67	17.71	15.77	14.18	11.95	10.12	7.95
0.83	25.76	23.16	20.06	17.66	14.58	11.99	9.40
0.97	30.90	27.95	24.36	21.62	17.24	14.43	11.30

**Local Nusselt Number,  $Nu_x$**

X/L	Re-46491	Re-40319	Re-36384	Re-30925	Re-26447	Re-21655	Re-15285
0.03	98.51	88.03	77.72	69.72	59.80	49.65	38.53
0.17	74.93	67.14	58.50	50.78	42.85	35.52	27.49
0.30	70.80	63.05	55.28	48.79	40.94	33.79	25.68
0.43	64.99	58.24	50.96	45.73	38.24	31.48	23.92
0.57	48.00	43.29	38.72	35.03	29.75	24.84	19.48
0.70	52.09	46.88	41.76	37.46	31.51	26.62	20.90
0.83	68.19	61.31	53.11	46.65	38.43	31.54	24.72
0.97	81.80	74.00	64.48	57.13	45.44	37.96	29.72

**Pressure drop,  $\Delta P$  ( $N/m^2$ )**

X/L	Re-46491	Re-40319	Re-36384	Re-30925	Re-26447	Re-21655	Re-15285
0.03	29.33	24.44	19.56	17.60	13.20	9.29	6.36
0.17	39.11	34.22	29.33	22.00	16.62	11.73	9.78
0.30	43.99	39.11	34.22	29.33	22.49	16.62	14.67
0.43	53.77	48.89	39.11	34.22	27.87	23.47	19.56
0.57	68.43	58.67	48.89	41.56	35.20	28.36	24.45
0.70	78.21	68.44	56.22	48.89	40.09	33.24	29.34
0.83	87.99	73.33	61.11	53.78	47.42	41.07	34.23
0.97	102.65	85.56	72.36	61.11	51.82	45.96	39.12

**Friction Factor,  $f_i$**

X/L	Re-46491	Re-40319	Re-36384	Re-30925	Re-26447	Re-21655	Re-15285
0.03	0.157	0.174	0.171	0.212	0.216	0.226	0.310
0.17	0.042	0.049	0.051	0.053	0.054	0.057	0.095
0.30	0.026	0.031	0.033	0.039	0.041	0.045	0.079
0.43	0.022	0.027	0.026	0.032	0.035	0.044	0.073
0.57	0.022	0.025	0.025	0.029	0.034	0.041	0.070
0.70	0.020	0.023	0.023	0.028	0.031	0.038	0.068
0.83	0.019	0.021	0.021	0.026	0.031	0.040	0.067
0.97	0.019	0.021	0.022	0.025	0.029	0.039	0.066

**Average heat transfer coefficient, Nusselt number, Pumping power, Total heat transfer rate, Effectiveness, Total pressure drop and Average friction factor**

Re	h	Nu	$P_m$	$Q_{out}$	$\epsilon$	$\Delta p$	$f_i$
15285	10.00	26.31	0.53	207.63	0.171	39.12	0.104
21655	12.90	33.93	0.88	257.84	0.157	45.96	0.066
26447	15.50	40.87	1.21	294.34	0.155	51.82	0.059
30925	18.51	48.91	1.66	329.51	0.158	61.11	0.056
36384	20.80	55.07	2.30	346.61	0.152	72.36	0.047
40319	23.70	62.74	3.02	364.16	0.155	85.56	0.046
46491	26.41	69.91	4.17	387.00	0.150	102.65	0.041

**Tube with Rectangular Strip Insert  
Local Wall Temperature,  $T_{wx}$  ( $^{\circ}C$ )**

X/L	Re-46687	Re-40152	Re-36166	Re-30424	Re-26686	Re-21664	Re-15310
0.03	54	57	60	62	63	64	65
0.17	62	64.5	67	69.5	72.5	75.5	77.5
0.30	69.5	71.5	73.5	76	79	81.5	84
0.43	73	75.5	78	80.5	84	86	88
0.57	83	88	92	96	98.5	101.5	105
0.70	80.5	84.5	89	93	96	99	102
0.83	69	74	78	82.5	86	88.5	92
0.97	66	70.5	73.5	76.5	78.5	81	84



**Local Bulk Temperature,  $T_{bx}$  ( $^{\circ}\text{C}$ )**

X/L	Re-46687	Re-40152	Re-36166	Re-30424	Re-26686	Re-21664	Re-15310
0.03	24.47	24.50	24.52	24.45	24.56	24.51	24.42
0.17	25.94	26.09	26.19	26.26	26.41	26.54	26.50
0.30	27.41	27.67	27.86	28.07	28.26	28.57	28.58
0.43	28.88	29.26	29.53	29.88	30.11	30.60	30.66
0.57	30.36	30.85	31.19	31.68	31.97	32.62	32.74
0.70	31.83	32.44	32.86	33.49	33.82	34.65	34.82
0.83	33.30	34.03	34.53	35.30	35.67	36.68	36.90
0.97	34.77	35.61	36.20	37.11	37.52	38.71	38.98

**Local Heat Transfer Coefficient,  $h_x$  ( $\text{W}/\text{m}^2\text{ }^{\circ}\text{C}$ )**

X/L	Re-46687	Re-40152	Re-36166	Re-30424	Re-26686	Re-21664	Re-15310
0.03	54.37	45.88	39.83	34.33	30.13	26.14	18.43
0.17	44.53	38.82	34.63	29.81	25.13	21.09	14.66
0.30	38.15	34.03	30.96	26.89	22.82	19.50	13.50
0.43	36.40	32.25	29.15	25.46	21.49	18.63	13.04
0.57	30.50	26.10	23.24	20.04	17.40	14.99	10.35
0.70	32.99	28.65	25.17	21.66	18.62	16.04	11.13
0.83	44.98	37.31	32.51	27.31	23.01	19.92	13.57
0.97	51.42	42.75	37.89	32.72	28.26	24.41	16.61

**Local Nusselt Number,  $\text{Nu}_x$**

X/L	Re-46687	Re-40152	Re-36166	Re-30424	Re-26686	Re-21664	Re-15310
0.03	143.95	121.33	105.23	90.59	79.44	68.82	48.51
0.17	117.89	102.66	91.48	78.66	66.26	55.51	38.60
0.30	101.01	89.98	81.80	70.96	60.19	51.35	35.52
0.43	96.36	85.29	77.02	67.19	56.67	49.06	34.33
0.57	80.75	69.00	61.40	52.88	45.89	39.46	27.24
0.70	87.34	75.75	66.51	57.16	49.11	42.24	29.30
0.83	119.08	98.65	85.90	72.06	60.67	52.45	35.73
0.97	136.13	113.04	100.11	86.34	74.51	64.27	43.72

**Pressure drop,  $\Delta P$  (N/m<sup>2</sup>)**

X/L	Re-46687	Re-40152	Re-36166	Re-30424	Re-26686	Re-21664	Re-15310
0.03	46.94	36.67	29.34	24.45	19.56	16.63	10.76
0.17	70.41	53.79	46.45	39.12	29.34	25.43	14.67
0.30	85.08	66.01	51.34	46.45	36.19	31.30	20.54
0.43	96.81	75.30	60.63	53.79	42.06	37.17	26.90
0.57	109.53	88.01	72.37	58.67	50.86	43.03	34.24
0.70	119.31	97.79	82.14	65.52	56.73	50.86	39.13
0.83	128.11	104.64	88.01	70.41	61.62	55.75	44.02
0.97	135.93	110.50	92.90	75.79	66.51	60.64	48.91

**Fanning friction factor,  $f_i$**

X/L	Re-46687	Re-40152	Re-36166	Re-30424	Re-26686	Re-21664	Re-15310
0.03	0.250	0.263	0.259	0.304	0.315	0.405	0.524
0.17	0.075	0.077	0.082	0.097	0.095	0.124	0.143
0.30	0.050	0.053	0.050	0.064	0.065	0.085	0.111
0.43	0.040	0.042	0.041	0.051	0.052	0.070	0.101
0.57	0.034	0.037	0.038	0.043	0.048	0.062	0.098
0.70	0.030	0.033	0.034	0.039	0.044	0.059	0.091
0.83	0.027	0.030	0.031	0.035	0.040	0.054	0.086
0.97	0.025	0.027	0.028	0.032	0.037	0.051	0.082

**Average heat transfer coefficient, Nusselt number, Pumping power, Total heat transfer rate, Effectiveness, Total pressure drop and Average friction factor**

Re	h	Nu	$P_m$	$Q_{out}$	$\epsilon$	$\Delta p$	$f_i$
15310	13.91	36.62	0.66	246.71	0.232	48.91	0.154
21664	20.09	52.90	1.16	340.57	0.236	60.64	0.114
26686	23.36	61.59	1.56	381.99	0.225	66.51	0.087
30424	27.28	71.98	2.03	425.17	0.230	75.79	0.083
36166	31.67	83.68	2.95	466.16	0.225	92.90	0.070
40152	35.72	94.46	3.89	491.95	0.228	110.50	0.070
46687	41.66	110.31	5.55	529.64	0.228	135.93	0.066

**Tube with Perforated Rectangular Strip insert**

For Porosity,  $R_p = 1.1\%$

Local Wall Temperature,  $T_{wx}$  ( $^{\circ}\text{C}$ )

X/L	Re-46654	Re-40123	Re-36160	Re-30731	Re-26668	Re-21612	Re-15375
0.03	52	53	55	57	58.5	60	61.5
0.17	59	62	65	67.5	69.5	72.5	74.5
0.30	62.5	65	68.5	71	73	76	78.5
0.43	67	69	72.5	75.5	78	80.5	83
0.57	81	84.5	88	92	95	97.5	100.5
0.70	76	80.5	84.5	88.5	90.5	94	96.5
0.83	65.5	69	73	76	78	82.5	86.5
0.97	63	66	70	72.5	74.5	78.5	81

Local Bulk Fluid Temperature,  $T_{bx}$  ( $^{\circ}\text{C}$ )

X/L	Re-46654	Re-40123	Re-36160	Re-30731	Re-26668	Re-21612	Re-15375
0.03	24.87	24.81	24.84	24.96	24.99	24.95	24.94
0.17	26.73	26.83	27.01	27.19	27.37	27.53	27.52
0.30	28.60	28.86	29.18	29.43	29.74	30.12	30.09
0.43	30.47	30.89	31.34	31.66	32.11	32.71	32.66
0.57	32.33	32.91	33.51	33.89	34.49	35.29	35.24
0.70	34.20	34.94	35.68	36.13	36.86	37.88	37.81
0.83	36.07	36.97	37.84	38.36	39.23	40.47	40.38
0.97	37.93	38.99	40.01	40.59	41.61	43.05	42.96

Local Heat Transfer Coefficient,  $h_x$  ( $\text{W}/\text{m}^2\text{ }^{\circ}\text{C}$ )

X/L	Re-46654	Re-40123	Re-36160	Re-30731	Re-26668	Re-21612	Re-15375
0.03	75.33	67.77	61.13	50.44	44.54	37.67	25.56
0.17	63.34	54.34	48.52	40.10	35.42	29.37	19.89
0.30	60.29	52.87	46.88	38.88	34.50	28.78	19.30
0.43	55.95	50.13	44.79	36.87	32.53	27.63	18.57
0.57	42.00	37.04	33.83	27.82	24.66	21.23	14.32
0.70	48.90	41.94	37.76	30.86	27.82	23.53	15.92
0.83	69.44	59.65	52.43	42.94	38.50	31.41	20.26
0.97	81.54	70.75	61.47	50.65	45.37	37.25	24.56

**Local Nusselt Number,  $Nu_x$**

X/L	Re-46654	Re-40123	Re-36160	Re-30731	Re-26668	Re-21612	Re-15375
0.03	198.43	178.28	160.55	132.36	116.70	98.50	66.85
0.17	166.86	142.93	127.45	105.22	92.81	76.79	52.02
0.30	158.82	139.08	123.12	102.01	90.39	75.26	50.48
0.43	147.37	131.88	117.64	96.74	85.22	72.24	48.55
0.57	110.63	97.43	88.85	72.99	64.62	55.50	37.45
0.70	128.80	110.32	99.17	80.97	72.90	61.52	41.64
0.83	182.92	156.91	137.72	112.67	100.87	82.14	53.00
0.97	214.79	186.11	161.44	132.91	118.88	97.40	64.24

**Pressure drop,  $\Delta P$  ( $N/m^2$ )**

X/L	Re-46654	Re-40123	Re-36160	Re-30731	Re-26668	Re-21612	Re-15375
0.03	33.24	29.33	22.00	19.56	15.64	11.73	7.82
0.17	51.81	43.99	34.22	28.36	22.00	16.62	12.71
0.30	59.15	53.77	39.11	33.24	26.89	21.51	17.11
0.43	71.37	60.61	48.88	38.13	31.78	26.40	21.51
0.57	83.59	70.88	58.66	45.96	39.11	31.29	26.89
0.70	93.36	80.65	68.43	50.84	44.00	36.18	31.29
0.83	103.14	86.03	70.88	57.69	48.89	42.04	36.18
0.97	117.32	95.32	80.17	65.51	53.78	47.91	42.05

**Friction Factor,  $f_i$**

X/L	Re-46654	Re-40123	Re-36160	Re-30731	Re-26668	Re-21612	Re-15375
0.03	0.175	0.208	0.191	0.234	0.248	0.281	0.371
0.17	0.054	0.062	0.059	0.068	0.070	0.080	0.121
0.30	0.035	0.042	0.038	0.044	0.047	0.057	0.090
0.43	0.029	0.033	0.033	0.035	0.039	0.049	0.078
0.57	0.026	0.030	0.030	0.032	0.036	0.044	0.075
0.70	0.023	0.027	0.028	0.029	0.033	0.041	0.071
0.83	0.022	0.024	0.025	0.028	0.031	0.040	0.069
0.97	0.021	0.023	0.024	0.027	0.029	0.040	0.069

**Average heat transfer coefficient, Nusselt number, Pumping power, Total heat transfer rate, Effectiveness, Total pressure drop and Average friction factor**

Re	h	Nu	$P_m$	$Q_{out}$	$\epsilon$	$\Delta p$	$f_i$
15375	19.80	51.78	0.58	308.27	0.312	42.05	0.118
21612	29.61	77.42	0.93	435.58	0.328	47.91	0.079
26668	35.42	92.80	1.28	492.33	0.319	53.78	0.067
30731	39.82	104.48	1.79	533.17	0.312	65.51	0.062
36160	48.35	126.99	2.58	608.09	0.321	80.17	0.053
40123	54.31	142.87	3.39	630.31	0.324	95.32	0.056
46654	62.10	163.58	4.83	674.21	0.320	117.32	0.048

**For Porosity,  $R_p = 2.5\%$   
Local Wall Temperature,  $T_{wx}(^{\circ}C)$**

X/L	Re-46360	Re-39940	Re-36046	Re-30643	Re-26562	Re-21390	Re-15469
0.03	50.5	52.5	55	56.5	58.5	60	61
0.17	55.5	58	61	63	66	69	72
0.30	58.5	62	64.5	67	70	74	77
0.43	63	66	69	71.5	75	79.5	82.5
0.57	77	82	86	89.5	93.5	98	99.5
0.70	72.5	78	81.5	84.5	89	93	97
0.83	65	68.5	72	75.5	79	84.5	89.5
0.97	58.5	62	65	67.5	71	76	79.5

**Local Bulk Fluid Temperature,  $T_{bx}(^{\circ}C)$**

X/L	Re-46360	Re-39940	Re-36046	Re-30643	Re-26562	Re-21390	Re-15469
0.03	24.08	24.23	24.36	24.30	24.53	24.40	24.12
0.17	26.00	26.34	26.62	26.72	27.07	27.18	27.02
0.30	27.92	28.46	28.87	29.13	29.60	29.97	29.91
0.43	29.84	30.57	31.12	31.54	32.13	32.76	32.80
0.57	31.76	32.68	33.38	33.96	34.67	35.54	35.70
0.70	33.68	34.80	35.63	36.37	37.20	38.33	38.59
0.83	35.60	36.91	37.88	38.78	39.73	41.12	41.48
0.97	37.52	39.02	40.14	41.20	42.27	43.90	44.38

**Local Heat Transfer Coefficient,  $h_x$  ( $W/m^2 \text{ } ^\circ C$ )**

X/L	Re-46360	Re-39940	Re-36046	Re-30643	Re-26562	Re-21390	Re-15469
0.03	78.95	70.11	62.35	54.09	46.73	39.56	28.69
0.17	70.71	62.61	55.56	48.00	40.77	33.68	23.52
0.30	68.21	59.09	53.61	45.99	39.29	31.99	22.47
0.43	62.90	55.94	50.43	43.58	37.03	30.13	21.29
0.57	46.11	40.19	36.30	31.35	26.98	22.55	16.58
0.70	53.73	45.88	41.65	36.18	30.64	25.76	18.11
0.83	70.95	62.74	55.99	47.43	40.42	32.47	22.03
0.97	99.42	86.26	76.83	66.21	55.24	43.88	30.12

**Local Nusselt Number,  $Nu_x$**

X/L	Re-46360	Re-39940	Re-36046	Re-30643	Re-26562	Re-21390	Re-15469
0.03	208.32	184.56	163.85	141.93	122.39	103.40	74.96
0.17	186.57	164.82	146.00	125.95	106.78	88.04	61.45
0.30	179.99	155.55	140.89	120.67	102.90	83.61	58.70
0.43	165.98	147.26	132.53	114.37	96.98	78.76	55.62
0.57	121.66	105.80	95.39	82.27	70.66	58.94	43.33
0.70	141.78	120.77	109.44	94.95	80.25	67.34	47.33
0.83	187.21	165.16	147.14	124.46	105.87	84.85	57.57
0.97	262.34	227.08	201.90	173.73	144.68	114.69	78.70

**Pressure drop,  $\Delta P$  ( $N/m^2$ )**

X/L	Re-46360	Re-39940	Re-36046	Re-30643	Re-26562	Re-21390	Re-15469
0.03	39.13	31.30	24.45	22.01	17.12	12.72	9.78
0.17	53.80	46.46	36.68	30.32	24.46	18.59	13.70
0.30	61.14	55.76	41.57	36.19	29.35	23.48	18.59
0.43	75.81	63.58	50.87	42.06	34.24	28.37	23.48
0.57	94.89	75.81	63.58	48.91	41.09	34.24	27.40
0.70	103.69	88.04	73.36	54.78	45.98	39.13	32.29
0.83	114.94	92.93	78.26	60.65	51.36	44.03	37.18
0.97	122.27	97.82	83.15	68.47	56.25	49.90	43.05

**Friction Factor,  $f_i$**

X/L	Re-46360	Re-39940	Re-36046	Re-30643	Re-26562	Re-21390	Re-15469
0.03	0.209	0.224	0.214	0.265	0.273	0.311	0.457
0.17	0.058	0.067	0.064	0.073	0.078	0.091	0.128
0.30	0.036	0.044	0.040	0.048	0.052	0.064	0.097
0.43	0.031	0.035	0.034	0.039	0.042	0.053	0.084
0.57	0.030	0.032	0.033	0.035	0.039	0.049	0.075
0.70	0.026	0.030	0.031	0.031	0.035	0.046	0.072
0.83	0.025	0.027	0.027	0.029	0.033	0.043	0.069
0.97	0.023	0.024	0.025	0.028	0.031	0.042	0.069

**Average heat transfer coefficient, Nusselt number, Pumping power, Total heat transfer rate, Effectiveness, Total pressure drop and Average friction factor**

Re-	h	Nu	$P_m$	$Q_{out}$	$\epsilon$	$\Delta p$	$f_i$
15469	22.85	59.71	0.60	348.98	0.348	43.05	0.132
21390	32.50	84.95	0.96	464.61	0.356	49.90	0.087
26562	39.63	103.81	1.33	523.55	0.350	56.25	0.073
30643	46.60	122.29	1.87	574.45	0.355	68.47	0.069
36046	54.09	142.14	2.66	630.14	0.351	83.15	0.059
39940	60.35	158.87	3.46	653.82	0.353	97.82	0.060
46360	68.87	181.73	4.99	688.05	0.349	122.27	0.055

**For porosity,  $R_p = 4.4\%$   
Local Wall Temperature,  $T_{wx}(^{\circ}C)$**

X/L	Re-46169	Re-39984	Re-36081	Re-30329	Re-26251	Re-21372	Re-15307
0.03	49.5	51.5	53	55	56.5	58	59
0.17	55	57	60	62	65.5	68.5	70.5
0.30	58	61	63.5	66	69	73	75
0.43	62.5	65	68	71.5	74.5	78	80
0.57	75.5	81	85	89	93	96	97.5
0.70	72	77.5	81	84	89	91.5	93.5
0.83	63.5	68	71	75	79	82	84.5
0.97	57.5	61	64	67	70.5	73.5	75.5

**Local Bulk Fluid Temperature,  $T_{bx}$ (°C)**

X/L	Re-46169	Re-39984	Re-36081	Re-30329	Re-26251	Re-21372	Re-15307
0.03	24.49	24.54	24.48	24.43	24.46	24.42	24.24
0.17	26.45	26.70	26.78	26.93	27.12	27.28	27.21
0.30	28.41	28.86	29.09	29.43	29.77	30.15	30.18
0.43	30.37	31.02	31.40	31.93	32.42	33.02	33.14
0.57	32.33	33.18	33.70	34.43	35.08	35.88	36.11
0.70	34.29	35.34	36.01	36.93	37.73	38.75	39.08
0.83	36.25	37.50	38.32	39.43	40.38	41.61	42.04
0.97	38.21	39.66	40.62	41.93	43.04	44.48	45.01

**Local Heat Transfer Coefficient,  $h_x$  (W/m<sup>2</sup> °C)**

X/L	Re-46169	Re-39984	Re-36081	Re-30329	Re-26251	Re-21372	Re-15307
0.03	84.91	75.32	68.68	58.46	51.33	43.14	30.91
0.17	74.38	67.01	58.97	50.96	42.84	35.15	24.82
0.30	71.76	63.18	56.93	48.87	41.92	33.81	23.97
0.43	66.09	59.76	53.52	45.17	39.08	32.21	22.93
0.57	49.19	42.46	38.19	32.75	28.39	24.10	17.50
0.70	56.31	48.16	43.54	37.97	32.07	27.46	19.74
0.83	77.93	66.57	59.94	50.24	42.58	35.87	25.30
0.97	110.08	95.15	83.80	71.28	59.87	49.93	35.24

**Local Nusselt Number,  $Nu_x$**

X/L	Re-46169	Re-39984	Re-36081	Re-30329	Re-26251	Re-21372	Re-15307
0.03	223.69	198.00	180.32	153.22	134.31	112.66	80.68
0.17	195.95	176.17	154.84	133.56	112.10	91.79	64.78
0.30	189.07	166.09	149.47	128.09	109.68	88.29	62.56
0.43	174.12	157.09	140.51	118.38	102.26	84.11	59.85
0.57	129.59	111.63	100.27	85.84	74.28	62.93	45.68
0.70	148.35	126.61	114.32	99.52	83.92	71.72	51.53
0.83	205.30	175.02	157.37	131.69	111.42	93.68	66.05
0.97	290.02	250.14	220.02	186.83	156.67	130.38	91.97



**Pressure drop,  $\Delta P$  (N/m<sup>2</sup>)**

X/L	Re-46169	Re-39984	Re-36081	Re-30329	Re-26251	Re-21372	Re-15307
0.03	44.01	34.23	27.39	23.47	18.59	14.67	9.78
0.17	57.71	48.90	39.12	33.25	26.90	22.01	14.68
0.30	67.49	58.68	45.97	38.14	31.79	26.90	19.57
0.43	83.13	68.46	53.79	44.01	37.17	31.30	24.46
0.57	100.25	83.13	68.46	52.82	44.02	37.17	29.35
0.70	112.48	92.92	78.24	57.71	48.91	42.06	34.25
0.83	119.81	97.81	83.13	63.57	53.80	47.93	39.14
0.97	127.15	102.70	88.03	71.40	58.69	52.82	44.03

**Friction Factor,  $f_i$**

X/L	Re-46169	Re-39984	Re-36081	Re-30329	Re-26251	Re-21372	Re-15307
0.03	0.236	0.244	0.238	0.288	0.303	0.359	0.466
0.17	0.062	0.070	0.068	0.082	0.088	0.108	0.140
0.30	0.040	0.046	0.044	0.052	0.058	0.073	0.103
0.43	0.034	0.037	0.036	0.042	0.047	0.059	0.090
0.57	0.032	0.035	0.035	0.038	0.042	0.053	0.082
0.70	0.029	0.031	0.032	0.034	0.038	0.049	0.078
0.83	0.026	0.028	0.029	0.031	0.035	0.047	0.074
0.97	0.024	0.025	0.026	0.030	0.033	0.045	0.072

**Average heat transfer coefficient, Nusselt number, Pumping power, Total heat transfer rate, Effectiveness, Total pressure drop and Average friction factor**

Re	h	Nu	$P_m$	$Q_{out}$	$\epsilon$	$\Delta p$	$f_i$
15307	25.05	65.39	0.61	354.41	0.376	44.03	0.138
21372	35.21	91.95	1.01	477.90	0.378	52.82	0.099
26251	42.26	110.58	1.38	542.42	0.370	58.69	0.080
30329	49.46	129.64	1.93	589.62	0.374	71.40	0.074
36081	57.94	152.14	2.82	646.18	0.369	88.03	0.064
39984	64.70	170.10	3.64	669.80	0.371	102.70	0.065
46169	73.83	194.51	5.18	700.47	0.369	127.15	0.060

**For Porosity,  $R_p = 6.8\%$   
Local Wall Temperature,  $T_{wx} (^{\circ}C)$**

X/L	Re-46545	Re-39925	Re-36091	Re-30612	Re-26610	Re-21613	Re-15574
0.03	51	52.5	55	56.5	59	61	62.5
0.17	56	58	61.5	64.5	67.5	70	72
0.30	59.5	62.5	65.5	68	71	74	78
0.43	64.5	67.5	71.5	73.5	76.5	80	83.5
0.57	78	83	87	91	95	99	101.5
0.70	73	79	82.5	85.5	89.5	94	98
0.83	66	69.5	72.5	76.5	81	85	89.5
0.97	60	64	66.5	68.5	72	77.5	80.5

**Local Bulk Fluid Temperature,  $T_{bx} (^{\circ}C)$**

X/L	Re-46545	Re-39925	Re-36091	Re-30612	Re-26610	Re-21613	Re-15574
0.03	24.77	25.02	25.06	25.07	24.91	24.77	24.49
0.17	26.67	27.08	27.28	27.36	27.34	27.47	27.27
0.30	28.56	29.15	29.51	29.65	29.78	30.17	30.04
0.43	30.45	31.22	31.74	31.94	32.21	32.86	32.81
0.57	32.35	33.28	33.96	34.22	34.64	35.56	35.59
0.70	34.24	35.35	36.19	36.51	37.08	38.25	38.36
0.83	36.13	37.42	38.42	38.80	39.51	40.95	41.13
0.97	38.03	39.48	40.64	41.09	41.94	43.65	43.91

**Local Heat Transfer Coefficient,  $h_x (W/m^2 \text{ } ^{\circ}C)$**

X/L	Re-46545	Re-39925	Re-36091	Re-30612	Re-26610	Re-21613	Re-15574
0.03	78.89	70.64	63.24	52.54	44.82	37.91	26.87
0.17	70.53	62.79	55.34	44.46	38.05	32.29	22.83
0.30	66.87	58.21	52.62	43.06	37.06	31.33	21.29
0.43	60.77	53.51	47.62	39.73	34.50	29.14	20.15
0.57	45.32	39.05	35.70	29.09	25.31	21.65	15.49
0.70	53.38	44.48	40.89	33.71	29.15	24.64	17.12
0.83	69.27	60.51	55.56	43.80	36.83	31.18	21.11
0.97	94.16	79.19	73.24	60.24	50.83	40.57	27.91

**Local Nusselt Number,  $Nu_x$**

X/L	Re-46545	Re-39925	Re-36091	Re-30612	Re-26610	Re-21613	Re-15574
0.03	207.81	185.62	165.90	137.75	117.38	99.43	70.22
0.17	185.80	165.01	145.18	116.57	99.65	84.69	59.66
0.30	176.15	152.97	138.03	112.88	97.07	82.17	55.65
0.43	160.08	140.60	124.93	104.16	90.35	76.41	52.65
0.57	119.38	102.61	93.67	76.25	66.30	56.77	40.49
0.70	140.61	116.87	107.27	88.37	76.33	64.61	44.75
0.83	182.48	159.01	145.75	114.83	96.45	81.77	55.18
0.97	248.04	208.08	192.13	157.93	133.14	106.39	72.93

**Pressure drop,  $\Delta P$  (N/m<sup>2</sup>)**

X/L	Re-46545	Re-39925	Re-36091	Re-30612	Re-26610	Re-21613	Re-15574
0.03	46.94	36.18	29.34	24.45	21.52	16.63	11.74
0.17	66.01	51.34	42.05	37.17	30.32	24.45	14.67
0.30	80.68	61.12	48.90	44.01	34.23	29.34	20.54
0.43	95.35	73.34	58.67	48.90	41.57	33.25	25.43
0.57	112.46	88.01	72.37	56.24	46.95	41.08	30.32
0.70	122.24	97.79	83.12	66.02	51.84	45.97	35.22
0.83	129.57	103.66	88.01	70.91	56.73	50.86	40.11
0.97	136.91	110.02	90.95	75.80	61.13	55.75	44.02

**Friction Factor,  $f_i$**

X/L	Re-46545	Re-39925	Re-36091	Re-30612	Re-26610	Re-21613	Re-15574
0.03	0.248	0.258	0.255	0.294	0.342	0.402	0.541
0.17	0.070	0.073	0.073	0.090	0.096	0.118	0.135
0.30	0.047	0.048	0.047	0.059	0.060	0.079	0.105
0.43	0.039	0.040	0.039	0.045	0.051	0.062	0.090
0.57	0.035	0.037	0.037	0.040	0.044	0.058	0.082
0.70	0.031	0.033	0.034	0.038	0.039	0.053	0.077
0.83	0.027	0.030	0.031	0.034	0.036	0.049	0.074
0.97	0.025	0.027	0.027	0.031	0.034	0.046	0.070

**Average heat transfer coefficient, Nusselt number, Pumping power, Total heat transfer rate, Effectiveness, Total pressure drop and Average friction factor**

Re	h	Nu	$P_m$	$Q_{out}$	$\epsilon$	$\Delta p$	$f_i$
15574	21.60	56.44	0.62	336.87	0.331	44.02	0.147
21613	31.09	81.53	1.07	453.05	0.341	55.75	0.109
26610	37.07	97.09	1.45	504.02	0.331	61.13	0.088
30612	43.33	113.59	2.07	544.73	0.334	75.80	0.079
36091	53.03	139.11	2.92	624.66	0.345	90.95	0.068
39925	58.55	153.85	3.90	640.39	0.345	110.02	0.068
46545	67.40	177.54	5.63	682.50	0.342	136.91	0.065

**For porosity,  $R_p = 13.3\%$   
Local Wall Temperature,  $T_{wx}(^{\circ}C)$**

X/L	Re-46432	Re-40150	Re-36197	Re-30278	Re-26298	Re-21606	Re-15292
0.03	51.5	53	56	57.5	60	61.5	63
0.17	58	59.5	62.5	65.5	68.5	71	73
0.30	61.5	64	67	70	72.5	76	79
0.43	66	68.5	73	75	79	82	85
0.57	80	84	89	92.5	96	99.5	102
0.70	75	80	84.5	87.5	91	95	98.5
0.83	66.5	70	74.5	77.5	81.5	85.5	89.5
0.97	62	65	68	70	73	78	81.5

**Local Bulk Fluid Temperature,  $T_{bx}(^{\circ}C)$**

X/L	Re-46432	Re-40150	Re-36197	Re-30278	Re-26298	Re-21606	Re-15292
0.03	23.67	23.61	23.45	23.67	23.61	23.37	23.38
0.17	25.57	25.66	25.66	25.96	26.07	26.03	26.08
0.30	27.46	27.70	27.87	28.25	28.53	28.70	28.79
0.43	29.35	29.74	30.08	30.54	30.99	31.37	31.50
0.57	31.25	31.79	32.28	32.82	33.44	34.03	34.20
0.70	33.14	33.83	34.49	35.11	35.90	36.70	36.91
0.83	35.03	35.88	36.70	37.40	38.36	39.37	39.62
0.97	36.93	37.92	38.91	39.69	40.82	42.03	42.32

**Local Heat Transfer Coefficient,  $h_x$  ( $W/m^2 \text{ } ^\circ C$ )**

X/L	Re-46432	Re-40150	Re-36197	Re-30278	Re-26298	Re-21606	Re-15292
0.03	73.94	65.43	57.60	48.10	41.77	35.58	24.60
0.17	63.44	56.82	50.89	41.15	35.82	30.17	20.78
0.30	60.44	52.97	47.91	38.97	34.56	28.68	19.42
0.43	56.14	49.61	43.67	36.59	31.65	26.79	18.22
0.57	42.20	36.83	33.05	27.26	24.29	20.72	14.38
0.70	49.15	41.65	37.49	31.06	27.58	23.27	15.83
0.83	65.39	56.35	49.59	40.57	35.23	29.41	19.54
0.97	82.06	71.01	64.44	53.67	47.22	37.72	24.88

**Local Nusselt Number,  $Nu_x$**

X/L	Re-46432	Re-40150	Re-36197	Re-30278	Re-26298	Re-21606	Re-15292
0.03	195.38	172.67	151.82	126.59	109.77	93.37	64.55
0.17	167.63	149.94	134.13	108.30	94.14	79.18	54.51
0.30	159.72	139.79	126.27	102.57	90.83	75.27	50.94
0.43	148.36	130.93	115.12	96.31	83.19	70.32	47.80
0.57	111.52	97.19	87.12	71.76	63.85	54.38	37.72
0.70	129.88	109.91	98.81	81.74	72.49	61.07	41.52
0.83	172.78	148.71	130.72	106.79	92.58	77.18	51.27
0.97	216.84	187.38	169.85	141.28	124.10	98.99	65.28

**Pressure drop,  $\Delta P$  ( $N/m^2$ )**

X/L	Re-46432	Re-40150	Re-36197	Re-30278	Re-26298	Re-21606	Re-15292
0.03	48.92	39.13	31.30	25.44	22.01	18.59	14.68
0.17	75.82	53.80	44.02	39.13	31.31	26.90	19.57
0.30	90.50	63.58	50.87	44.03	36.20	31.31	24.46
0.43	105.17	78.26	63.58	50.87	42.07	35.22	29.35
0.57	120.34	97.82	78.26	58.70	51.85	44.03	34.24
0.70	127.18	107.60	90.48	68.48	56.25	48.92	39.13
0.83	136.97	114.94	96.84	75.82	60.66	53.81	44.03
0.97	143.82	122.27	105.16	81.20	66.04	58.70	48.92

**Friction Factor,  $f_i$**

X/L	Re-46432	Re-40150	Re-36197	Re-30278	Re-26298	Re-21606	Re-15292
0.03	0.262	0.279	0.274	0.317	0.362	0.451	0.710
0.17	0.081	0.077	0.077	0.097	0.103	0.130	0.189
0.30	0.054	0.050	0.049	0.061	0.066	0.084	0.131
0.43	0.043	0.043	0.043	0.049	0.053	0.066	0.109
0.57	0.038	0.041	0.040	0.043	0.050	0.063	0.097
0.70	0.032	0.037	0.038	0.041	0.044	0.056	0.090
0.83	0.029	0.033	0.034	0.038	0.040	0.052	0.085
0.97	0.027	0.030	0.032	0.035	0.037	0.049	0.082

**Average heat transfer coefficient, Nusselt number, Pumping power, Total heat transfer rate, Effectiveness, Total pressure drop and Average friction factor**

Re	h	Nu	$P_m$	$Q_{out}$	$\epsilon$	$\Delta p$	$f_i$
15292	19.71	51.70	0.67	321.59	0.313	48.92	0.187
21606	29.04	76.22	1.13	447.50	0.324	58.70	0.119
26298	34.77	91.37	1.54	501.31	0.318	66.04	0.094
30278	39.67	104.42	2.18	536.69	0.315	81.20	0.085
36197	48.08	126.73	3.36	618.40	0.320	105.16	0.073
40150	53.83	142.07	4.32	634.31	0.322	122.27	0.074
46432	61.59	162.76	5.86	678.69	0.320	143.82	0.071

**For porosity,  $R_p=17.4\%$   
Local Wall Temperature,  $T_{wx}(^{\circ}C)$**

X/L	Re-46316	Re-40149	Re-36219	Re-30759	Re-26469	Re-21384	Re-15341
0.03	52	54	57.5	59.5	61	62	63
0.17	59.5	61.5	64	67	70.5	73	75
0.30	63.5	66	68.5	71.5	74	78	81
0.43	68	71	75	77	81	83.5	86.5
0.57	81.5	85.5	90.5	94	97	100	102.5
0.70	77	82	86.5	90	93.5	96	99
0.83	67	71	76	78.5	82	86	90
0.97	64	67	70.5	72	75	79	82

**Local Bulk Fluid Temperature,  $T_{bx}$ (°C)**

X/L	Re-46316	Re-40149	Re-36219	Re-30759	Re-26469	Re-21384	Re-15341
0.03	25.16	25.29	25.03	25.04	24.49	24.54	24.45
0.17	27.00	27.27	27.15	27.22	26.84	27.09	27.03
0.30	28.84	29.24	29.27	29.39	29.18	29.64	29.61
0.43	30.68	31.21	31.39	31.56	31.53	32.19	32.20
0.57	32.52	33.19	33.51	33.74	33.88	34.74	34.78
0.70	34.36	35.16	35.63	35.91	36.23	37.29	37.37
0.83	36.20	37.13	37.75	38.08	38.58	39.84	39.95
0.97	38.04	39.11	39.87	40.26	40.92	42.39	42.53

**Local Heat Transfer Coefficient,  $h_x$  (W/m<sup>2</sup> °C)**

X/L	Re-46316	Re-40149	Re-36219	Re-30759	Re-26469	Re-21384	Re-15341
0.03	74.56	64.90	55.65	45.68	40.08	34.35	24.26
0.17	61.57	54.42	49.03	39.56	33.51	28.03	19.50
0.30	57.73	50.68	46.06	37.37	32.65	26.61	18.20
0.43	53.62	46.83	41.43	34.64	29.58	25.08	17.22
0.57	40.85	35.61	31.70	26.12	23.18	19.72	13.81
0.70	46.93	39.78	35.52	29.10	25.55	21.92	15.17
0.83	64.97	55.01	47.24	38.94	33.70	27.88	18.69
0.97	77.08	66.79	58.99	49.58	42.94	35.15	23.70

**Local Nusselt Number,  $Nu_x$**

X/L	Re-46316	Re-40149	Re-36219	Re-30759	Re-26469	Re-21384	Re-15341
0.03	196.28	170.58	146.15	119.89	105.18	89.94	63.52
0.17	162.10	143.04	128.77	103.84	87.95	73.39	51.05
0.30	152.00	133.21	120.96	98.10	85.69	69.67	47.66
0.43	141.16	123.07	108.81	90.92	77.63	65.67	45.10
0.57	107.56	93.60	83.27	68.55	60.84	51.63	36.16
0.70	123.55	104.54	93.28	76.37	67.06	57.39	39.73
0.83	171.05	144.59	124.06	102.21	88.44	73.00	48.93
0.97	202.94	175.55	154.92	130.14	112.70	92.04	62.05

**Pressure drop,  $\Delta P$  (N/m<sup>2</sup>)**

X/L	Re-46316	Re-40149	Re-36219	Re-30759	Re-26469	Re-21384	Re-15341
0.03	44.96	34.21	29.33	23.46	19.56	16.62	13.69
0.17	65.49	51.32	41.55	36.17	29.33	24.44	18.58
0.30	75.27	61.09	46.93	41.55	34.22	28.36	23.47
0.43	97.75	75.27	60.61	48.88	39.11	33.24	27.38
0.57	112.41	95.31	75.28	56.21	48.89	40.09	32.27
0.70	122.19	104.59	87.99	65.99	53.78	45.96	38.13
0.83	131.96	110.46	94.83	71.37	58.67	50.84	42.04
0.97	138.80	119.25	102.65	78.21	65.51	55.73	48.89

**Friction Factor,  $f_i$**

X/L	Re-46316	Re-40149	Re-36219	Re-30759	Re-26469	Re-21384	Re-15341
0.03	0.239	0.241	0.254	0.281	0.316	0.409	0.654
0.17	0.070	0.072	0.072	0.087	0.095	0.120	0.178
0.30	0.045	0.048	0.045	0.055	0.061	0.078	0.125
0.43	0.040	0.041	0.040	0.045	0.049	0.063	0.101
0.57	0.035	0.040	0.038	0.040	0.046	0.058	0.091
0.70	0.031	0.035	0.036	0.038	0.041	0.054	0.087
0.83	0.028	0.031	0.033	0.034	0.038	0.050	0.080
0.97	0.025	0.029	0.031	0.032	0.037	0.047	0.081

**Average heat transfer coefficient, Nusselt number, Pumping power, Total heat transfer rate, Effectiveness, Total pressure drop and Average friction factor**

Re	h	Nu	$P_m$	$Q_{out}$	$\epsilon$	$\Delta p$	$f_i$
15341	18.82	49.28	0.67	308.49	0.299	48.89	0.174
21384	27.34	71.59	1.06	424.43	0.310	55.73	0.110
26469	32.65	85.69	1.54	482.71	0.300	65.51	0.085
30759	37.62	98.75	2.14	519.15	0.297	78.21	0.076
36219	45.70	120.03	3.30	596.02	0.306	102.65	0.069
40149	51.75	136.02	4.25	614.58	0.311	119.25	0.067
46316	59.66	157.08	5.69	660.09	0.311	138.80	0.064



For porosity,  $R_p=22\%$   
Local Wall Temperature,  $T_{wx}(^{\circ}C)$

X/L	Re-46617	Re-40054	Re-36194	Re-30739	Re-26598	Re-21632	Re-15204
0.03	52	54.5	57.5	60.5	61	62.5	63.5
0.17	60.5	62.5	65	68	71	73.5	75.5
0.30	63.5	66.5	69	72	75	79	81
0.43	68.5	71.5	76	79	82	84	86
0.57	82	86	90.5	95	97.5	100	103
0.70	79	82.5	88.5	90	95	97	100
0.83	68	71.5	77	79	83	87	91
0.97	64	67.5	70.5	73	77	79.5	83

Local Bulk Fluid Temperature,  $T_{bx}(^{\circ}C)$

X/L	Re-46617	Re-40054	Re-36194	Re-30739	Re-26598	Re-21632	Re-15204
0.03	24.35	24.38	24.42	24.63	24.67	24.82	24.43
0.17	26.15	26.32	26.49	26.74	26.95	27.28	26.97
0.30	27.95	28.26	28.57	28.85	29.23	29.74	29.51
0.43	29.75	30.20	30.64	30.96	31.51	32.20	32.04
0.57	31.55	32.13	32.71	33.07	33.79	34.66	34.58
0.70	33.35	34.07	34.79	35.18	36.07	37.12	37.11
0.83	35.15	36.01	36.86	37.29	38.35	39.58	39.65
0.97	36.95	37.95	38.93	39.40	40.63	42.04	42.19

Local Heat Transfer Coefficient,  $h_x (W/m^2 \text{ } ^{\circ}C)$

X/L	Re-46617	Re-40054	Re-36194	Re-30739	Re-26598	Re-21632	Re-15204
0.03	71.09	60.44	53.27	42.51	39.30	33.33	23.27
0.17	57.22	50.31	45.77	36.96	32.41	27.17	18.74
0.30	55.29	47.59	43.59	35.34	31.19	25.49	17.66
0.43	50.72	44.07	38.85	31.74	28.28	24.24	16.85
0.57	38.96	33.79	30.50	24.63	22.41	19.22	13.29
0.70	43.06	37.58	32.81	27.82	24.23	20.97	14.46
0.83	59.83	51.28	43.90	36.56	31.98	26.49	17.71
0.97	72.66	61.58	55.83	45.39	39.26	33.53	22.28

**Local Nusselt Number,  $Nu_x$**

X/L	Re-46617	Re-40054	Re-36194	Re-30739	Re-26598	Re-21632	Re-15204
0.03	187.66	159.31	140.22	111.79	103.15	87.28	60.98
0.17	151.06	132.61	120.46	97.19	85.08	71.16	49.09
0.30	145.96	125.46	114.72	92.93	81.88	66.77	46.26
0.43	133.90	116.15	102.26	83.48	74.22	63.50	44.15
0.57	102.85	89.06	80.27	64.75	58.82	50.34	34.81
0.70	113.67	99.06	86.36	73.15	63.59	54.93	37.88
0.83	157.95	135.18	115.56	96.15	83.93	69.37	46.39
0.97	191.82	162.33	146.95	119.36	103.04	87.82	58.36

**Pressure drop,  $\Delta P$  (N/m<sup>2</sup>)**

X/L	Re-46617	Re-40054	Re-36194	Re-30739	Re-26598	Re-21632	Re-15204
0.03	41.08	31.79	26.90	21.52	17.12	14.68	12.72
0.17	61.13	48.90	39.12	32.28	26.90	22.50	17.61
0.30	70.91	58.68	44.01	38.14	31.79	26.42	21.52
0.43	92.92	70.91	58.68	44.01	36.68	31.31	26.42
0.57	103.67	90.47	73.35	51.84	46.46	38.16	31.31
0.70	113.45	100.25	83.13	60.64	51.36	43.05	36.69
0.83	123.24	105.14	90.47	66.02	56.25	47.94	41.58
0.97	133.02	114.92	97.81	75.80	63.58	52.83	46.47

**Friction Factor,  $f_i$**

X/L	Re-46617	Re-40054	Re-36194	Re-30739	Re-26598	Re-21632	Re-15204
0.03	0.218	0.227	0.234	0.259	0.274	0.353	0.620
0.17	0.065	0.070	0.068	0.078	0.086	0.108	0.172
0.30	0.042	0.047	0.043	0.051	0.057	0.071	0.117
0.43	0.038	0.039	0.039	0.041	0.045	0.058	0.099
0.57	0.032	0.038	0.038	0.037	0.044	0.054	0.090
0.70	0.029	0.034	0.034	0.035	0.039	0.049	0.085
0.83	0.026	0.030	0.032	0.032	0.036	0.046	0.081
0.97	0.024	0.028	0.029	0.031	0.035	0.044	0.078

**Average heat transfer coefficient, Nusselt number, Pumping power, Total heat transfer rate, Effectiveness, Total pressure drop and Average friction factor**

Re	h	Nu	$P_m$	$Q_{out}$	$\epsilon$	$\Delta p$	$f_i$
15204	18.03	47.24	0.63	299.92	0.291	46.47	0.168
21632	26.31	68.90	1.02	414.28	0.297	52.83	0.098
26598	31.13	81.71	1.50	470.96	0.287	63.58	0.077
30739	35.12	92.35	2.07	503.06	0.282	75.80	0.070
36194	43.06	113.35	3.13	581.36	0.291	97.81	0.065
40054	48.33	127.40	4.06	600.38	0.295	114.92	0.064
46617	56.11	148.11	5.45	648.38	0.294	133.02	0.059

**For porosity,  $R_p=27.1\%$   
Local Wall Temperature,  $T_{wx}(^{\circ}C)$**

X/L	Re-46307	Re-40272	Re-36117	Re-30453	Re-26325	Re-21552	Re-15631
0.03	53	55	58	60	61	62	63.5
0.17	60.5	63.5	66	68.5	70.5	72.5	75
0.30	65	68	70	73	76	79.5	82
0.43	70	73	77	79.5	83.5	85	86.5
0.57	81.5	86.5	90	96	98	101	103.5
0.70	79	83	87.5	91	95.5	98	100
0.83	69.5	73	78	80	84	88	92
0.97	64.5	67.5	71	74	77	80	83.5

**Local Bulk Fluid Temperature,  $T_{bx}(^{\circ}C)$**

X/L	Re-46307	Re-40272	Re-36117	Re-30453	Re-26325	Re-21552	Re-15631
0.03	26.12	26.15	26.18	26.11	25.85	25.98	25.49
0.17	27.82	27.97	28.12	28.13	28.04	28.32	27.87
0.30	29.51	29.78	30.05	30.16	30.24	30.65	30.25
0.43	31.20	31.59	31.98	32.19	32.43	32.98	32.62
0.57	32.90	33.41	33.92	34.21	34.62	35.32	35.00
0.70	34.59	35.22	35.85	36.24	36.82	37.65	37.37
0.83	36.28	37.03	37.78	38.27	39.01	39.98	39.75
0.97	37.98	38.85	39.72	40.29	41.20	42.32	42.13

**Local Heat Transfer Coefficient,  $h_x$  ( $W/m^2 \text{ } ^\circ C$ )**

X/L	Re-46307	Re-40272	Re-36117	Re-30453	Re-26325	Re-21552	Re-15631
0.03	68.58	59.58	51.71	42.93	38.76	32.99	23.07
0.17	56.40	48.37	43.43	36.04	32.09	26.89	18.61
0.30	51.94	44.97	41.18	33.96	29.77	24.32	16.94
0.43	47.51	41.51	36.55	30.75	26.67	22.84	16.28
0.57	37.93	32.37	29.33	23.55	21.50	18.09	12.80
0.70	41.51	35.97	31.85	26.57	23.21	19.69	14.00
0.83	55.49	47.78	40.91	34.86	30.28	24.75	16.78
0.97	69.50	59.98	52.59	43.17	38.06	31.53	21.20

**Local Nusselt Number,  $Nu_x$**

X/L	Re-46307	Re-40272	Re-36117	Re-30453	Re-26325	Re-21552	Re-15631
0.03	180.33	156.45	135.61	112.51	101.47	86.23	60.36
0.17	148.29	127.01	113.89	94.46	84.01	70.29	48.68
0.30	136.56	118.08	108.00	89.01	77.94	63.58	44.33
0.43	124.92	108.99	95.84	80.59	69.84	59.71	42.58
0.57	99.72	85.00	76.93	61.72	56.28	47.28	33.49
0.70	109.13	94.45	83.53	69.63	60.78	51.46	36.63
0.83	145.91	125.48	107.28	91.37	79.28	64.68	43.91
0.97	182.73	157.50	137.92	113.13	99.64	82.42	55.45

**Pressure drop,  $\Delta P$  ( $N/m^2$ )**

X/L	Re-46307	Re-40272	Re-36117	Re-30453	Re-26325	Re-21552	Re-15631
0.03	39.09	29.32	24.43	19.54	16.61	12.71	12.22
0.17	58.63	46.42	36.65	31.76	24.43	20.52	15.64
0.30	68.40	53.75	41.53	36.65	29.32	24.43	19.55
0.43	87.95	68.40	56.19	43.97	34.21	29.32	24.44
0.57	97.72	85.51	70.85	51.30	43.98	36.16	29.32
0.70	109.94	95.28	78.18	61.08	48.87	41.05	34.21
0.83	117.27	100.16	85.51	65.96	53.75	44.96	39.10
0.97	128.99	109.94	92.83	73.29	61.08	50.82	44.96

**Friction Factor,  $f_i$**

X/L	Re-46307	Re-40272	Re-36117	Re-30453	Re-26325	Re-21552	Re-15631
0.03	0.207	0.205	0.212	0.238	0.270	0.306	0.561
0.17	0.062	0.065	0.063	0.077	0.079	0.099	0.144
0.30	0.040	0.042	0.040	0.050	0.053	0.065	0.100
0.43	0.036	0.037	0.037	0.041	0.043	0.054	0.086
0.57	0.031	0.035	0.036	0.037	0.042	0.051	0.079
0.70	0.028	0.032	0.032	0.035	0.038	0.047	0.075
0.83	0.025	0.028	0.030	0.032	0.035	0.043	0.072
0.97	0.024	0.027	0.028	0.031	0.034	0.042	0.071

**Average heat transfer coefficient, Nusselt number, Pumping power, Total heat transfer rate, Effectiveness, Total pressure drop and Average friction factor**

Re	h	Nu	$P_m$	$Q_{out}$	$\epsilon$	$\Delta p$	$f_i$
15631	17.46	45.68	0.63	289.27	0.276	44.96	0.148
21552	25.14	65.71	0.98	391.98	0.285	50.82	0.089
26325	30.04	78.66	1.44	449.39	0.280	61.08	0.074
30453	33.98	89.05	1.99	479.96	0.275	73.29	0.068
36117	40.94	107.38	2.99	542.68	0.279	92.83	0.060
40272	46.31	121.62	3.93	566.91	0.282	109.94	0.059
46307	53.61	140.95	5.30	608.04	0.284	128.99	0.057

**For porosity,  $R_p = 39\%$   
Local Wall Temperature,  $T_{wx}$  ( $^{\circ}C$ )**

X/L	Re-46702	Re-40118	Re-36152	Re-30716	Re-26352	Re-21687	Re-15238
0.03	53.5	55.5	58.5	60.5	61.5	62.5	64
0.17	61	64	66.5	69	71	74	76
0.30	66	68.5	71	74	77	80	83
0.43	71	73.5	77	80	84	86	87.5
0.57	82	87	90.5	96.5	98.5	101.5	103.5
0.70	79.5	83.5	88	92	96	98.5	100.5
0.83	69.5	73.5	78	81	85	89	92.5
0.97	65	68.5	72	74.5	77	80.5	84

**Local Bulk Fluid Temperature,  $T_{bx}$  (°C)**

X/L	Re-46702	Re-40118	Re-36152	Re-30716	Re-26352	Re-21687	Re-15238
0.03	25.71	25.74	25.96	25.98	25.92	25.35	25.16
0.17	27.33	27.50	27.78	27.88	28.00	27.55	27.42
0.30	28.96	29.26	29.61	29.79	30.08	29.75	29.67
0.43	30.59	31.02	31.44	31.70	32.16	31.95	31.92
0.57	32.21	32.78	33.26	33.60	34.24	34.15	34.18
0.70	33.84	34.54	35.09	35.51	36.32	36.35	36.43
0.83	35.47	36.30	36.92	37.42	38.40	38.55	38.68
0.97	37.09	38.06	38.74	39.32	40.48	40.75	40.94

**Local Heat Transfer Coefficient,  $h_x$  (W/m<sup>2</sup> °C)**

X/L	Re-46702	Re-40118	Re-36152	Re-30716	Re-26352	Re-21687	Re-15238
0.03	64.15	55.81	47.86	40.07	36.39	30.38	20.92
0.17	52.96	45.51	40.23	33.65	30.11	24.29	16.72
0.30	48.13	42.33	37.63	31.29	27.60	22.46	15.23
0.43	44.12	39.10	34.18	28.64	24.98	20.88	14.62
0.57	35.81	30.64	27.21	22.00	20.15	16.76	11.72
0.70	39.05	33.93	29.44	24.49	21.70	18.16	12.68
0.83	52.39	44.65	37.91	31.74	27.79	22.37	15.09
0.97	63.89	54.57	46.83	39.33	35.45	28.39	18.86

**Local Nusselt Number,  $Nu_x$**

X/L	Re-46702	Re-40118	Re-36152	Re-30716	Re-26352	Re-21687	Re-15238
0.03	168.98	146.63	125.37	104.78	95.16	79.30	54.60
0.17	139.50	119.55	105.38	87.98	78.74	63.43	43.65
0.30	126.80	111.21	98.57	81.82	72.16	58.63	39.76
0.43	116.21	102.72	89.55	74.89	65.31	54.51	38.15
0.57	94.33	80.48	71.28	57.51	52.69	43.74	30.59
0.70	102.86	89.13	77.11	64.04	56.73	47.40	33.10
0.83	138.00	117.30	99.31	83.00	72.65	58.40	39.40
0.97	168.29	143.35	122.68	102.84	92.71	74.11	49.24

**Pressure drop,  $\Delta P$  (N/m<sup>2</sup>)**

X/L	Re-46702	Re-40118	Re-36152	Re-30716	Re-26352	Re-21687	Re-15238
0.03	36.65	26.88	21.99	17.10	14.66	11.73	9.78
0.17	55.71	42.03	34.21	29.32	21.99	17.59	12.71
0.30	64.51	51.31	38.12	33.23	26.88	22.48	16.62
0.43	83.07	65.48	53.75	41.05	31.76	26.39	21.51
0.57	93.83	81.12	67.44	48.87	41.05	33.23	26.40
0.70	104.58	90.89	74.28	58.64	46.42	38.12	31.28
0.83	112.40	96.76	82.10	61.57	51.31	42.03	36.17
0.97	123.15	105.07	89.92	69.39	58.64	48.87	43.02

**Friction Factor,  $f_i$**

X/L	Re-46702	Re-40118	Re-36152	Re-30716	Re-26352	Re-21687	Re-15238
0.03	0.192	0.190	0.189	0.203	0.237	0.278	0.469
0.17	0.058	0.059	0.059	0.070	0.071	0.083	0.122
0.30	0.038	0.040	0.036	0.044	0.048	0.059	0.089
0.43	0.034	0.036	0.036	0.037	0.039	0.048	0.079
0.57	0.029	0.034	0.034	0.034	0.039	0.046	0.075
0.70	0.026	0.031	0.030	0.033	0.036	0.043	0.072
0.83	0.024	0.027	0.028	0.029	0.033	0.040	0.069
0.97	0.022	0.026	0.027	0.028	0.033	0.040	0.071

**Average heat transfer coefficient, Nusselt number, Pumping power, Total heat transfer rate, Effectiveness, Total pressure drop and Average friction factor**

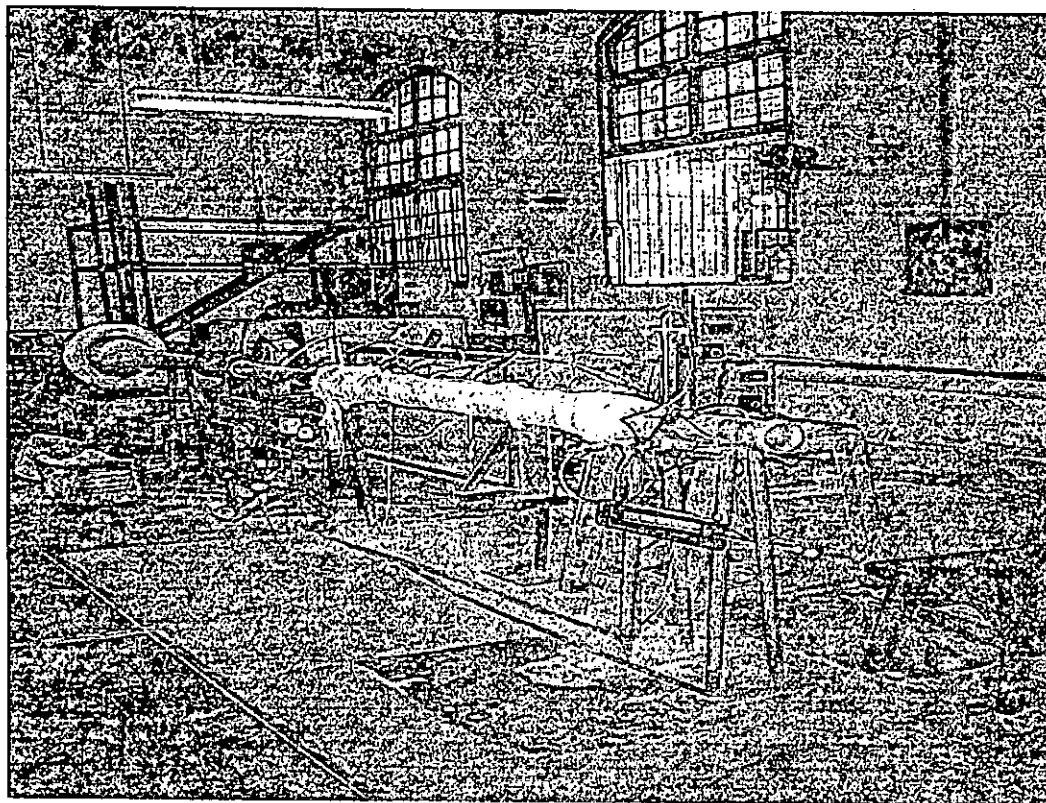
Re	h	Nu	Pm	Q <sub>out</sub>	$\epsilon$	$\Delta p$	$f_i$
15238	15.73	41.06	0.59	267.96	0.258	43.02	0.131
21687	22.96	59.94	0.95	372.25	0.263	48.87	0.080
26352	28.02	73.27	1.38	427.11	0.263	58.64	0.067
30716	31.40	82.11	1.91	456.35	0.254	69.39	0.060
36152	37.66	98.66	2.90	513.76	0.260	89.92	0.055
40118	43.32	113.80	3.74	547.93	0.268	105.07	0.055
46702	50.06	131.87	5.08	588.12	0.266	123.15	0.053

**Performance Parameter, R for different inserts at different pumping power**

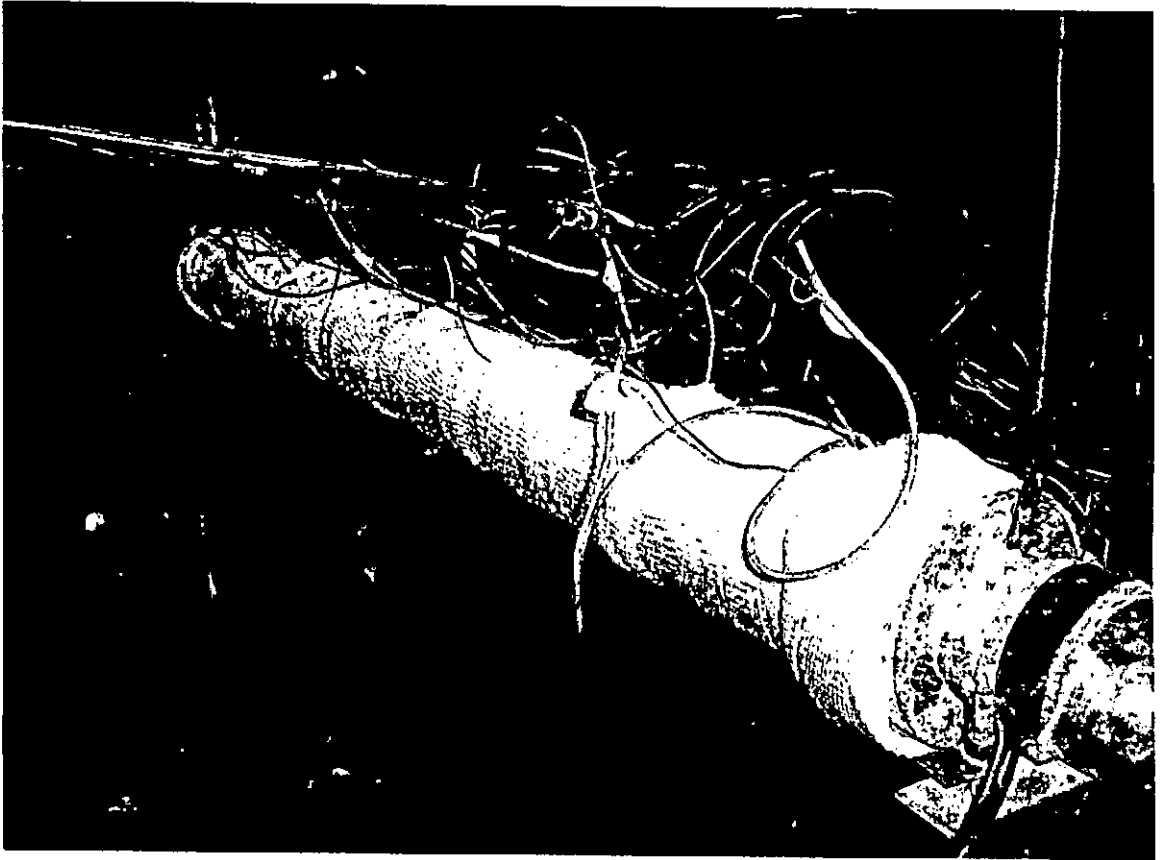
$R_p$	$P_m = 0.88$ watt	$P_m = 1.21$ watt	$P_m = 1.66$ watt	$P_m = 2.30$ watt	$P_m = 3.02$ watt	$P_m = 4.17$ watt
For $R_p = 1.1\%$	1.97	2.05	2.01	2.09	2.00	2.09
For $R_p = 2.5\%$	1.91	1.99	1.95	2.03	1.95	2.01
For $R_p = 4.4\%$	1.83	1.92	1.89	1.97	1.91	1.94
For $R_p = 6.8\%$	1.77	1.87	1.86	1.93	1.87	1.89
For $R_p = 13.3\%$	1.72	1.82	1.81	1.88	1.82	1.84
For $R_p = 17.4\%$	1.77	1.88	1.88	1.92	1.88	1.90
For $R_p = 22\%$	1.84	1.95	1.93	1.96	1.91	1.95
For $R_p = 27.1\%$	1.90	1.97	1.96	2.02	1.97	1.98
For $R_p = 39\%$	1.97	2.04	2.04	2.07	2.01	2.03
For Rectangular Strip insert ( $R_p = 0$ )	1.75	1.87	1.82	1.91	1.85	1.88



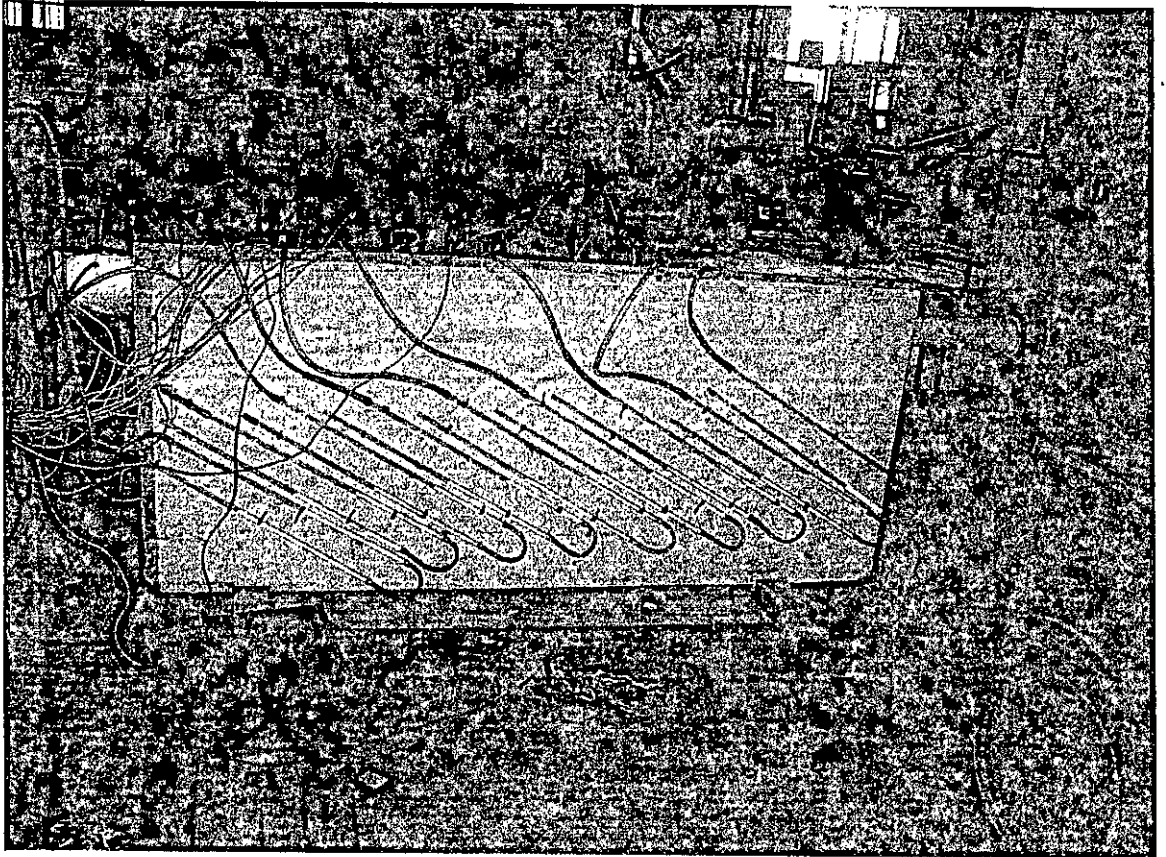
**APPENDIX-F  
PHOTOGRAPH**



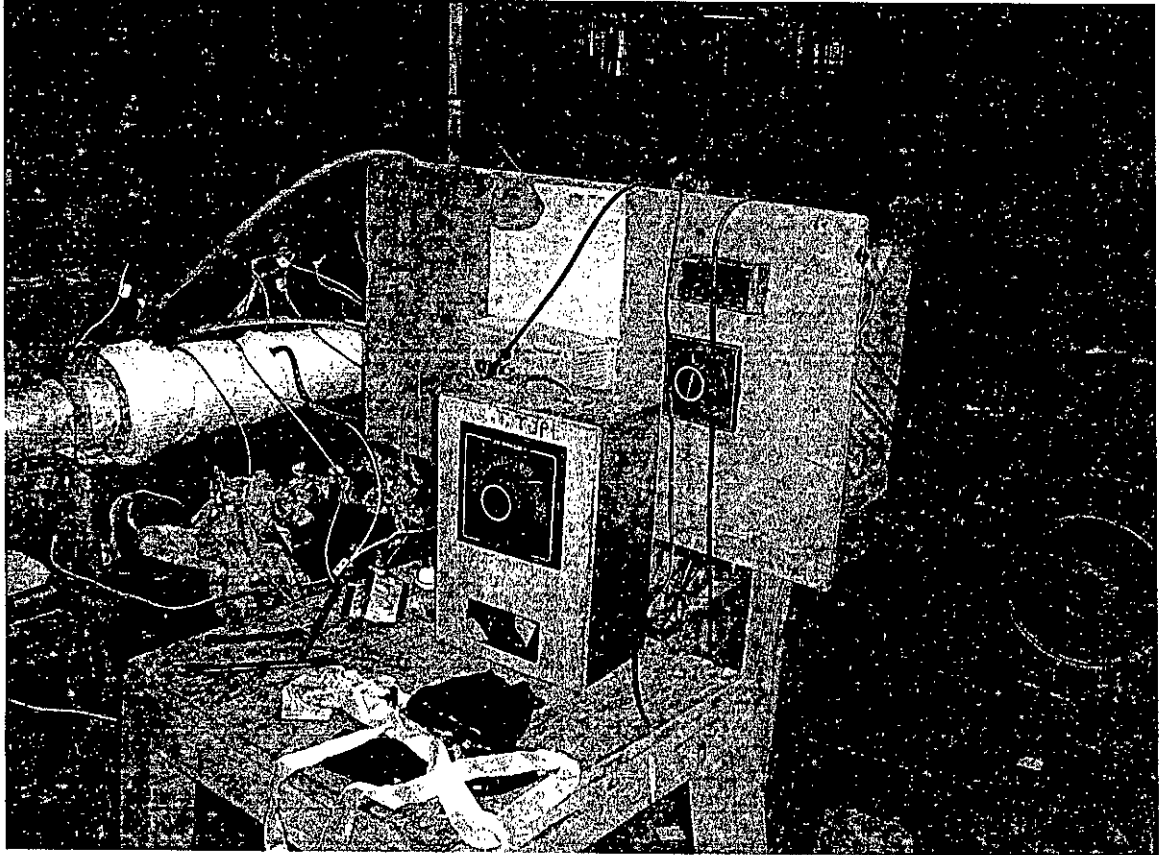
**FIGURE 1: Experimental Facility.**



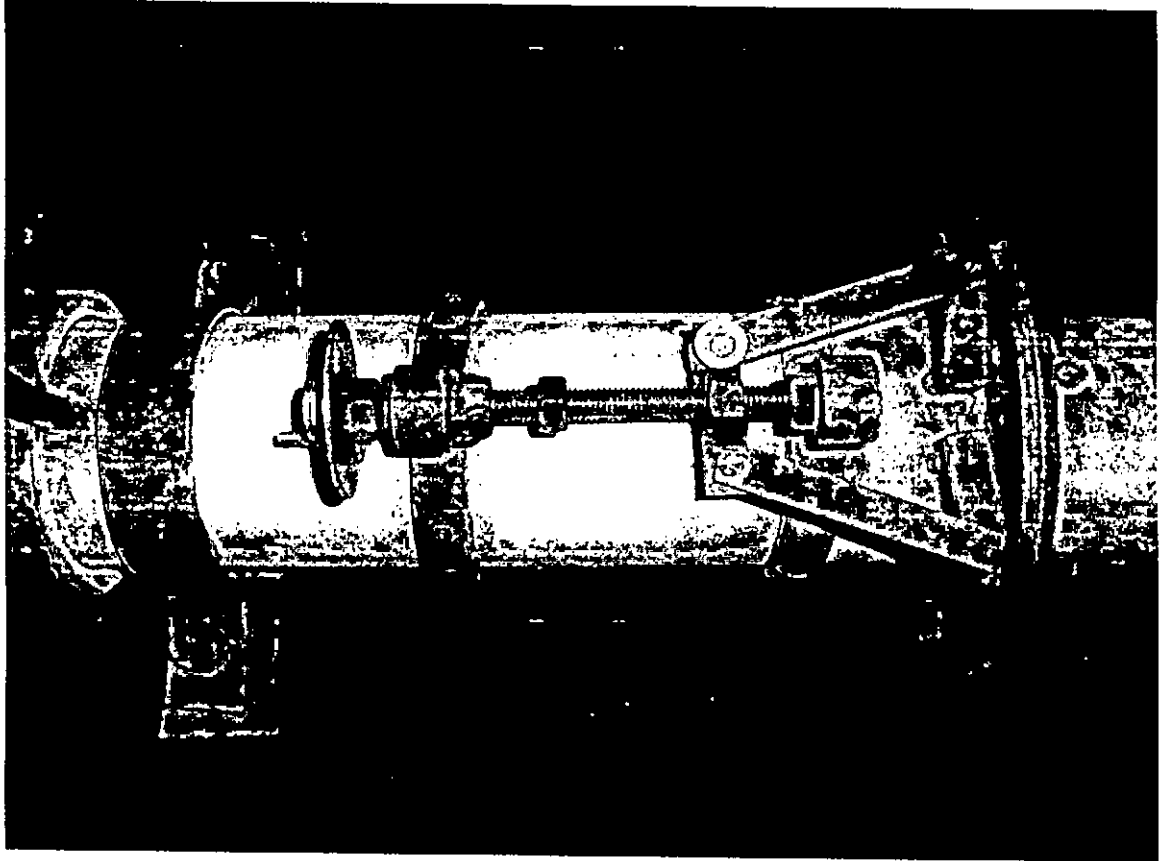
**FIGURE 2: Insulated Test Section**



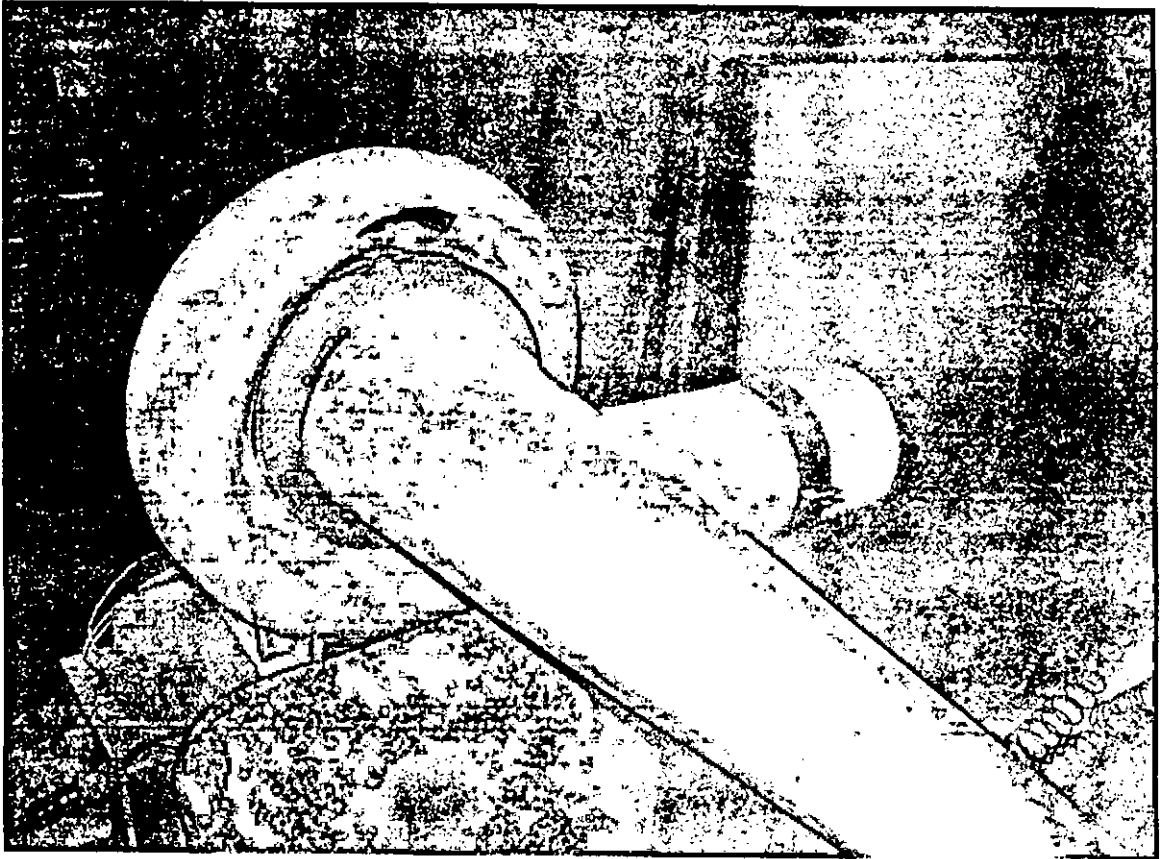
**FIGURE 3: 30° Inclined U-tube Manometer**



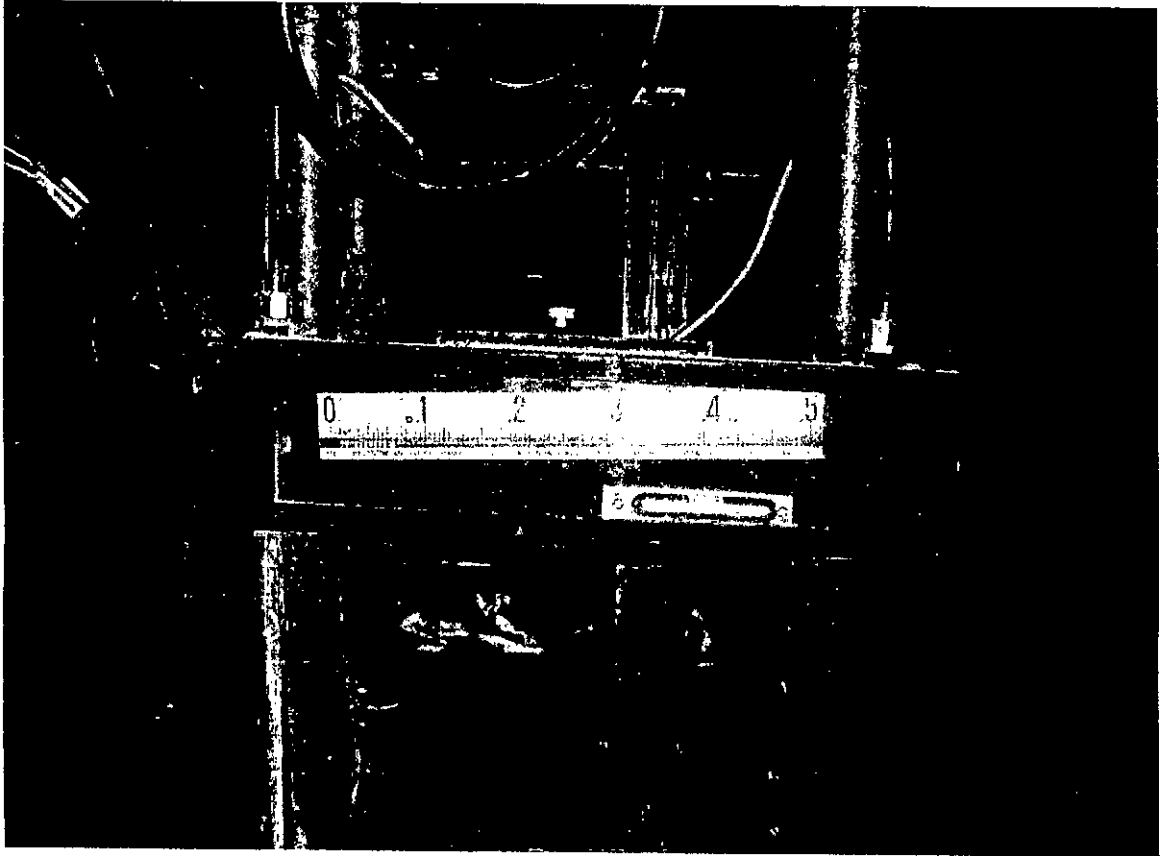
**FIGURE 4: Thermocouples and their positions**



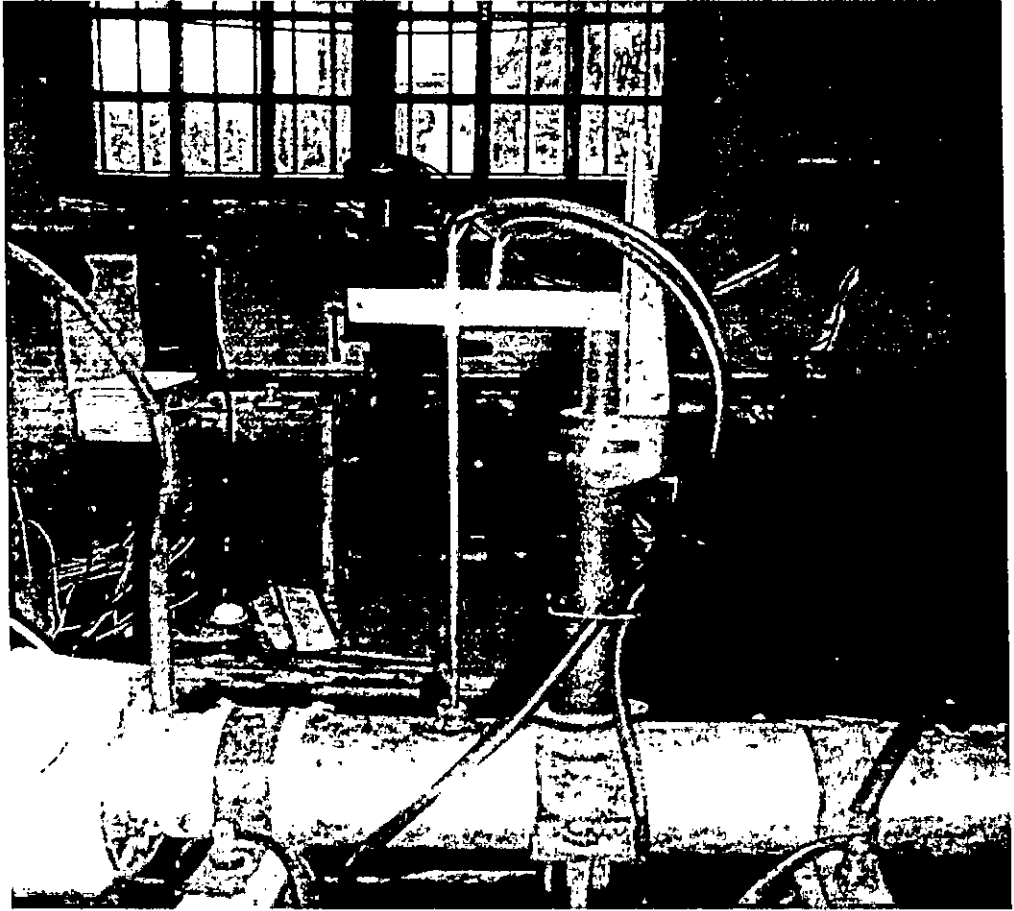
**FIGURE 5: Butterfly Valve**



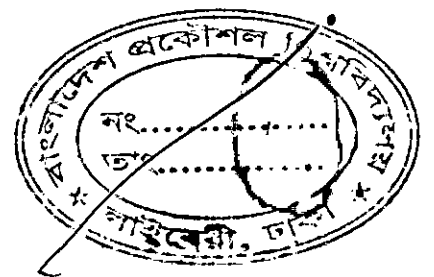
**FIGURE 6: Centrifugal Blower**



**FIGURE 7: Inclined Tube Manometer**



**FIGURE 8: Traversing Pitot Tube.**





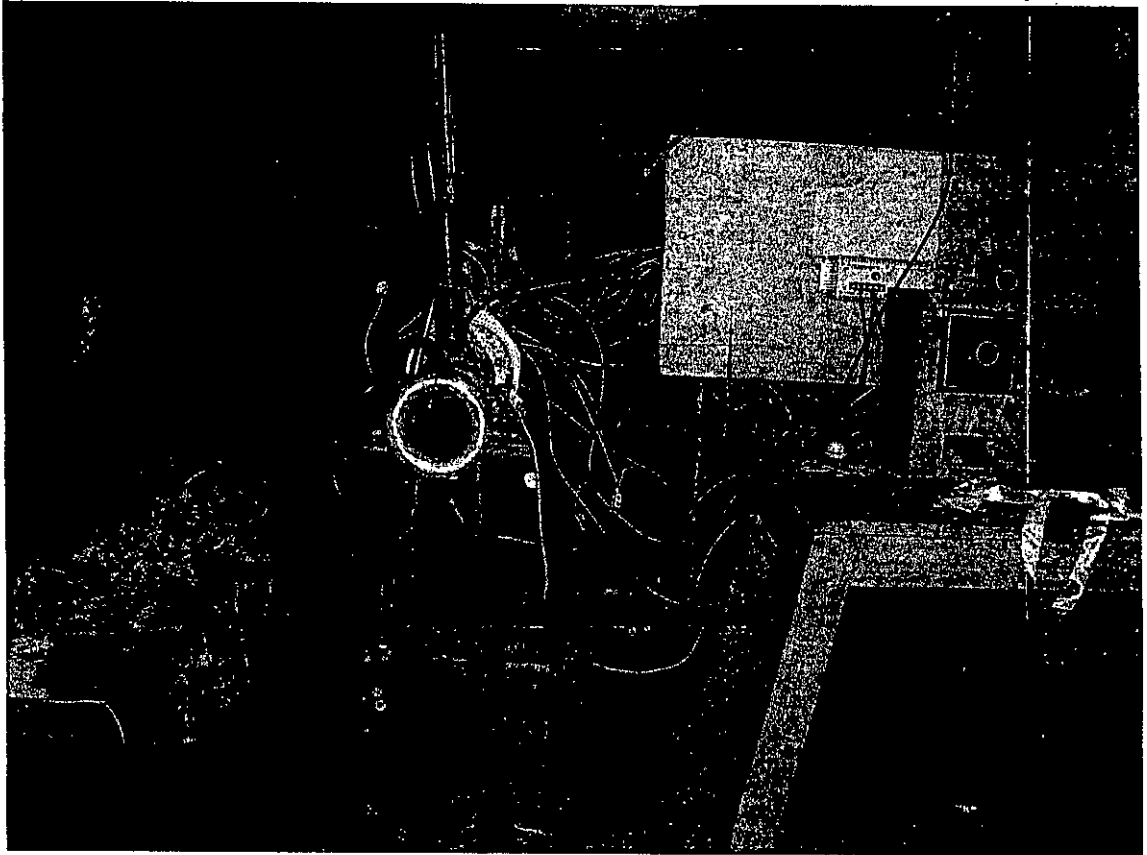


**FIGURE 11: Inlet Section.**

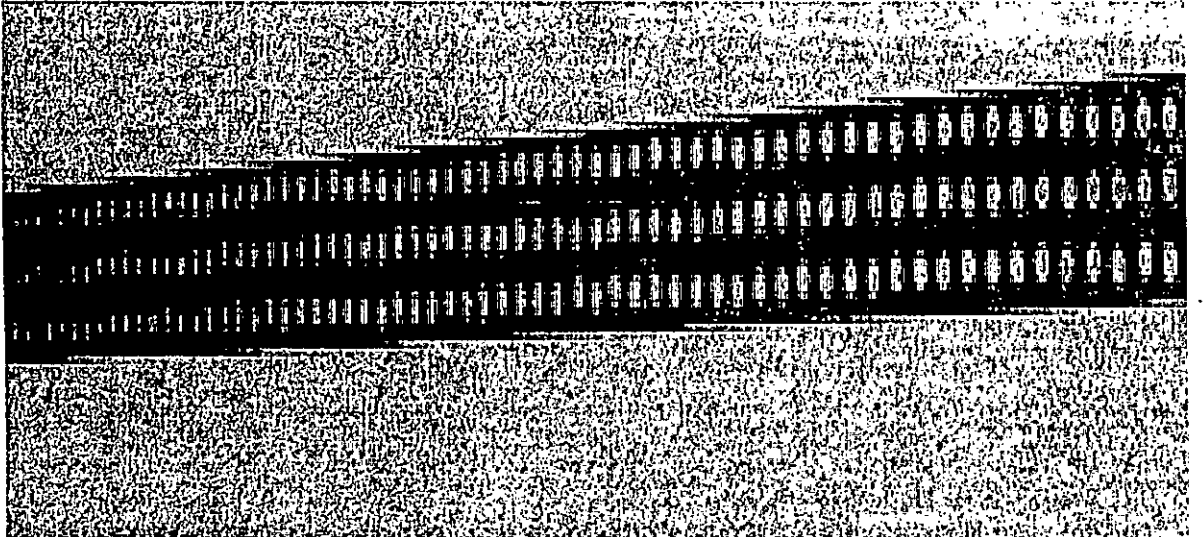


**FIGURE 9: Perforated Rectangular Strip.**

